Biophysical Investigation of Small-Molecule Glyco-Amphiphiles for Membrane-Protein Research

Vom Fachbereich Biologie der Technischen Universität Kaiserslautern

zur Erlangung des akademischen Grades

Doktor der Naturwissenschaften

(Doctor rerum naturalium)

– Genehmigte Dissertation –

von

Herrn Diplom-Biophysiker Florian Mahler

geboren am 28.08.1992 in Karlsruhe

Erstgutachter: Prof. Dr. Sandro Keller

Zweitgutachter: Prof. Dr. Matthias Hahn

Vorsitzender: Prof. Dr. Stefan Kins

Wissenschaftliche Aussprache am 25. März 2022

D 386

Table of Contents

Abstract

Membrane proteins are of high pharmacological interest as they are involved in a variety of vital functions. However, to make them accessible to *in vitro* studies, they often need to be extracted from their natural lipid environment and stabilized with the aid of membrane-mimetic systems. Such membrane mimics can consist of diverse amphiphilic molecules. Small-molecule amphiphiles that can solubilize lipid bilayers, so-called detergents, have been invaluable tools for membrane-protein research in recent decades. Herein, novel small-molecule glyco-amphiphiles embodying three distinct design principles are introduced, and their biophysical and physicochemical properties are investigated. In doing so, the major aims consist in establishing new promising amphiphiles and in determining structure–efficacy relationships for their synthesis and application.

First, the software package D/STAIN was introduced to facilitate the analysis of demicellization curves obtained by isothermal titration calorimetry. The robustness of the underlying algorithm was demonstrated by analyzing demicellization curves representing large variations in amphiphile concentrations and thermodynamic parameters.

Second, the interactions of diastereomeric cyclopentane maltoside amphiphiles (CPMs) with lipid bilayers and membrane proteins were investigated. To this end, lipid model membranes, cellular membranes, and model membrane proteins were treated with different stereoisomer CPMs. These investigations pointed out the importance of stereochemical configuration in the solubilization of lipid bilayers, in the extraction of membrane proteins, and, ultimately, in the stabilization of the latter. Ultimately, CPM-*C*12 could be identified as a particularly stabilizing agent.

Third, the influence of a polymerizable group attached to detergent-like amphiphiles was characterized regarding their micellization, micellar properties, and ability to solubilize lipid membranes. This revealed that such chemical modifications can have different degrees of impact regarding the investigated properties. In particular, micellization was influenced substantially, whereas the sizes of the resulting micelles varied slightly. The polymerizable amphiphiles were shown to solubilize artificial and natural lipid membranes and, consequently, to extract membrane proteins.

Last, the self-assembly of diglucoside amphiphiles bearing either a hydrocarbon or a lipophobic fluorocarbon chain to form native nanodiscs was investigated. It was

shown that the presence of a fluorocarbon hydrophobic chain conveys superior stabilization properties onto the amphiphile and the resulting nanodiscs. Moreover, the kinetics of lipid exchange were fundamentally altered by the presence of the fluorocarbon amphiphiles in the nanodisc rim.

Zusammenfassung

Membranproteine sind von hohem pharmakologischem Interesse, da sie an einer Vielzahl lebenswichtiger Funktionen beteiligt sind. Um sie jedoch für *In-vitro*-Studien zugänglich zu machen, müssen sie oft aus ihrer natürlichen Lipidumgebung extrahiert und mit Hilfe von membranmimetischen Systemen stabilisiert werden. Solche Membranmimetika können aus verschiedenen amphiphilen Molekülen bestehen. Kleinmolekulare Amphiphile, die Lipiddoppelschichten auflösen können, sogenannte Detergenzien, waren in den letzten Jahrzehnten unschätzbare Werkzeuge für die Membranproteinforschung. Hier werden neuartige kleinmolekulare Glykoamphiphile vorgestellt, die auf drei verschiedenen Konstruktionsprinzipien basieren, und ihre biophysikalischen und physiko-chemischen Eigenschaften untersucht. Die Hauptziele bestehen dabei darin, neue vielversprechende Amphiphile zu etablieren und Struktur-Wirkungs-Beziehungen für deren Synthese und Anwendung zu bestimmen.

Zuerst wurde das Softwarepaket D/STAIN eingeführt, um die Analyse von Demizellisierungskurven zu erleichtern, die durch isotherme Titrationskalorimetrie erhalten wurden. Die Robustheit des zugrunde liegenden Algorithmus wurde durch die Analyse von Demizellisierungskurven mit großen Variationen in Amphiphilkonzentrationen und thermodynamischen Parametern demonstriert.

Zweitens wurden die Wechselwirkungen von diastereomeren Cyclopentanmaltosid-Amphiphilen (CPMs) mit Lipiddoppelschichten und Membranproteinen untersucht. Zu diesem Zweck wurden Lipidmodellmembranen, Zellmembranen und Modellmembranproteine mit verschiedenen stereoisomeren CPMs behandelt. Diese Untersuchungen wiesen auf die Bedeutung der stereochemischen Konfiguration bei der Solubilisierung von Lipiddoppelschichten, bei der Extraktion von Membranproteinen und letztendlich bei deren Stabilisierung hin. Letztlich konnte CPM-*C*12 als besonders stabilisierendes Amphiphil identifiziert werden.

Drittens wurde der Einfluss einer polymerisierbaren Gruppe, die an detergensartige Amphiphile gebunden ist, in Bezug auf ihre Mizellbildung, ihre mizellaren Eigenschaften und ihre Fähigkeit, Lipidmembranen zu aufzulösen, charakterisiert. Dabei zeigte sich, dass sich solche chemischen Modifikationen unterschiedlich stark auf die untersuchten Eigenschaften auswirken können. Insbesondere die Mizellisierung wurde stark beeinflusst, während die Größe der

resultierenden Mizellen leicht variierte. Es wurde gezeigt, dass die polymerisierbaren Amphiphile künstliche und natürliche Lipidmembranen solubilisieren und so Membranproteine extrahieren.

Zuletzt wurde die Selbstorganisation von Diglucosid-Amphiphilen mit entweder einer Kohlenwasserstoff- oder einer lipophoben Fluorkohlenstoffkette zu nativen Nanodiscs untersucht. Es wurde gezeigt, dass die Anwesenheit einer hydrophoben Fluorkohlenstoffkette dem Amphiphil und den resultierenden Nanodiscs überlegene Stabilisierungseigenschaften verleiht. Darüber hinaus wurde die Kinetik des Lipidaustauschs durch die Anwesenheit der Fluorkohlenstoff-Amphiphile im Rand der Nanodiscs grundlegend verändert.

List of Included Manuscripts

Manuscript 1

Fast and Robust Quantification of Detergent Micellization Thermodynamics from Isothermal Titration Calorimetry

Shih-Chia Tso, Florian Mahler, Jonas Höring, Sandro Keller, and Chad A. Brautigam

Analytical Chemistry **2020**, 92, 1154–1161

Manuscript 2

Diastereomeric Cyclopentane-Based Maltosides (CPMs) as Tools for Membrane Protein Study

Manabendra Das, Florian Mahler, Parameswaran Hariharan, Haoqing Wang, Yang Du, Jonas S. Mortensen, Eugenio Pérez Patallo, Lubna Ghani, David Glück, Ho Jin Lee, Bernadette Byrne, Claus J. Loland, Lan Guan, Brian K. Kobilka, Sandro Keller, and Pil Seok Chae

Journal of the American Chemical Society **2020**, 142, 51, 21382–21392

Manuscript 3

Detergent-Like Polymerizable Monomers: Synthesis, Physicochemical, and Biochemical Characterization

Christophe Bonnet, Pierre Guillet, Florian Mahler, Sébastien Igonet, Sandro Keller, Anass Jawhari, and Grégory Durand

European Journal of Organic Chemistry **2020**, 33, 5340–5349

Manuscript 4

Self-Assembly of Protein-Containing Lipid-Bilayer Nanodisc from Small-Molecule Amphiphiles

Florian Mahler, Annette Meister, Carolyn Vargas, Grégory Durand, and Sandro Keller

Small **2021**, 2103603

Chapter 1: Introduction

1.1. Biological Membranes

Biological membranes surround all cells, thus providing a barrier to separate them from the environment. Moreover, membranes are found inside eukaryotic cells forming separated compartments called organelles. All these membranes are **highly complex and dynamic structures** consisting mainly of lipids and membrane proteins (MPs). Both components are amphiphilic molecules, containing hydrophilic and hydrophobic groups.[1] The hydrophobic effect leads to minimization of the interfacial area between the hydrophobic groups and the aqueous solvent, thus driving self-assembly of the bilayer membrane.[2] The separation by such membranes is of utter importance in order to establish and maintain specific conditions required within the cell and its organelles.[1] The lipids in the bilayer membrane act primarily as barrier for aqueous solutes, but at the same time, they provide a two-dimensional matrix for the incorporation of MPs.[3] Membranes can consist of hundreds of different lipids species and thousands of different MPs with different functions.[1,4] Thus, membranes are not just simple barriers but **can perform rather complex and specific tasks**. This includes the selective transmembrane transport of solutes such as metabolites and ions, signal transduction and amplification, as well as gradient build-up and subsequent energy conversion.[5]

MPs can be classified into peripheral and integral MPs.[1,3] The latter are embedded within the bilayer, whereas peripheral MPs are bound to the membrane by interactions with lipid headgroups or integral MPs. By contrast, integral MPs can either be located in one of the leaflets or span through the entire membrane.[1,3] In particular, channel-forming and receptor MPs build a bridge between the extra- and intracellular space by enabling and regulating mass and information flow. These unique functions paired with their overall large abundance within the membrane (25–75%[6]) render **MPs important drug targets**. Hence, by 2015, more than 50% of FDA-approved drug targets in humans were MPs.[7,8]

1.2. Challenges in Membrane-Protein Studies

Despite their importance, the structures and functions of MPs often remain elusive, as reflected in the fact that, today, only a low percentage of available 3D structures come from MPs (https://blanco.biomol.uci.edu/mpstruc/, 08.10.2021). The reason for this is that MPs need to be extracted from the bulk membrane and the MP of

interest needs to be enriched, compared with others. By this, MPs are made amenable in a simplified model system for biophysical techniques under *in vitro* conditions, which often leads to **loss of structure and function**. Usually, this is accomplished by the application of amphiphilic, membrane-solubilizing agents. These agents are able to fragment lipid bilayers and form small complexes with lipids and MPs, thus shielding hydrophobic surfaces from the aqueous environment and, hence, prevent aggregation of MPs. However, MP extraction bears a major issue: As mentioned above, the biological membrane is a highly complex and heterogeneous structure, which provides numerous interaction partners. This includes other proteins, co-factors, and specific lipid species. In particular, protein–lipid interactions have gained increasing interest over recent years and turned out to be decisive for proper structure,[9–11] oligomerization,[10,12,13] and function[10,14,15] of different MPs. Hence, it is **crucial to provide adequate and mild solubilizing agents** that are able to mimic the membrane and its physicochemical properties required by individual MPs.

1.3. Membrane-Mimetic Systems

Amphiphilic molecules can provide a hydrophobic environment for MPs after extraction from their natural membrane, thus, acting as membrane mimics. Over the last decades, many different approaches and membrane-mimetic systems have been developed. These can be distinguished by the type of aggregates they form when interacting with MPs and lipids. For certain applications there is a requirement for non-bilayer systems that are as small as possible. Therefore, amphiphiles are applied that form a belt-like structure around the hydrophobic surfaces of the MPs.[16,17] On the contrary, for other experiments or particularly sensitive MPs, the imitation of a native bilayer membrane plays a key role. Therefore, amphiphiles that form bilayer systems either made of vesicular lipid bilayers[18] or containing a nano-sized bilayer core[19–21] are used.

Additionally, amphiphiles can be distinguished by their ability to extract MPs directly from the natural membrane. On the one hand, detergents and nanodisc-forming amphiphilic polymers can directly extract MPs. Other systems, such as artificial vesicles, amphipols, bilayered micelles, and nanodisc-forming proteins are not able to effectively extract MPs from natural membranes.[22]

In the following, the most **prominent membrane mimics are presented** with a special focus on detergent micelles.

1.3.1. Non-Bilayer Systems

Detergent Micelles are composed of detergents that are surface active, small-molecule amphiphiles, so-called surfactants, that are able to solubilize lipids and other water-insoluble molecules.[23] The ability to solubilize lipid bilayers and hydrophobic molecules such as MPs renders detergents **invaluable tools for MP research**. They can be directly applied to extract MPs from their natural membrane and form small MP/detergent complexes.

Structurally, detergents consist of a defined hydrophilic and a hydrophobic group, often referred to as head and tail, respectively. Geometrically, most head-and-tail detergents exhibit a conical structure, with the hydrophilic headgroup occupying a larger cross-section area than the flexible hydrophobic chain (Fig. 1A). Hence, owed to the hydrophobic effect, detergents self-assemble into micelles, in which the hydrophobic tail groups are buried inside, whereas the hydrophilic headgroups are exposed to the aqueous solvent with which they interact (Fig. 1B). By this, the **hydrophobic tails are shielded from the aqueous environment**. This self-assembly of detergent monomers into micelles is termed micellization and happens above a certain threshold concentration, the so-called *critical micellization concentration* (CMC). In detail, when increasing the detergent concentration in a solution, first, the concentration of monomers increases linearly. When the concentration reaches the CMC, the monomer concentration stays constant and micellization begins, thus, the micellar concentration starts to increase (Fig. 1C).[22] The CMC of a detergent is an important property to pay attention to and must be accounted for when working with detergent solutions.

The CMC of classical head-and-tail detergents is determined by the **balance between its hydrophilicity and hydrophobicity**, this is, the charge and size of headgroup and length of the alkyl chain. Headgroups can be classified in three different types, which are ionic, zwitterionic, and non-ionic. In general, a higher charge results in higher hydrophilicity and, consequently, in higher CMC values (Fig. 1D). However, one must keep in mind that the actual charge strongly depends on buffer conditions. For non-ionic headgroups, the situation becomes particularly complex because of the widespread use of sugar moieties, which will be discussed in section 1.3.3. Glyco-Amphiphiles. Moreover, the size of the hydrophobic tail also plays an important role. For a homologous amphiphile series, an increase or decrease in alkyl chain length leads to a higher or lower CMC, respectively. This correlation is well known and quantitatively understood. An

increase in chain length by two CH_2 groups results in a ~10-fold lower CMC according to Traube's law.[24]

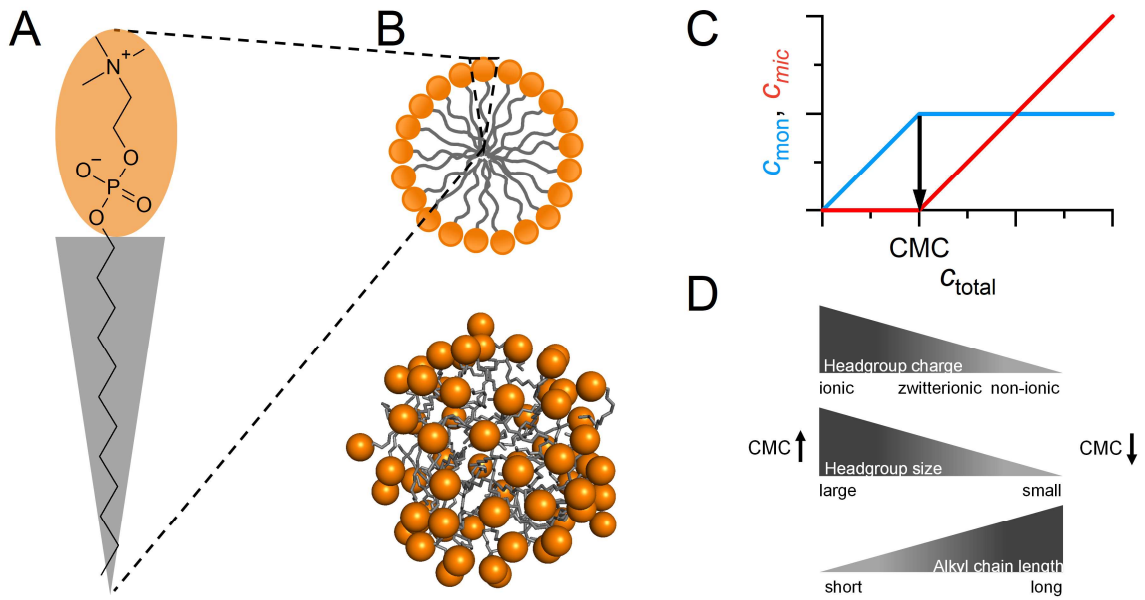

Figure 1. Structure of conventional detergents and micellization. (A) Chemical structure of dodecyl phosphocholine (DPC) with the hydrophilic headgroup and the hydrophobic alkyl chain highlighted in orange and gray, respectively. (B) Structure of a spherical micelle. *Top*: Cross-section of a schematic micelle. *Bottom*: Snapshot of a molecular dynamics simulation of a DPC micelle after 1.1 ns simulation time.[25] Headgroups are presented as orange spheres at the position of the phosphate group. The coordinate files are kindly provided online by Prof. Tieleman from the University of Calgary. (C) Change in monomeric (*blue*) and micellar (*red*) detergent concentration around the CMC as function of the total concentration. (D) General influence of important chemical and structural features on the CMC.

The structures and CMC values of detergent micelles are often assumed to be fixed and static properties. However, from different methods monitoring changes in physical properties of detergent solutions, such as isothermal titration calorimetry, dynamic light scattering, or surface tensiometry, it can be seen that the CMC is not a sharply defined threshold concentration.[26,27] Thus, additionally reporting a monomer/micelle transition range of concentrations is more appropriate than a single number value. Regarding the misconception about micelle structures, this arises from simplified cartoon schemes that show detergents with a fully extended hydrophobic chain in micellar cross-sections. **Micelles are rather flexible and dynamic** (Fig. 1B).[25,27,28] However, this dynamic nature is often the reason for issues with fragile MPs by not providing them with a stable supporting environment as in the bilayer membrane. The flexible alkyl chains of conventional head-and-tail detergents are likely to interfere with important protein–protein, protein–lipid, or other interactions (cf., 1.2. Biological Membranes). This is particularly pronounced for short-chained detergents.[29,30] To this end, two major approaches were used

in the synthesis of novel small-molecule amphiphiles: Fluorinated surfactants and amphiphiles with branched hydrophobic chains.

Fluorinated surfactants resemble the structure of conventional head-and-tail detergents but substitute the hydrophobic alkyl chains with fluorinated chains. Fluorocarbon chains convey useful properties, which are twofold.[31] First, the substitution of hydrogen atoms by larger fluorine atoms results in slower dynamics inside the micelle owed to steric hindrance, as fluorocarbon chains are stiff, compared with hydrocarbon chains. Second, the bulkier nature of the fluorocarbon chain caused by the larger fluorine paired with the high electronegativity of fluorine leads to unfavorable interactions with hydrocarbon groups. Together, the lower interior micellar dynamics, the bulky chains, and unfavorable interactions render fluorocarbon chains **mild and less prone to interfere with native interactions** (*Manuscript 4*). However, on a downside, this mild character renders fluorinated surfactants rather poor solubilizing agents.[31,32]

Branched detergents are a novel group of small-molecule amphiphiles that deviate from the classical head-and-tail structure (*Manuscript 2*). The most popular member of this group is lauryl maltose neopentylglycol (LMNG)[33] which consists of two maltose groups as headgroup and two alkyl chains as hydrophobic groups. It proved particularly useful for G protein-coupled receptors (GPCRs).[34] The potential reason for these stabilizing properties is **lower mobility of the individual amphiphile molecules** because of two reasons. First, the central connection between the branches restricts mobility of the groups, compared with conventional detergents. Second, the maltose headgroups can intertwine and establish sustained hydrogen bonds, which further lower the mobility and, hence, the dynamics in the micellar complex.[34]

The effect of amphiphile headgroups on MP stability will be discussed in section 1.3.3. Glyco-Amphiphiles.

Short Amphiphilic Polymers, or amphipols, are short, amphiphilic polymers with both hydrophobic and hydrophilic moieties, designed to tightly bind onto the hydrophobic surface of MPs, thus, forming a thin layer.[16,35] The hydrophilic moieties can either be ionic groups such as carboxylic groups (APol, A8-35[36]), or non-ionic groups such as branched glucose (NAPol[37]) or maltose (*Manuscript 3*) groups. Non-ionic groups help to overcome the limitations of anionic polymers, these are, precipitation at low pH values[38] or high divalent cation concentrations.[39] Because of their slow dynamics and high hydrophobicity,

amphipols **wrap tightly around the hydrophobic surfaces** of MPs and, thus, have turned out to have stabilizing properties for MPs, when compared with conventional detergents.[36] However, amphipols exhibit very low solubilization and extraction efficiencies; therefore, it is common practice to extract MPs from their native bilayer by using detergents and subsequently exchange the MPs into amphipols.[40,41] In particular, for fragile MPs that require the stabilizing effect of amphipols, this initial detergent exposure can be detrimental.

1.3.2. Lipid-Bilayer Systems

Lipids usually consist of a hydrophilic headgroup connected by a glycerol backbone to a hydrophobic tail group, typically comprising two fatty acyl chains (Fig. 2A). In contrast with detergents, lipids possess a rather cylindrical shape because the two acyl chains occupy a cross-sectional area comparable to the headgroup. Therefore, **self-assembly of lipids results in the formation of bilayers** in which the hydrophobic acyl chains of lipids from both monolayers are shielded from water inside the bilayer. At the same time, the hydrophilic headgroups are exposed to the aqueous solvent at both sides of the bilayer (Fig. 2B).

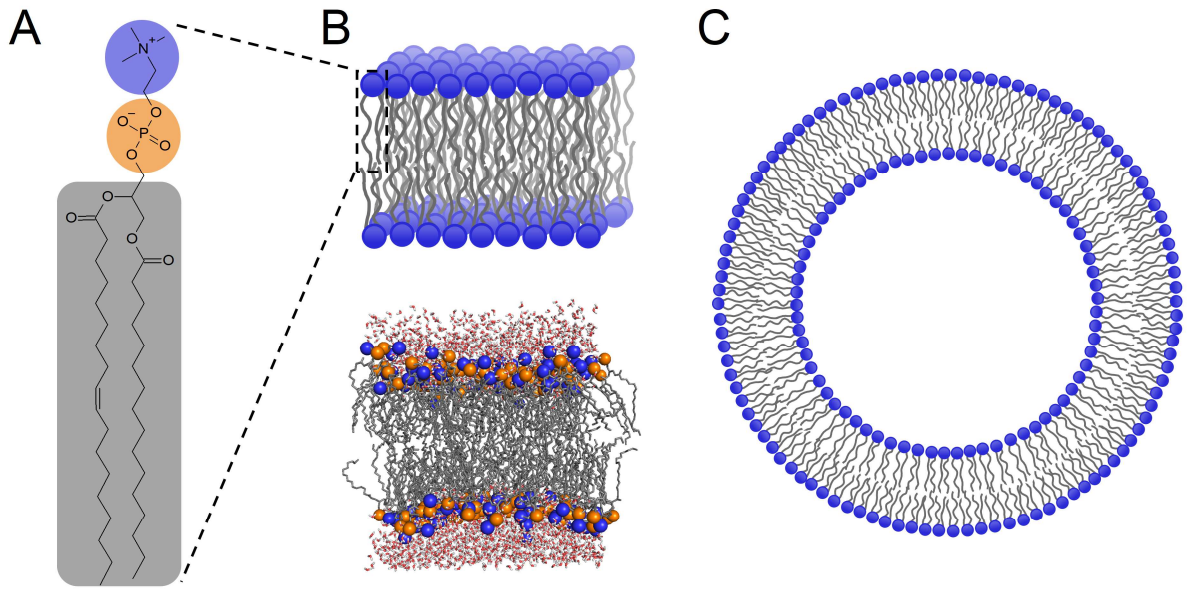

Figure 2. Chemical structure of phospholipids and vesicle structure. (A) Chemical structure of 1-palmitoyl-2-oleoyl-*sn*-glycero-3-phosphocholine (POPC) with the hydrophilic headgroup and the hydrophobic alkyl chain highlighted in blue/orange and gray, respectively. The positively charged choline group is highlighted in blue and the negatively charged phosphate group is highlighted in orange. (B) Structure of a lipid bilayer. *Top*: Cross-section of a schematic bilayer. *Bottom*: Snapshot of a molecular dynamics simulation of a POPC bilayer after 1.6 ns simulation time.[42] Charged groups are presented as blue and orange spheres centered at the nitrogen and phosphate, respectively. Water molecules are shown in stick representation and red/white. The coordinate files are kindly provided online by Prof. Tieleman from the University of Calgary. (C) Cross-section of a schematic unilamellar lipid vesicle.

Artificial vesicles made from synthetic lipids represent a simplified but native-like model system for studying MPs *in vitro*. Typically, such artificial vesicles consist of just a few or even one single lipid species. In most cases, this are phospholipids because of their high natural abundance in membranes.[43] To get a vesicle population with a defined size distribution, unilamellar vesicles can be prepared in a way that a single lipid bilayer encloses an aqueous compartment (Fig. 2C). Such vesicles can be prepared, for instance, by extrusion,[44] sonication,[45] or microfluidics.[46,47] Depending on the technique used to produce the unilamellar vesicles, diameters between 30 nm and 1 µm can be obtained.

Nanodiscs mimic a whole native-like membrane within a 10–40-nm sized lipid-bilayer patch, surrounded by a belt consisting of amphiphilic agents. Thus, MPs can be embedded under mild conditions in a native-like lipid bilayer while being amenable to biophysical techniques due to their small size. These agents can either be certain lipids, amphipathic proteins, or amphiphilic polymers.

Bilayered micelles, or bicelles, are the oldest membrane mimics that contain nanosized lipid-bilayers (Fig. 3A). Typically, their belt is made of 1,2-dihexanoyl-*sn*-glycero-3-phosphocholine (DHPC). Unfortunately, these lipid amphiphiles are **unable to directly recruit lipids and MPs** from a native membrane into bicelles.[48] Therefore, bicelles need to be assembled from lipids for the bilayer patch, MPs, and the rim-forming agent. However, the formation of bicelles is restricted to certain combinations of lipids and, moreover, is only stable under certain experimental conditions such as defined lipid/amphiphile ratios and certain temperatures.[49] This renders bicelles rather complicated membrane-mimetic systems to handle.

Protein-bounded nanodiscs use mostly amphipathic proteins from the membrane scaffold protein (MSP) family, which are derived from apolipoprotein A1, in order to stabilize the lipid-bilayer patch (Fig. 3B).[20] Similarly to bicelle-forming lipids, MSP **cannot recruit nanodisc material directly** from a native membrane but need to be assembled with the single components.[50] However, MSP nanodiscs are stable over a wide range of conditions.

Polymer-bounded nanodiscs are formed by amphiphilic copolymers, which mostly rely on a maleic acid unit as hydrophilic group (Fig. 3C). The most prominent members of this group are the negatively charged styrene/maleic acid (SMA)[19] and di-isobutylene/maleic acid (DIBMA)[51] copolymers. In contrast with the other nanodisc-forming agents mentioned above, these polymers form nanodiscs upon

direct application onto native membranes.[19,51] Currently, researchers try to overcome the disadvantages inherent to the negatively charged maleic acid groups by derivatization of these groups to produce zwitterionic or nonionic alternatives.[52]

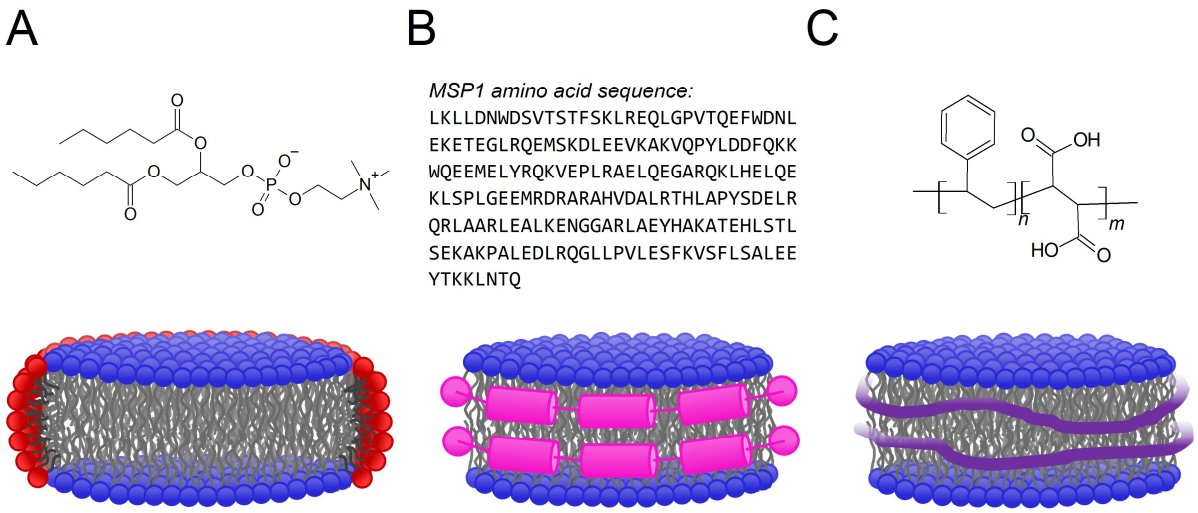

Figure 3. Schematic structure of different nanodisc types. (A) *Top*: Chemical structure of short-chained, bicelle-forming DHPC. *Bottom*: Schematic structure of a bicelle composed of such short-chained DHPC (*red/gray*) and long-chained phospholipids (*blue/gray*). For clarity, DHPC molecules in the front are not shown. (B) *Top*: Amino acid sequence of nanodisc-stabilizing MSP1.[53] *Bottom*: Schematic structure of a MSP nanodisc stabilized by helical MSP1 (*magenta*). (C) *Top*: Chemical structure of nanodisc-forming SMA copolymer. *Bottom*: Schematic structure of a copolymer nanodisc stabilized by SMA (*violet*).

1.3.3. Glyco-Amphiphiles

In MP research, the role of the nature of the hydrophilic groups of amphiphiles is particularly well understood for conventional head-and-tail detergents. In general, ionic, zwitterionic, and non-ionic **headgroups can be ranked from harsh to mild**, in this order.[17,54,55] Therefore, ionic amphiphiles are good solubilizing agents but are prone to denature MPs.[54] A well-known example is the use of sodium dodecyl sulfate (SDS) for protein unfolding.[56,57] However, owed to the varying properties of individual MPs, this does not necessarily exclude ionic detergents as membrane mimics; in fact, some ionic detergents, such as lysophospholipids, are popular in NMR spectroscopy.[17,54,58]

From a physicochemical point of view, ionic or zwitterionic amphiphiles are particularly sensitive to solution properties such as ionic strength, pH, and additives because these properties influence the ionization state of the ionic headgroups (cf., amphiphilic polymers). In particular for polymeric amphiphiles containing carboxy groups, such as APols, SMA, and DIBMA, the presence of divalent cations or low pH values are major restrictions in the usage of these

amphiphiles.[51,59] Moreover, in the case of conventional detergents, this leads to changes of the CMC,[60–62] which leads to practical restrictions for buffer conditions. Additionally, changes of the buffer conditions can also affect the solubilization efficiency of ionic amphiphiles as exemplified by poor solubilization efficiency of anionic SDS and SMA at an acidic pH.[63]

Because of above reasons, **non-ionic detergents have experienced great popularity** in MP research as mild alternatives to ionic and zwitterionic detergents.[64] Glyco-amphiphiles contain a sugar moiety as headgroup and are a particularly interesting group within the non-ionic amphiphiles. The most popular sugars used as headgroups are glucose (glucosides; Fig. 4A) and maltose (maltosides; Fig. 4B), but the large chemical variety of sugars can be exploited to tune the physicochemical properties of newly developed amphiphiles.[65–69] The striking majority of 3D MP structures in the last decade were obtained by using glyco-amphiphiles, where n-dodecyl-β-D-maltopyranoside (DDM, Fig. 4B) has been the most popular choice by far.[64] This popularity is reflected in both MP solubilization and structure determination and, therefore it counts as the gold standard in MP research.

Currently, a trend toward nanodisc-forming polymers can be observed in which researchers try to substitute or derivatize the maleic acid moieties by sugar moieties to render the polymers less charged.[52] Interestingly, this is the same historic development that happened to detergents[70] and amphipols.[37]

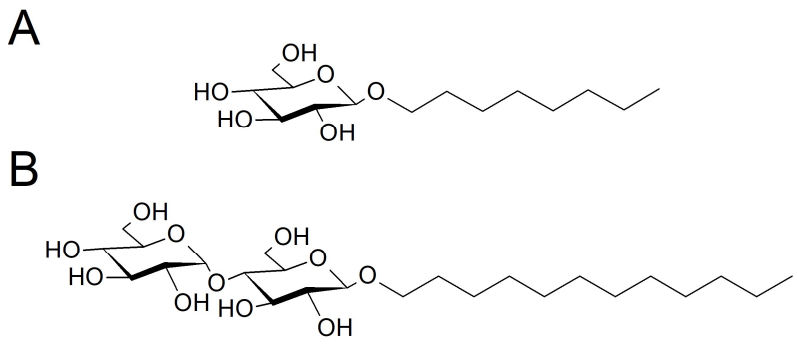

Figure 4. Exemplary chemical structures of two popular small-molecule glyco-amphiphiles. (A) n-octyl-β-D-glucopyranoside (OG) with a glucose moiety as headgroup and (B) DDM with a maltose moiety as headgroup.

1.4. Objectives

Although glyco-amphiphiles have gained increasing popularity in recent years, two major problems persist in membrane-protein research. From an applicational viewpoint, there is **no magic bullet amphiphile** suitable for all membrane proteins because they all have unique structures, properties, and requirements. Additionally, from a physicochemical viewpoint, we lack the **knowledge of a complete structure–efficacy relationship** between proteins and amphiphiles that would facilitate choosing the adequate amphiphile or even enable smart, rational design of new amphiphiles. Hence, the objectives of this thesis can be concluded to:

I. Introduction and characterization of novel small-molecule glyco-amphiphiles that exhibit favorable properties for the ever-growing toolbox of membrane-protein research. This includes:
    a. Investigation of the self-association process including determination of the CMC and assessment of the colloidal structure.
    b. Investigation of their detergency, that is, solubilization of artificial lipid membranes and protein extraction from native membranes.
    c. Assessment of stabilization properties of model membrane proteins in the matter of binding, activity, and unfolding assays.

II. Derive conclusions on structure–efficacy relationships between glyco-amphiphiles and natural membranes regarding the structural and chemical variations tested within the individual manuscripts presented in this thesis.

Chapter 2: Examination of Micellization Thermodynamics

2.1. Synopsis (Manuscript 1)

Isothermal titration calorimetry (ITC) is a powerful technique to characterize the micellization process of micelle-forming amphiphiles. *Manuscript 1* introduces the software package D/STAIN that facilitates and standardizes ITC demicellization-curve analysis. To this end, previous methods to determine CMC values and related thermodynamic parameters were extended in order to relieve inherent parameter correlation. This altered approach is termed as quasi-phenomenological sigmoid algorithm (QPSA), as no physical meaning is ascribed to the pre- and post-transitional baselines. The robustness of the QPSA was tested by analyzing demicellization curves spanning a wide range of CMC values, changes in micellization enthalpy (ΔH^{o}_{mic}), and temperatures.

D/STAIN offers automated, adaptive, and rigorous confidence-interval determination, which is a measure on how reliable obtained fitting parameters are. If necessary, the software can use these confidence intervals to detect possible parameter correlations. Moreover, D/STAIN was designed to read output files obtained from the well-established peak-integration software NITPIC[71] and optionally makes use of the herein calculated heat error estimates to weigh the integrated heats. Together with a simple interface and an integrated graphical parameter view, **D/STAIN facilitates investigation of the micellization process** for newcomers in the field and amphiphile veterans.

2.2. Manuscript 1

Fast and Robust Quantification of Detergent Micellization Thermodynamics from Isothermal Titration Calorimetry

Shih-Chia Tso, Florian Mahler, Jonas Höring, Sandro Keller, and Chad A. Brautigam

Analytical Chemistry, **2020**, 92, 1154–1161

Contribution

For this work, I performed ITC experiments to thoroughly test the software. Furthermore, I suggested software features and participated in editing and revising the manuscript.

analytical chemistry

Article

Cite This: *Anal. Chem.* 2020, 92, 1154–1161

pubs.acs.org/ac

Fast and Robust Quantification of Detergent Micellization Thermodynamics from Isothermal Titration Calorimetry

Shih-Chia Tso,[†] Florian Mahler,[‡] Jonas Höring,[‡] Sandro Keller,[‡] and Chad A. Brautigam*[,†,∥]

[†]Departments of Biophysics and [∥]Microbiology, UT Southwestern Medical Center, 5323 Harry Hines Boulevard, Dallas, Texas 75390, United States

[‡]Molecular Biophysics, Technische Universität Kaiserslautern (TUK), Erwin-Schrödinger-Str. 13, 67663 Kaiserslautern, Germany

Supporting Information

ABSTRACT: Detergents are widely used in modern in vitro biochemistry and biophysics, in particular to aid the characterization of integral membrane proteins. An important characteristic of these chemicals in aqueous solutions is the concentration above which their molecular monomers self-associate to form micelles, termed the critical micellar concentration (CMC). Micelles are supramolecular assemblies arranged with the hydrophobic portions oriented inward and the hydrophilic head groups positioned outward to interact with the aqueous solvent. Knowledge of the CMC is not only of practical relevance but also of theoretical interest because it provides thermodynamic insights. Isothermal titration calorimetry (ITC) is a powerful method to determine CMCs, as it furnishes additional information on the enthalpy and entropy of micellization. Here we describe our extension of previous methods to determine CMCs and other thermodynamic parameters from ITC demicellization curves. The new algorithm, incorporated into the stand-alone software package D/STAIN, analyzes ITC demicellization curves by taking advantage of state-of-the-art thermogram-integration techniques and automatically providing rigorous confidence intervals on the refined parameters. As a demonstration of the software's capabilities, we undertook ITC experiments to determine the respective CMCs of *n*-octyl β-D-glucopyranoside (OG), *n*-dodecyl β-D-maltopyranoside (DDM), and lauryldimethylamine *N*-oxide (LDAO). Motivated by the fact that in vitro membrane protein studies often require additives such as precipitants (e.g., polyethylene glycol (PEG)), we also carried out ITC demicellization studies in the presence of PEG3350, finding in all cases that PEG had significant effects on the thermodynamics of detergent micellization.

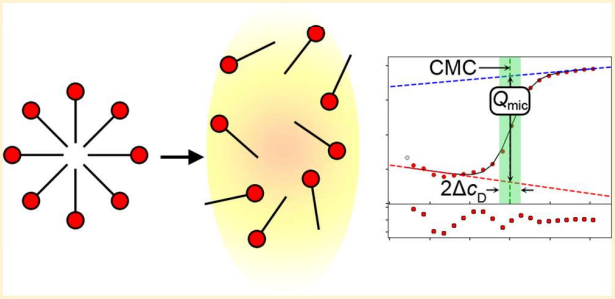

Detergents are amphiphilic molecules usually having hydrophobic chains ("tails") attached to hydrophilic moieties ("head groups") and play central roles in modern molecular science. They are particularly relevant for the in vitro study of integral membrane proteins; taking these very hydrophobic polypeptides out of their native phospholipid environments and purifying them to homogeneity generally requires extracting them from biological membranes using detergents or other amphiphilic agents.[1−4] Downstream studies on the function and structure of the target protein may also employ detergents, and it is widely accepted that the choice of detergent has a significant impact on the results of such experiments.[1,5]

For success in detergent-based studies, it is crucial that researchers consider the physical characteristics of the detergent used. Most importantly, above a certain concentration in aqueous solution, these chemicals spontaneously self-associate into micelles, which can adopt a variety of shapes[6] but always feature an assemblage of detergent molecules oriented such that the head groups contact the solvent, shielding the interior hydrophobic tails from exposure to water. The concentration above which this occurs is called the critical micellar concentration (CMC). Different detergents have vastly different CMC values, which is understood as a thermodynamic parameter related to the change in the free energy between the monomeric and micellar forms of a given detergent.[6] The CMC of course depends on the chemical composition of the detergent; for example, an increase in the size of the hydrophobic tail (e.g., with growing alkyl-chain length) results in stronger self-association as reflected in a lower CMC value.[6,7] For many detergent applications (including the aforementioned membrane protein research), it is imperative to have micelles present, and thus using detergent concentrations above the CMC is necessary.

The measurement of CMC values can be undertaken in many different ways. Conductivity, surface tension, dye binding, and nuclear magnetic resonance (NMR) spectroscopy have all been employed,[6,8] and still others exist.[9] However, the

Received: September 19, 2019
Accepted: December 12, 2019
Published: December 12, 2019

DOI: 10.1021/acs.analchem.9b04281
Anal. Chem. 2020, 92, 1154−1161

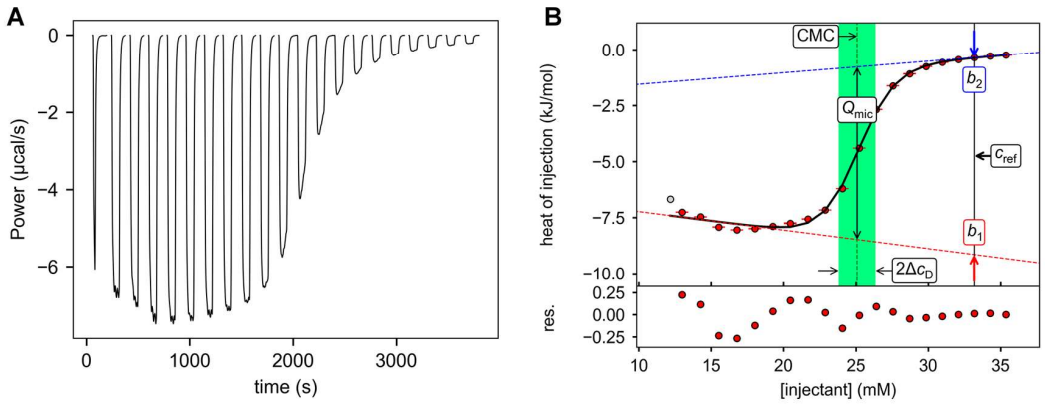

Figure 1. Thermogram and demicellization isotherm for OG. (A) The SVD-truncated, baseline-corrected thermogram as outputted by NITPIC.[19] The widths of the peaks are due to longer-than-usual injection times (see Experimental Section). (B) Graphical Parameter View from D/STAIN. The upper graph shows the demicellization curve, with red circles (with error bars provided by NITPIC) representing the integrated heats of injection used for the analysis and the gray circle denoting an excluded data point that arose from the first injection. The fit to the data is shown as a black line. The red and blue dashed lines are the lines fitted to the pre- and postinflection-point data points, respectively (see eqs 1 and 2). The green-shaded area has a width of $2\Delta c_D$, which is meant to show the magnitude of the parameter Δc_D in concentration space. The vertical black dashed line shows the position of the CMC. All other relevant parameters are annotated with arrows. Q_{mic} is related to ΔH_{mic} by $\Delta H_{mic} = Q_{mic}(c_{syr}/c_{syr} - \mathrm{CMC})$. The lower graph shows the residuals between the fit and the data.

technique par excellence for determining CMC values is isothermal titration calorimetry (ITC).[10−12] In such experiments, it is the demicellization process that is monitored: a solution of the detergent at a concentration well above the CMC (i.e., containing both micelles and free detergent monomers) is titrated into a detergent-free solution, and the heats of demicellization are recorded. As the concentration of the detergent in the calorimeter's monitored volume (the "cell") reaches the CMC, the heats diminish, eventually becoming very small when the concentration in the cell is well above the CMC. This titration results in the classic sigmoid ITC demicellization curve (e.g., Figure 1). One advantage that ITC demicellization experiments have over other CMC-determination methods is that they reveal more thermodynamic information about the micellization process, as the changes in enthalpy and entropy are simultaneously observed in conjunction with the changes in free energy. Additionally, ITC studies can be used to monitor the enthalpy of micellization, ΔH_{mic}, as a function of temperature, thus revealing the corresponding change in heat capacity, $\Delta C_{p,mic}$. ITC studies have demonstrated that detergent micellization is entropically favored and has a negative $\Delta C_{p,mic}$, both hallmarks of processes driven by the hydrophobic effect.[13] Thus, ITC can be used to infer detailed mechanistic information about micellization,[10,11] and it has been used to study the effects of excipients on this process.[7,14,15]

Recently, a method for the analysis of ITC demicellization curves has been presented[7] and refined.[16] That method, extended herein, relies on fitting demicellization data to a quasi-phenomenological sigmoid function and rests on the approximation that the self-association of detergents with sufficiently high aggregation numbers can be treated as pseudophase separation between the aqueous phase containing detergent monomers and the micellar phase.[12,17,18] We have extended this algorithm by adding the features of (a) defining a reference concentration to minimize the correlation of parameters, (b) automatic confidence-interval searches on all fitted parameters, (c) the (optional) use of confidence intervals on the integrated heats[19] as weights for the least-squares fitting algorithms, (d) automatic alternation of fitting algorithms to maximize the probability of parameter convergence, and (e) the ability to examine parameter correlations to understand the nuances of the quasi-phenomenological fitting process. All of these are implemented in a new, stand-alone software called D/STAIN, which is freely available (see below). The performances of these strategies and features were tested by conducting demicellization experiments on various detergents in the absence and presence of a polyethylene glycol having a weight-average molar mass of 3350 g/mol (PEG3350), which is a common precipitant used for protein crystallization. Analysis of the demicellization data using the aforementioned techniques revealed that the presence of PEG3350 not only substantially influences the CMC but also has significant effects on the enthalpic and entropic contributions to micellization.

■ EXPERIMENTAL SECTION

Detergents and Buffers. LDAO and DDM were purchased in their solid forms from Anatrace (Maumee, OH). OG was purchased in its solid form from Gold Biotechnology (St. Louis, MO) and PEG3350 from Hampton Research (Aliso Viejo, CA). Throughout, the buffer used was 10 mM sodium phosphate, 1.8 mM potassium phosphate, 137 mM NaCl, and 2.7 mM KCl, adjusted to pH 7.4 with HCl, hereinafter referred to as phosphate-buffered saline (PBS). All stock solutions of detergents and PEG were prepared by dissolving the respective solid in PBS and readjusting the pH to 7.4 when necessary. All PEG concentrations are given in units of weight per volume (*w*/*v*).

Isothermal Titration Calorimetry. All solutions were degassed prior to the titrations. All ITC experiments were performed in a Malvern iTC200 microcalorimeter (Malvern, UK). The detergent under study was loaded in the syringe at a concentration around 10 to 12-fold of the estimated CMC and titrated into the cell, which contained only buffer (PBS). The cell was held at 20 °C, and the solution was stirred at 750 rpm. Experiments were also performed at 10, 30, 40, 50, and 60 °C as needed for the determination of the heat capacity change upon micellization, $\Delta C_{p,mic}$. A typical experiment encompassed

DOI: 10.1021/acs.analchem.9b04281
Anal. Chem. 2020, 92, 1154−1161

one injection of 0.5 μL followed by 20 injections of 1.9 μL each. The spacing between injections was set to at least 150 s, and in the experiments with PEG, a longer interinjection time (up to 300 s) was used to allow the heat exchange from one injection to return completely to baseline levels before the start of the next injection. In the experiment with OG, which has a high CMC, up to 25 mM of the detergent was included in the cell before the beginning of the titration; furthermore, because of the very high heat of demicellization of this detergent, the syringe contents were injected much more slowly (e.g., an injection velocity of 0.026 μL/s instead of the typical 0.5 μL/s). The enthalpy of detergent demicellization in this study varied significantly depending on the detergent and the experimental temperature, and thus the reference power for each experiment was set accordingly to keep the differential power within the dynamic range of the instrument, i.e., 0 to +52.3 μJ/s (+12.5 μcal/s in the instrument's units).

Data Analysis. Data were loaded into NITPIC[19,20] and integrated using that software's "[Injectant]" mode; that is, the data were plotted as a function of injectant concentration in the cell rather than as a function of molar ratio. The data were outputted using NITIPC's "Save Everything" function. Our new software, D/STAIN, is designed to read one of the files outputted in this process, specifically, a file with a ".nitpkl" extension. This is a compact binary file containing all of the information about the integrated heats and their respective estimated errors. The equation used to fit the heat data $q(j)$ is based on the logistic function, a generic sigmoid-generating equation. This approach is quasi-phenomenological, as no attempts to ascribe a physical meaning to the properties of the line segments on either side of the sigmoid's inflection point are made, yet the physical parameters CMC, the enthalpy change upon micellization ΔH_{mic}, and a parameter related to the cooperativity of micellization, Δc_D, can be estimated:[16]

$$q(c_j) = \frac{[(m_1 - m_2)(c_j - \mathrm{CMC})] - [\Delta H_{mic}(c_{syr} - \mathrm{CMC})/c_{syr}]}{1 + e^{(c_j - \mathrm{CMC})/\Delta c_D}} + [m_2(c_j - c_{ref})] + b_2 \quad (1)$$

where c_j is the average concentration of the detergent in the sample cell during injection j, m_1 is the slope of the preinflection-point heats, m_2 is the slope of the post-inflection-point heats, b_2 is the y-intercept of the post-inflection-point heats at c_{ref} is a reference concentration of detergent, and c_{syr} is the concentration of detergent in the syringe. The quality of the fits resulting from eq 1 is dependent on the assumptions that the preinflection-point and post-inflection-point portions of the curve can be approximated by straight lines. D/STAIN allows data that do not conform to these assumptions to be excluded to arrive at realistic parameter estimates.[16] Equation 1 differs from that presented earlier,[16] in that a new term, c_{ref}, has been introduced. We have found that this term, when chosen judiciously, relieves some parameter correlations inherent in the equation (not shown). This term is set by D/STAIN to be the average of the last five calculated concentrations of the demicellization curve. The approach detailed in eq 1 is hereinafter termed the quasi-phenomenological sigmoid algorithm (QPSA). Once the NITPIC-integrated data were loaded into D/STAIN, preliminary estimates of the fitted parameters (usually CMC, ΔH_{mic}, m_1, m_2, b_2, and Δc_D) were made by the program. These estimates were accomplished as described previously,[16] except as detailed in the following. The CMC was estimated using the extremum of the first derivative of the demicellization curve with respect to concentration, $q'(c_j)$. Δc_D was estimated using an iterative procedure that examined the changes in $q'(c_j)$. Starting at the maximum, a walk in the positive c direction was executed until the respective $q'(c_j)$ was 75% of the maximum; at this point, the search was halted, and the c value designated as c_+. The same procedure was conducted in the negative direction, resulting in the determination of c_-. Finally, the estimated Δc_D was calculated as $\Delta c_{D,\,est} = | c_+ - c_- | /2$. Notably, the intercept of the preinflection-point line at c_{ref}, called b_1, is not a fitted parameter. Rather, it can be calculated from the others:

$$b_1 = [(m_2 - m_1)(\mathrm{CMC} - c_{ref})] + b_2 - \left[\left(\frac{\Delta H_{mic}}{c_{syr}}\right)(c_{syr} - \mathrm{CMC})\right] \quad (2)$$

Where necessary, eq 2 was used to calculate b_1, and confidence-interval estimates for this parameter were propagated from those of the fitted parameters.

For nonlinear least-squares fitting, the Nelder–Mead Simplex (NMS)[21] and Levenberg–Marquardt (LM)[22] algorithms were automatically alternated until convergence was reached (defined as the refined parameter set in which the results from NMS and LM differed by no greater than 0.1% in any refined parameter value). Rigorous confidence-interval estimation was accomplished using the one-dimensional error-surface projection (ESP) methodology described elsewhere.[23] For the two-dimensional ESPs used to visualize parameter correlations, a similar procedure was undertaken over a grid area that spanned ca. 3 times the extent of parameter space that was scanned in the respective one-dimensional search. Any parameter pairs that resulted in values of χ^2 that were greater than 5 times the value of the critical χ^2 were represented in the two-dimensional contour plots by white space (see Supplemental Methods in Supporting Information). Bootstrap calculations for confidence-interval estimates were conducted using 10 000 iterations. For each iteration, data from the best-fit line were taken as starting points, and noise was added by sampling (with replacement) from the table of residuals between the best-fit line and the observed data.[24] These new data were fitted by alternating between the NMS and LM optimization algorithms as described above using the same convergence criterion, and the resulting parameter values were recorded into sets. To investigate correlations of parameters x and y, a two-dimensional histogram of the resulting parameter sets $\{x\}$ and $\{y\}$ could be plotted (see below). Additionally, Pearson's correlation coefficient (r) was determined from these data.[25] We found that the contour plot produced by the two-dimensional ESP could be statistically sampled and an analogous value, which we called the ESP correlation coefficient (r_{ESP}), could be computed (see Supplemental Methods), yielding values that were quantitatively similar to r. Calculations of the thermodynamic parameters for the standard Gibbs free-energy change of micellization (ΔG^0_{mic}), the standard entropy change of micellization (ΔS^0_{mic}), the mole-fraction CMC (CMC′), and the mole-fraction equilibrium constant (K'_{mic}) were performed as previously outlined.[7,12] The confidence intervals on these parameters were calculated by propagation of the confidence limits of the refined parameters ΔH_{mic} and CMC. In the case of ΔS^0_{mic}, limits of both ΔH_{mic} and ΔG^0_{mic} were propagated.

DOI: 10.1021/acs.analchem.9b04281
Anal. Chem. 2020, 92, 1154−1161

Table 1. Thermodynamic Parameters of Micellization at 20 °C

parameter	detergent		
	OG	DDM	LDAO
CMC (mM)	25.1 [24.5, 25.6]	0.147 [0.137, 0.154]	1.89 [1.86, 1.91]
ΔH_{mic} (kJ/mol)	9.3 [7.3, 12.5]	3.8 [3.0, 5.1]	8.6 [8.0, 9.3]
$-T\Delta S^0_{mic}$ (kJ/mol)	−28 [−31, −26]	−35.1 [−36.6, −34.2]	−33.7 [−34.4, −33.0]
ΔG^0_{mic} (kJ/mol)	−18.77 [−18.83, −18.72]	−31.30 [−31.46, −31.18]	−25.07 [−25.11, −25.04]
CMC′ ($\times 10^{-5}$)[a]	45.2 [44.2, 46.2]	0.265 [0.247, 0.278]	3.41 [3.36, 3.45]
K' ($\times 10^3$ M^{-1})[b]	2.21 [2.16, 2.26]	378 [360, 404]	29.4 [29.0, 29.8]

[a]CMC′ is the critical micellar concentration on a mole-fraction basis. [b]K' is the water-to-micelle partition coefficient on a mole-fraction basis.

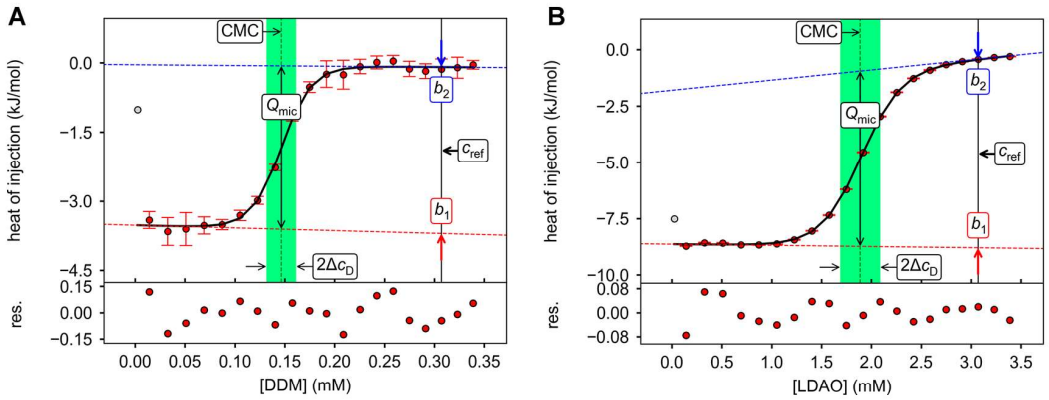

Figure 2. Demicellization isotherms for DDM and LDAO. (A) Demicellization curve for DDM. Heats of injection are shown as circles, with error bars from NITPIC[19] also shown. The black line is the fit to the data. The arrangement of the panels is the same as in Figure 1B. (B) Demicellization curve for LDAO. D/STAIN is capable of passing data to GUSSI for an alternative rendering of these data.[26]

RESULTS

Performance of the Analytical Methods. To examine the performance of the QPSA and the related confidence-interval searches, we analyzed data collected from the demicellization of three detergents: LDAO, OG, and DDM. The first detergent features a zwitterionic (or "1,2-dipolar") headgroup, whereas the other two are neutral, containing carbohydrate head groups. We conducted all of our studies in PBS at 20 °C rather than in water, with the goal of rendering the results relevant to researchers studying buffered solutions of proteins or other macromolecules.

We first used D/STAIN to analyze a demicellization curve obtained from OG (Figure 1). The analysis yielded a positive ΔH_{mic} of 9.3 [7.3, 12.5] kJ/mol and a CMC of 25.1 [24.5, 25.6] mM (we present 95% confidence intervals in brackets in this work). The remainder of the parameters are tabulated in Table 1. These values agree reasonably with previous results obtained under somewhat different buffer conditions.[12,27] D/STAIN offers the user a "Graphical Parameter View", which intuitively maps CMC, ΔH_{mic}, m_1, b_1, m_2, b_2, and Δc_D into demicellization-curve space (Figure 1B). This view is valuable as a secondary check on the veracity of the optimized parameters. The parameter b_1 was not fitted in the analysis; rather, it was calculated by inserting the refined parameters into eq 2

Next, we studied the micellization properties of DDM in PBS (Figure 2A). We obtained a CMC of 147 [137, 154] μM and a ΔH_{mic} of 3.8 [3.0, 5.1] kJ/mol. The CMC value compares well with literature values, while the magnitude of ΔH_{mic} is larger than an earlier value determined at lower ionic strength.[7]

Most of the experiments in this paper were conducted on the zwitterionic detergent LDAO (Figure 2B). We found that the detergent has a high ΔH_{mic} at 20 °C (8.6 [8.0, 9.3] kJ/mol) and a CMC between those of the other two detergents studied (1.89 [1.86, 1.91] mM) (Table 1). Again, the CMC agrees with earlier reported values, while ΔH_{mic} differs by about 4 kJ/mol from an earlier report conducted in a different buffer.[14]

Parameter Correlations. The data-to-parameter ratio for fitting demicellization data using eq 1 is usually only about 5:1 using a constant-volume calorimeter; even in very favorable cases, it approaches only about 10:1. These low data-to-parameter ratios, coupled with the unknown relationships of the physical parameters (e.g., ΔH_{mic}) with the unphysical ones (e.g., m_1), raised the prospect that the fitted parameters could be correlated with one another. In other words, changes in the value of one parameter can be compensated by changing the values of others with little penalty in the goodness of the fit. An insightful way to examine this possibility is to perform repeated fits of the data while fixing pairs of the two parameters in question at nonoptimal values and scrutinizing plots of χ^2 as a function of the value pairs.[28,29] For N parameters, there are $N!/2!(N-2)!$ pairwise possibilities, or 15 in our case ($N = 6$). All of these plots can be visualized using D/STAIN, and an example is shown in Figure 3 for LDAO; all 15 plots from this fitting session are assembled in Figure S1. If the two subject parameters are uncorrelated, such plots should not have any diagonal character; that is, they should appear as circles or untilted ovals in such plots. Conversely, correlations are revealed by strong diagonal features.

The physical parameters of most interest in the present case are CMC and ΔH_{mic}. We used the visualization tools present in D/STAIN to examine the correlations of these parameters for

DOI: 10.1021/acs.analchem.9b04281
Anal. Chem. 2020, 92, 1154−1161

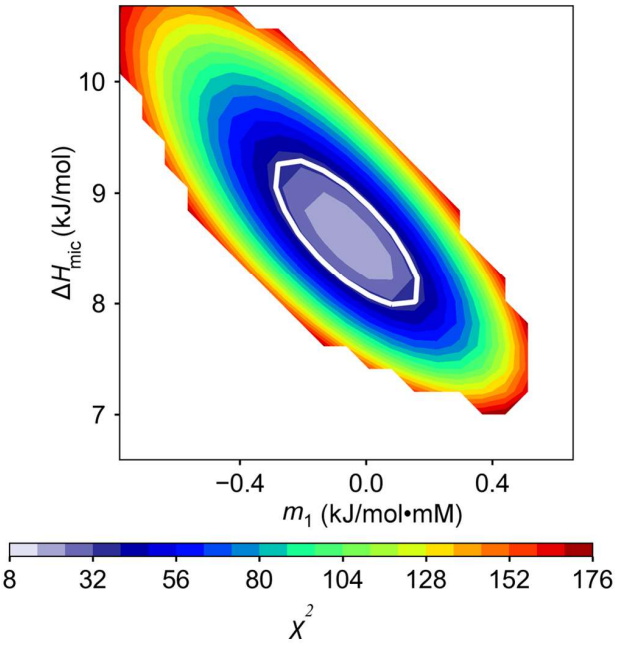

Figure 3. An example of parameter correlations for the QPSA. A two-dimensional contour plot is shown for the refined parameters ΔH_{mic} and m_1 of LDAO (Figure 2B). The dimension shown by the colors (see key at bottom) is the χ^2 value for the parameter pair. The white line depicts the 95% confidence level of χ^2.[28] White space in the contour plots represents areas where the χ^2 was greater than 5 times the 95% confidence level. The r_{ESP} for this plot is −0.747.

the micellization of LDAO (Figure 3, Figure S1). The CMC showed a weak correlation with m_2, but it was essentially uncorrelated with ΔH_{mic} and Δc_D. ΔH_{mic}, on the other hand, was strongly correlated with Δc_D and the phenomenological parameters m_1 and m_2.

Another means of discovering these correlations is through the bootstrap resampling method (or the related Monte Carlo resampling method) of determining confidence intervals[24] (see Experimental Section). By organizing the results of the resampling method into two-dimensional histograms, correlations can be easily discerned (Figure S2). From this treatment, it is straightforward to calculate Pearson's correlation coefficient (r) (Table 2). The trends observed with the

Table 2. Pearson's Correlation Coefficients between Refined Parameters for LDAO

	ΔH_{mic}	m_1	m_2	b_2	Δc_D
CMC	0.232	0.360	−0.582	0.073	0.136
ΔH_{mic}		−0.758	−0.870	0.284	0.880
m_1			0.389	−0.223	−0.679
m_2				−0.030	−0.710
b_2					0.378

error-surface projection are recapitulated in these resampled results. We found that it is also possible to represent the features of the two-dimensional error-surface projections as a correlation coefficient, r_{ESP} (see Supplemental Methods, Figure S3, and Table S1). For example, the r_{ESP} value for the plot in Figure 3 is −0.747, compared to the r value for that pair of −0.758 (Table 2).

Addressing the Accuracy of ΔH_{mic}. The physical parameter showing the strongest, most consistent correlations in the above analysis is ΔH_{mic}. This fact may raise some concern regarding the accuracy of fitting ΔH_{mic} using the QPSA as embodied in eq 1. To examine whether this potential problem had the capability of resulting in inaccurate or inconsistent values of ΔH_{mic}, we chose to perform a series of LDAO demicellization experiments at different temperatures and to globally fit the resulting CMC and ΔH_{mic} values using a van't Hoff approach.[30] Specifically, $\Delta H_{mic}(T)$ values were fitted in a custom Python script using a linear temperature dependence of the form

$$\Delta H_{mic}(T) = \Delta C_{p,mic}(T - T_0) \tag{3}$$

while CMC(T) values were simultaneously fitted using the following expression:

$$\mathrm{CMC}(T) = \mathrm{CMC}(T_0)\exp\left(\frac{\Delta C_{p,mic}}{R}\left(1 - \frac{T_0}{T} + \ln\frac{T_0}{T}\right)\right) \tag{4}$$

where T_0 is the temperature at which $\Delta H_{mic}(T_0) = 0$ and at which the CMC assumes its minimum value, CMC(T_0). eqs 3 and 4 thus imply that the $\Delta H_{mic}(T)$ and CMC(T) data may be fitted with the adjustable parameters $\Delta C_{p,mic}$, T_0, and CMC(T_0). Reassuringly, these data across the entire temperature range studied could be globally fitted to yield $\Delta C_{p,mic}$ = −375 [−389, − 361] J/(mol·K), CMC(T_0) = 1.7 [1.4, 1.9] mM, and T_0 = 314.0 [313.8, 314.2] K or 40.9 °C (Figure 4). Importantly, $\Delta C_{p,mic}$ was found to be negative, as expected for a process dominated by the hydrophobic effect, and similar in magnitude to the decrease in heat capacity observed for other detergents of the same hydrocarbon chain length.[30]

Micellization in the Presence of Polyethylene Glycol. To our knowledge, no systematic calorimetric studies of detergent micellization have been undertaken in the presence of the commonly used crowding and precipitating agent polyethylene glycol (PEG). Previous studies of ethoxy-type detergents in glycerol[15] have shown that the presence of this widely adopted kosmotrope also causes an increase in the CMC. It seemed likely that the detergents in this study would follow this pattern, and thus we systematically varied the concentration of PEG3350 and studied its effects on the micellization of OG, DDM, and LDAO at 20 °C.

OG was the first detergent that was subjected to this treatment (Figure S4). The PEG mass concentrations studied were 5%, 10%, and 15%. Because of the high CMC of OG, we included a low starting concentration of the detergent in the sample cell (see Experimental Section). The presence of PEG systematically and significantly increased the CMC of OG (Figure 5A). The trend appeared close to linear between 0% and 10% PEG3350 but demonstrated a sharp increase at 15%. In this last isotherm, the CMC was the most uncertain, as the curve was only weakly sigmoid (Figure S5). Additionally, we attempted a titration in 20% PEG3350, but the resulting data were uninterpretable (Figure S6), evincing high, nonsaturating heats of injection. It is possible that the PEG lowered the cloud point of OG such that a phase separation caused by interactions between the micelles occurred, and thus the heats measured were those of breakage of micelle/micelle interactions. Although the effects of PEG on the CMC of OG were readily evident, more profound effects were observed on the parameter ΔH_{mic} (Figure 5B), which decreased from 9.3

DOI: 10.1021/acs.analchem.9b04281
Anal. Chem. 2020, 92, 1154−1161

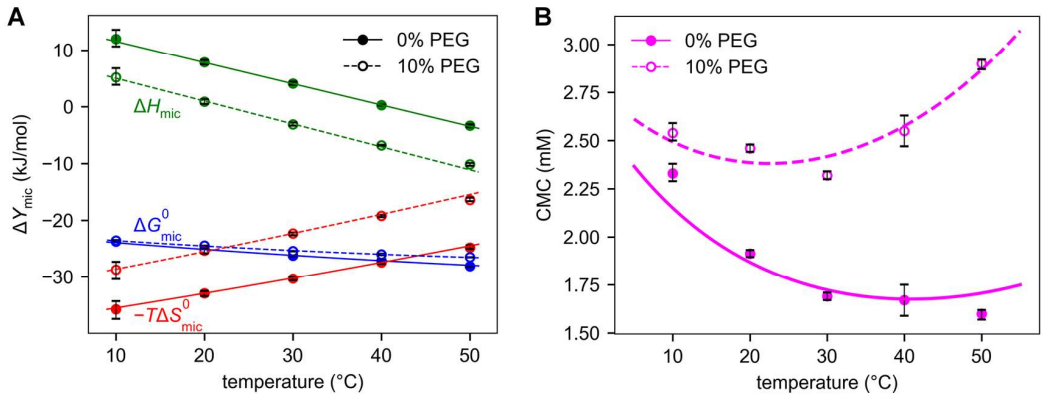

Figure 4. Temperature-dependent thermodynamic values for LDAO micellization. (A) Effects of temperature on molar changes in thermodynamic quantities (ΔY_{mic}). Colors depict different thermodynamic quantities as identified in the figure. (B) CMC changes with temperature. In both parts, all data points are associated with their respective 95% confidence intervals (error bars), solid lines show values obtained with no PEG, and dashed lines show those obtained with 10% PEG. All lines in both parts are the results of global van't Hoff fits based on eqs 3 and 4 .

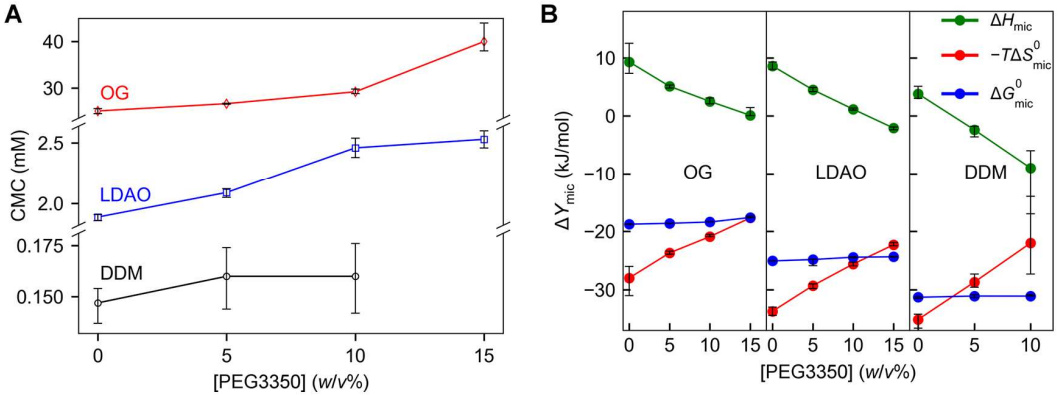

Figure 5. Effects of PEG3350 on demicellization. (A) CMC as a function of PEG3350 concentration. The widely differing CMC values necessitate breaking the *y*-axis to show details; text colors identify the detergents in the plot. (B) Changes in thermodynamic quantities (ΔY_{mic}) for three detergents as functions of PEG3350 concentration. Colors, markers, and detergent identities are given in the figure. Lines are shown as visual aids and do not represent the results of fits to the data.

[7.3, 12.5] kJ/mol with no PEG present to 0.1 [0.03, 1.43] kJ/mol when 15% PEG3350 was included. This trend was countered by an increase in the magnitude of $-T\Delta S^0_{mic}$, in an apparent case of enthalpy−entropy compensation (Figure 5B).

We next tested the consequences of PEG inclusion on the micellization behavior of DDM (Figure 5 and Figure S7). In this case, the effect of the polymer on CMC was not as stark. As in the case of OG, the general trend was toward higher CMCs in the presence of PEG3350. However, no discernible difference was observed between the CMCs of DDM in the presence of 5% or 10% of the polymer (Figure 5A). Experiments designed to explore the trend at higher PEG3350 concentrations could not be completed because DDM precipitated under these conditions. Still, PEG3350 again had a strong and significant influence on ΔH_{mic}. The trend in ΔH_{mic} as a function of PEG concentrations was negative and approximately linear over this narrow range (Figure 5B). As with OG, the diminishing ΔH_{mic} was compensated by a rising magnitude of $-T\Delta S^0_{mic}$. Unlike OG, however, the ΔH_{mic} changed from being endothermic with 0% PEG3350 present to exothermic at both tested concentrations of the polymer.

The last detergent examined was LDAO. The CMC of LDAO exhibited a significant upward trend as a function of the PEG3350 concentration (Figure 5A and Figure S8): with 15% PEG present, it was 33% higher than without any of the polymer in solution. Again, there was a substantial, negative, linear trend in the ΔH_{mic} of LDAO as PEG3350 was added. As with DDM, there was a transition (this time between 10% and 15% PEG3350) from endothermic to exothermic ΔH_{mic} (Figure 5B). Provocatively, the observed CMC did not change substantially in this PEG concentration range, whereas the linearity of the ΔH_{mic} trend was unperturbed.

Heat Capacity Change of LDAO in the Presence of PEG. As a first step to explore the ramifications of PEG inclusion on micelle formation, we undertook a series of experiments to examine the $\Delta C_{p,mic}$ value of LDAO with 10% PEG3350 included in solution. To arrive at this value, we again varied the experimental temperature from 10 to 50 °C, evaluated the resulting data with D/STAIN, and undertook the global van't Hoff fitting strategy embodied in eqs 3 and 4 (Figure 4). Although the observed ΔH_{mic} values were consistently more negative with PEG present than without (Figure 4A), we observed only a small change in $\Delta C_{p,mic}$, as the value was −400 [−430, − 380] J/(mol·K) in the presence of the polymer. The values of CMC(T_0) and T_0 from the fit were 2.4 [1.8, 3.0] mM and 295.6 [295.1, 296.2] K (22.5 °C), respectively. Thus, with PEG3350 present, the CMC of LDAO

DOI: 10.1021/acs.analchem.9b04281
Anal. Chem. 2020, 92, 1154−1161

assumes a minimum value at a lower temperature (Figure 4B), but this CMC is significantly higher than that observed with no PEG in solution.

DISCUSSION

In this report, we have introduced and tested the software "D/STAIN" as a new, user-friendly implementation of a quasi-phenomenological approach to determining the thermodynamic parameters of detergent micellization using ITC. We tested its ability to characterize the thermodynamics of micellization in the buffer PBS for three widely employed detergents (Figures 1 and 2; Table 1). In all cases, the algorithms underpinning the software quickly determined the demicellization parameters (CMC, ΔH_{mic}, Δc_D, m_1, m_2, and b_2; see eq 1) and automatically provided rigorous confidence-interval estimates for them (Table 1, Figures 4 and 5).

An area of concern for any fitting algorithm is parameter correlation. This is because inaccuracies in one parameter can be compensated by adjustments in the correlated parameter. D/STAIN has on-demand tools to aid the user in detecting these correlations (Figure 3, Figures S1 and S2, Table 2, Table S1). We examined these correlations in the QPSA for the micellization of LDAO and found that ΔH_{mic} was the physical parameter most likely to be compromised by them. Nevertheless, we observed that ΔH_{mic} varied linearly with changes in temperature (Figure 4), as expected for a system with no coupled equilibria across a reasonably narrow temperature range. This observation implies that ΔH_{mic} is robustly and accurately determined by the QPSA algorithm despite evident parameter correlations. Previously, it has been suggested that the parameter Δc_D be constrained to 15% of the CMC.[31] While this approach may yield acceptable results under some circumstances, universal application of such a constraint would likely compromise the accuracy of refinement of physical parameters. In D/STAIN, there is the option to fix the adjustable parameters individually, if desired.

We also characterized the effect that PEG3350 has on the micellization of the three detergents targeted in this study. For DDM, the effect on the CMC was not substantial, whereas for OG and LDAO, the respective CMCs were significantly higher in the presence of PEG (Figure 5A). Moreover, PEG had the consistent effect of lowering the ΔH_{mic} values of all detergents studied herein (Figure 5B). The means by which the polymer disfavored the formation of the micelle are not immediately obvious and are likely to be complex and multifaceted. A study including calorimetry and other methods on the effects of glycerol on micellization of the ethoxylated detergent octaethylene glycol dodecyl ether and on OG[15] concluded that glycerol had complex effects on micellization that could not easily be classified by, for example, its status as a kosmotrope. In that study, glycerol, like PEG3350 in our case, was found to slightly increase the CMC but drastically alter ΔH_{mic}.[15] Other researchers have studied the effects of PEG on OG/octyl-POE mixed micelles,[32] but that research was mainly concerned with examining the effects of the polymer on the cloud point of the detergent mixture, a parameter thought to be relevant for membrane protein crystallization.

Our observations hold important implications for membrane protein research. For example, in a typical vapor-diffusion[33] crystallization experiment with PEG as the precipitant, the concentration of PEG starts relatively low and increases over time. According to our results (Figure 5), such an increase could potentially raise the CMC enough to cause disruption of micelles and thus aggregation or precipitation of the protein. Therefore, the best chance of success in such experiments is brought about by including the detergent at relatively high concentrations, typically 2−3 times above the CMC.

Finally, we point out that the calculations of several thermodynamic quantities presented herein (e.g., K') are predicated on the assumption that the aggregation number of the detergent is high, typically greater than ten.[12] If the aggregation number is substantially lower, this assumption breaks down. In such cases, there is the intriguing possibility of fitting the calorimetric demicellization curve using a stoichiometric model rather than the pseudophase approximation used here, which is applicable only in the case of high aggregation numbers.[12] Future work will focus on whether the current experimental and computational framework can be expanded to support such detailed modeling.

CONCLUSIONS

This study introduced software (D/STAIN; available at http://biophysics.swmed.edu/MBR/software.html) that extends the capabilities of a quasi-phenomenological sigmoid algorithm (QPSA) for the fitting of detergent demicellization isotherms obtained using isothermal titration calorimetry (ITC). The program offered automated, adaptive, and rigorous confidence-interval determination, on-demand tools for the detection of parameter correlations, optional use of injection-heat error estimates to weight the fitting, advanced result reporting, and a simple interface to graphing software. The fact that the algorithm facilitated the analysis of experiments spanning a wide range of ΔH_{mic} values and CMC values demonstrated its robustness. Experiments conducted at different temperatures were also accommodated, as shown by the tabulation of parameters from the QPSA and subsequent global fitting to determine $\Delta C_{p,mic}$ values. The finding that the presence of PEG shifts the CMC to higher values provided a rational basis for membrane protein researchers to employ detergent concentrations well above the CMC.

ASSOCIATED CONTENT

Supporting Information

The Supporting Information is available free of charge at https://pubs.acs.org/doi/10.1021/acs.analchem.9b04281.

Supplemental methods, Figures S1−S8, and Table S1 (PDF)

AUTHOR INFORMATION

Corresponding Author

*E-mail: chad.brautigam@utsouthwestern.edu.

ORCID

Sandro Keller: 0000-0001-5469-8772

Chad A. Brautigam: 0000-0001-6563-1338

Author Contributions

The manuscript was written through contributions of all authors. S.-C.T., F.M., J.H., and C.A.B. designed and performed experiments. F.M., J.H., S.K., and C.A.B. analyzed data. S.K. and C.A.B. wrote algorithms.

Notes

The authors declare no competing financial interest.

DOI: 10.1021/acs.analchem.9b04281
Anal. Chem. 2020, 92, 1154−1161

■ ACKNOWLEDGMENTS

The authors thank Drs. Joel Tellinghuisen (Vanderbilt University) and Anthony Mittermaier (McGill University) for helpful comments on the QPSA. S.K. acknowledges funding from the Deutsche Forschungsgemeinschaft (DFG) through grant KE 1478/7-1.

■ REFERENCES

(1) *Membrane Protein Purification and Crystallization*, 2nd ed.; Hunte, C., von Jagow, G., Schagger, H., Eds.; Academic Press: San Diego, CA, 2003.
(2) Garavito, R. M.; Ferguson-Miller, S. *J. Biol. Chem.* **2001**, *276*, 32403−32406.
(3) Le Bon, C.; Marconnet, A.; Masscheleyn, S.; Popot, J. L.; Zoonens, M. *Methods* **2018**, *147*, 95−105.
(4) Simon, K. S.; Pollock, N. L.; Lee, S. C. *Biochem. Soc. Trans.* **2018**, *46*, 1495−1504.
(5) Dorwart, M. R.; Wray, R.; Brautigam, C. A.; Jiang, Y.; Blount, P. S. *PLoS Biol.* **2010**, *8*, No. e1000555.
(6) Wennerström, H.; Lindman, B. *Phys. Rep.* **1979**, *52*, 1−86.
(7) Broecker, J.; Keller, S. *Langmuir* **2013**, *29*, 8502−8510.
(8) Natalini, B.; Sardella, R.; Gioiello, A.; Ianni, F.; Di Michele, A.; Marinozzi, M. *J. Pharm. Biomed. Anal.* **2014**, *87*, 62−81.
(9) Mukerjee, P.; Mysels, K. J. *Critical Micelle Concentrations of Aqueous Surfactant Systems*; National Bureau of Standards (U.S.): Washington, DC, 1971.
(10) Olofsson, G.; Loh, W. *J. Braz. Chem. Soc.* **2009**, *20*, 577−593.
(11) Loh, W.; Brinatti, C.; Tam, K. C. *Biochim. Biophys. Acta, Gen. Subj.* **2016**, *1860*, 999−1016.
(12) Paula, S.; Süs, W.; Tuchtenhagen, J.; Blume, A. *J. Phys. Chem.* **1995**, *99*, 11742−11751.
(13) Blokzijl, W.; Engberts, J. B. F. N. *Angew. Chem., Int. Ed. Engl.* **1993**, *32*, 1545−1579.
(14) Broecker, J.; Fiedler, S.; Gimpl, K.; Keller, S. *J. Am. Chem. Soc.* **2014**, *136*, 13761−13768.
(15) Patel, H.; Raval, G.; Nazari, M.; Heerklotz, H. *Biophys. Chem.* **2010**, *150*, 119−128.
(16) Textor, M.; Keller, S. *Anal. Biochem.* **2015**, *485*, 119−121.
(17) Tsamaloukas, A. D.; Beck, A.; Heerklotz, H. *Langmuir* **2009**, *25*, 4393−4401.
(18) Heerklotz, H.; Tsamaloukas, A. D.; Keller, S. *Nat. Protoc.* **2009**, *4*, 686−697.
(19) Keller, S.; Vargas, C.; Zhao, H.; Piszczek, G.; Brautigam, C. A.; Schuck, P. *Anal. Chem.* **2012**, *84* (11), 5066−5073.
(20) Brautigam, C. A.; Zhao, H.; Vargas, C.; Keller, S.; Schuck, P. *Nat. Protoc.* **2016**, *11*, 882−894.
(21) Nelder, J.; Mead, R. *Comput. J.* **1965**, *7*, 308−313.
(22) Marquardt, D. W. *J. Soc. Ind. Appl. Math.* **1963**, *11*, 431−441.
(23) Scheuermann, T. H.; Padrick, S. B.; Gardner, K. H.; Brautigam, C. A. *Anal. Biochem.* **2016**, *496*, 79−83.
(24) Johnson, M. L. *Methods Cell Biol.* **2008**, *84*, 781−805.
(25) Taylor, J. R. *An Introduction to Error Analysis: The Study of Uncertainties in Physical Measurements*; Oxford University Press: Mill Valley, CA, 1982.
(26) Brautigam, C. A. *Methods Enzymol.* **2015**, *562*, 109−134.
(27) Majhi, P. R.; Blume, A. *Langmuir* **2001**, *17*, 3844−3851.
(28) Bevington, P. R.; Robinson, D. K. *Data Reduction and Error Analysis for the Physical Sciences*, 2nd ed.; WCB/McGraw-Hill: Boston, MA, 1992.
(29) Zhao, H.; Piszczek, G.; Schuck, P. *Methods* **2015**, *76*, 137−148.
(30) Keller, S.; Heerklotz, H.; Jahnke, N.; Blume, A. *Biophys. J.* **2006**, *90*, 4509−4521.
(31) Shimizu, S.; Pires, P. A. R.; Loh, W.; El Seoud, O. A. *Colloid Polym. Sci.* **2004**, *282*, 1026−1032.
(32) Hitscherich, C. J.; Aseyev, V.; Wiencek, J.; Loll, P. J. *Acta Crystallogr., Sect. D: Biol. Crystallogr.* **2001**, *57*, 1020−1029.
(33) McPherson, A. *Crystallization of Biological Macromolecules*; Cold Spring Harbor Laboratory Press: New York, 1999.

DOI: 10.1021/acs.analchem.9b04281
Anal. Chem. 2020, 92, 1154−1161

SUPPORTING INFORMATION

Fast and robust quantification of detergent micellization thermo-dynamics from isothermal titration calorimetry

Shih-Chia Tso†, Florian Mahler‡, Jonas Höring‡, Sandro Keller‡, and Chad A. Brautigam*†,‖

Departments of Biophysics† and Microbiology‖, UT Southwestern Medical Center, 5323 Harry Hines Boulevard, Dallas, TX 75390, USA

Molecular Biophysics‡, Technische Universität Kaiserslautern (TUK), Erwin-Schrödinger-Str. 13, 67663 Kaiserslautern, Germany

Contents

Supplemental Methods

Calculation of error-surface projections

One-dimensional error-surface projections (ESPs) were performed automatically by D/STAIN [1]. In brief, a critical χ^2 value, χ_c^2, was calculated; if χ^2 values from subsequent fits exceeded χ_c^2, they were deemed to be statistically different from the best fit. To perform the error-surface projection (ESP) for two parameters simultaneously, a 21 x 21 grid was established covering in both dimensions approximately three times the parameter space that was explored in the respective one-dimensional searches. Then, at each grid point, the respective pair of parameter values was fixed at the search values, and all other fitted parameters were allowed to refine, alternating the Nelder–Mead Simplex and Levenberg–Marquardt algorithms until convergence was achieved. The χ^2 of the fit was recorded for the grid point if it was less than $5\chi_c^2$; if greater than this value, the grid point was given a value of "not a number," which, when rendered in the contour plot, would appear white (*see* main text, Fig. 3 and Fig. S1). These steps were repeated for all grid points, resulting in the final contour plot. The process is fully automated in D/STAIN.

When the correlation is strong, we observed that it could cause steep gradients in the observed χ^2 values. These gradients cause artifactual features and poor sampling in the resulting contour plot. Thus, the algorithm detects these gradients and increases the resolution of the grid automatically. The maximum grid size allowed was 81 x 81.

Computation of a correlation coefficient from the two-dimensional ESP

A correlation coefficient, r_{ESP}, was calculated from the results of the two-dimensional ESP search. To accomplish this, a point with the ordinal i in the previously established parameter space of the

ESP search was randomly chosen (points were not restricted to grid points). Through two-dimensional interpolation, the point was assigned its respective χ^2 value (χ_i^2). The probability of accepting this point was calculated as

$$P_i = 1 - C\left\{\chi_i^2, \nu\right\}, \tag{0.1}$$

where ν is the degrees of freedom and the function C is the cumulative distribution function of the χ^2 distribution given χ_i^2 and ν. If accepted, the point was added to the set of points that were used for the calculation of the correlation coefficient. If not accepted, it was discarded. This process was iterated until 1,000 accepted points were accumulated, at which point the simulation was terminated and the pseudo-Pearson correlation coefficient, r_{ESP}, was computed using the standard equation[2]. If the grid resolution had been increased because of steep gradients (see above), the threshold number of accepted points was lowered; the minimum allowed number of points was 10.

Supplemental Figures

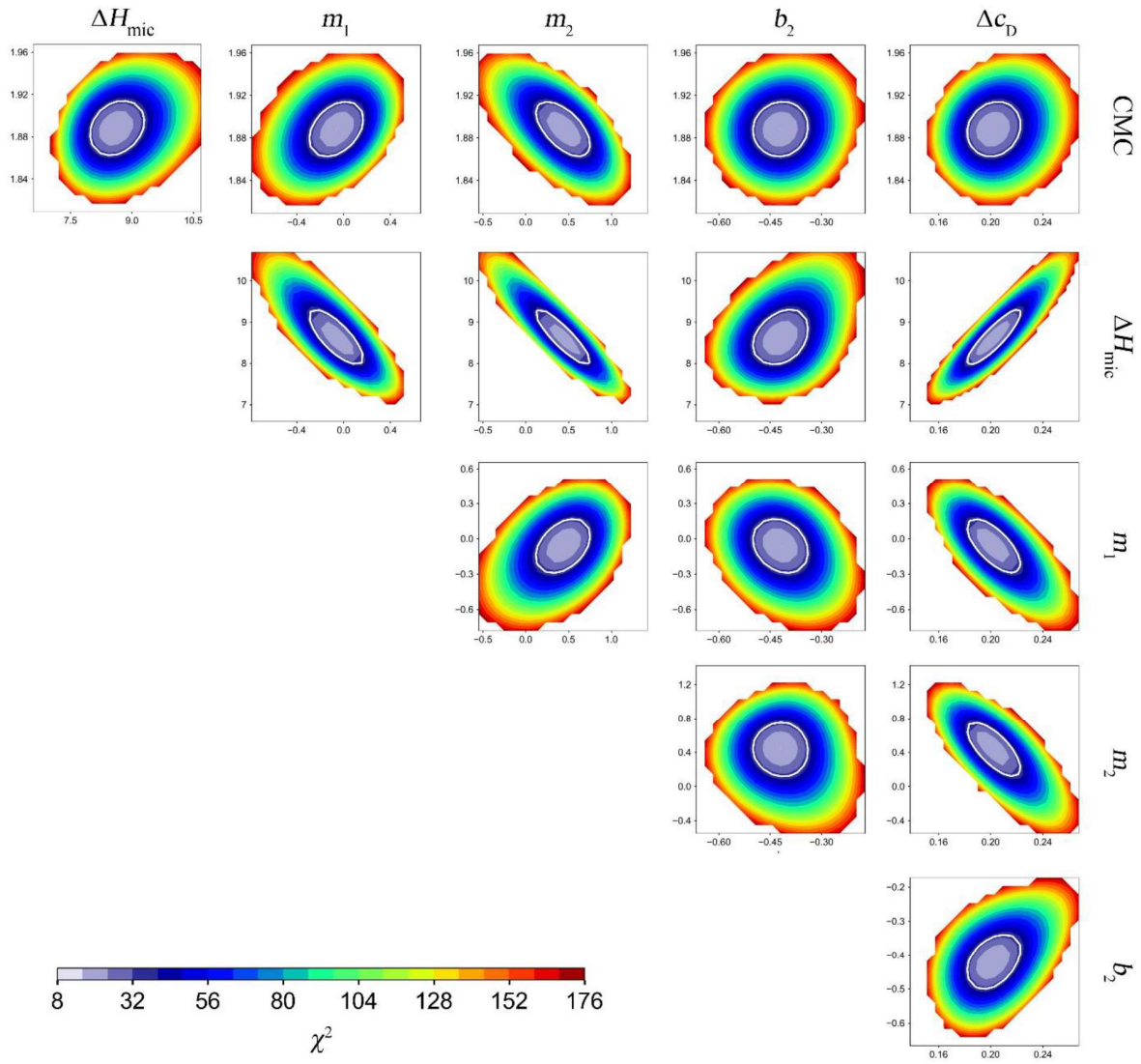

Figure S1.
Two-dimensional error-surface projections for all refined parameters derived from the LDAO demicellization curve at 20 °C. Conventions established in Fig. 3 of the main text are followed here.

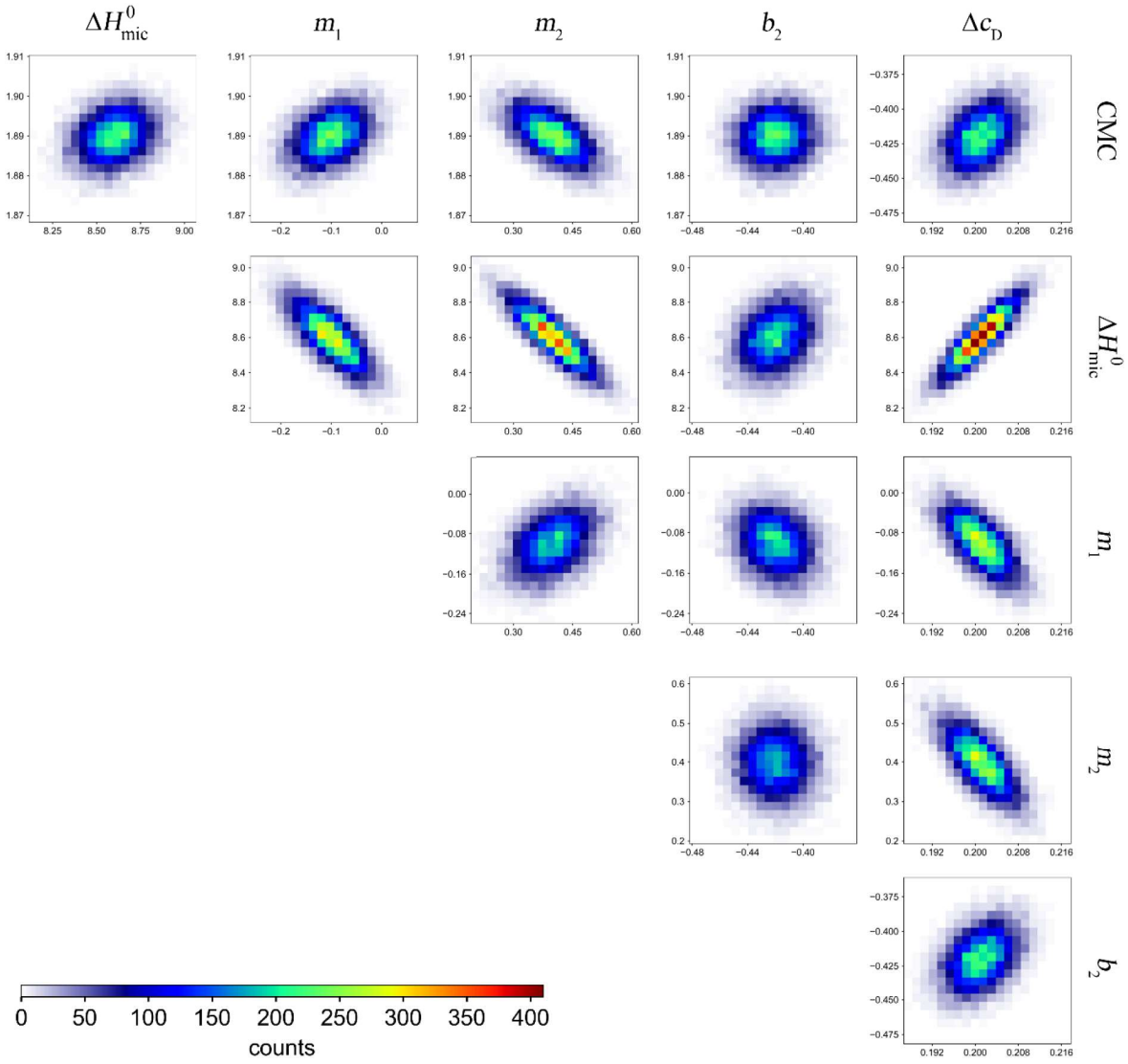

Figure S2.
Two-dimensional histograms for all refined parameters for LDAO. Parameter identities are at the top and right sides of the plot. Colors represent counts in the histograms according to the color legend at the lower left. Pearson correlation coefficients for these plots are presented in Table 2 of the main text.

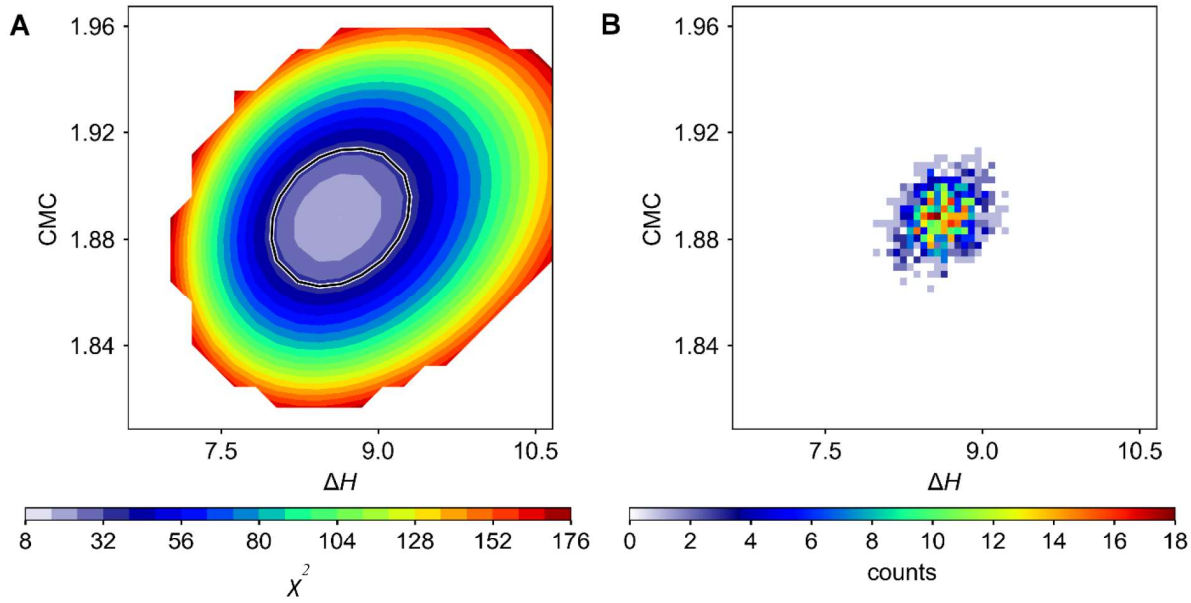

Figure S3

Illustration of the r_{ESP} correlation. (A) The regular ESP two-dimensional contour plot for the parameters CMC and ΔH_{mic}. See the upper-left graph of Fig. 3 in the main text. (B) The randomly sampled ESP plot. The plot in part (A) was used as a probability distribution that was randomly sampled until 1,000 accepted points were produced. The r_{ESP} was calculated from these points using the standard equation for Pearson's correlation coefficient[2]; it was 0.283 (see Table S1).

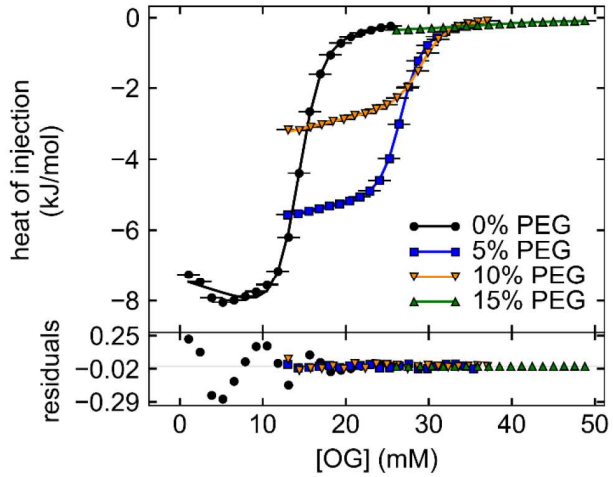

Figure S4
The effect of PEG3350 on the micellization properties of OG. Markers and colors are as depicted in the inset legend.

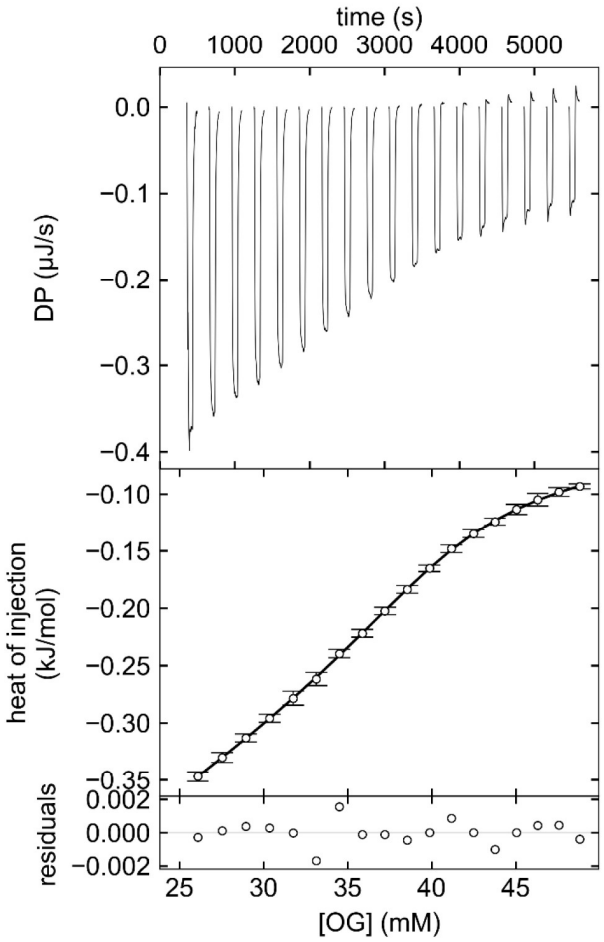

Figure S5
The thermogram/demicellization isotherm pair for OG at 15% (*w*/*v*) PEG3350.

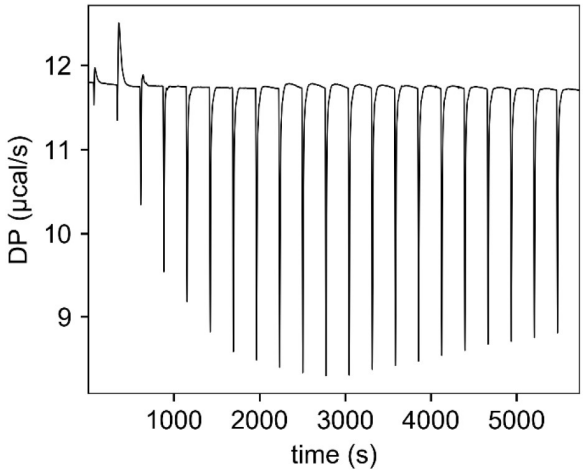

Figure S6
Non-saturating heats of OG demicellization in the presence of 20% (*w/v*) PEG3350. There were 20 mM of detergent in the calorimetric cell and 180 mM in the syringe.

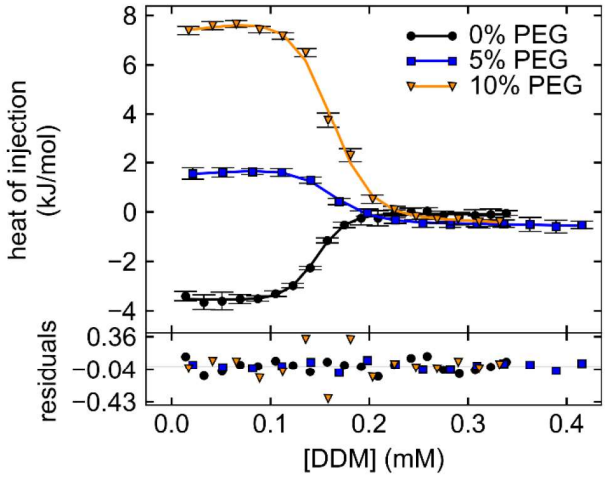

Figure S7
The effect of including PEG3350 on the micellization properties of DDM.

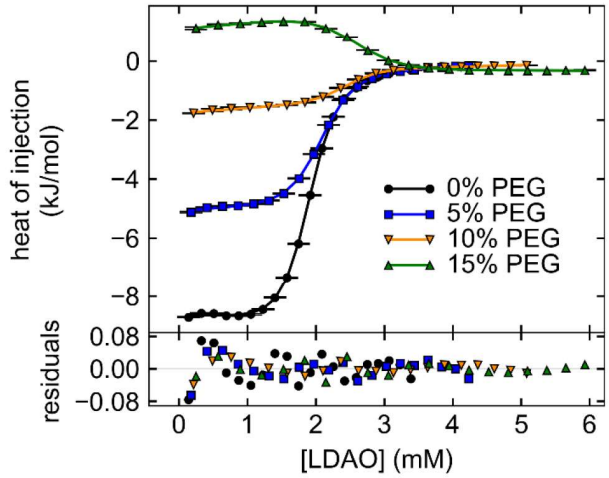

Figure S8
The effect of including PEG3350 on the micellization properties of LDAO.

Table S1
The r_{ESP} values between refined parameters for LDAO.

	ΔH_{mic}	m_1	m_2	b_2	Δc_D
CMC	0.256	0.357	−0.617	0.057	0.147
ΔH_{mic}		−0.747	−0.865	0.250	0.902
m_1			0.423	−0.231	−0.679
m_2				−0.041	−0.728
b_2					0.386

References

(1) Scheuermann, T. H.; Padrick, S. B.; Gardner, K. H.; Brautigam, C. A. On the Acquisition and Analysis of Microscale Thermophoresis Data. *Anal. Biochem.* **2016**, *496*, 79–83.

(2) Taylor, J. R. *An Introduction to Error Analysis: The Study of Uncertainties in Physical Measurements*; Oxford University Press: Mill Valley, CA, 1982.

Chapter 3: Investigation of Novel Small-Molecule Glyco-Amphiphiles

3.1. Synopsis (Manuscript 2)

Manuscript 2 introduces novel diastereomeric maltoside amphiphiles with a cyclopentane (CP) core group termed cyclopentane-based maltosides (CPMs). Two hydrophilic maltose groups and two hydrophobic alkyl chains are attached to the CP core group. The CPM series is derived from norbonane-based maltosides (NBMs) by breakage of one single bond in the norbonane core (cf., Figure 1 in *Manuscript 2*). Thus, the branched hydrophilic group has an **increased conformational flexibility** leading to (i) increased solubility and (ii) adaption of different conformations of the CP core depending on the stereochemical configuration of the alkyl chains (*cis*/*trans*, CPM-*C*/*T*).

The increased solubility allowed the preparation of CPMs with either C11 or C12 alkyl chains, contrary to the maximum of C11 for NBMs. As shown by dynamic light scattering (DLS), CPM-*T*s formed considerably smaller micelles compared with their NBM parent molecule. By contrast, the *cis* configuration (CPM-*C*s) led only to a minor difference in micelle size. All CPMs showed CMCs between 4 µM and 7 µM, comparable to the NBM parent molecules.

Furthermore, the CPMs were evaluated regarding MP solubilization and long-term stabilization using various model MPs including the bacterial leucine transporter (LeuT), the melibiose permease ($MelB_{St}$), the human β_2 adrenergic receptor (β_2AR), and mouse μ-opioid receptor (MOR). In short, CPM-*C*12 turned out to be the most **promising MP-stabilizing agent** in this study. It outperformed the gold standard DDM on all tested MPs and, moreover, outperformed established amphiphiles of similar structures such as NBMs and the GPCR-optimized LMNG. Although, the efficacy in particular cases depended on the alkyl chain length and the investigated MP, overall, the ***cis* configuration was favorable** compared to the *trans* configuration for CPMs. This can be related to the different conformations of the CP core. The half-chair conformation of CPM-*C*s led to an uneven effective chain length between the two hydrophobic chains, which possibly improves adaption to the also uneven hydrophobic MP surface.

Because of the above-mentioned promising results, CPM-*C*12 was further investigated. In addition to the MP stabilization assays, it was used to extract and purify the bacterial voltage-dependent potassium ion channel KvAP. Furthermore,

to gain a better insight into the solubilization efficiency of CPM-*C*12, it was tested on a broad range of MPs by shotgun MP-extraction from *E. coli* membranes. Additionally, the two comparison detergents *X*-NBM-C11 and DDM, as well as the *trans* isomer CPM-*T*12 were tested. CPM-*C*12 outperformed all three amphiphiles. This emphasizes, on the one hand, the wide application of CPM-*C*12 and, on the other hand, the superior properties regarding MP extraction by *cis* isomers compared with *trans* isomers.

Moreover, the micellar properties and vesicle solubilization by CPM-*C*12 were investigated. Multi-detection size-exclusion chromatography revealed homogeneous micelles and an aggregation number between 60 and 85. When applied to artificial POPC vesicles, CPM-*C*12 solubilized them faster compared with *X*-NBM-C11 and formed considerably smaller micelles as shown by DLS. This smaller size is preferable for most biophysical techniques.

In conclusion, the results presented in this manuscript showed that, in addition to the overall structure of branched small-molecule glyco-amphiphiles, the **stereochemical configuration has a strong effect** on both the micellar properties as well as on the solubilizing properties.

3.2. Manuscript 2

Diastereomeric Cyclopentane-Based Maltosides (CPMs) as Tools for Membrane Protein Study

Manabendra Das, Florian Mahler, Parameswaran Hariharan, Haoqing Wang, Yang Du, Jonas S. Mortensen, Eugenio Pérez Patallo, Lubna Ghani, David Glück, Ho Jin Lee, Bernadette Byrne, Claus J. Loland, Lan Guan, Brian K. Kobilka, Sandro Keller, and Pil Seok Chae

Journal of the American Chemical Society, **2020**, 142, 51, 21382–21392

Contribution

For this work, I designed and performed size-exclusion chromatography (Fig. 4a–b), artificial vesicle solubilization (Fig. 4c-d and Fig. S10), and *E. coli* membrane-protein extraction experiments (Fig. 5). I also analyzed and interpreted the corresponding data. For the original draft, I wrote the corresponding sections of the manuscript.

JACS
JOURNAL OF THE AMERICAN CHEMICAL SOCIETY
pubs.acs.org/JACS
Article

Diastereomeric Cyclopentane-Based Maltosides (CPMs) as Tools for Membrane Protein Study

Manabendra Das, Florian Mahler, Parameswaran Hariharan, Haoqing Wang, Yang Du, Jonas S. Mortensen, Eugenio Pérez Patallo, Lubna Ghani, David Glück, Ho Jin Lee, Bernadette Byrne, Claus J. Loland, Lan Guan, Brian K. Kobilka, Sandro Keller, and Pil Seok Chae*

Cite This: J. Am. Chem. Soc. 2020, 142, 21382−21392

ABSTRACT: Amphiphilic agents, called detergents, are invaluable tools for studying membrane proteins. However, membrane proteins encapsulated by conventional head-to-tail detergents tend to denature or aggregate, necessitating the development of structurally distinct molecules with improved efficacy. Here, a novel class of diastereomeric detergents with a cyclopentane core unit, designated cyclopentane-based maltosides (CPMs), were prepared and evaluated for their ability to solubilize and stabilize several model membrane proteins. A couple of CPMs displayed enhanced behavior compared with the benchmark conventional detergent, *n*-dodecyl-*β*-D-maltoside (DDM), for all the tested membrane proteins including two G-protein-coupled receptors (GPCRs). Furthermore, CPM-C12 was notable for its ability to confer enhanced membrane protein stability compared with the previously developed conformationally rigid NBMs [*J. Am. Chem. Soc.* **2017**, *139*, 3072] and LMNG. The effect of the individual CPMs on protein stability varied depending on both the detergent configuration (*cis*/*trans*) and alkyl chain length, allowing us draw conclusions on the detergent structure−property−efficacy relationship. Thus, this study not only provides novel detergent tools useful for membrane protein research but also reports on structural features of the detergents critical for detergent efficacy in stabilizing membrane proteins.

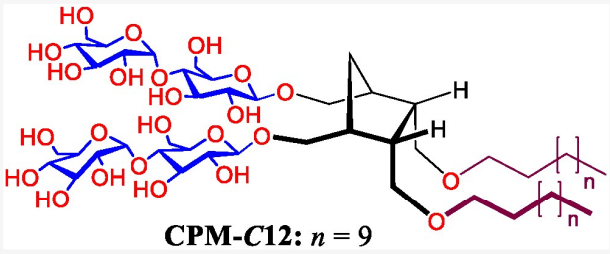

INTRODUCTION

Integral membrane proteins are essential for cell functions such as inter- or intracellular material transfer, signal transduction, photosynthetic electron transport, protein trafficking, and cell adhesion and comprise more than 50% of human drug targets.[1] Structural and functional information about membrane proteins is essential for a fundamental understanding of their mechanism of action as well as for rational design of new drug molecules. Unfortunately, these biomacromolecules represent only ∼2−3% of 3D-resolved protein structures,[2] even with the recent advances in cryo-electron microscopy and the substantial successes achieved with X-ray crystallography.[3] Membrane protein extraction, purification, and structural investigation are often challenging mainly because of the low natural abundance of these molecules and their tendency to denature or aggregate once extracted from native membranes into aqueous buffer. A key prerequisite for isolation and structural studies of membrane proteins is that they must be maintained in a soluble and stable state in buffer solution by an amphiphilic additive that shields the large hydrophobic protein surfaces from polar aqueous environments. Conventional detergents with a polar head and a hydrophobic tail group such as *n*-dodecyl-*β*-D-maltoside (DDM), *n*-octyl-*β*-D-glucoside (OG), and lauryldimethylamine-*N*-oxide (LDAO) are widely used to extract membrane proteins from native lipid bilayers and to maintain the native states of the proteins in solution.[4,5] However, in addition to being more dynamic than lipid assemblies, detergent micelles tend to expose hydrophobic regions of membrane proteins to buffer solution,[6,7] resulting in irreversible nonspecific aggregation. Thus, it is of great importance to develop novel agents or membrane-mimetic systems displaying favorable behaviors for membrane protein solubilization and stabilization.[8] Notable examples of several large membrane-mimetic systems are bicelles,[9] nanodiscs (NDs),[10] amphiphilic polymers [styrene−maleic acid (SMA)[11a] and diisobutylene−maleic acid (DIBMA)[11b] co-polymers, amphipols (APols)],[12] and peptide detergents [*β*-peptides (BPs),[13] lipopeptide detergents (LPDs),[14a] Salipro,[14b] and peptidiscs[14c]]. These agents have been shown to maintain several membrane proteins in native-like conformations but were often found to be inefficient at protein extraction and

Received: September 8, 2020
Published: December 14, 2020

https://dx.doi.org/10.1021/jacs.0c09629
J. Am. Chem. Soc. 2020, 142, 21382−21392

tend to form large protein−detergent complexes (PDCs). More importantly, with few exceptions (*e.g.*, SMA),[11a] they are yet to produce protein crystals with high quality. As an alternative strategy, several small amphiphilic agents have been developed as exemplified by neopentyl glycol (NG)-based amphiphiles (MNGs/GNGs),[15] mannitol-based amphiphiles (MNAs),[16] tripod amphiphiles (TPAs),[17] calix[4]arene-based amphiphiles (C4Cs),[18] tandem malonate-based glucosides (TMGs),[19] pentasaccharide amphiphiles (PSEs),[20] butane−tetraol-based maltosides (BTMs),[21] glycosyl-substituted dicarboxylate detergents (DCODs),[22] dendronic group-containing trimaltosides (DTMs),[23] and 1,3,5-triazine-cored maltosides (TEMs).[24] GNG-3 and MNG-3 have contributed to the determination of more than 40 membrane protein crystal structures including a sodium-pumping pyrophosphatase, human aquaporin 2 (AQP2), and acetylcholine and opioid G-protein-coupled receptors (GPCRs) in the past 10 years.[25] Departing from the canonical "polar head and nonpolar tail" design of conventional detergents, facial amphiphiles (FAs) represent a highly innovative approach for studying membrane proteins, and some of these amphiphiles (*e.g.*, FA-5 and FA-7) were utilized for 3D crystal structure determinations of the ATP-binding cassette transporter (MsbA) and the GPCR-like bacteriorhodopsin.[26] Recently, we developed norbornane (NB)-based maltosides (NBMs)[27] with two flexible alkyl arms and two maltoside head groups connected by a conformationally locked norbornane linker. Of these agents, X-NBM-C11 showed remarkable stabilization behavior with several model membrane proteins including human β_2 adrenergic receptor (β_2AR). Despite the favorable effects on protein stability, this NBM tends to form larger micelles (hydrodynamic radius (R_h) = 17.3 nm), which is potentially unfavorable for protein crystallization and NMR-based structural studies. In addition, the rigid NB linker used to build the NBMs could be associated with suboptimal detergent efficacy for protein stabilization. Herein, we made efforts to address these issues by converting the linker from the rigid NB (NBMs) to a more flexible cyclopentane (CP) unit (CPMs) (Figure 1). This monocyclic linker provides conformational flexibility relative to the bicyclic NB linker, which can result in enhanced detergent efficacy for protein stabilization. When the new detergents were evaluated, we found that CPM-*C*12 was significantly better than DDM and X-NBM-C11 at stabilizing several model membrane proteins including two GPCRs.

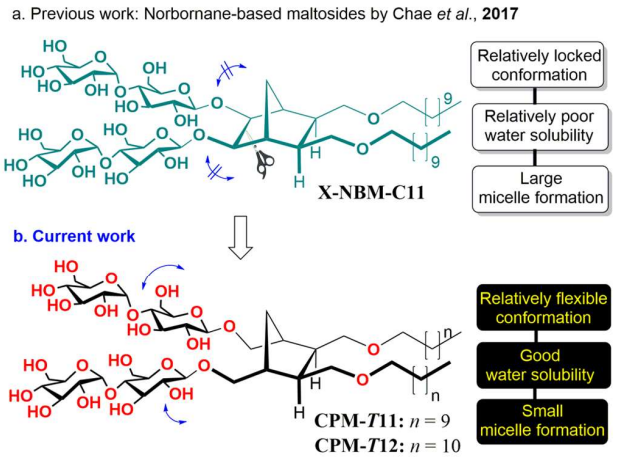

Figure 1. Background for this study. The chemical structures of (a) previously reported X-NBM-C11 detergent with conformationally restricted maltoside head groups and (b) new cyclopentane-based maltoside-*trans* detergents (CPM-*T*s) with the more conformationally flexible head groups. The CPM-*T*s were created by disconnecting a C−C bond from the norbornane scaffold. The blue arrows show the relative conformational flexibility of the head groups. Unlike X-NBM-C11, these new detergents gave increased water solubility and formed smaller micelles.

RESULTS

Detergent Structures and Physical Characterizations. The CPMs feature two alkyl chains and two dimaltosides as the hydrophobic and hydrophilic groups, respectively, connected via a monocyclic CP ring (Figure 2). Depending on the relative orientation of the alkyl chains with respect to the head groups (*cis*/*trans*), these agents can be categorized into two sets. The two alkyl chains were connected to the C2 and C3 positions of the CP linker in a *cis* configuration (2*R*,3*S*) with respect to the head groups for CPM-*C*s while a *trans* configuration was used for this connection of the alkyl chains in the case of CPM-*T*s (Figure 2). As a result, the CPM-*C*s and CPM-*T*s are CP variants of D-NBMs and X-NBMs, respectively; D (*endo*) and X (*exo*) notations were previously used to represent the relative orientation of the NBM tail groups with respect to their head groups.[27] Because of the torsional and angle strains of the central CP ring, the CPM-*C*s and CPM-*T*s are likely to preferentially adopt energy-minimized puckered conformations, half-chair ($\mathbf{C_2}$) and envelope ($\mathbf{C_s}$), respectively (Figure 2 and Figure S1). This is in contrast with the conformationally locked NB linker in the NBMs. The configuration (*cis*/*trans*) and conformational variations (half-chair ($\mathbf{C_2}$)/envelope ($\mathbf{C_s}$)) between the CPM-*C*s and CPM-*T*s could affect amphiphile efficacy for membrane protein stabilization in spite of their identical chemical compositions (*i.e.*, identical polar and nonpolar segments). As the hydrophile−lipophile balance (HLB) is important in determining detergent property,[28] we prepared detergent variants with two alkyl chain lengths (C11 and C12) for both sets of CPMs, used for detergent designation. Density functional theory (DFT) calculations at a B3LYP/6-31G* level supported a half-chair/twist conformation of the CP ring for CPM-C11 with a hydrophobic length of 15.2 Å, while its *trans* isomer (CPM-*T*11) was calculated to give an envelope conformation of the CP ring, with the hydrophobic length of 15.1 Å (Figure S1). Thus, the two different conformations (half-chair ($\mathbf{C_2}$)/envelope ($\mathbf{C_s}$)) along with alkyl chain length variations (C11/C12) serve as a way to change or fine-tune the detergent hydrophobic length. This is important as detergent hydrophobic length needs to be compatible with the hydrophobic dimensions of membrane proteins for optimal protein stability in solution.

The individual hydrophobic groups of the CPM-*C*s/*T*s are optically inactive *meso* compounds due to the presence of an internal symmetry plane dissecting the CP linker (compounds **B** and **D** in Figure 2). Because these *meso*-1,5-diols (**B** and **D**) are nonsuperimposable stereoisomers, they are diastereomers to each other. The CPM-*C*s/*T*s are also diastereomers of each other but are optically active because of the lack of an internal symmetry plane. The new agents were prepared according to a protocol comprising five high-yielding synthetic steps: (1) dialkylation, (2) alkene *syn*-dihydroxylation using osmium tetroxide−*N*-methylmorpholine *N*-oxide (OsO_4−NMO) (*i.e.*, 1,2-diol derivatives **A** and **C**), (3) periodate-mediated oxidative cleavage of 1,2-diol, followed by *in situ* $NaBH_4$ reduction of

https://dx.doi.org/10.1021/jacs.0c09629
J. Am. Chem. Soc. 2020, 142, 21382−21392

Journal of the American Chemical Society pubs.acs.org/JACS Article

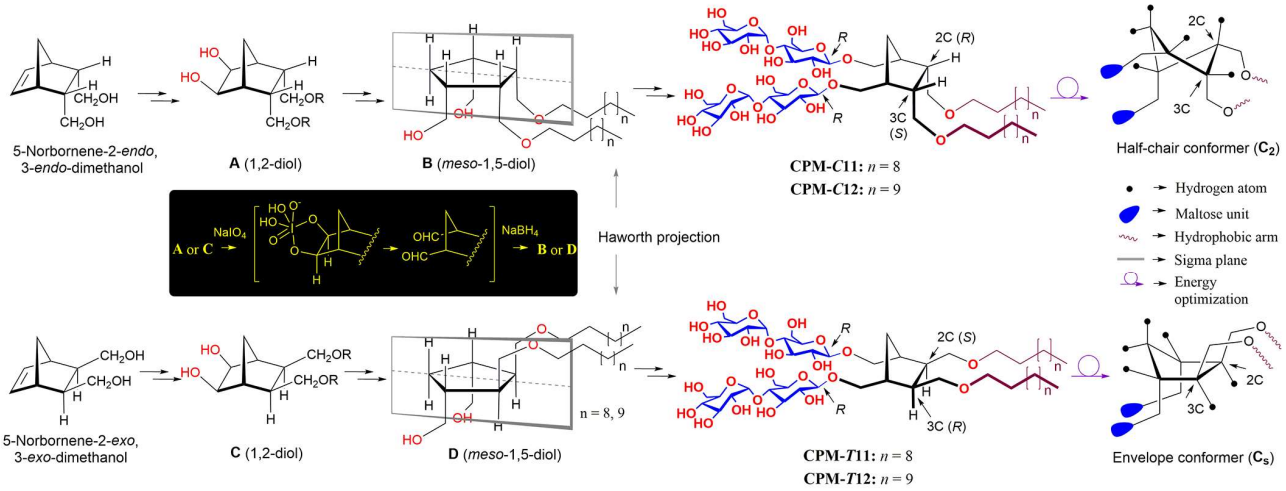

Figure 2. (a) Chemical structures of novel cyclopentane-based maltosides (CPMs) (middle right) and their energy-optimized puckered conformers (far right). The CPM-*C*s were derived from 5-norbornene-2-*endo*,3-*endo*-dimethanol, while CPM-*T*s were derived from isomeric 2-*exo*,3-*exo*-dimethanol (far left). *Syn*-dihydroxylation using OsO_4–NMO was used for 1,2-diol generation (**A**/**C**, left). The inset within the rectangle represents periodate-mediated oxidative cleavage of 1,2-diols (**A** and **C**), followed by $NaBH_4$ reduction to afford *meso*-1,5-diol derivatives (**B** and **D**). **B** and **D** are *meso* compounds due to the presence of a symmetry plane which perpendicularly bisects the central cyclopentane (CP) ring of the molecule (indicated by the gray line in the Haworth projection). The CPM-C/*T*s commonly contain a dimaltoside head group connected to the two alkyl chains using a cyclopentane linker (middle right). *R* or *S* designation was used to specify the stereochemistry of the two chiral carbons (C2 and C3). Half-chair (C_2) and envelope (C_s) are two energy-minimized CP conformations of CPM-Cs and CPM-*T*s, respectively, optimized by DFT calculations at the energy level of B3LYP/6-31G*) (far right).

dialdehyde (**B** and **D**; inset in Figure 2), (4) AgOTf-promoted glycosylation, and (5) global deprotection (see amphiphile synthesis in the Supporting Information for details). Glycosylation could generate two stereochemical outcomes depending on the approaching direction of a glycosyl acceptor toward a glycosyl donor, resulting in either an α- or a β-glycosidic bond. Consequently, the final products containing two newly formed glycosidic bonds could be a mixture of multiple diastereomers. We solved this stereochemistry issue by utilizing β-selective glycosylation attained via neighboring group participation.[29] The high diastereomeric purity of the CPMs was confirmed by the ^{1}H NMR spectroscopic method (Figures S2 and S3). For example, the axial protons of CPM-C11 attached to the anomeric carbons, designated H_a, produce two narrowly separated peaks at 4.25 and 4.24 ppm as doublets (Figure 3b and Figure S2). By contrast, the same axial protons of the *trans* isomer (*i.e.*, CPM-*T*11) gave two nonseparable doublets, located at 4.26 ppm (Figure 3c and Figure S2). In addition, these anomeric protons (H_a) of both isomers interact with their neighboring protons (H) with a vicinal coupling constant ($^3J_{aa}$) of 8.0 Hz, revealing that β-selective glycosylation had occurred. We also observed another doublet peak at 5.16 ppm with a relatively small coupling constant ($^3J_{ae}$ = 4.0 Hz), which corresponds to the α-anomeric protons (H_e) in the terminal glucose units of these detergents (Figure 3 and Figure S2). Few additional peaks were detected in the α- or β-anomeric region (4.3–5.2 ppm), indicative of high diastereomeric purity of the CPMs. The only detectable peaks in this region were the doublets at 4.48 and 5.09 ppm, which correspond to the anomeric protons of maltose (Figure S4). This disaccharide impurity in our detergent samples originates from the hydrolyzed product of perbenzoylated maltosyl bromide used in glycosylation. Based on the NMR spectra of the CPMs (Figures S2 and S3), the amounts of this impurity varied from ~1 (CPM-*T*12) to ~5% (CPM-C11), but the

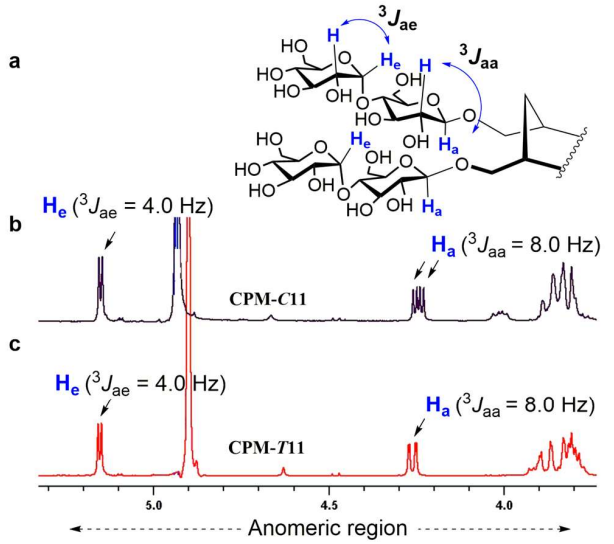

Figure 3. (a) Chemical structure of the dimaltoside head group of the CPMs is shown to illustrate the anomeric protons of interest (H_e and H_a) and their vicinal couplings with the neighboring protons (H in blue). (b, c) Anomeric regions of the ^{1}H NMR spectra for CPM-C11 (b) and CPM-*T*11 (c) showing their high diastereomeric purity (see Figure S2 for the full range of ^{1}H NMR spectra). Each isomer gave unique spectral features in the anomeric region, indicative of the clear differentiation of the individual isomers by their ^{1}H NMR spectra. Vicinal coupling constants ($^3J_{aa}$ and $^3J_{ae}$) are indicated above individual peaks to differentiate the α- and β-anomeric protons (H_e and H_a, respectively).

detergent efficacy for protein stabilization is unlikely to be affected by the presence of this highly hydrophilic compound. Because of the high efficiency of each synthetic step, the final amphiphiles could be prepared with overall yields of ~75%,

https://dx.doi.org/10.1021/jacs.0c09629
J. Am. Chem. Soc. 2020, 142, 21382−21392

Table 1. Molecular Weights (MWs), Critical Micelle Concentrations (CMCs; n = 3), Water Solubility of the Novel Agents (CPM-Cs and CPM-Ts) and Control Detergents (DDM and X/D-NBM-C11), and Hydrodynamic Radii (R_h; n = 4) of Their Micelles in Double-Distilled Water at Room Temperature

detergent	MW[a] (Da)	CMC (μM)	R_h (nm)[b]	solubility (wt %)
CPM-C11	1147.4	6.7 ± 0.3	3.8 ± 0.1	~10
CPM-C12	1175.5	5.0 ± 0.1	4.0 ± 0.1	~10[c]
CPM-T11	1147.4	4.8 ± 0.1	4.8 ± 0.1	~10
CPM-T12	1175.5	3.8 ± 0.5	5.5 ± 0.1	~10[c]
X-NBM-C11	1145.4	6	17.3 ± 0.2	~5[c]
D-NBM-C11	1145.4	7	3.7 ± 0.1	~5
DDM	510.6	170	3.4 ± 0.1	>10

[a]Molecular weight of detergents. [b]Hydrodynamic radius of detergent micelles measured at 1.0 wt % detergent concentration by dynamic light scattering. [c]Sonication required to obtain a clear solution.

making preparation of multigram quantities of material at a reasonable cost highly feasible.

High water solubility (10 wt %) was a feature of all four new detergents, yet as for a long alkyl-chain detergent (i.e., CPM-C12/T12) a brief sonication was required for an initial dissolution (Table 1). Detergent solutions remained clear during a month of incubation at room temperature. Critical micelle concentrations (CMCs) were measured by monitoring dye solubilization using diphenylhexatriene[30] with increasing detergent concentration, and the hydrodynamic radii (R_h) of the detergent micelles were estimated through dynamic light scattering (DLS) measurements. The summarized results for the CPMs along with D/X-NBM-C11 and DDM are presented in Table 1. The CMC values of all CPMs (from 3.8 to 6.7 μM) were more or less comparable to those of D/X-NBM-C11 but much smaller than that of DDM (170 μM), which indicates stronger tendencies to form self-assemblies than DDM (Figure S5). Within the same set of detergents (*e.g.*, the CPM-Cs), the CMC values decreased with increasing alkyl chain length because of the increased hydrophobicity. For instance, the CMCs of the CPM-Cs reduced from 6.7 to 5.0 μM when the alkyl chain length increased from C11 to C12. Micelles formed by the individual sets of detergents were enlarged along with increasing alkyl chain length. The detergent micelle size increased from 4.8 (C11) to 5.5 nm (C12) for the *trans* isomers. The detergent micelle size is determined by the geometry of the detergent molecule, estimated by the volume ratio of detergent head and tail groups.[31] It is interesting to note that the micelle size of the *trans* isomers significantly decreased with change from the NB to CP linker. For instance, the R_h value of CPM-T11 micelles was 4.8 nm, smaller than X-NBM-C11 (17.3 nm). Even the C12 alkyl chain CPM (CPM-T12) formed smaller micelles than X-NBM-C11 with the shorter alkyl chain (5.5 *vs* 17.3 nm). This comparison reveals that the geometry of the detergent molecules substantially changes from a cylindrical to a conical shape for the *trans* isomers with the linker modification. This change in detergent geometry likely originates from increased flexibility of the two maltoside head groups, resulting in an increased hydrophilic volume with little effect on the hydrophobic volume (Figure 1). Interestingly, a different trend was observed for the *cis* isomers. CPM-C11/C12 was comparable to the D-NBM-C11 with respect to micelle size (3.8/4.0 vs 3.7 nm).

The variation in the conformation of the CP linker (half-chair (C_2) or envelope (C_s)) is likely associated with the different behaviors of the CPM-Cs and CPM-Ts in self-assembly formation (Figure S1). The DFT calculations show substantial variation in the linker conformation (NB *vs* CP) between D-NBM-C11 and CPM-C11 but show little variation in the linker conformation between CPM-T11 and X-NBM-C11. The CPM-Cs formed smaller micelles than the *trans* isomers (*i.e.*, the CPM-Ts), as exemplified by CPM-C11 (3.8 nm) vs CPM-T11 (4.8 nm). Our results indicate that a small change in detergent architecture (*i.e.*, just eliminating a single C−C bond) can result in a large variation in self-assembly, which could also affect detergent efficacy for membrane protein stabilization. When we investigated the size distribution of detergent micelles, all new agents showed only one set of micellar populations in number- or volume-weighted DLS profiles, indicative of high homogeneity (Figures S6 and S7). The appearance of a peak corresponding to large aggregates in the intensity-weighted DLS profiles results from the high sensitivity of light scattering to large particles.[27]

The detergent micelle size was further investigated with increasing temperature from 15 to 65 °C (Figure S9). DDM

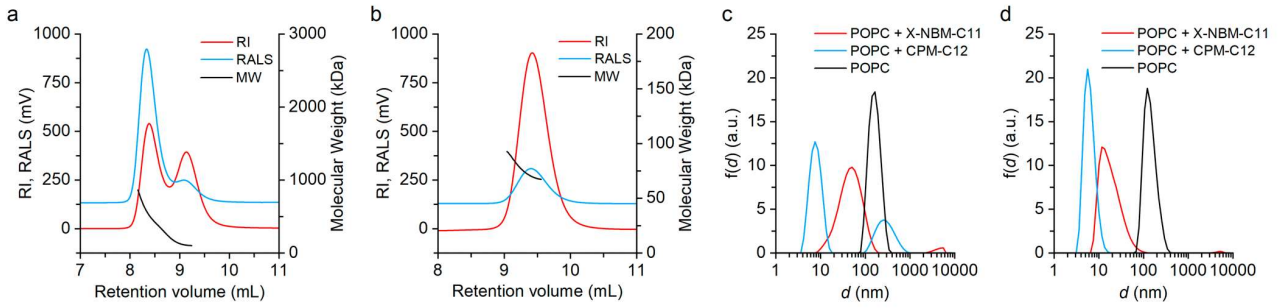

Figure 4. (a, b) SEC elution profiles and (c, d) particle size distributions from DLS for X-NBM-C11 and CPM-C12. (a) RI and RALS signals (left axis) of X-NBM-C11 showed a bimodal distribution corresponding to micellar molecular weights ranging from 860 to 210 kDa across the first peak and from 210 to 100 kDa across the second one, as indicated by the black line (right axis). (b) RI and RALS signals (left axis) of CPM-C12 showed a unimodal distribution giving molecular weights ranging from 70 to 100 kDa, as indicated by the black line (right axis). The black lines indicate peak widths correlated to homogeneity of detergent self-assemblies. (c) Intensity- or (d) volume-weighted particle size distribution profiles derived from DLS for mixtures of either X-NBM-C11 or CPM-C12 with POPC show a major population of small micelles. Profiles of POPC vesicles only were included for comparison. DLS: dynamic light scattering; SEC: size exclusion chromatography; RI: refractive index; RALS: right-angle light scattering.

https://dx.doi.org/10.1021/jacs.0c09629
J. Am. Chem. Soc. 2020, 142, 21382−21392

gave little change in micelle size over this range of temperature variation. Consistent with the previous result,[27] the size of the D-NBM-C11 micelles was not affected by temperature, while micelles formed by X-NBM-C11 were substantially enlarged with increasing solution temperature. A similar trend was observed for the CPM analogues (CPM-*C*11 and CPM-*T*11), indicating that micelles formed by the *endo*/*cis* isomer are significantly more stable than the *exo*/*trans* isomer under the conditions tested. There was little difference in micelle sizes formed by CPM-C11 and D-NBM-C11, while micelles formed by CPM-*T*11 were substantially smaller than those formed by X-NBM-C11 over the temperature range tested. As the best protein stabilization efficiency was obtained from CPM-C12 (*vide infra*), we performed in-depth physical characterizations for this agent along with X-NBM-C11 as a reference. X-NBM-C11 and CPM-C12 micelles investigated by multidetection size exclusion chromatography (SEC) showed different distributions when detected using refractive index (RI) and right-angle light scattering (RALS) (Figure 4 and Figure S8). Micelles formed by X-NBM-C11 showed two separated peaks in the SEC profile, indicating a bimodal size distribution for these micelles (Figure 4a). The peak at 8.4 mL corresponds to an aggregation number (N_{agg}) of between 90 and 180, while the peak at 9.1 mL gives N_{agg} of 180−750. By contrast, micelles formed by CPM-C12 gave a well-defined unimodal distribution, showing only one peak at 9.4 mL, corresponding to N_{agg} of 60−85 (Figure 4b). This N_{agg} is much smaller than DDM micelles (~175).[31] The higher N_{agg} of X-NBM-C11 than that of CPM-C12 reflects the larger micelle size observed by DLS experiment (Table 1).

To gain insights into the solubilizing efficiency of the new agents, unilamellar vesicles made of 1-palmitoyl-2-oleoyl-*sn*-glycero-3-phosphocholine (POPC) were separately mixed with 5 mM CPM-*C*12 and X-NBM-C11. The scattering intensity and mass-averaged (*z*-average) particle diameters decreased over incubation time for both detergents (Figure S10), thus demonstrating liposome solubilization. Interestingly, the solubilization kinetic of POPC vesicles was faster for CPM-C12 than for X-NBM-C11. DLS profiles following the liposome solubilization indicate the formation of the small aggregates with hydrodynamic diameters well below the initial size of the POPC vesicles (~120 nm) (Figure 4c). The volume-weighted size distribution suggested the formation of small assemblies following detergent mixing, with hydrodynamic diameters close to 5.6 nm (CPM-C12) and 11.7 nm (X-NBM-C11) (Figure 4d). Based on the liposome solubilization result, these two detergents along with DDM were further tested for extracting diverse membrane proteins from native *Escherichia coli* (*E. coli*) membranes. Of the tested detergents, CPM-C12 gave the highest extraction yields of various *E. coli* membrane proteins, followed by X-NBM-C11 and DDM (Figure 5). The trans analogue (*i.e.*, CPM-*T*12) was inferior to CPM-C12 in this regard.

Detergent Evaluation with Diverse Model Membrane Proteins. To assess the potential utility of new amphiphiles as tools for membrane protein study, we evaluated several model protein systems with the CPMs using DDM and X/D-NBM-C11 as controls. The suitability of the isomeric CPMs (CPM-*C*s and CPM-*T*s) for the membrane protein study was first investigated with the bacterial leucine transporter (LeuT), a prokaryotic homologue of the mammalian neurotransmitter: sodium symporter (NSS) family from *Aquifex aeolicus*.[33,34] This transporter was initially expressed and extracted from *E.*

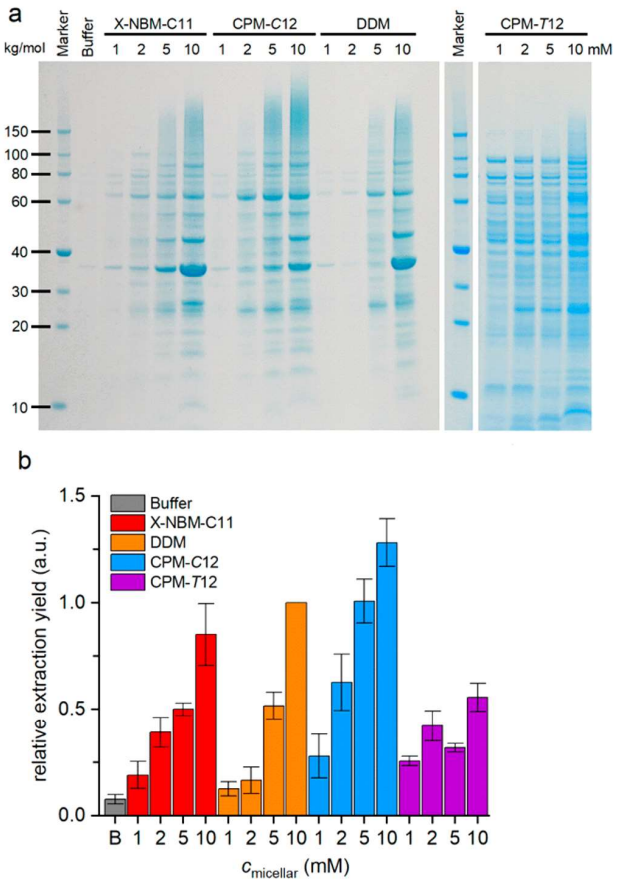

Figure 5. (a) SDS-PAGE of detergent-solubilized fractions and (b) relative protein extraction yields of CPM-C12 from the native *E. coli* membranes. X-NBM-C11 and DDM were used for comparison, with the amount of membrane protein extracted by 10 mM DDM serving as reference value (1.0 or 100%). Cell membrane fragments from *E. coli* BL21 (DE3) were incubated with three individual detergents (X-NBM-C11, CPM-C12, CPM-*T*12, and DDM) for 16 h at four different concentrations (1, 2, 5, and 10 mM). The band intensity in each lane was measured by densitometry using ImageJ;[32] error bars indicate standard errors of the mean from three or four separate solubilizations.

coli C41 (DE3) membranes with 1.0 wt % DDM and purified in 0.05 wt % of the same detergent. DDM-purified LeuT was diluted into buffer solutions containing individual agents (CPM-C11/C12, CPM-*T*11/*T*12, D/X-NBM-C11, or DDM) to reach final detergent concentrations of CMC + 0.04 wt % or CMC + 0.2 wt %. We assessed protein stability by measuring the ability of the transporter to bind radiolabeled leucine ([^{3}H]-Leu) using scintillation proximity assay (SPA)[35] at regular intervals during a 13-day incubation at room temperature. At both detergent concentrations, LeuT in DDM-containing buffer underwent a gradual loss of protein activity over the incubation period, resulting in ~10% residual activity after the 13-day incubation (Figure 6). Consistent with a previous result,[27] X/D-NBM-C11 was markedly superior to DDM in terms of preserving the functional state of the transporter. All CPMs were similar to X/D-NBM-C11 in maintaining transporter activity (Figure 6a,b). No clear difference between the isomers (i.e., CPM-Cs vs CPM-*T*s) was observed in this regard although the *cis* isomers look slightly better than the *trans* isomers. This result suggests that

https://dx.doi.org/10.1021/jacs.0c09629
J. Am. Chem. Soc. 2020, 142, 21382−21392

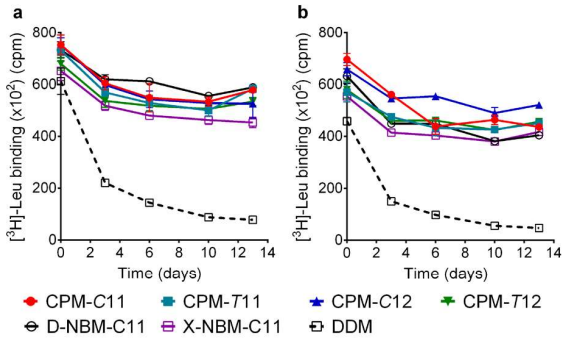

Figure 6. Long-term stability of LeuT solubilized in CPMs (CPM-*C*11/*T*11/*C*12/*T*12) at the two detergent concentrations: (a) CMC + 0.04 wt % and (b) CMC + 0.2 wt %. X/D-NBM-C11 and DDM were used as positive controls. The ligand binding ability of the transporter was measured by using the radio-labeled substrate ([^{3}H]-leucine (Leu)) via scintillation proximity assay (SPA). Protein stability was monitored at regular intervals during a 13-day incubation at room temperature. Data are shown as means ± SEM (error bars), n = 3.

overall the CPM architecture is favorable for long-term LeuT stability. There was little observed difference in stability of the LeuT in the CPM agents with different stereochemistry.

The new agents were further investigated for the extraction and stabilization of melibiose permease from *Salmonella typhimurium* ($MelB_{St}$).[36] *E. coli* membrane fractions containing overexpressed $MelB_{St}$ were treated with 1.5 wt % of individual detergents (DDM, D/X-NBM-C11, or CPM-C11/*T*11/*C*12/*T*12) for 90 min at 0 °C, and the resulting detergent extracts were further incubated at an elevated temperature (45, 55, or 65 °C) for another 90 min. The amounts of soluble $MelB_{St}$ under the tested conditions were quantified by Western blot analysis and expressed as percentages of the initial amount of $MelB_{St}$ present in the untreated membranes. As a mild detergent is unlikely to destroy transporter integrity at low temperature, the amount of soluble $MelB_{St}$ obtained at 0 °C would mainly reflect detergent extraction efficiency. If detergent-extracted $MelB_{St}$ is further treated at a high temperature of 45, 55, or 65 °C, the amount of soluble $MelB_{St}$ depends on detergent ability to prevent protein aggregation under the conditions tested. Consistent with a previous result,[27] X-NBM-C11 failed to solubilize $MelB_{St}$, while its *endo* isomer (D-NBM-C11) was efficient in this regard (Figure 7a). DDM and D-NBM-C11 quantitatively extracted the transporter at 0 °C. Similar efficiencies for protein solubilization (90−100%) were observed for the CPM agents with the exception of CPM-*T*12. CPM-*T*12 was similar to X-NBM-C11 in terms of $MelB_{St}$ extraction efficiency. At an elevated temperature of 45 °C, the amounts of soluble $MelB_{St}$ were similar to those observed at 0 °C. When the incubation temperature was further increased to 55 °C, however, the detergent efficacy for $MelB_{St}$ solubilization was clearly differentiated. At this high temperature, DDM and X-NBM-C11 gave only ~10% soluble $MelB_{St}$, while D-NBM-C11 yielded 75% solubilized $MelB_{St}$. CPM-*T*12 was inferior to D-NBM-C11, but the other three CPMs (CPM-C11, CPM-*T*11, and CPM-C12) were more effective than DDM at maintaining MelB solubility, with the best performance observed for CPM-*C*11 and CPM-C12 (~100%). This result indicates that these CPM agents were not only efficient at extracting the transporter but also effective at preserving the transporter in

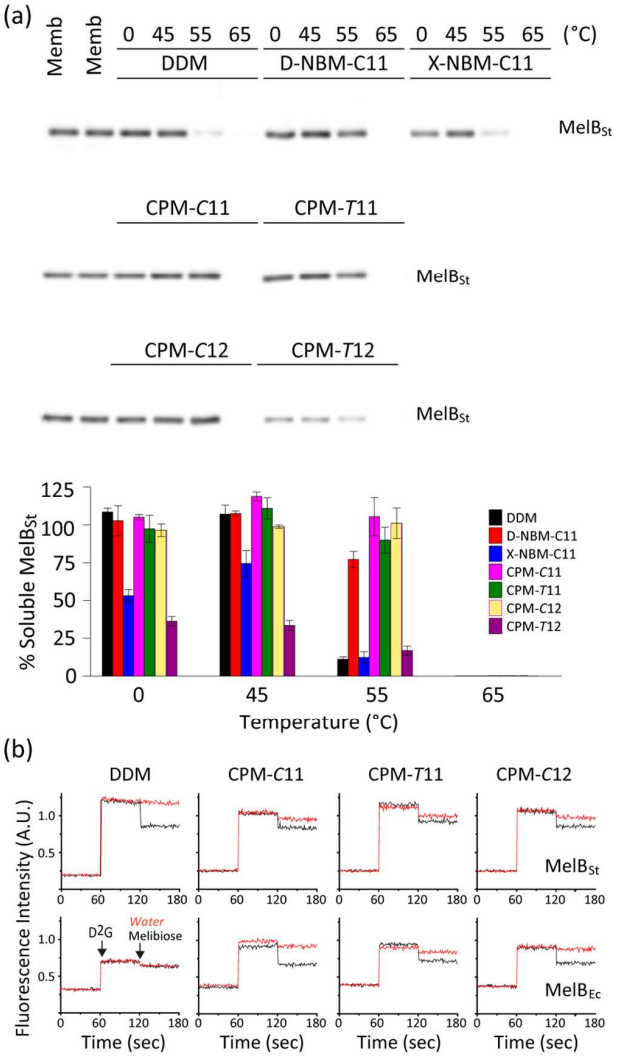

Figure 7. (a) Thermo-solubility of $MelB_{St}$ solubilized in four CPM agents. DDM and D/X-NBM-C11 were used as controls. $MelB_{St}$ was extracted from *E. coli* membranes by using 1.5 wt % individual detergents for 90 min at 0 °C. These detergent extracts were further incubated for another 90 min at an elevated temperature (45, 55, or 65 °C). Following ultracentrifugation to remove insoluble proteins and debris, the soluble $MelB_{St}$ was separated by SDS-PAGE and visualized by Western blot (top panel). The amount of soluble $MelB_{St}$ was expressed as a percentage of total $MelB_{St}$ in the untreated membrane (Memb) and presented as a histogram (a, bottom panel). Error bars, SEM, n = 2. (b) Melibiose binding-mediated FRET reversal. Right-side-out (RSO) membrane vesicles containing $MelB_{St}$ or $MelB_{Ec}$ were solubilized with DDM, CPM-C11, CPM-*T*11, or CPM-*C*12. The detergent extracts were used to measure melibiose reversal of FRET from Trp to dansyl-2-galactoside (D^2G). D^2G at 10 μM and melibiose at a saturating concentration were added at 1 and 2 min time points, respectively (black lines). Control data (red lines) were obtained by addition of water instead of melibiose.

a soluble state upon heating. Additionally, the CPM-*C*s appeared to be superior to the *trans* isomers (CPM-*T*s) at maintaining $MelB_{St}$ in a soluble form. To further evaluate relative detergent effectiveness to DDM, the three CPMs (CPM-C11, CPM-*T*11, and CPM-C12) were selected for the $MelB_{St}$ functional assay. The $MelB_{St}$ function was assessed by melibiose reversal of Förster resonance energy transfer

https://dx.doi.org/10.1021/jacs.0c09629
J. Am. Chem. Soc. 2020, 142, 21382−21392

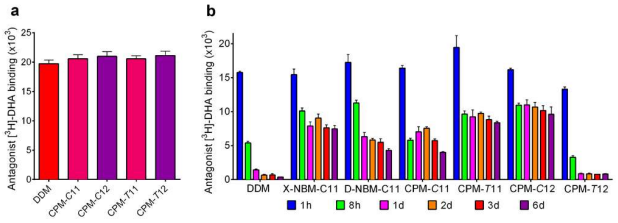

Figure 8. (a) Initial or (b) long-term ligand binding ability of β_2AR solubilized in individual detergents (DDM, CPM-Cs, and CPM-*T*s). DDM and X/D-NBM-C11 were used as positive controls. DDM-purified receptor was diluted into buffer solutions containing the individual new agents or DDM/CHS to reach the final detergent concentration of 0.2 wt %. Ligand binding activity of the receptor was measured using the radio-labeled ligand ([^{3}H]-dihydroalprenolol (DHA)). The receptor activity was measured following 30 min dilution (a) or at regular intervals during a 6-day incubation (b) at room temperature. Error bars, SEM, n = 3.

(FRET) from tryptophan to 2′-(*N*-dansyl)aminoalkyl-1-thio-β-D-galactopyranoside (D^2G).[36a,d,e] An active transporter binds to both fluorescent galactoside ligand (D^2G) and non-fluorescent substrate (melibiose). Consequently, D^2G addition to active $MelB_{St}$ gives a strong fluorescent signal that could be reversed by addition of a competitive melibiose as a ligand–substrate exchange occurs in the binding pocket. The DDM-solubilized $MelB_{St}$ showed a response to the addition of both D^2G and melibiose (Figure 7b). However, a complete loss in transporter function was observed when a less stable homologue, $MelB_{EC}$ obtained from *E. coli*, was used under the same conditions.[36d] By contrast, all the tested CPMs (CPM-C11, CPM-*T*11, and CPM-C12) preserved the functionality of both MelB homologues. Collectively, these three CPMs were superior to DDM at maintaining MelB in a soluble and functional form.

We next assessed the new agents using a GPCR, the human β_2 adrenergic receptor (β_2AR).[37] The receptor was first extracted and purified by using DDM. The DDM-purified receptor was diluted in buffer solutions supplemented with either the new individual agents without cholesteryl hemisuccinate (CHS) or DDM with CHS. The final detergent concentration was 0.2 wt % for all tested detergents. As a direct assessment of receptor stability, the ability of the receptor to bind the radioactive antagonist ([^{3}H]-dihydroalprenolol (DHA)) was measured.[38−40] Preliminary results were obtained by measuring the initial ability of the detergent-solubilized receptor to bind the ligand. All CPM agents were as effective as DDM at maintaining receptor activity (Figure 8a). To further investigate detergent efficacy, ligand binding activity of the receptor solubilized in the individual detergents was monitored at regular intervals over a 6-day incubation at room temperature (Figure 8b). The DDM-solubilized receptor showed high initial activity but rapidly lost its activity, giving only ∼5% residual activity at the end of the incubation. A similar trend was observed for CPM-*T*12. X/D-NBM-C11-solubilized receptor retained approximately 50/30% of the initial activity at day 6. There is little difference in β_2AR stabilization between the CPMs and the NBMs, as exemplified by CPM-C11 vs D-NBM-C11 and CPM-*T*11 vs X-NBM-C11. CPM-C12-solubilized receptor showed the highest retention in receptor activity over the incubation period (Figure 8b).

The promising results with LeuT, MelB, and β_2AR prompted us to select three CPMs (CPM-C11, CPM-C12, and CPM-*T*11) for the further evaluation with another GPCR, namely, the mouse μ-opioid receptor (MOR).[41] The individual detergents were used at 0.5 wt %. MOR stability was assessed by measuring receptor T_m *via* CPM assay. Along with DDM, LMNG, widely used for GPCR study, was included as a control in detergent evaluation. As expected, LMNG-solubilized MOR gave a higher T_m than found for the DDM-solubilized receptor (33.7 vs 28.0 °C) (Figure 9). CPM-*T*11 was comparable to LMNG at stabilizing the receptor, while the *cis* isomers (CPM-C11 and CPM-C12) were notably more effective than LMNG. MOR solubilized in CPM-C11 and CPM-C12 gave T_ms of 36.3 and 39.3 °C, respectively. The receptor T_m was further increased by 5.6 °C when solubilized in CPM-C12 instead of LMNG, indicating the promise of this agent for GPCR structural study, particularly when combined with the β_2AR result.

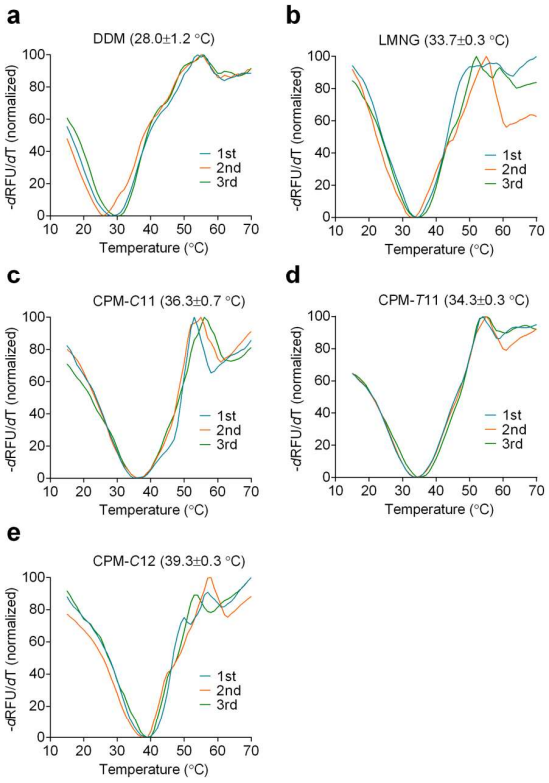

Figure 9. Melting temperatures (T_m) of MOR solubilized in the designated detergents and derivative functions (normalized) of CPM profiles. T_m values were obtained from the derivative functions of the CPM profiles. For the CPM assay, the receptor was solubilized in DDM (a), LMNG (b), CPM-C11 (c), CPM-*T*11 (d), and CPM-C12 (e), and temperatures of individual samples were increased from 15 to 70 °C. The value in parentheses represents average receptor T_m ± SEM (n = 3). "1st", "2nd", and "3rd" represent experimental numbers of three independent samples.

As CPM-C12 was most effective in stabilizing multiple membrane proteins, we investigated whether this agent can be effectively used for protein extraction/solubilization and purification. To this end, we utilized the prokaryotic voltage-dependent potassium ion channel KvAP cloned from *Aeropyrum pernix* and expressed in *E. coli*.[42] Cells were subjected to homogenization by sonication, followed by two-step centrifugation (7000*g* and 100000*g*), and the resulting KvAP-containing membranes were incubated with CPM-C12

https://dx.doi.org/10.1021/jacs.0c09629
J. Am. Chem. Soc. 2020, 142, 21382−21392

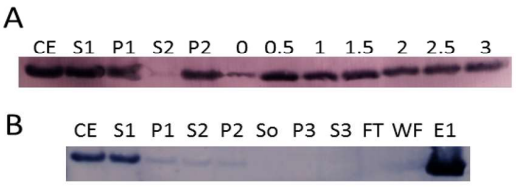

Figure 10. Western blots of prokaryotic voltage-dependent potassium channel (KvAP) over (a) *E. coli* BL21 membrane preparation and solubilization and (b) extraction and purification of the channel protein by immobilized metal affinity chromatography (IMAC) using Talon Co^{2+} beads. CPM-C12 was used at seven different concentrations (0, 0.5, 1, 1.5, 2, 2.5, and 3 wt %) (a) or 1.0 wt % (b) for KvAP extraction. CE: crude extract; S1 and P1: supernatant and pellet after the first centrifugation (7000*g*); S2 and P2: supernatant and pellet after the second centrifugation (100000*g*); So: solubilized material; S3 and P3: supernatant and pellet after the third centrifugation (100000*g*); FT: flow through; WF: washed fraction; E1: eluted fraction.

at a range of concentrations from 0 to 3.0 wt % for 3 h at room temperature. The amounts of KvAP solubilized under these conditions were estimated by SDS-PAGE (Figure S11) and Western blot (Figure 10a). CPM-C12 was efficient at KvAP extraction and solubilization, and the amount of solubilized KvAP showed little dependency on detergent concentration over the range of 0.5−3.0 wt % tested. To gauge the compatibility of this detergent with protein purification, KvAP extracted and solubilized by using 1.0 wt % CPM-C12 was loaded onto immobilized metal affinity chromatography (IMAC). CPM-C12-purified KvAP was eluted in good yields upon addition of 1.5 column volumes of elution buffer containing 0.25 wt % CPM-C12 and 400 mM imidazole at pH 8.0 (Figure 10b and Figure S12). Combined together, these results indicate that CPM-12 can be effectively used for membrane protein extraction and purification.

■ DISCUSSION

Membrane proteins display different tendencies to denature or aggregate in solution because of large variations in the structures and properties. This is the reason we lack a magic bullet detergent suitable for working with all membrane proteins. Despite the protein-specific nature of detergent efficacy for protein stabilization, DDM is widely used for membrane protein research and thus is an accepted gold standard for membrane protein structural study. In this study, we developed a novel class of diastereomeric amphiphiles (CPMs) based on our previous NBM study and evaluated their efficacy for protein stabilization with multiple membrane proteins (LeuT, MelB, β_2AR, and MOR). The best detergent was CPM-C12, which turned out to be markedly superior to DDM for all the membrane proteins tested here. In addition, this C12 alkyl-chained CPM was even better than X/D-NBM-C11 at stabilizing the membrane proteins. When compared with LMNG, a detergent optimized for GPCR stability, CPM-C12 was notably better than this NG class detergent for stabilization of two GPCRs (β_2AR and MOR). CPM-C12 was better at stabilizing β_2AR than X-NBM-C11, an agent shown previously to be better than LMNG at stabilizing the receptor in our previous NBM study.[27] CPM-C12 gave 5.6 °C higher T_m of the receptor than LMNG in the case of MOR. Furthermore, CPM-C12 was efficient at extracting membrane proteins ($MelB_{St}$) and successfully used for both solubilization and purification of the channel protein (KvAP). Thus, these results reveal that this CPM will find wide use in studying membrane proteins, particularly GPCRs. Development of such detergents with enhanced protein stabilization efficacy and good protein extraction efficiency is challenging as multiple detergent properties need to be individually optimized within a single small architecture.

It is important to identify structural features responsible for the observed superiority of CPM-C12 over X/D-NBM-C11 in terms of protein stabilization. These detergents (CPM-C12 vs X/D-NBM-C11) mainly differ in their core structure (CP/NB) and alkyl chain length (C11/C12). To unravel the effects of the detergent core unit on protein stability, it is necessary to compare detergent efficacy between a pair of detergents with the same alkyl chain length and the same relative configuration of detergent head and tail groups (*e.g.*, CPM-C11 *vs* D-NBM-C11). CPM-C11 was similar to D-NBM-C11 at stabilizing the membrane proteins (LeuT, $MelB_{St}$, and β_2AR). A similar trend was observed for the *trans*/*exo* versions (CPM-*T*11 vs X-NBM-C11), with the exception of $MelB_{St}$ stability. This comparison indicates that the presence of a CP rather than an NB core is unlikely to be responsible for the favorable protein stabilization behavior of the CPMs compared to the NBMs. In other words, the increase in the hydrophilic group flexibility attained by the introduction of the CP core is not a *direct* reason for the enhanced protein stabilization efficacy of CPM-C12 relative to X/D-NBM observed here. Rather, the increased hydrophilic group flexibility appears to give an *indirect* effect on protein stability as it conferred enhanced water solubility to the CPM molecules, allowing for preparation of the most effective detergent with good water solubility (*i.e.*, CPM-C12). As a result, we conceive that CPM-C12 was observed to be better for protein stabilization than D/X-NBM-C11 not because of enhanced flexibility of this CPM in the hydrophilic region but because of the increased alkyl chain length from C11 to C12. The increase in alkyl chain length could provide greater compatibility of CPM-C12 to the hydrophobic dimensions of protein surfaces as compared with D/X-NBM-C11. In addition, this alkyl chain extension endows detergent molecules with stronger interactions with the protein hydrophobic surfaces, leading to effective prevention of protein aggregation. At first glance, this conclusion seems inconsistent with the general concept that detergent flexibility is critical for membrane protein stabilization.[43,44] However, such detergent flexibility is associated with the detergent hydrophobic group rather than the hydrophilic group. Thus, the current result is still compatible with the previous results, yet it implies a distinctive role for detergent flexibility associated with the head group in protein stability.

It is interesting to compare the *cis* and *trans* versions of CPMs in terms of protein stabilization as this configuration difference generates variation in the relative directions of the detergent head and tail groups. The relative efficacy of the CPM-*C*s and CPM-*T*s for protein stabilization was dependent on both detergent alkyl chain length (C11/C12) and target membrane protein (MelB, MOR, LeuT, or β_2AR). In the cases of the C11 versions, the *cis*-configured CPM (CPM-C11) was slightly better than the *trans* isomer (CPM-*T*11) for MelB and MOR stability, while the opposite trend was observed for β_2AR stability. When it comes to the C12 versions, CPM-C12 was clearly superior to CPM-*T*12 at stabilizing MelB and β_2AR, while little difference was observed for LeuT stability. Thus, there was no clear-cut trend for detergent efficacy between the CPMs with the *cis* and *trans* configurations. However, the

https://dx.doi.org/10.1021/jacs.0c09629
J. Am. Chem. Soc. 2020, 142, 21382−21392

CPM-Cs showed overall favorable behaviors for stabilizing the membrane proteins compared to the *trans* counterparts. The general outperformance of the *cis* isomers compared to the *trans* isomers is likely associated with a difference in conformation of the CP core unit (half-chair or envelope) between these stereoisomers, in addition to the relative configuration of the tail group to the head group (*cis*/*trans*). The conformation of the CP ring not only determines the relative directions of the alkyl chains and two maltose groups but also affects detergent hydrophobic length and molecular symmetry. The half-chair conformation of the CP ring in the CPM-Cs places the two alkyl chains in a nonparallel arrangement: one alkyl chain in an axial position and the other alkyl chain in the equatorial position. This asymmetric conformation results in a difference in the effective chain length between the two alkyl chains. Membrane proteins have uneven protein hydrophobic surfaces, and thus the difference in the effective chain length of the CPM-Cs could be more beneficial for interactions with membrane proteins than the *trans* counterparts (*i.e.*, CPM-*T*s).

■ CONCLUSIONS

Through variations of stereochemistry and alkyl chain length, we report herein two sets of diastereomeric cyclopentane-based maltosides. Of the new agents, we found CPM-C12 to be markedly more effective than optimized novel detergents (X-NBM-C11 and LMNG) as well as a gold standard detergent (DDM) at stabilizing GPCRs. Successful extraction and purification of a voltage-gated potassium ion channel, along with the efficient solubilization of $MelB_{St}$ and *E. coli* membrane proteins, further underline the utility of this agent. Hence, this CPM represents an invaluable tool for membrane protein structural study. Additionally, detergent comparison enabled us to propose roles for both detergent flexibilities associated with the hydrophilic group and detergent core conformation in protein stability, which will assist rational design of novel detergents in the future.

■ ASSOCIATED CONTENT

Supporting Information

The Supporting Information is available free of charge at https://pubs.acs.org/doi/10.1021/jacs.0c09629.

Figures S1−S12, supplementary methods for protein stability assays, and detergent synthetic protocols and characterizations (PDF)

■ AUTHOR INFORMATION

Corresponding Author

Pil Seok Chae − *Department of Bionanotechnology, Center for Bionano Intelligence Education and Research, Hanyang University, Ansan 155-88, Korea;* orcid.org/0000-0003-1799-3304; Email: pchae@hanyang.ac.kr

Authors

Manabendra Das − *Department of Bionanotechnology, Center for Bionano Intelligence Education and Research, Hanyang University, Ansan 155-88, Korea; Technische Universität Kaiserslautern (TUK), 67663 Kaiserslautern, Germany*

Florian Mahler − *Technische Universität Kaiserslautern (TUK), 67663 Kaiserslautern, Germany*

Parameswaran Hariharan − *Department of Cell Physiology and Molecular Biophysics, Center for Membrane Protein Research, School of Medicine, Texas Tech University Health Sciences Center, Lubbock, Texas 79430, United States*

Haoqing Wang − *Department of Molecular and Cellular Physiology, Stanford University, Stanford, California 94305, United States*

Yang Du − *Department of Molecular and Cellular Physiology, Stanford University, Stanford, California 94305, United States*

Jonas S. Mortensen − *Department of Neuroscience, University of Copenhagen, Copenhagen DK-2200, Denmark*

Eugenio Pérez Patallo − *Technische Universität Kaiserslautern (TUK), 67663 Kaiserslautern, Germany*

Lubna Ghani − *Department of Bionanotechnology, Center for Bionano Intelligence Education and Research, Hanyang University, Ansan 155-88, Korea*

David Glück − *Technische Universität Kaiserslautern (TUK), 67663 Kaiserslautern, Germany*

Ho Jin Lee − *Department of Bionanotechnology, Center for Bionano Intelligence Education and Research, Hanyang University, Ansan 155-88, Korea*

Bernadette Byrne − *Department of Life Sciences, Imperial College London, London SW7 2AZ, United Kingdom;* orcid.org/0000-0001-9598-9832

Claus J. Loland − *Department of Neuroscience, University of Copenhagen, Copenhagen DK-2200, Denmark;* orcid.org/0000-0002-1773-1446

Lan Guan − *Department of Cell Physiology and Molecular Biophysics, Center for Membrane Protein Research, School of Medicine, Texas Tech University Health Sciences Center, Lubbock, Texas 79430, United States;* orcid.org/0000-0002-2274-361X

Brian K. Kobilka − *Department of Molecular and Cellular Physiology, Stanford University, Stanford, California 94305, United States*

Sandro Keller − *Technische Universität Kaiserslautern (TUK), 67663 Kaiserslautern, Germany; Institute of Molecular Biosciences (IMB), NAWI Graz and Field of Excellence BioHealth, University of Graz, 8010 Graz, Austria; BioTechMed-Graz, Graz, Austria;* orcid.org/0000-0001-5469-8772

Complete contact information is available at: https://pubs.acs.org/10.1021/jacs.0c09629

Notes

The authors declare the following competing financial interest(s): P.S.C. and M.D. are inventors on a patent application that covers the CPM agents.

■ ACKNOWLEDGMENTS

This work was supported by the National Research Foundation of Korea (NRF) (2016R1A2B2011257 and 2018R1A6A1A03024231 to P.S.C.). We acknowledge Julia Lenz for preparing native *E. coli* membranes for extraction studies. This study was also supported by the National Institutes of Health (Grants R01GM122759 and R21NS105863 to L.G.).

■ REFERENCES

(1) (a) Sanders, C. R.; Myers, J. K. Disease-related misassembly of membrane proteins. *Annu. Rev. Biophys. Biomol. Struct.* **2004**, *33*, 25−51. (b) Overington, J. P.; Al-Lazikani, B.; Hopkins, A. L. How many drug targets are there? *Nat. Rev. Drug Discovery* **2006**, *5*, 993−996.

https://dx.doi.org/10.1021/jacs.0c09629
J. Am. Chem. Soc. 2020, 142, 21382−21392

(2) Membrane proteins of known 3D structure; http://blanco.biomol.uci.edu/mpstruc/.
(3) Kuhlbrandt, W. Microscopy: cryo-EM enters a new era. *eLife* **2014**, *3*, No. e03678.
(4) (a) Garavito, R. M.; Ferguson-Miller, S. Detergents as tools in membrane biochemistry. *J. Biol. Chem.* **2001**, *276*, 32403−32406. (b) Serrano-Vega, M. J.; Magnani, V.; Shibata, Y.; Tate, C. G. Co-evolving stability and conformational homogeneity of the human adenosine A2A receptor. *Proc. Natl. Acad. Sci. U. S. A.* **2008**, *105*, 10744−10749.
(5) (a) Newstead, S.; Ferrandon, S.; Iwata, S. Rationalizing R-helical membrane protein crystallization. *Protein Sci.* **2008**, *17*, 466−472. (b) He, Y.; Wang, K.; Yan, N. The recombinant expression systems for structure determination of eukaryotic membrane proteins. *Protein Cell* **2014**, *5*, 658−672. (c) Parker, J. L.; Newstead, S. Current trends in α-helical membrane protein crystallization. *Protein Sci.* **2012**, *21*, 1358−1365.
(6) Israelachvili, J. N.; Mitchell, D. J.; Ninham, B. W. Theory and self-assembly of lipid bilayers and vesicles. *Biochim. Biophys. Acta, Biomembr.* **1977**, *470*, 185−201.
(7) Chaptal, V.; Delolme, F.; Kilburg, A.; Magnard, S.; Montigny, C.; Picard, M.; Prier, C.; Monticelli, L.; Bornert, O.; Agez, M.; Ravaud, S.; Orelle, C.; Wagner, R.; Jawhari, A.; Broutin, I.; Pebay-Peyroula, E.; Jault, J.-M.; Kaback, R.; Le Maire, M.; Falson, P. Quantification of detergents complexed with membrane proteins. *Sci. Rep.* **2017**, *7*, 41751.
(8) (a) Loll, P. J. Agrobacterium: from biology to biotechnology. *J. Struct. Biol.* **2003**, *142*, 144−153. (b) White, S. H. The progress of membrane protein structure determination. *Protein Sci.* **2004**, *13*, 1948−1949.
(9) Faham, S.; Bowie, J. U. Bicelle crystallization; a new method for crystallizing membrane protein yields a monomeric bacteriorhodopsin structure. *J. Mol. Biol.* **2002**, *316*, 1−6.
(10) Nath, A.; Atkins, W. M.; Sligar, S. G. Applications of phospholipid bilayer nanodiscs in the study of membranes and membrane proteins. *Biochemistry* **2007**, *46*, 2059−2069.
(11) (a) Broecker, J.; Eger, B. T.; Ernst, O. P. Crystallogenesis of membrane proteins mediated by polymer-bounded lipid nanodiscs. *Structure* **2017**, *25*, 384−392. (b) Oluwole, A. O.; Danielczak, B.; Meister, A.; Babalola, J. O.; Vargas, C.; Keller, S. Solubilization of membrane proteins into functional lipid-bilayer nanodiscs by diisobutylene/maleic acid copolymer. *Angew. Chem., Int. Ed.* **2017**, *56*, 1919−1924.
(12) (a) Tribet, C.; Audebert, R.; Popot, J.-L. Amphipols: polymers that keep membrane proteins soluble in aqueous solutions. *Proc. Natl. Acad. Sci. U. S. A.* **1996**, *93*, 15047−15050. (b) Popot, J.-L.; Althoff, T.; Bagnard, D.; Banéres, J.-L.; Bazzacco, P.; Billon-Denis, E.; Catoire, L. J.; Champeil, P.; Charvolin, D.; Cocco, M. J.; Cremel, G.; Dahmane, T.; de la Maza, L. M.; Ebel, C.; Gabel, F.; Giusti, F.; Gohon, Y.; Goormaghtigh, E.; Guittet, E.; Kleinschmidt, J. H.; Kuhlbrandt, W.; Le Bon, C.; Martinez, K. L.; Picard, M.; Pucci, B.; Sachs, J. N.; Tribet, C.; van Heijenoort, C.; Wien, F.; Zito, F.; Zoonens, M. Amphipols from A to Z. *Annu. Rev. Biophys.* **2011**, *40*, 379−408.
(13) Tao, H.; Lee, S. C.; Moeller, A.; Roy, R. S.; Siu, F. Y.; Zimmermann, J.; Stevens, R. C; Potter, C. S; Carragher, B.; Zhang, Q. Engineered nanostructured β-sheet peptides protect membrane proteins. *Nat. Methods* **2013**, *10*, 759−761.
(14) (a) McGregor, C.-L.; Chen, L.; Pomroy, N. C.; Hwang, P.; Go, S.; Chakrabartty, A.; Privé, G. G. Lipopeptide detergents designed for the structural study of membrane proteins. *Nat. Biotechnol.* **2003**, *21*, 171−176. (b) Frauenfeld, J.; Loving, R.; Armache, J.-P.; Sonnen, A. F-P; Guettou, F.; Moberg, P.; Zhu, L.; Jegerschold, C.; Flayhan, A.; Briggs, J. A G; Garoff, H.; Low, C.; Cheng, Y.; Nordlund, P. A saposin-lipoprotein nanoparticle system for membrane proteins. *Nat. Methods* **2016**, *13*, 345−351. (c) Carlson, M. L.; Young, J. W.; Zhao, Z.; Fabre, L.; Jun, D.; Li, J.; Li, J.; Dhupar, H. S.; Wason, I.; Mills, A. T.; Beatty, J. T.; Klassen, J. S.; Rouiller, I.; Duong, F. The peptidisc, a simple method for stabilizing membrane proteins in detergent-free solution. *eLife* **2018**, *7*, No. e34085.
(15) (a) Chae, P. S.; Rasmussen, S. G.; Rana, R. R.; Gotfryd, K.; Chandra, R.; Goren, M. A.; Kruse, A. C.; Nurva, S.; Loland, C. J.; Pierre, Y.; et al. Maltose-neopentyl glycol (MNG) amphiphiles for solubilization, stabilization and crystallization of membrane proteins. *Nat. Methods* **2010**, *7*, 1003−1008. (b) Chae, P. S.; Rana, R. R.; Gotfryd, K.; Rasmussen, S. G.; Kruse, A. C.; Cho, K. H.; Gether, U.; et al. Glucose-neopentyl glycol (GNG) amphiphiles for membrane protein study. *Chem. Commun.* **2013**, *49*, 2287−2289. (c) Cho, K. H.; Husri, M.; Amin, A.; Gotfryd, K.; Lee, H. J.; Go, J.; Chae, P. S.; et al. Maltose neopentyl glycol-3 (MNG-3) analogues for membrane protein study. *Analyst* **2015**, *140*, 3157−3163. (d) Bae, H. E.; Du, Y.; Hariharan, P.; Mortensen, J. S.; Kumar, K. K.; Ha, B.; Kobilka, B. K.; et al. Asymmetric maltose neopentyl glycol amphiphiles for a membrane protein study: effect of detergent asymmetricity on protein stability. *Chem. Sci.* **2019**, *10*, 1107−1116.
(16) Hussain, H.; Du, Y.; Scull, N. J.; Mortensen, J. S.; Tarrasch, J.; Bae, H. E.; Loland, C. J.; Byrne, B.; Kobilka, B. K.; Chae, P. S. Accessible mannitol-based amphiphiles (MNAs) for membrane protein solubilization and stabilization. *Chem. - Eur. J.* **2016**, *22*, 7068−7073.
(17) Chae, P. S.; Laible, P. D.; Gellman, S. H. Tripod amphiphiles for membrane protein manipulation. *Mol. BioSyst.* **2010**, *6*, 89−94.
(18) Matar-Merheb, R.; Rhimi, M.; Leydier, A.; Huché, F.; Galián, C.; Desuzinges-Mandon, E.; Ficheux, D.; Flot, D.; Aghajari, N.; Kahn, R.; Di Pietro, A.; Jault, J. M.; Coleman, A. W.; Falson, P. Structuring detergents for extracting and stabilizing functional membrane proteins. *PLoS One* **2011**, *6*, No. e18036.
(19) Hussain, H.; Mortensen, J. S.; Du, Y.; Santillan, C.; Ribeiro, O.; Go, J.; Hariharan, P.; Loland, C. J.; Guan, L.; Kobilka, B. K.; Byrne, B.; Chae, P. S. Tandem malonate-based glucosides (TMGs) for membrane protein structural studies. *Sci. Rep.* **2017**, *7*, 3963.
(20) Ehsan, M.; Du, Y.; Scull, N. J.; Tikhonova, E.; Tarrasch, J.; Mortensen, J. S.; Loland, C. J.; Skiniotis, G.; Guan, L.; Byrne, B.; Kobilka, B. K.; Chae, P. S. Highly branched pentasaccharide-bearing amphiphiles for membrane protein studies. *J. Am. Chem. Soc.* **2016**, *138*, 3789−3796.
(21) Das, M.; Du, Y.; Mortensen, J. S.; Ribeiro, O.; Hariharan, P.; Guan, L.; Loland, C. J.; Kobilka, B. K.; Byrne, B.; Chae, P. S. Butane-1,2,3,4-tetraol-based amphiphilic stereoisomers for membrane protein study: importance of chirality in the linker region. *Chem. Sci.* **2017**, *8*, 1169−1177.
(22) Nguyen, K. A.; Peuchmaur, M.; Magnard, S.; Haudecoeur, R.; Boyère, C.; Mounien, S.; Benammar, I.; Zampieri, V.; Igonet, S.; Chaptal, V.; Jawhari, A.; Boumendjel, A.; Falson, P. Glycosyl-Substituted Dicarboxylates as Detergents for the Extraction, Over-stabilization, and Crystallization of Membrane Proteins. *Angew. Chem., Int. Ed.* **2018**, *57*, 2948−2952.
(23) Sadaf, A.; Du, Y.; Santillan, C.; Mortensen, J.; Molist, I.; Seven, A.; Hariharan, P.; Skiniotis, G.; Loland, C.; Kobilka, B. K.; Guan, L.; Byrne, B.; Chae, P. S. Dendronic trimaltose amphiphiles (DTMs) for membrane protein study. *Chem. Sci.* **2017**, *8*, 8315−8324.
(24) Ghani, L.; Munk, C. F.; Zhang, X.; Katsube, S.; Du, Y.; Cecchetti, C.; Huang, W.; Bae, H. E.; Saouros, S.; Ehsan, M.; Guan, L.; Liu, X.; Loland, C. J.; Kobilka, B. K.; Byrne, B.; Chae, P. S. 1,3,5-Triazine-Cored Maltoside Amphiphiles for Membrane Protein Extraction and Stabilization. *J. Am. Chem. Soc.* **2019**, *141*, 19677−19687.
(25) (a) Rasmussen, S. G. F.; Choi, H.-J.; Fung, J. J.; Pardon, E.; Casarosa, P.; Chae, P. S.; DeVree, B. T.; Rosenbaum, D. M.; Thian, F. S.; Kobilka, T. S.; Schnapp, A.; Konetzki, I.; Sunahara, R. K.; Gellman, S. H.; Pautsch, A.; Steyaert, J.; Weis, W. I.; Kobilka, B. K. Structure of a nanobody-stabilized active state of the β_2 adrenoceptor. *Nature* **2011**, *469*, 175−180. (b) Kruse, A. C.; Hu, J.; Pan, A. C.; Arlow, D. H.; Rosenbaum, D. M.; Rosemond, E.; Green, H. F.; Liu, T.; Chae, P. S.; Dror, R. O.; Shaw, D. E.; Weis, W. I.; Wess, J.; Kobilka, B. K. Activation and allosteric modulation of a muscarinic acetylcholine receptor. *Nature* **2012**, *482*, 552−556. (c) Ring, A. M.; Manglik, A.;

https://dx.doi.org/10.1021/jacs.0c09629
J. Am. Chem. Soc. 2020, 142, 21382−21392

Kruse, A. C.; Enos, M. D.; Weis, W. I.; Garcia, K. C.; Kobilka, B. K. Adrenaline-activated structure of β2-adrenoceptor stabilized by an engineered nanobody. *Nature* **2013**, *502*, 575−579. (d) Miller, V.; Aricescu, A. R. Crystal structure of a human GABAA receptor. *Nature* **2014**, *512*, 270−275. (e) Karakas, E.; Furukawa, H. Crystal structure of a heterotetrameric NMDA receptor ion channel. *Science* **2014**, *344*, 992−997. (f) Suzuki, H.; Nishizawa, T.; Tani, K.; Yamazaki, Y.; Tamura, A.; Ishitani, R.; Dohmae, N.; Tsukita, S.; Nureki, O.; Fujiyoshi, Y. Crystal Structure of a Claudin Provides Insight into the Architecture of Tight Junctions. *Science* **2014**, *344*, 304−307. (g) Frick, A.; Eriksson, U. K.; de Mattia, F.; Oberg, F.; Hedfalk, K.; Neutze, R.; de Grip, W. J.; Deen, P. M. T.; Tornroth-Horsefield, S. X-ray structure of human aquaporin 2 and its implications for nephrogenic diabetes insipidus and trafficking. *Proc. Natl. Acad. Sci. U. S. A.* **2014**, *111*, 6305−6310. (h) Yin, J.; Mobarec, J. C.; Kolb, P.; Rosenbaum, D. M. Crystal structure of the human OX2 orexin receptor bound to the insomnia drug suvorexant. *Nature* **2015**, *519*, 247−250. (i) Kang, Y.; Zhou, X. E.; Gao, X.; He, Y.; Liu, W.; Ishchenko, A.; Xu, Q.; et al. Crystal structure of rhodopsin bound to arrestin by femtosecond X-ray laser. *Nature* **2015**, *523*, 561−567. (j) Perez, C.; Gerber, S.; Boilevin, J.; Bucher, M.; Darbre, T.; Aebi, M.; Reymond, J.-L.; Locher, K. P. Structure and mechanism of an active lipid-linked oligosaccharide flippase. *Nature* **2015**, *524*, 433−438. (k) Taniguchi, R.; Kato, H. E.; Font, J.; Deshpande, C. N.; Wada, M.; Ito, K.; Ishitani, R.; Jormakka, M.; Nureki, O. Outward- and inward-facing structures of a putative bacterial transition-metal transporter with homology to ferroportin. *Nat. Commun.* **2015**, *6*, 8545. (l) Dong, Y. Y.; Pike, A. C.; Mackenzie, A.; McClenaghan, C.; Aryal, P.; Dong, L.; Ruda, G. F.; et al. K2P channel gating mechanisms revealed by structures of TREK-2 and a complex with Prozac. *Science* **2015**, *347*, 1256−1259. (m) Paulsen, C. E.; Armache, J.-P.; Gao, Y.; Cheng, Y.; Julius, D. Structure of the TRPA1 ion channel suggests regulatory mechanisms. *Nature* **2015**, *520*, 511−517. (n) Kellosalo, J.; Kajander, T.; Kogan, K.; Pokharel, K.; Goldman, A. The structure and catalytic cycle of a sodium-pumping pyrophosphatase. *Science* **2012**, *337*, 473−476.

(26) (a) Zhang, Q.; Ma, X.; Ward, A.; Hong, W.-X.; Jaakola, V.-P.; Stevens, R. C.; Finn, M. G.; Chang, G. Designing facial amphiphiles for the stabilization of integral membrane proteins. *Angew. Chem., Int. Ed.* **2007**, *46*, 7023−7025. (b) Lee, S. C.; Bennett, B. C.; Hong, W.-X.; Fu, Y.; Baker, K. A.; Marcoux, J.; Robinson, C. V.; Ward, A. B.; Halpert, J. R.; Stevens, R. C.; Stout, C. D.; Yeager, M. J.; Zhang, Q. Steroid-based facial amphiphiles for stabilization and crystallization of membrane protein. *Proc. Natl. Acad. Sci. U. S. A.* **2013**, *110*, E1203−E1211. (c) Das, M.; Du, Y.; Mortensen, J. S.; Bae, H. E.; Byrne, B.; Loland, C. J.; Kobilka, B. K.; Chae, P. S. An engineered lithocholate-based facial amphiphile stabilizes membrane proteins: assessing the impact of detergent customizability on protein stability. *Chem. - Eur. J.* **2018**, *24*, 9860−9868.

(27) Das, M.; Du, Y.; Ribeiro, O.; Hariharan, P.; Mortensen, J. S.; Patra, D.; Skiniotis, G.; Loland, C. J.; Guan, L.; Kobilka, B. K.; Byrne, B.; Chae, P. S. Conformationally preorganized diastereomeric norbornane-based maltosides for membrane protein study: Implications of detergent kink for micellar properties. *J. Am. Chem. Soc.* **2017**, *139*, 3072−3081.

(28) Chae, P. S.; Kruse, A. C.; Gotfryd, K.; Rana, R. R.; Cho, K. H.; Rasmussen, S. G. F.; Bae, H. E.; Chandra, R.; Gether, U.; Guan, L.; Kobilka, B. K.; Loland, C. J.; Byrne, B.; Gellman, S. H. Novel tripod amphiphiles for membrane protein analysis. *Chem. - Eur. J.* **2013**, *19*, 15645−15651.

(29) Nukada, T.; Berces, A.; Zgierski, M. Z.; Whitfield, D. M. Exploring the mechanism of neighboring group assisted glycosylation reactions. *J. Am. Chem. Soc.* **1998**, *120*, 13291−13295.

(30) Chattopadhyay, A.; London, E. Fluorometric determination of critical micelle concentration avoiding interference from detergrent charge. *Anal. Biochem.* **1984**, *139*, 408−412.

(31) (a) Oliver, R. C.; Lipfert, J.; Fox, D. A.; Lo, R. H.; Doniach, S.; Columbus, L. Dependence of micelle size and shape on detergent alkyl chain length and head group. *PLoS One* **2013**, *8*, No. e62488.

(b) Chae, P. S.; Gotfryd, K.; Pacyna, J.; Miercke, L. J.; Rasmussen, S. G.; Robbins, R. A.; Rana, R. R.; Loland, C. J.; Kobilka, B.; Stroud, R.; Byrne, B.; Gether, U.; Gellman, S. H. Tandem Facial Amphiphiles for Membrane Protein Stabilization. *J. Am. Chem. Soc.* **2010**, *132*, 16750−16752.

(32) Schneider, C. A.; Rasband, W. S.; Eliceiri, K. W. NIH Image to ImageJ: 25 years of image analysis. *Nat. Methods* **2012**, *9*, 671−675.

(33) Deckert, G.; Warren, P. V.; Gaasterland, T.; Young, W. G.; Lenox, A. L.; Graham, D. E.; Overbeek, R.; Snead, M. A.; Keller, M.; Aujay, M.; Huber, R.; Feldman, R. A.; Short, J. M.; Olsen, G. J.; Swanson, R. V. The complete genome of the hyperthermophilic bacterium Aquifex aeolicus. *Nature* **1998**, *392*, 353−358.

(34) Yamashita, A.; Singh, S. K.; Kawate, T.; Jin, Y.; Gouaux, E. Crystal structure of a bacterial homologue of Na^+/Cl^--dependent neurotransmitter transporters. *Nature* **2005**, *437*, 215−223.

(35) Quick, M.; Javitch, J. A. Monitoring the function of membrane transport proteins in detergent-solubilized form. *Proc. Natl. Acad. Sci. U. S. A.* **2007**, *104*, 3603−3608.

(36) (a) Guan, L.; Nurva, S.; Ankeshwarapu, S. P. Mechanism of melibiose/cation symport of the melibiose permease of Salmonella typhimurium. *J. Biol. Chem.* **2011**, *286*, 6367−6374. (b) Ethayathulla, A. S.; Yousef, M. S.; Amin, A.; Leblanc, G.; Kaback, H. R.; Guan, L. Structure-based mechanism for Na^+/melibiose symport by MelB. *Nat. Commun.* **2014**, *5*, 3009. (c) Amin, A.; Ethayathulla, A. S.; Guan, L. Suppression of conformation-compromised mutants of *Salmonella enterica* serovar Typhimurium MelB. *J. Bacteriol.* **2014**, *196*, 3134−3139. (d) Amin, A.; Hariharan, P.; Chae, P. S.; Guan, L. Effect of detergents on galactoside binding by Melibiose permeases. *Biochemistry* **2015**, *54*, 5849−5855. (e) Cordat, E.; Mus-Veteau, I.; Leblanc, G. Structural Studies of the Melibiose Permease of *Escherichia coli* by Fluorescence Resonance Energy Transfer II. Identification of the tryptophan residues. *J. Biol. Chem.* **1998**, *273*, 33198−33202.

(37) Rosenbaum, D. M.; Cherezov, V.; Hanson, M. A.; Rasmussen, S. G. F.; Thian, F. S.; Kobilka, T. S.; Choi, H.-J.; Yao, X.-J.; Weis, W. I.; Stevens, R. C.; Kobilka, B. K. High-resolution crystal structure of an engineered human β2-adrenergic G protein-coupled receptor. *Science* **2007**, *318*, 1266−1273.

(38) Mansoor, S. E.; Mchaourab, H. S.; Farrens, D. L. Mapping proximity within proteins using fluorescence spectroscopy. A study of T4 lysozyme showing that tryptophan residues quench bimane fluorescence. *Biochemistry* **2002**, *41*, 2475−2484.

(39) Yao, X.; Parnot, C.; Deupi, X.; Ratnala, V. R P; Swaminath, G.; Farrens, D.; Kobilka, B. Coupling ligand structure to specific conformational switches in the β2-adrenoceptor. *Nat. Chem. Biol.* **2006**, *2*, 417−422.

(40) Swaminath, G.; Steenhuis, J.; Kobilka, B.; Lee, T. W. Allosteric modulation of β2-adrenergic receptor by Zn^{2+}. *Mol. Pharmacol.* **2002**, *61*, 65−72.

(41) Manglik, A.; Kruse, A. C.; Kobilka, T. S.; Thian, F. S.; Mathiesen, V.; Sunahara, R. K.; Pardo, L.; Weis, W. I.; Kobilka, B. K.; Granier, S. Crystal structure of the μ-opioid receptor bound to a morphinan antagonist. *Nature* **2012**, *485*, 321−326.

(42) Ruta, V.; Jiang, Y.; Lee, A.; Chen, J.; MacKinnon, R. Functional analysis of an archaebacterial voltage-dependent K^+ channel. *Nature* **2003**, *422*, 180−185.

(43) Sadaf, A.; Mortensen, J. S.; Capaldi, S.; Tikhonova, E.; Hariharan, P.; Ribeiro, O.; Loland, C. J.; Guan, L.; Byrne, B.; Chae, P. S. A class of rigid linker-bearing glucosides for membrane protein structural study. *Chem. Sci.* **2016**, *7*, 1933−1939.

(44) Hussain, H.; Du, Y.; Tikhonova, E.; Mortensen, J. S.; Ribeiro, O.; Santillan, C.; Das, M.; Ehsan, M.; Loland, C. J.; Guan, L.; Kobilka, B. K.; Byrne, B.; Chae, P. S. Resorcinarene-based facial glycosides: implication of detergent flexibility on membrane protein stability. *Chem. - Eur. J.* **2017**, *23*, 6724−6729.

https://dx.doi.org/10.1021/jacs.0c09629
J. Am. Chem. Soc. 2020, 142, 21382−21392

Supporting Information

Diastereomeric Cyclopentane-Based Maltosides (CPMs) as Tools for Membrane Protein Study

*Manabendra Das, Florian Mahler, Parameswaran Hariharan, Haoqing Wang, Yang Du, Jonas S. Mortensen, Eugenio Pérez Patallo, Lubna Ghani, David Glück, Ho Jin Lee, Bernadette Byrne, Claus J. Loland, Lan Guan, Brian K. Kobilka, Sandro Keller, and Pil Seok Chae**

Table of Contents

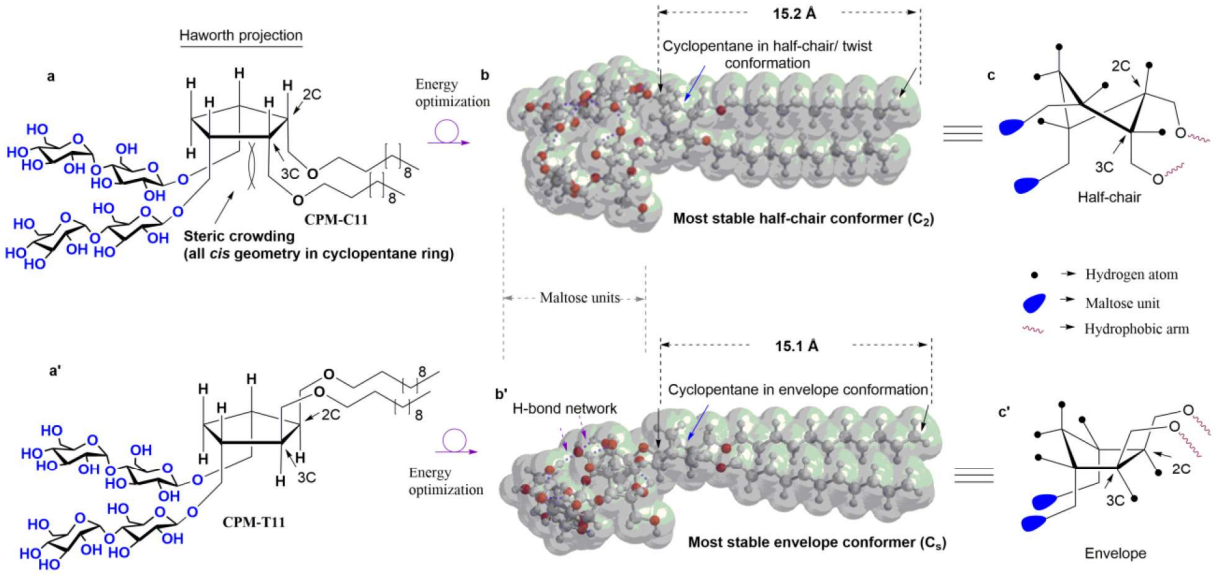

Figure S1. Chemical structures (left) of CPM-*C*11 (a) and CPM-*T*11 (a'), and their energy-minimized conformations (b and b', respectively). The energy-minimized conformations of the CPM were obtained from DFT calculations at the energy level B3LYP/6-31G*. Half chair (***C*₂**) and envelope (***C*ₛ**) are the conformations of the cyclopentane (CP) core in the energy-minimized structures of CPM-*C*11 and CPM-*T*11, respectively. The lengths of the hydrophobic groups of CPM-*C*11 and CPM-*T*11 estimated from the energy minimized conformations were 15.2 and 15.1 Å for CPM-*C*11 and CPM-*T*11, respectively. The hydrophobic lengths were determined by measuring distances between the two carbon atoms indicated in the black arrows in the energy-minimized conformations (b and b'). Atoms are indicated by different colors and size in the energy minimized conformations; gray-large for carbon atoms, gray small for hydrogen atoms and red for oxygen atoms. Purple arrows indicate hydrogen-bond networks in the maltoside head group, while blue arrows indicate the location of the central cyclopentane ring in the energy-minimized structures.

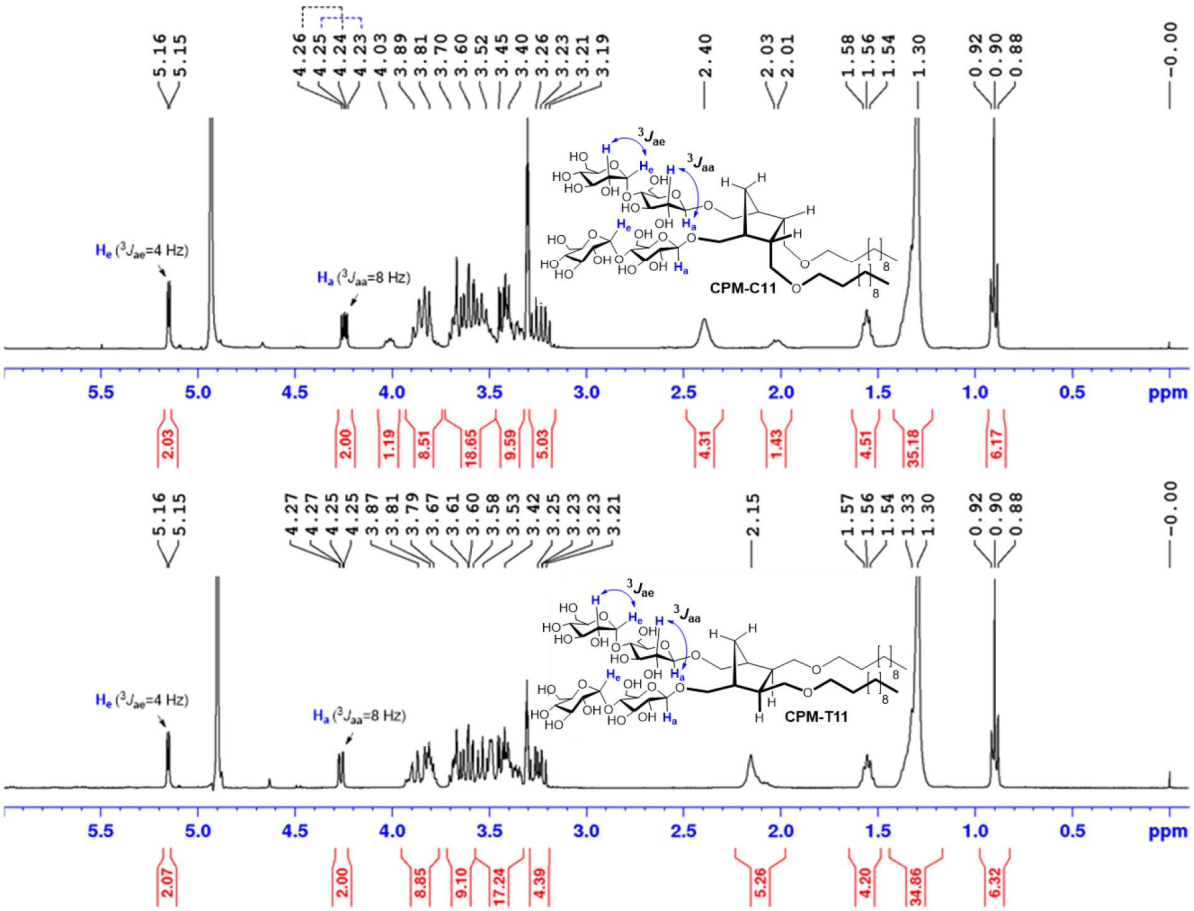

Figure S2. ^{1}H NMR spectra of CPM-*C*11 (*top*) and CPM-*T*11 (*bottom*) along with the chemical structures. Two sets of anomeric protons in the maltoside head group, labeled H_a and H_e in the chemical structures, are different in terms of their chemical shift (δ) and vicinal coupling constant (^{3}J). In CPM-*C*11, the peaks for α-anomeric protons (*i.e.*, H_e) appeared at 5.16 ppm as doublets with a vicinal axial-equatorial coupling constant ($^{3}J_{ae}$) of 4.0 Hz, whereas the peaks for β-anomeric protons (*i.e.*, H_a) appeared as two narrowly separated doublets at 4.25 and 4.24 ppm, with a vicinal axial-axial coupling ($^{3}J_{aa}$) of 8.0 Hz. In the case of CPM-*T*11, the peaks for α-anomeric protons (*i.e.*, H_e) also appeared at 5.16 ppm as doublets with 4.0 Hz vicinal coupling constant ($^{3}J_{ae}$), but the peaks for β-anomeric protons (*i.e.*, H_a) appeared as two non-separable doublets, located at 4.26 ppm, with the same coupling constant value ($^{3}J_{aa}$ = 8.0 Hz). The chemical shifts and coupling constants observed here are typical of anomeric protons with α- and β-glycosidic bonds (H_e and H_a), respectively.

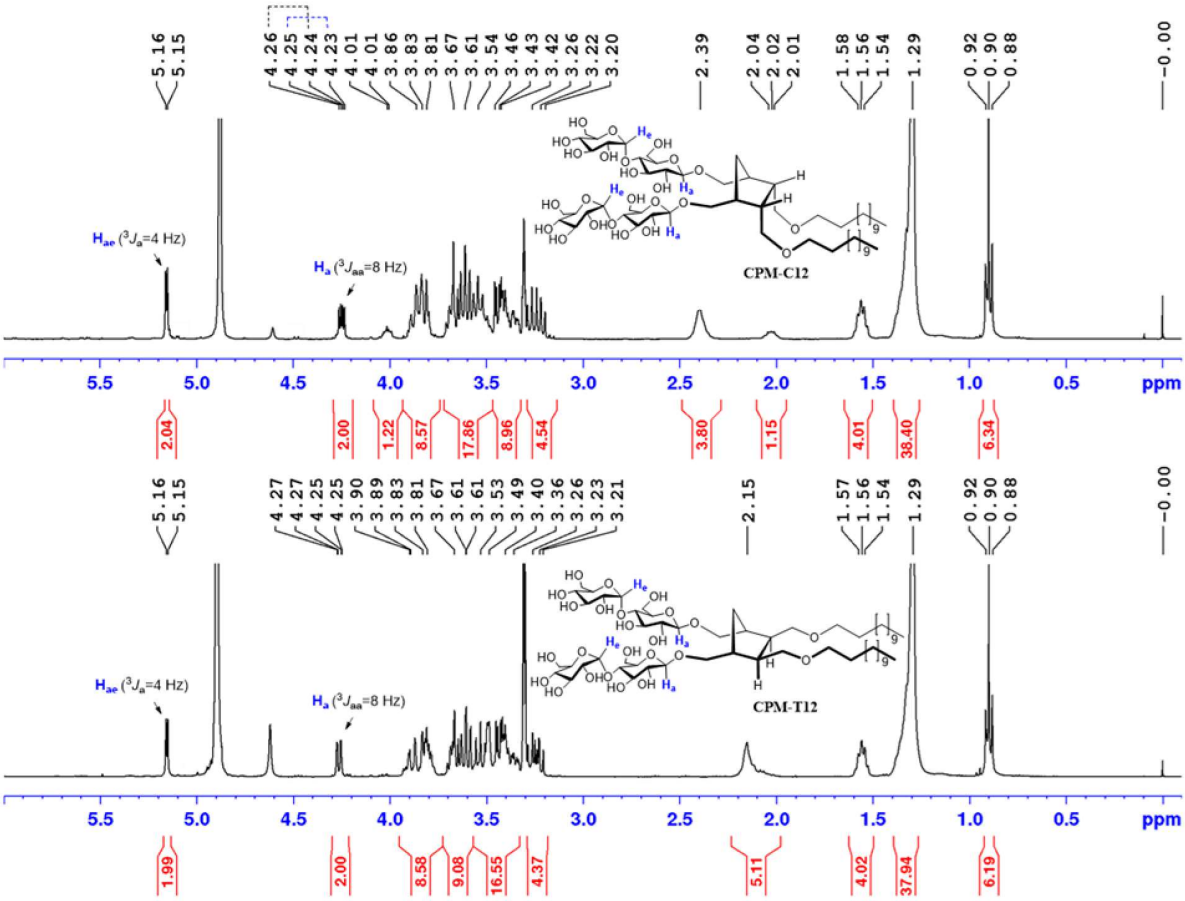

Figure S3. ^{1}H NMR spectra of CPM isomers (*top*) CPM-*C*12 and (*bottom*) CPM-*T*12). High diastereomeric purity of each isomer was confirmed by the respective ^{1}H NMR spectrum. A typical vicinal axial–axial coupling constant ($^{3}J_{aa}$ = 8.0 Hz) was observed for the β-anomeric protons (H_a) of both isomers, whereas a vicinal axial-equatorial coupling constant ($^{3}J_{ae}$ = 4.0 Hz) was observed for another anomeric proton with α-configuration (H_e). The two sets of anomeric protons (H_a and H_e) of the maltoside head group were indicated in the chemical structures. Assignments of the anomeric protons along with the measured coupling constants ($^{3}J_{aa}$ and $^{3}J_{ae}$) are given above the peaks in the spectra.

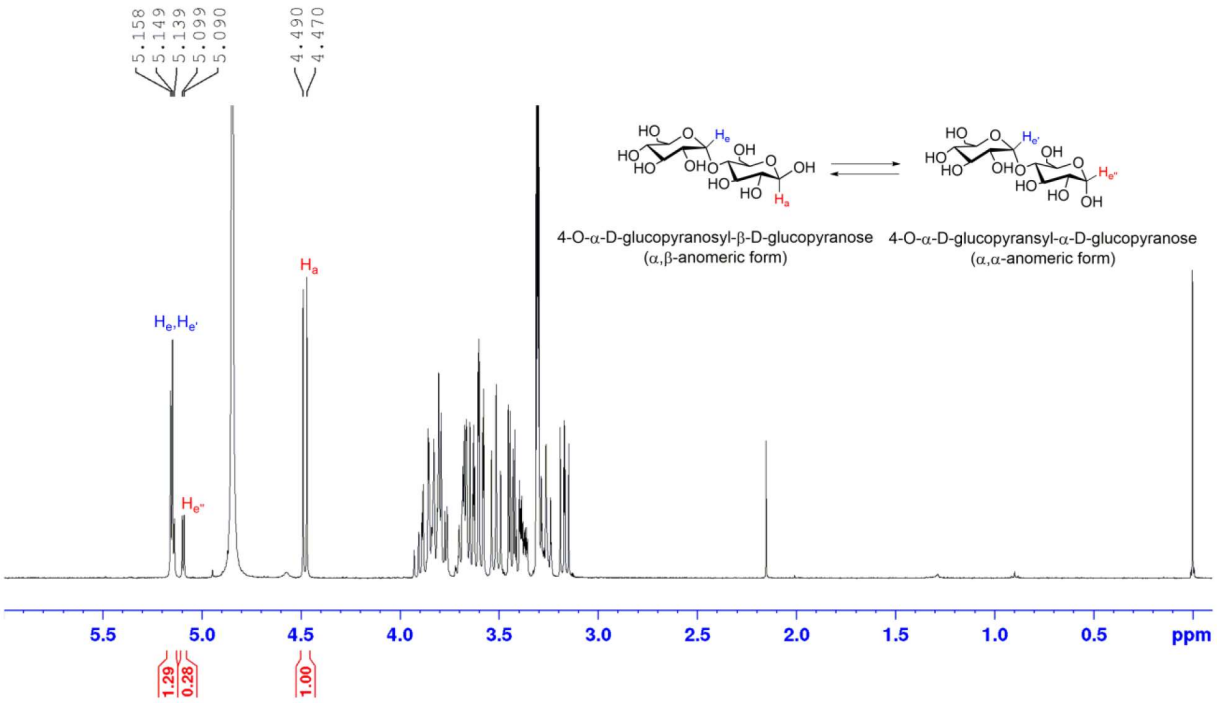

Figure S4. ^{1}H NMR spectrum of D-(+)-maltose in MeOD. For the measurement, D-(+)-maltose monohydrate purchased from Sigma-Aldrich was dissolved in water and then lyophilized. The chemical structures of two anomeric forms of D-(+)-maltoside were inserted for anomeric peak assignments. Due to ring-chain tautomerism, the α,α- and α,β-anomeric forms of D-(+)-maltose are present together at equilibrium. The peaks at 4.48 and 5.09 ppm correspond to α, β-anomeric form (*left* in the insert) of D-(+)-maltose, while the peaks at 5.14 and 5.15 ppm correspond to α, α-anomeric form (*right* in the insert).

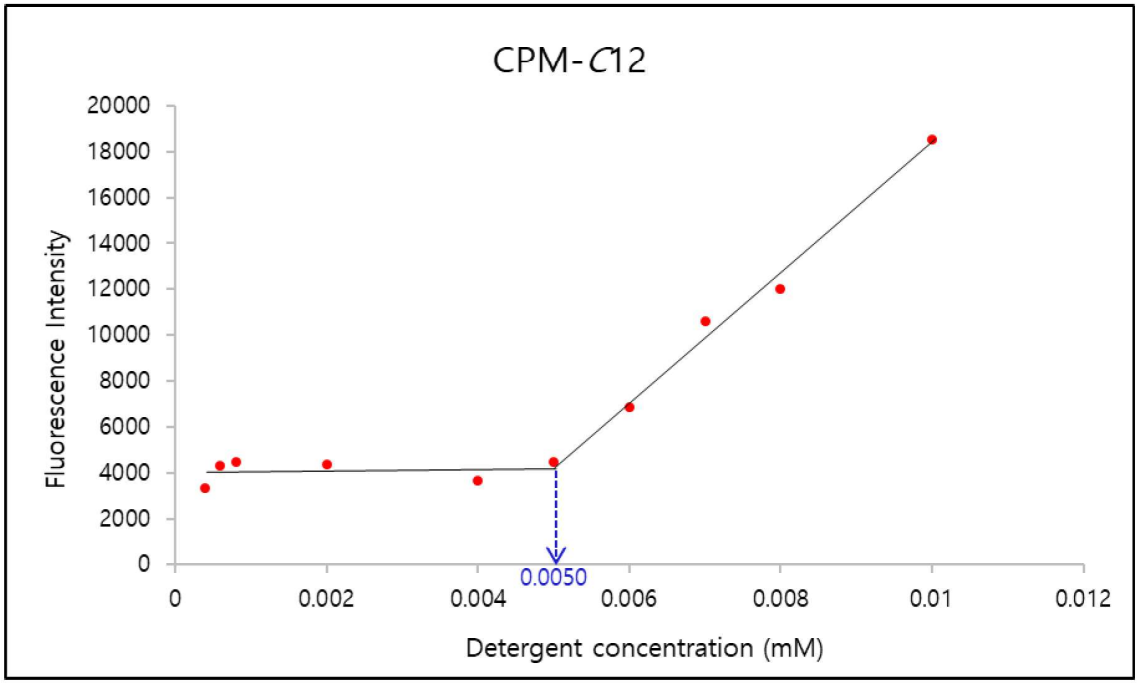

Figure S5. CMC determination of CPM-*C*12. Fluorescence intensity of CPM-*C*12 was monitored with increasing detergent concentration from 0.0006 to 0.01 mM. Detergent CMC was estimated by locating the intersection of two trend lines. This is a representative of three independent experiments.

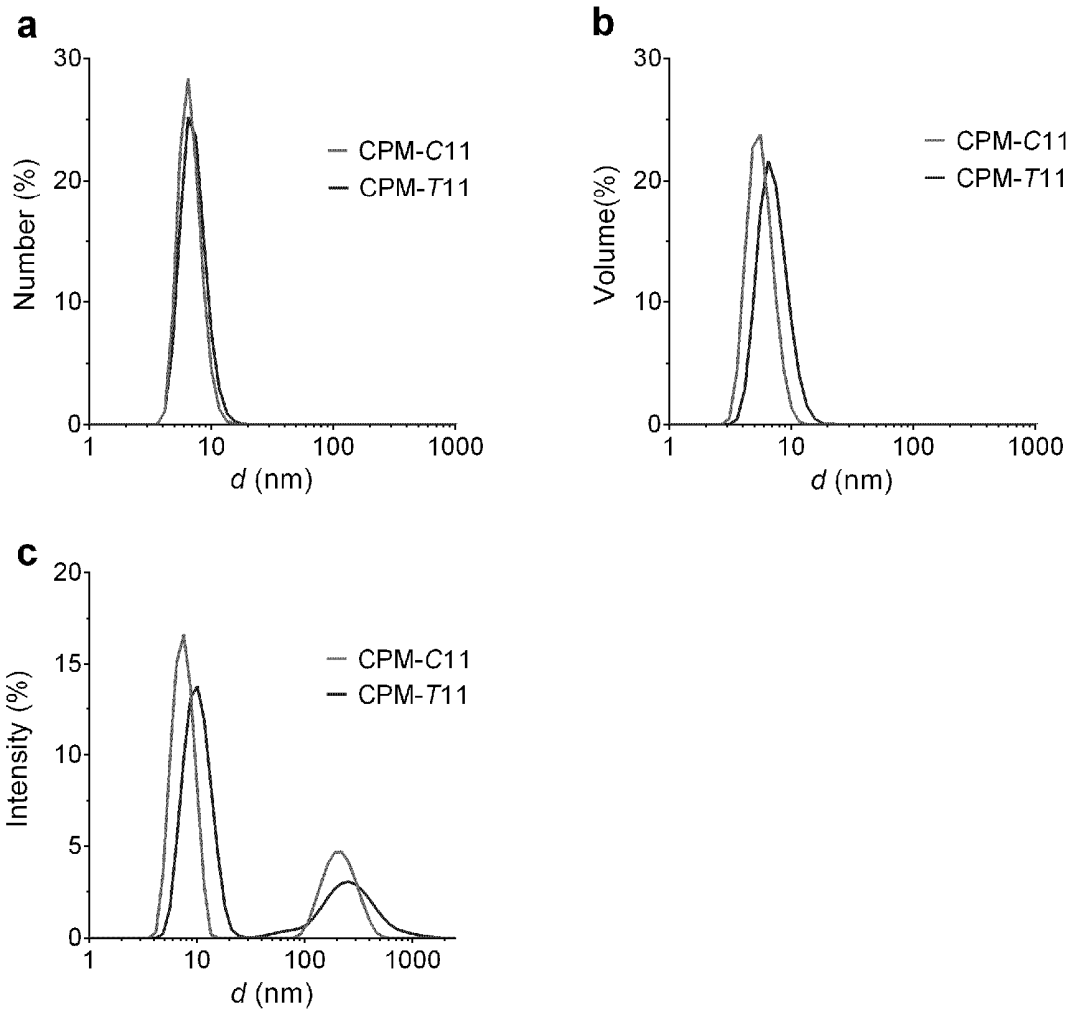

Figure S6. (a) Number-, (b) volume-, (c) intensity-weighted particle size distribution profiles derived with the aid of DLS for micelles formed by CPM-*C*11 and CPM-*T*11. Detergents were used at 1.0 wt%, and DLS measurements were carried out at 25 °C.

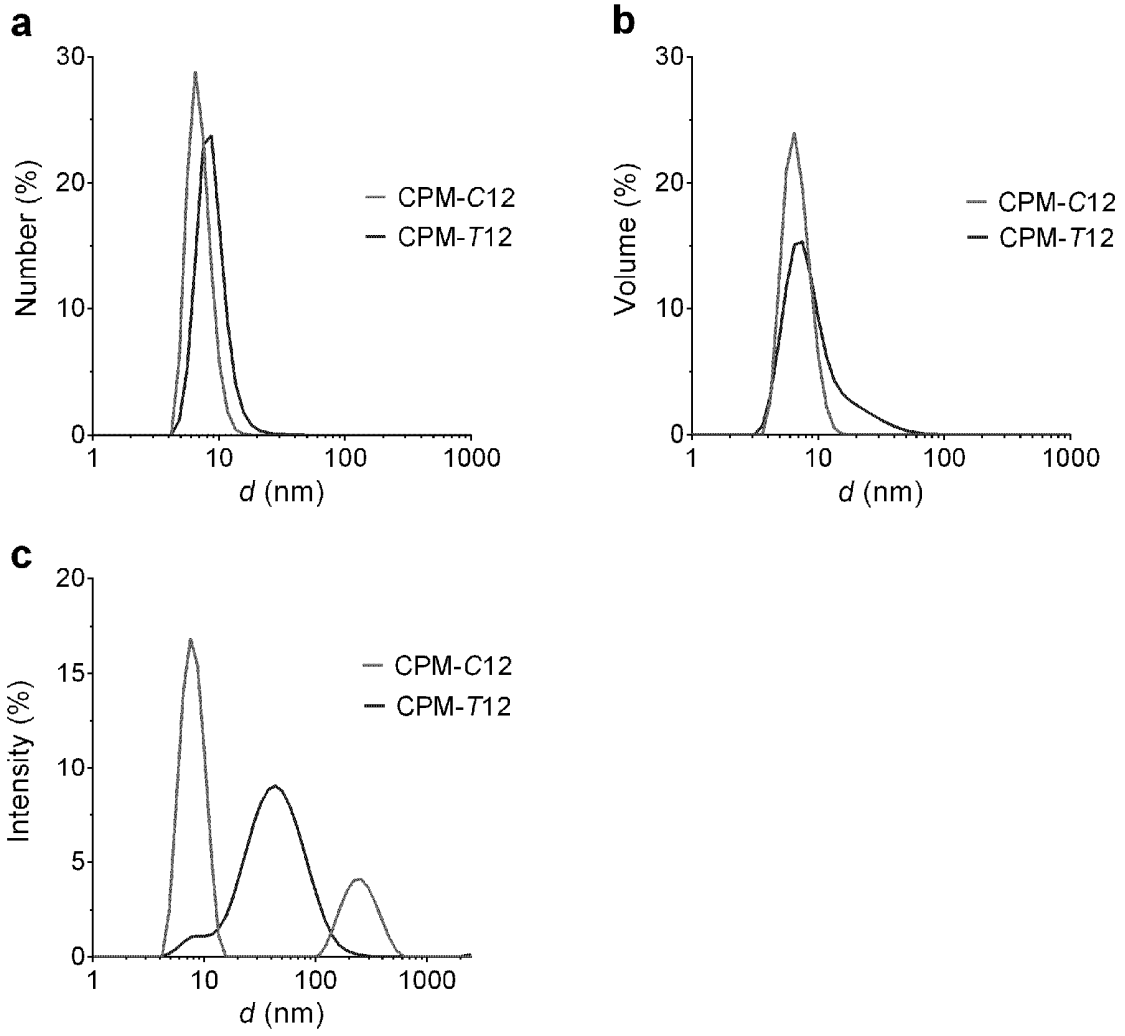

Figure S7. (a) Number-, (b) volume-, (c) intensity-weighted particle size distribution profiles derived with the aid of DLS for micelles formed by CPM-*C*12 and CPM-*T*12. Detergents were used at 1.0 wt%, and DLS measurements were carried out at 25 °C.

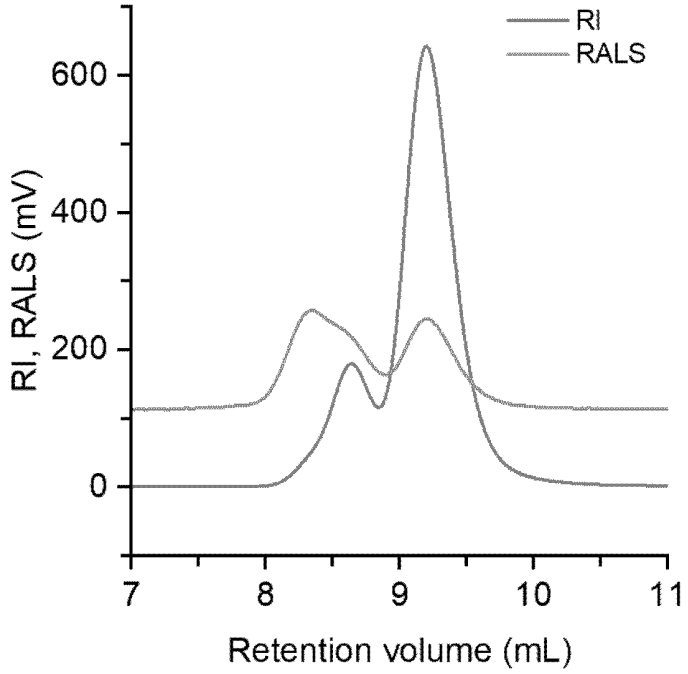

Figure S8. RI and RALS signals of bovine serum albumin (BSA) in SEC elution. These data were used as reference for determining N_{agg} of micelles formed by the detergents (X-NBM-C11 and CPM-*C*12).

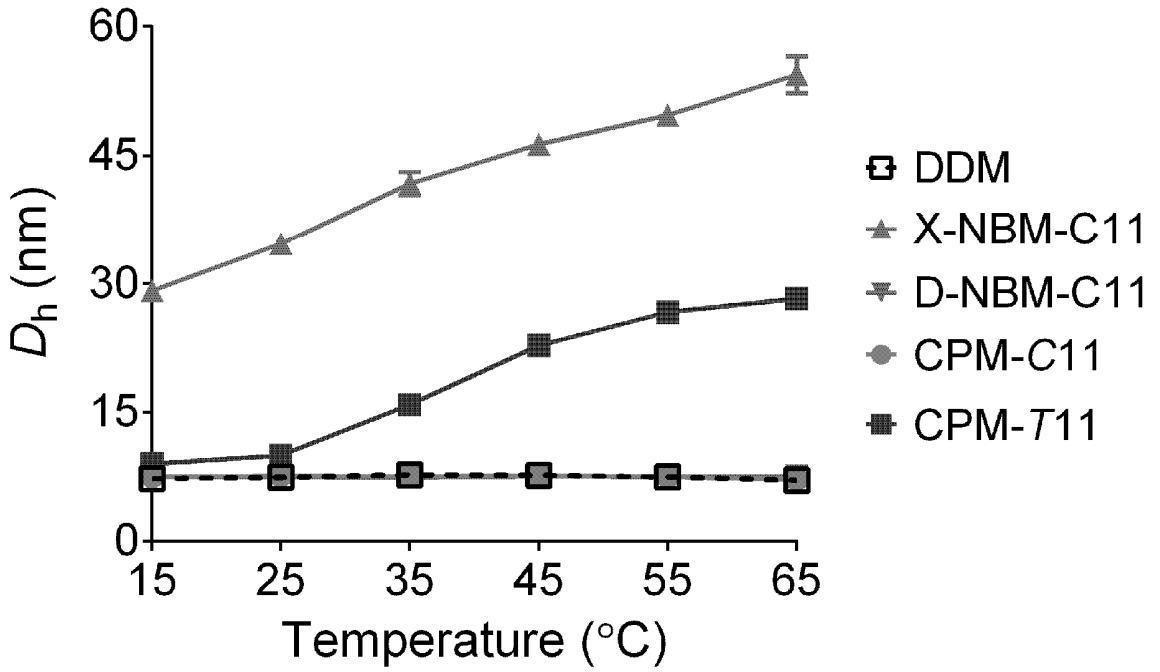

Figure S9. Temperature-dependent variation in the micelle sizes of DDM, D/X-NBM-C11, or CPM-*C11*/*T11*. The detergents were tested at 1.0 wt % in a range of temperature from 15 to 65 °C. Hydrodynamic diameters (D_h) were determined using DLS as described in the Methods section. Error bars, SD, $n = 4$.

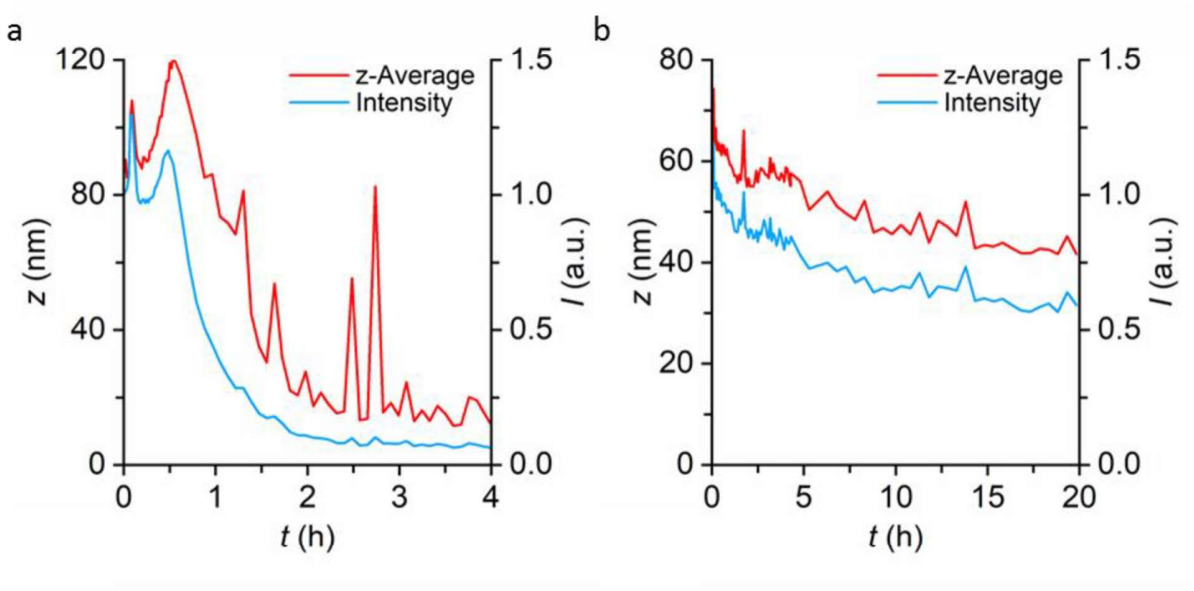

Figure S10. POPC vesicle solubilization by (a) CPM-*C*12 or (b) X-NBM-C11as monitored by static light scattering (intensity) and dynamic light scattering (*z*-average). POPC was used at 0.3 mM to form unilamellar vesicles that were mixed with 5 mM of individual detergents. The solubilization of POPC vesicles by CPM-*C*12 was completed within ~ 2 h (a), whereas for X-NBM-C11 complete solubilization took ~20 h (b).

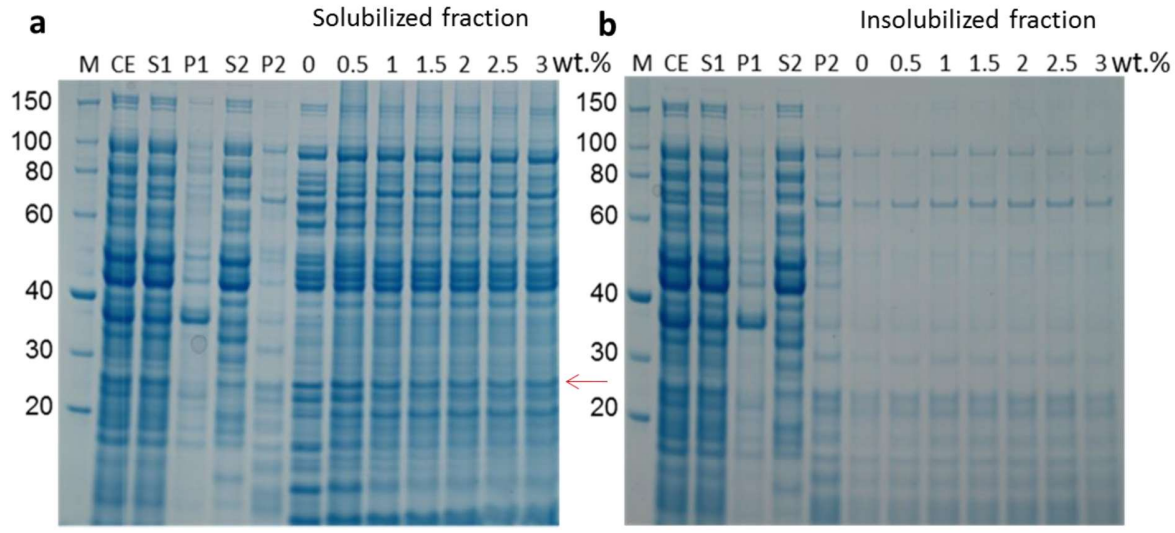

Figure S11. SDS-PAGE images containing the solubilized (a) and insolubilized fractions (b) after the treatment of *E. coli* BL21 membranes contained KvAP with different amounts of CPM-*C*12. M: Protein marker; CE: Crude extract; S1 and P1: Supernatant and pellet after the first centrifugation; S2 and P2: Supernatant and pellet after the second centrifugation; 0, 0.5, 1, 1.5, 2, 2.5 and 3 wt% are CPM-*C*12 concentrations used for protein extraction. The red arrow represents the KvAP signal (~25 kDa) in the solubilized fraction.

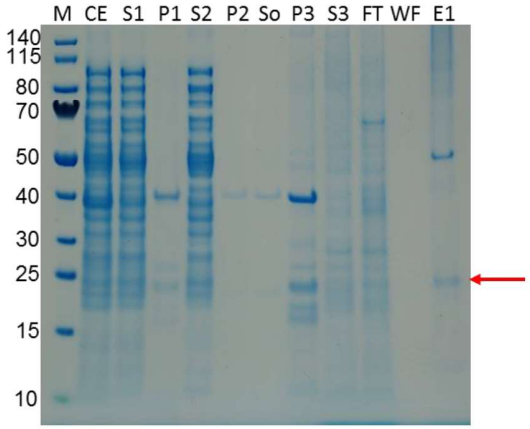

Figure S12. SDS-PAGE image showing the protein channel (KvAP) purified by immobilize metal affinity chromatography using Talon Co^{2+} beads. 1.0 wt % CPM-C12 was used for protein extraction. M: Protein marker; CE: Crude extract; S1 and P1: Supernatant and pellet after the first centrifugation; S2 and P2: Supernatant and pellet after the second centrifugation; So: Solubilized material; S3 and P3: Supernatant and pellet after the third centrifugation; FT: Flow through; WF: Washed fraction; E1: Eluted fraction. The red arrow represents the purified KvAP signal in eluted fraction after protein concentration using Amicon™ ultra centrifugal filter units with 10K MWCO).

Optical rotations

Optical rotations were measured with a Rudolph Research Analytical Autopol IV A1200-T polarimeter, [α] is given in degcm^{3}g^{-1}dm^{-1} and c is given in gcm^{-3}.

Detergent micelle size measurement by dynamic light scattering (DLS) experiment

The new agents (CPM-*C*s/CPM-*T*s) were dissolved individually in distilled and deionized water to give a detergent concentration of 1.0 wt %. These detergent solutions were filtered by a syringe filter with a pore size of 0.22 μm. The hydrodynamic radii of the micelles produced by the new agents were measured using a Malvern Zeta Sizer Nano ZS90 particle analyzer. With a maximum power of 5 mW, a He–Ne laser operating at 633 nm was used as the light source. The scattered light was collected at an angle of 90°, with temperature kept at 25 °C throughout all experiments. The hydrodynamic radius (R_h) of detergent micelles were calculated by autocorrelation analysis on time-dependent scattered light intensity. Hydrodynamic radius (R_h) values for micelles formed by the individual detergents were expressed as mean ± SD (n = 4). The micelle sizes of DDM, D/X-NBM-C11, and CPM-*C11*/*T11* were also measured with increasing temperature from 15 to 65 °C. Detergent micelle size was represented in terms of hydrodynamic diameter (D_h) and expressed as mean ± SD (n = 4).

Detergent CMC determination by diphenylhexatriene (DPH) encapsulation

Stock solutions containing 5.0 mM new agent (CPM-*C*s/CPM-*T*s) were prepared in deionized and distilled water. A series of detergent solutions with different concentrations were prepared from the stock solutions. 200 μL of each detergent sample was transferred to a 96-well plate in duplicate. A DPH stock solution was prepared by dissolving 3.0 mg DPH in 5.0 mL THF. 50 μL of the stock solution was diluted to 950 μL of distilled water to prepare a working solution and then 2.0 μL DPH working solution was added into each well containing a detergent solution. After ~15-20 min incubation at room temperature, fluorescence intensities were measured at 430 nm upon excitation at 358 nm using a Synergy Mx Monochromator-Based Multi-Mode Microplate reader. Detergent CMCs were determined by identifying the intersection of two trend lines in the plot of florescence intensity as a function of detergent concentrations. The detergent CMCs were obtained with triplicate and are expressed as mean ± SD (n = 3).

Aggregation number (N_{agg}) determination by size-exclusion chromatography

For either CPM-*C*12 or X-NBM-C11, 50 μL of 5 mM detergent samples in buffer (20 mM Tris, 100 mM NaCl, pH 7.4) were injected into the OmniSEC system (Malvern Instruments, Malvern, United Kingdom) equipped with a Superdex 75 10/300 SEC column (GE Healthcare) with a running buffer with 60 μM of the respective compound. All measurements were performed at 25 °C with a flow rate of 0.5 mL min^{-1}. The molar masses of detergent self-assemblies were calculated using the OmniSEC 11.01 software and were used to give aggregation numbers of the individual detergents (DDM, X-NBM-C11, and CPM-*C*12) (N_{agg} = molar masses of detergent self-assemblies / molar masses of detergents).

Solubilization of artificial, unilamellar lipid vesicles

Large unilamellar vesicles made of 1-palmitoyl-2-oleoyl-*sn*-glycero-3-phosphocholine (POPC) were prepared by dispersing the lipid powder in buffer (50 mM Tris, 200 mM NaCl, pH 7.4), vortexing for several minutes, and subsequent extrusion using a LiposoFast extruder (Avestin, Mannheim, Germany) with at least 35 extrusion steps through two stacked polycarbonate membranes with a pore diameter of 100 nm (Avestin). The hydrodynamic diameter of the LUVs was distributed around 120 nm, as verified by dynamic light scattering (DLS). Solubilization of POPC vesicles was monitored using a Nano Zetasizer S90 (Malvern Instruments), using a He–Ne Laser with a wavelength of 633 nm and a detection angle of 90°. To this end, 0.3 mM POPC vesicles and 5 mM detergent (X-NBM-C11 or CPM-*C*12) were mixed in a 3 mm x 3 mm quartz glass cuvette (Hellma, Munich, Germany) and the DLS measurements were immediately started after mixing without equilibration time.

Membrane-protein extraction from the native *E. coli* membranes

E. coli BL21(DE3) cells were transformed with an empty pET-24 vector and selected by kanamycin resistance. After incubation in lysogeny broth overnight under permanent agitation at 37 °C, the cells were harvested by centrifugation and subsequently washed with saline. The resulting pellets were resuspended in ice-cold alkaline buffer (100 mM Na_2CO_3, pH 11) and lysed by sonication using a sonopuls probe head (Bandelin, Berlin, Germany) (see below for a schematic protocol). The suspension was treated for 10 min with 0.4 s pulses and 0.6 s pauses. Subsequently, the lysate was centrifuged at 6000 *g* for 10 min. at 4°C to remove cell debris and residual intact cells. After ultracentrifugation (100,000 *g*, 4 °C, 1 h) the pellet was resuspended with a buffer (50 mM Tris, 200 mM NaCl, pH 7.4) and again ultra-centrifuged. Finally, the pellet was resuspended in a buffer to obtain a 100 g L^{-1} stock suspension. For protein solubilization, this membrane suspension was mixed 1:1 with detergent stocks (X-NBM-C11, CPM-*C*12, CPM-*T*12, or DDM) to give a desired membrane concentration of 50 g L^{-1} and incubated with an agitation for 16 hr. A subsequent ultracentrifugation (100,000 *g*, 4 °C, 1 h) separated residual bilayer fragments (P3) from mixed micelles (S3). Detergent-solubilized samples (S3) were analyzed using SDS-PAGE. Band intensity in each lane was further analyzed by densitometry using imageJ.[1] This experiment was carried out three or four times and the data are expressed as mean ± SEM (n = 3-4).

Detergent evaluation with diverse model membrane proteins

LeuT stability assay

Purification of the wild type leucine transporter (LeuT) from *Aquifex aeolicus* was performed according to the protocol described previously.[2] LeuT was expressed in *E. coli* C41 (DE3) transformed with pET16b encoding a C-terminally 8xHis-tagged LeuT. After isolation of bacterial membranes, the protein was solubilized by treatment of 1.0 wt% of DDM followed by immobilization to Ni^{2+}-NTA resin (Life Technologies). After ~2 hr incubation, the resin was washed extensively in wash buffer (20 mM Tris-HCl (pH 8.0), 1 mM NaCl, 199 mM KCl, 0.05 % DDM) and eluted with the addition of 300 mM imidazole. Subsequently, approx. 1.5 mg/ml protein stock was diluted ten-fold in identical buffer without DDM and imidazole, but supplemented with individual detergents (CPM-*C*s, CPM-*T*s, X-NBM-C11 or DDM

(control)) to a final detergent concentration of either CMC + 0.04 wt% or CMC + 0.2 wt%. The LeuT:detergent samples were stored for 13 days at room temperature and binding activity of the transporter was determined, at the indicated time points, using [^{3}H]-Leucine ([^{3}H]-Leu) via scintillation proximity assay (SPA).[3] The binding activity assay was performed with buffer (20 mM Tris-HCl, pH 8.0) containing 450 mM NaCl and the respective detergents at the concentrations specified above. The SPA reaction was carried out in the presence of 20 nM [^{3}H]-Leu and 1.25 mg/ml copper chelate (His-Tag) YSi beads (Perkin Elmer). YSi beads contain scintillants that emit light upon coming in close proximity to [^{3}H]-Leu. These beads are also coated with Cu^{2+} for the binding of His-tagged LeuT. Total [^{3}H]-Leu binding for the respective samples was measured using a MicroBeta liquid scintillation counter (PerkinElmer). Non-specific binding was determined in the presence of 1 mM leucine.

MelB$_{St}$ solubilization and thermal stability assay

A published protocol was used to evaluate detergent efficacy with MelB from *Salmonella typhimurium* (MelB$_{St}$).[4] The plasmid pK95ΔAHB/WT MelB$_{St}$/CH10 encoding the wild-type MelB$_{St}$ with a C-terminal 10-His tag was expressed in DW2 cells (*ΔmelB* and *ΔlacZY*). Cell growth and membrane preparation were carried out as reported.[5] Protein assays were carried out with a Micro BCA kit (Thermo Scientific, Rockford, IL). For the measurement of solubilization/stability, membrane samples containing MelB$_{St}$ (a final protein concentration was 10 mg mL^{-1}) in a solubilization buffer (20 mM sodium phosphate, pH 7.5, 200 mM NaCl, 10% glycerol, 20 mM melibiose) were mixed and incubated with 1.5 wt% of DDM, X/D-NBM-C11, or the individual CPMs (CPM-*C*11, CPM-*T*11, CPM-*C*12, and CPM-*T*12) for 90 min at 0 °C. The resulting detergent extracts were further incubated for another 90 min at an elevated temperature (45, 55, or 65 °C). Following ultracentrifugation at 355,590 *g* in a Beckman Optima™ MAX Ultracentrifuge using a TLA-100 rotor for 45 min at 4 °C, 20 μg of each protein sample was separated by SDS-16% PAGE, followed by immunoblotting with a Penta-His-HRP antibody (Qiagen, Germantown, MD). MelB$_{St}$ was detected using SuperSignal West Pico chemiluminescent substrate by the ImageQuant LAS 4000 Biomolecular Imager (GE Healthcare Life Science).

Preparation of RSO vesicles and Trp→D^{2}G FRET assay. RSO membrane vesicles were prepared from *E. coli* DW2 cells containing MelB$_{St}$ or MelB$_{Ec}$ by osmotic lysis.[6-8] The RSO membrane vesicles in a buffer (pH 7.5) containing 100 mM KP$_i$ and 100 mM NaCl at a protein concentration of 1 mg mL^{-1} were treated with 1.0 % DDM, CPM-*C*11, CPM-*T*11, or CPM-*C*12 at 23 °C for 30 min and subjected to ultracentrifugation using TLA 120.2 rotor at >300,000 *g* for 45 min at 4 °C. The supernatants were applied for Trp→D^{2}G FRET experiments using an Amico-Bowman Series 2 (AB2) Spectrofluorometer. Tryptophan residues were excited at 290 nm,[7] and Trp→D^{2}G FRET was recorded at 465 nm and 490 nm for MelB$_{Ec}$ and MelB$_{St}$, respectively. On a time trace, 10 μM D^{2}G and excess melibiose or equal volume of water were added at 1-min and 2-min points, respectively.

β_2AR stability assay

Soluble radioligand binding assay

The β_2AR in 0.1% DDM was purified based on the protocol as reported before and finally concentrated to around 10 mg/ml (approximately 200 μM).[9] The DDM-purified β_2AR was used to prepare a master binding mixture containing 10 nM [^{3}H]-dihydroalprenolol (DHA) supplemented with 0.5 mg/ml BSA, in 0.2% DDM/CPM-*C*s/CPM-*T*s, respectively. Activity of the detergent-purified receptor at 0.2 pmol was monitored at the regular intervals during a 6-day incubation at room temperature. Receptor activity was measured by the soluble radioactive ligand binding assay described below. The receptor purified in DDM or individual detergents (DDM, X/D-NBM-C11, CPM-*C*s, or CPM-*T*s) was incubated with 10 nM [^{3}H]-DHA for 30 min at room temperature. The mixture was loaded on a G-50 column and collected the follow-through with 1 mL binding buffer (20 mM HEPES pH 7.5, 100 mM NaCl, supplemented with 0.5 mg mL^{-1} BSA and 20 × CMC individual detergents), and further filled with 15 mL scintillation fluid. Receptor-bound [^{3}H]-DHA was measured with a scintillation counter (Beckman). Non-specific binding of [^{3}H]-DHA was calculated by adding 2 μM alprenolol (Sigma) in the same binding reaction. Each experiment was performed in triplicate.

MOR stability assay

CPM assay

N-[4-(7-diethylamino-4-methyl-3-coumarinyl)phenyl] maleimide (CPM) dye in DMSO (3 mg/ml stock) was diluted 40-fold into buffer containing 20 mM HEPES pH 7.5 and 150 mM NaCl. The mouse μ-opioid receptor (~ 4 μM) was purified in DDM (0.05%)/CHS (0.005%) with naloxone as described.[9] Differential scanning fluorimetry assays were performed in 96-well PCR plates using a real-time PCR machine (CFX96, Bio-Rad). Standard assay was performed using 50 μL samples including 20 mM HEPES pH 7.5, 100 mM NaCl, 0.5% detergent. The protein and CPM final concentrations were 0.75 and 20 μM, respectively. The receptor was first incubated with 1% individual detergents (DDM, LMNG, X-NBM-C11, CPM-*C*11/*C*12 or CPM-*T*11/*T*12) (25 μL) at 4 °C for 30 min to allow detergent exchange. Then CPM dye was added and mixed before scanning in the PCR machine. The fluorescence intensity was measured with increasing temperature from 15 to 70 °C by using the FAM filter set. The negative first order derivatives of relative fluorescence units (-*d*RFU/*d*T) were calculated from the individual CPM profiles to obtain the melting temperatures (T_ms) of the receptor, x-values corresponding to the minimum point of –*d*RFU/*d*T.

KvAP solubilization assay

Expression and solubilization protocol

The protocol for purifying KvAP followed a previously described method[11] with slight modification. 1 L of LB medium containing 100 μg mL^{-1} ampicillin was inoculated with 40 mL overnight preculture of *E. coli* BL21 harboring the plasmid pQE60, into which C-terminal hexa-histidine tag cDNA of the potassium ion channel of *Aeropyrum pernix* (KvAP) was cloned. When the culture reached an OD_{600} roughly 0.8-1.0 protein expression was induced by the addition of 0.4mM isopropyl-β-D-thiogalactopyranoside (IPTG) supplemented with 10 mM $BaCl_2$ for 4 hr at 37 °C. Cells were harvested by centrifugation for 15 min at 4 °C and 7000 *g*. Pellets were washed with a buffer (25 mM Tris, 100 mM KCl, 1 mM $MgCl_2$ pH 8.0).

Cells were resuspended (1:3 wt/v) in the same buffer containing EDTA free proteinase inhibitors and benzonase. Cell disruption was performed by four cycles of 6 min each of 5 s pulse, 10 s pause and 40% amplitude (Bandelin sonoplus MS73). The cell lysate (CE) was centrifuged for 15 min at 4 °C and 7000 *g* and the obtained supernatant (S1) was ultra-centrifuged for 90 min at 4 °C and 100,000 *g*. The resulting membrane fraction (P2) was weighed and resuspended to 60 mg mL^{-1} in a solubilization buffer containing 25 mM Tris, 100 mM KCl, 2 mM TCEP, and 1.0 wt % CPM-*C*12 pH 8.0. Solubilization was performed for three hours at room temperature with gently shaking. Non-solubilized material (P3) was removed by ultracentrifugation at 4 °C and 100,000 *g* during 90 min. The resulting supernatant fraction containing solubilized material (S3) was retained for KvAP purification.

Protein (KvAP) purification protocol

Immobilized metal affinity chromatography purification of the potassium channel was performed using a batch procedure. A volume of 10 mL of solubilized material was incubated with 2 mL of Talon Co^{2+} beads at 4 °C with gentle agitation. After 16 hr, the whole material was packed in a column and washed with 20 column volumes of a buffer (25 mM Tris, 100 mM KCl, 1 mM $MgCl_2$, 0.25 wt % CPM-*C*12, pH 8.0). KvAP was eluted by addition of 1.5 column volumes of elution buffer containing 25 mM Tris, 100 mM KCl, 1 mM $MgCl_2$, 0.25 wt % CPM-*C*12, 400 mM imidazole, pH 8.0. Eluted fractions (E) were pooled and concentrated using Amicon™ ultra centrifugal filter units 10 kDa MWCO.

Western Blot Detection Method (for KvAP)

Samples were mixed with 200 mM dithiothreitol (DTT) and SDS loading buffer (106 mM Tris HCl, 141 mM Tris Base, 2% SDS, 10% Glycerol, 0.51 mM EDTA, 0.22 mM SERVA Blue G250, 0.175 mM Phenol Red pH 8.5) and loaded onto an NuPAGE™ 4-12% Bis-Tris gel. After electrophoresis, proteins were transferred (15 V, 18 minutes) onto a PVDF membrane and incubated with blocking buffer (3% albumin in PBS). The membranes were washed with PBS-T (PBS buffer containing 0.1% Tween-20) and incubated 1 hr with the antibody His Tag primary Antibody at a dilution of 1:3000 in PBS-T. PVDF membrane was successively washed with PBS-T and PBS and then incubated with anti-Mouse IgG (Fc specific) alkaline phosphatase secondary antibody at a dilution of 1:1500 in PBS-T. After washing, signals were detected by color detection using nitroblue-tetrazolium and 5-bromo-4-chloro-2-indoxylphosphate (NBT/BCIP) as substrate.

Amphiphile Synthesis

General procedure for dialkylation (step a)

NaH (3.0 equiv.) and commercially available **compound A** or **G** (1 equiv., 500 mg) were dissolved in DMF (15 mL) at 0°C. Alkyl iodide (2.9 equiv.) was added dropwise, and the resulting solution was stirred at 70°C for 3 days. After completion of the reaction (as detected by TLC), the solution was diluted with diethyl ether (150 mL) and the washed successively with 1 M aqueous HCl (2 x 20 mL) and brine (100 mL). The organic layer was dried with anhydrous Na_2SO_4, and the solvent was removed by rotary evaporation. The residue was purified by silica gel column chromatography (EtOAc/hexane) providing a desired product (**B** or **H**) as a liquid.

General procedure for Upjohn Dihydroxylation (step b)

A solution of NMO (1.5 equiv.) in water (50 wt. %) was added to a mixture of THF and water (15 mL of a 9:1 mixture) at 0°C. **Compound B** or **H** (500 mg, 1.5 equiv.) was then added in one portion, the mixture allowed to stir for 15 minutes and then OsO_4 (1.4 mL of a 2.5 wt. % solution in t-BuOH) was added dropwise by syringe over 20 minutes. The mixture was stirred at room temperature for 5days. The reaction was quenched by the addition of sodium sulfite (8.0 g) and diluted with water (30 mL). The solution was then extracted with EtOAc (2 × 70 mL). The combined organic extracts were dried with anhydrious Na_2SO_4 and concentrated in vacuo and the residue was purified by silica gel column chromatography (EtOAc/hexane) providing a desired diol (**C** or **I**) as an orange gum.

General procedure for step c (two steps; periodate oxidative cleavage of 1,2-diol, followed by $NaBH_4$ reduction)

To a vigorously stirred suspension of chromatographic grade silica gel (1.1 g) in DCM (5 mL) was added dropwise a saturated aqueous solution of $NaIO_4$ (1.5 equiv.) whence a flaky suspension was formed. A solution of compound **C** or **I** (550 mg, 1 equiv.) in DCM (10 mL) was then added and the reaction was stirred for 3 hours. The mixture was filtered on a sintered glass, and the silica gel was thoroughly washed with DCM (50 mL). Concentrated in vacuum to remove DCM and then was dissolved in EtOH (20 mL). $NaBH_4$ (4 equiv.) was added to the cooled solution at 0°C. After stirring at 0°C for 3 hours, the reaction mixture was acidified with ambulate IR 120 resin until litmus paper showed neutral. All solvents were removed and residue was purified by silica gel column chromatography (EtOAc/hexane) providing a desired diol (**D** or **J**) as an orange gum.

General procedures for glycosylation reactions (step d)

This procedure followed a literature method[11] with slight modification. A mixture of **compound D** or **J** (1 equiv., 250 mg), AgOTf (2.4 equiv.) and collidine (1.0 equiv.) in anhydrous CH_2Cl_2 (40 mL) was stirred at -45°C. A solution of 2.4 equiv. of perbenzoylatedmaltosylbromide in CH_2Cl_2 (10 mL) was added dropwise over 0.5 h to this suspension. Stirring was continued for 0.5 h at -45°C, and then the reaction mixture was allowed to warm to 0°C and left stirring for 1 h. After completion of the reaction, pyridine was added to

the reaction mixture, and it was diluted with CH_2Cl_2 (40 mL) before being filtered through celite. The filtrate was washed successively with a 1 M aqueous $Na_2S_2O_3$ (40 mL), a 0.1 M aqueous HCl solution (40 mL), and brine (2 x 40 mL). The organic layer was dried with anhydrous Na_2SO_4, and the solvent was removed by rotary evaporation. The residue was purified by silica gel column chromatography (EtOAc/hexane), which provided the desired product (**E** or **K**) as a white solid.

General procedures for deprotection reactions (step e)

This procedure followed the de-*O*-benzoylation or de-O-acetylation under Zemplén's conditions.[12] The *O*-protected **compounds E** or **K** were dissolved in MeOH and treated with the required amount of a methanolic solution of 0.5 M NaOMe such that the final concentration of NaOMe was 0.05 M. The reaction mixture was stirred for 14 h at room temperature, and then neutralized with Amberlite IR-120 resin (H^+ form). The resin was removed by filtration and washed with MeOH, and the solvent was removed from the combined filtrate *in vacuo*. The residue was purified by silica gel column chromatography (eluting with MeOH/CH_2Cl_2). Further purification, by recrystallization using CH_2Cl_2/MeOH/diethyl ether, afforded fully deprotected final product (**F** or **L**) as a white solid.

Supplementary scheme 1

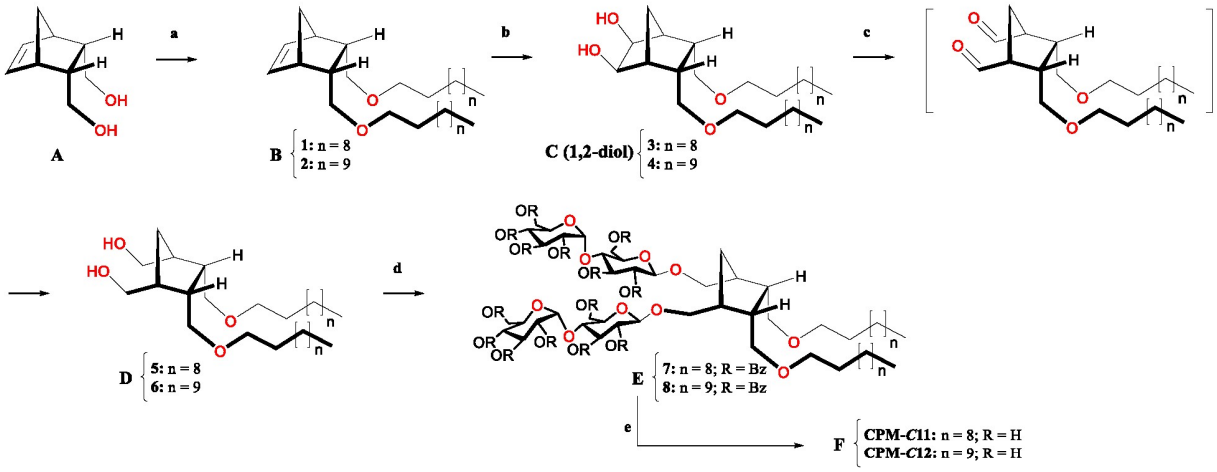

(a) alkyl iodide, NaH, 0°C → 70°C, 81-84%; (b) OsO_4, NMO, THF, H_2O, 0°C → room temperature, 5 days, 95-97%; (c) (i) $NaIO_4$, DCM, H_2O, room temperature, 3 hr (ii) $NaBH_4$, EtOH, 0°C, 3 hr, 92-94% (for two steps); (d) perbenzoylated malotsylbromide, AgOTf, DCM, -45°C → 0°C, 84-87%; (d) NaOMe, MeOH, room temperature, 14 hr, 94-96%.

Compound **1** was prepared in 81% yield according to the general procedure for dialkylation. **^{1}H NMR** (400 MHz, $CDCl_3$): δ 6.11 (s, 2H), 3.37-3.30 (m, 4H), 3.22 (dd, *J* = 11.8 Hz, 8.0 Hz, 2H), 3.00 (t, *J* = 8.0 Hz, 2H), 2.91 (br s, 2H), 2.45 (br s, 2H), 1.56-1.45 (m, 4H), 1.46 (d, *J* = 12.2 Hz, 1H), 1.38-1.21 (m, 34H), 0.88 (t, *J* = 7.9 Hz, 6H); **13C NMR** (100 MHz, CDCl3): δ 135.4, 71.2, 71.0, 49.2, 45.8, 41.6, 32.1, 29.9, 29.8, 29.7, 29.6, 26.5, 22.9, 14.3.

Compound **2** was prepared in 84% yield according to the general procedure for dialkylation. **^{1}H NMR** (400 MHz, $CDCl_3$): δ 6.11 (s, 2H), 3.37-3.30 (m, 4H), 3.22 (dd, *J* = 11.8 Hz, 8.0 Hz, 2H), 3.00 (t, *J* = 8.0 Hz, 2H), 2.91 (br s, 2H), 2.45 (br s, 2H), 1.56-1.52 (m, 4H), 1.46 (d, *J* = 12.2 Hz, 1H), 1.38-1.21 (m, 36H), 0.88 (t, *J* = 7.9 Hz, 6H); **13C NMR** (100 MHz, CDCl3): δ 135.5, 71.3, 71.0, 49.3, 45.8, 41.7, 32.1, 30.0, 29.9, 29.8, 29.7, 29.6, 26.5, 22.9, 14.3.

Compound **3** was prepared in 95% yield according to the general procedure for upjohn dihydroxylation. **^{1}H NMR** (400 MHz, $CDCl_3$): δ 4.00 (br s, 2H), 3.44 (dd, *J* = 8.2 Hz, 4.1 Hz, 2H), 3.37 (t, *J* = 7.9 Hz, 6H), 3.13 (br s, 2H), 2.26 (br s, 4H), 1.88 (d, *J* = 7.8 Hz, 1H), 1.60-1.53 (m, 4H), 1.39-1.17 (m, 34H), 0.88 (t, *J* = 7.8 Hz, 6H); **13C NMR** (100 MHz, CDCl3): δ 71.5, 69.6, 68.1, 47.3, 38.7, 33.2, 32.1, 29.9, 29.8, 29.7, 29.5, 26.4, 22.9, 14.3.

Compound **4** was prepared in 97% yield according to the general procedure for upjohn dihydroxylation. **^{1}H NMR** (400 MHz, $CDCl_3$): δ 4.00 (br s, 2H), 3.42 (dd, *J* = 8.2 Hz, 4.1 Hz, 2H), 3.35 (t, *J* = 7.9 Hz, 6H), 3.17 (br s, 2H), 2.24 (br s, 4H), 1.86 (d, *J* = 8.0 Hz, 1H), 1.55-1.52 (m, 4H), 1.39-1.17 (m, 38H), 0.86 (*t*, J = 7.8 Hz, 6H); **13C NMR** (100 MHz, CDCl3): δ 71.5, 69.6, 68.1, 47.3, 38.8, 33.2, 32.1, 29.9 (2C), 29.8, 29.7, 29.6, 26.4, 22.9, 14.3.

Compound **5** was prepared in 92% yield according to the general procedure for periodate oxidative cleavage of 1,2-diol, followed by $NaBH_4$ reduction. **^{1}H NMR** (400 MHz, $CDCl_3$): δ 3.75-3.34 (m, 12H), 2.48-2.31

(m, 4H), 1.85-1.83 (m, 1H), 1.57 (br s, 4H), 1.39-1.17 (m, 32H), 0.88 (*t*, J = 7.8 Hz, 6H); **^{13}C NMR** (100 MHz, CDCl3): δ 71.6, 68.6, 64.0, 43.2, 43.0, 32.0, 30.0, 29.8, 29.7, 29.6 (2C), 29.5, 29.4, 26.2, 22.8, 14.2.

Compound **6** was prepared in 94% yield according to the general procedure for periodate oxidative cleavage of 1,2-diol, followed by $NaBH_4$ reduction. **^{1}H NMR** (400 MHz, $CDCl_3$): δ 3.49-3.38 (m, 12H), 2.47-2.28 (m, 4H), 1.82-1.79 (m, 1H), 1.57 (br s, 4H), 1.39-1.17 (m, 36H), 0.85 (*t*, J = 7.8 Hz, 6H); **^{13}C NMR** (100 MHz, CDCl3): δ 71.8, 68.7, 64.2, 43.4, 43.1, 32.1, 30.0, 29.8 (2C), 29.7, 29.6 (2C), 29.5, 29.4, 26.3, 22.9, 14.3.

Compound **7** was prepared in 84% yield according to the general procedure for glycosylation reaction. **^{1}H NMR** (400 MHz, $CDCl_3$): δ 8.11-7.64 (m, 42H), 7.42-7.19 (m, 60H), 6.21-2.97 (m, 42H), 3.15-3.00 (m, 8H), 2.22 (br s, 4H), 1.49-1.23 (m, 32H), 0.88 (app. t, *J* = 4.0 Hz, 6H); **^{13}C NMR** (100 MHz, CDCl3): δ 166.3 (2C), 166.1, 165.9, 165.8, 165.7, 165.5, 165.2 (2C), 165.0, 164.8, 164.4, 133.4 (2C), 133.2, 133.1, 130.2, 130.1, 130.0, 129.9 (2C), 129.7 (3C), 129.5 (2C), 129.1, 129.0, 128.9 (2C), 128.8, 128.7 (2C), 128.6, 128.5 (3C), 128.3 (2C), 128.2, 128.1, 99.6, 98.7, 97.2, 97.0, 75.3, 75.0, 74.9, 74.3, 73.9, 72.8, 72.5, 71.8, 71.6, 71.3, 71.2, 71.1, 70.6, 70.2, 69.2 (2C), 68.2, 67.5, 64.7, 64.1, 62.7, 62.6, 60.5, 46.5, 44.7, 38.6, 37.8, 33.9, 32.1 (2C), 30.1, 29.9, 29.8, 29.7, 29.6, 29.5 (2C), 26.5, 26.4, 22.9, 14.3.

Compound **8** was prepared in 87% yield according to the general procedure for glycosylation reaction. **^{1}H NMR** (400 MHz, $CDCl_3$): δ 8.09-7.74 (m, 42H), 7.40-7.19 (m, 60H), 6.11-2.97 (m, 42H), 3.15-2.96 (m, 8H), 2.22 (br s, 4H), 1.49-1.23 (m, 34H), 0.87 (app. t, *J* = 4.0 Hz, 6H); **^{13}C NMR** (100 MHz, CDCl3): δ 166.2 (2C), 166.1, 166.0, 165.9, 165.8, 165.7, 165.5, 165.2 (2C), 165.0, 164.8, 164.4, 133.4 (2C), 133.2, 133.1, 130.2, 130.1, 130.0, 129.9 (2C), 129.7 (3C), 129.5 (2C), 129.1, 129.0, 128.9 (2C), 128.8, 128.7 (2C), 128.6, 128.5 (3C), 128.3 (2C), 128.2, 128.1, 99.6, 98.7, 97.2, 97.0, 75.3, 75.0, 74.9, 74.3, 73.9, 72.8, 72.5, 71.8, 71.6, 71.3, 71.2, 71.1, 70.6, 70.2, 69.2 (2C), 68.2, 67.5, 64.7, 64.1, 62.8, 62.6, 60.5, 46.5, 44.7, 38.7, 37.8, 33.9, 32.1 (2C), 30.1, 29.9, 29.8, 29.7, 29.5 (3C), 26.5, 26.4, 22.8, 14.3.

CPM-*C*11 was prepared in 94% yield according to the general procedure for deprotection reaction (purity: ~ 94% based on ^{1}H NMR spectrum). $[\alpha]^{20}_D$ = +51 ($c = 0.16 \times 10^{-2}$, MeOH, *l* = 1 dm); **^{1}H NMR** (400 MHz, CD_3OD): δ 5.15 (app. d, *J* = 4.0 Hz, 2H), 4.25 (d, *J* = 8.0 Hz, 1H), 4.24 (d, *J* = 8.0 Hz, 1H), 4.03 (m, 1H), 3.89-3.81 (m, 9H), 3.70-3.19 (m, 33H), 2.40 (br s, 4H), 2.03 (br s, 1H), 1.56 (app. t, *J* = 8.0 Hz, 4H), 1.42-1.28 (m, 35H), 0.90 (t, *J* = 8.0 Hz, 6H); **^{13}C NMR** (100 MHz, CD3OD): δ 104.7, 103.1, 81.5, 78.0, 76.7, 75.2, 74.9, 74.8, 74.3, 72.8, 72.7, 72.3, 71.6, 69.8, 62.9, 62.3, 44.6, 44.5, 41.6, 33.3, 31.0 (2C), 30.8, 30.7, 27.7, 23.9, 14.7; HRMS (EI): calcd. for $C_{55}H_{102}O_{24}Na^+$ $[M+Na]^+$ 1169.6659, found 1169.6663.

CPM-*C*12 was prepared in 96% yield according to the general procedure for deprotection reaction (purity: ~ 96% based on ^{1}H NMR spectrum). $[\alpha]^{21}_D$ = +43 ($c = 0.12 \times 10^{-2}$, MeOH, *l* = 1 dm); **^{1}H NMR** (400 MHz, CD_3OD): δ 5.16 (app. d, *J* = 4.0 Hz, 2H), 4.25 (d, *J* = 8.0 Hz, 1H), 4.24 (d, *J* = 8.0 Hz, 1H), 4.01 (m, 1H), 3.89-3.81 (m, 9H), 3.67-3.20 (m, 31H), 2.39 (br s, 4H), 2.02 (br s, 1H), 1.56 (app. t, *J* = 8.0 Hz, 4H), 1.42-1.28 (m, 38H), 0.90 (t, *J* = 8.0 Hz, 6H); **^{13}C NMR** (100 MHz, CD3OD): δ 104.7, 104.6, 103.1, 81.5, 78.0 (2C), 76.7, 75.2, 74.9, 74.8, 74.4, 74.3, 72.8, 72.7, 72.3, 71.6, 69.8, 62.9, 62.3, 44.6, 44.5, 41.6, 34.1, 33.2, 31.0 (3C), 30.8, 30.7, 27.7, 23.9, 14.6; HRMS (EI): calcd. for $C_{57}H_{106}O_{24}Na^+$ $[M+Na]^+$ 1197.6972, found 1197.6970.

Supplementary scheme 2

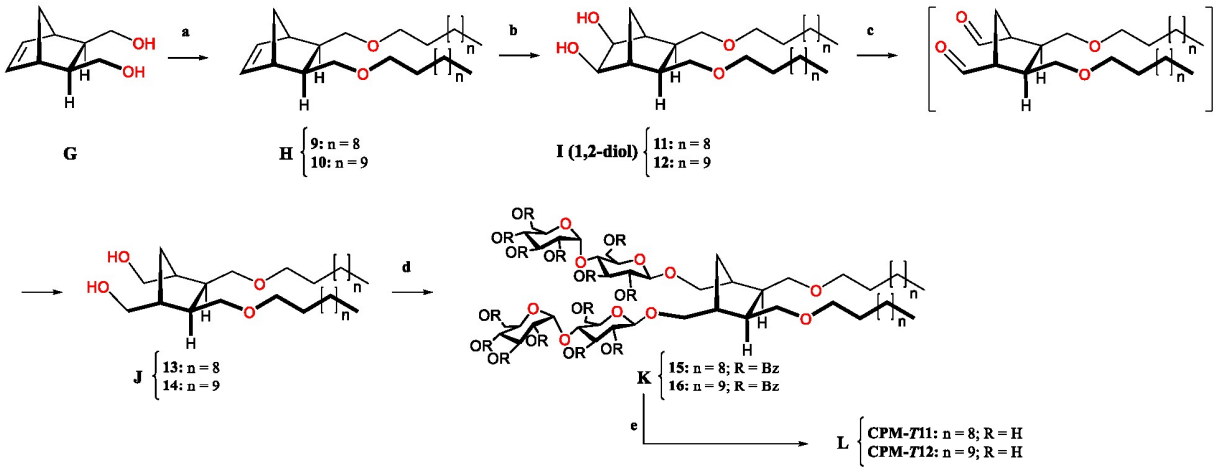

(a) alkyl iodide, NaH, 0°C → 70°C, 85-87%; (b) OsO_4, NMO, THF, H_2O, 0°C → room temperature, 5 days, 91-94%; (c) (i) $NaIO_4$, DCM, H_2O, room temperature, 3 hr (ii) $NaBH_4$, EtOH, 0°C, 3 hr, 88-92% (for two steps); (d) perbenzoylated malotsylbromide, AgOTf, DCM, -45°C → 0°C, 94-97%; (d) NaOMe, MeOH, room temperature, 14 hr, 95-97%.

Compound **9** was prepared in 85% yield according to the general procedure for dialkylation. **^{1}H NMR** (400 MHz, $CDCl_3$): δ 6.14 (t, *J* = 4.2 Hz, 2H), 3.56 (dd, *J* = 8.0 Hz, 4.0 Hz, 2H), 3.41-3.36 (m, 4H), 3.27 (app. t, *J* = 7.8 Hz, 2H), 2.74 (t, *J* = 4.4 Hz, 2H), 1.77-1.75 (m, 2H), 1.60-1.53 (m, 4H), 1.48 (d, *J* = 8.2 Hz, 1H), 1.40-1.20 (m, 41H), 0.88 (t, *J* = 7.9 Hz, 6H); **^{13}C NMR** (100 MHz, $CDCl_3$): δ 137.5, 72.3, 71.4, 45.0, 42.9, 40.7, 32.1, 30.0, 29.8 (2C), 29.7, 29.6, 29.5 (2C), 26.5, 22.9, 14.3.

Compound **10** was prepared in 87% yield according to the general procedure for dialkylation. **^{1}H NMR** (400 MHz, $CDCl_3$): δ 6.14 (t, *J* = 4.2 Hz, 2H), 3.56 (dd, *J* = 8.0 Hz, 4.0 Hz, 2H), 3.41-3.36 (m, 4H), 3.27 (app. t, *J* = 7.8 Hz, 2H), 2.74 (t, *J* = 4.4 Hz, 2H), 1.77-1.75 (m, 2H), 1.60-1.53 (m, 4H), 1.48 (d, *J* = 8.2 Hz, 1H), 1.40-1.20 (m, 48H), 0.88 (t, *J* = 7.9 Hz, 6H); **^{13}C NMR** (100 MHz, $CDCl_3$): δ 137.5, 72.3, 71.4, 71.2, 45.0, 42.9, 40.7, 32.1, 30.0, 29.9 (2C), 29.8, 29.7, 29.6 (2C),, 29.4, 28.7, 26.5, 26.4, 26.0, 22.9, 14.3.

Compound **11** was prepared in 91% yield according to the general procedure for upjohn dihydroxylation. **^{1}H NMR** (400 MHz, $CDCl_3$): δ 3.84 (br s, 2H), 3.71 (br s, 2H), 3.44 (dd, *J* = 8.1 Hz, 4.1 Hz, 2H), 3.40-3.31 (m, 4H), 3.24 (app. t, *J* = 7.8 Hz, 2H), 2.10 (br s, 2H), 1.80-1.70 (m, 2H), 1.62 (d, *J* = 8.0 Hz, 1H), 1.56-1.51 (m, 4H), 1.40-1.20 (m, 34H), 0.88 (t, *J* = 7.9 Hz, 6H); **^{13}C NMR** (100 MHz, $CDCl_3$): δ 74.2, 71.4, 70.3, 46.8, 40.5, 32.1, 29.8, 29.6, 29.5, 27.5, 26.4, 22.8, 14.3.

Compound **12** was prepared in 94% yield according to the general procedure for upjohn dihydroxylation. **^{1}H NMR** (400 MHz, $CDCl_3$): δ 3.84 (br s, 1H), 3.68 (br s, 2H), 3.44 (dd, *J* = 8.1 Hz, 4.1 Hz, 2H), 3.33-3.31 (m, 4H), 3.22 (app. t, *J* = 8.0 Hz, 2H), 2.07 (br s, 2H), 1.72-1.51 (m, 6H), 1.40-1.20 (m, 38H), 0.85 (*t*, *J* = 7.9 Hz, 6H); **^{13}C NMR** (100 MHz, $CDCl_3$): δ 74.2, 71.4, 70.3, 46.8, 40.5, 32.1, 29.9, 29.8, 29.7, 29.5, 27.5, 26.4, 22.8, 14.3.

Compound **13** was prepared in 88% yield according to the general procedure for periodate oxidative cleavage of 1,2-diol, followed by $NaBH_4$ reduction. **^{1}H NMR** (400 MHz, $CDCl_3$): δ 3.70 (br s, 2H), 3.58-3.22 (m, 12H), 2.08-1.87 (m, 4H), 1.85-1.83 (m, 1H), 1.56 (br s, 4H), 1.39-1.16 (m, 31H), 0.88 (t, J = 7.8 Hz, 6H); **^{13}C NMR** (100 MHz, $CDCl_3$): δ 71.7 (2C), 66.6, 46.3 (2C), 32.0, 32.6, 32.1, 29.8, 29.7 (2C), 29.6, 29.5, 26.3, 22.8, 14.3.

Compound **14** was prepared in 92% yield according to the general procedure for periodate oxidative cleavage of 1,2-diol, followed by $NaBH_4$ reduction. **^{1}H NMR** (400 MHz, $CDCl_3$): δ 3.63 (br s, 2H), 3.58-3.25 (m, 12H), 2.10-1.88 (m, 4H), 1.85-1.83 (m, 1H), 1.57 (br s, 4H), 1.40-1.16 (m, 34H), 0.90 (t, J = 8.0 Hz, 6H); **^{13}C NMR** (100 MHz, $CDCl_3$): δ 71.9, 71.7, 66.7, 46.5, 32.8, 32.1, 29.9, 29.8, 29.7, 29.6 (2C), 26.4, 22.9, 14.3.

Compound **15** was prepared in 94% yield according to the general procedure for glycosylation reaction. **^{1}H NMR** (400 MHz, $CDCl_3$): δ 8.03-7.66 (m, 28H), 7.42-7.21 (m, 43H), 6.09 (t, J = 8.2 Hz, 1H), 5.78-5.67 (m, 6H), 5.52-5.24 (m, 3H), 4.72-2.90 (m, 28H), 1.86-1.50 (m, 8H), 1.44-1.23 (m, 36H), 0.87 (app. t, J = 6.4 Hz, 6H); **^{13}C NMR** (100 MHz, $CDCl_3$): δ 166.4, 166.0, 165.9, 165.6, 165.2, 165.1, 133.7, 133.6, 133.4, 133.2, 130.1, 130.0, 129.9, 129.8, 129.7, 129.5, 129.4, 129.1, 129.0, 128.9 (2C), 128.8, 128.7 (2C), 128.6, 128.5, 128.3, 101.4, 101.2, 96.4, 75.2, 75.1, 74.5, 73.2, 73.1, 72.9, 72.5, 71.4, 71.1, 70.1 (2C), 69.7, 63.7 62.7, 62.6, 43.6, 43.2, 32.1(2C), 29.9, 29.8, 29.7, 29.6 (2C), 29.5, 26.5(2C), 26.4, 22.8 (2C), 14.3.

Compound **16** was prepared in 97% yield according to the general procedure for glycosylation reaction. **^{1}H NMR** (400 MHz, $CDCl_3$): δ 8.13-7.64 (m, 28H), 7.42-7.21 (m, 45H), 6.00 (t, J = 8.2 Hz, 1H), 5.78-5.67 (m, 6H), 5.52-5.24 (m, 4H), 4.72-2.88 (m, 28H), 1.84-1.50 (m, 8H), 1.44-1.20 (m, 40H), 0.87 (app. t, J = 6.8 Hz, 6H); **^{13}C NMR** (100 MHz, $CDCl_3$): δ 166.5, 166.4, 165.8, 165.7, 165.2, 165.1, 133.8, 133.5, 133.4 (2C), 133.2, 130.0 (2C), 129.9 (2C), 129.8 (2C), 129.5, 129.4 (2C), 129.1, 129.0, 128.9, 128.8, 128.7, 128.6, 128.5, 128.4 (2C), 101.5, 101.3, 96.4, 75.2, 75.1, 74.5, 73.2, 73.1, 72.8, 72.5 (2C), 71.4, 71.1, 70.1 (2C), 69.9, 63.7 62.7, 62.6, 43.6, 43.2, 32.1, 29.9 (2C), 29.8, 29.7 (3C), 29.5, 26.5 (3C), 26.4, 22.7, 14.2.

CPM-*T*11 was prepared in 95% yield according to the general procedure for deprotection reaction (purity: ~ 96% based on ^{1}H NMR spectrum). $[\alpha]^{22}_D$ = +46 ($c = 0.21 \times 10^{-2}$, MeOH, l = 1 dm); **^{1}H NMR** (400 MHz, CD_3OD): δ 5.16 (app. d, J = 4.0 Hz, 2H), 4.26 (app. d, J = 8.0 Hz, 2H), 3.87-3.79 (m, 9H), 3.67-3.21 (m, 30H), 2.15 (br s, 5H), 1.56 (app. t, J = 8.0 Hz, 4H), 1.42-1.28 (m, 35H), 0.90 (t, J = 8.0 Hz, 6H); **^{13}C NMR** (100 MHz, CD_3OD): δ 104.7, 104.6, 103.1, 81.5, 78.0, 76.7, 75.2, 74.9, 74.8, 74.7, 74.3, 72.6, 72.3, 71.6, 62.9, 62.3, 45.0, 44.9, 43.1, 43.0, 33.9, 33.3, 31.0 (2C), 30.8, 30.7, 27.6, 23.9, 14.7; HRMS (EI): calcd. for $C_{55}H_{102}O_{24}Na^+$ $[M+Na]^+$ 1169.6659, found 1169.6662.

CPM-*T*12 was prepared in 97% yield according to the general procedure for deprotection reaction (purity: ~ 98% based on ^{1}H NMR spectrum). $[\alpha]^{22}_D$ = +42 ($c = 0.21 \times 10^{-2}$, MeOH, l = 1 dm); **^{1}H NMR** (400 MHz, CD_3OD): δ 5.16 (app. d, J = 4.0 Hz, 2H), 4.26 (app. d, J = 8.0 Hz, 2H), 3.90-3.81 (m, 9H), 3.67-3.21 (m, 30H), 2.15 (br s, 5H), 1.56 (app. t, J = 8.0 Hz, 4H), 1.42-1.28 (m, 38H), 0.90 (t, J = 8.0 Hz, 6H); **^{13}C NMR** (100 MHz, CD_3OD): δ 104.7 (2C), 103.1, 81.5, 78.0, 76.7, 75.2, 74.9, 74.7, 74.3, 72.6, 72.4, 72.3, 71.6, 62.9, 62.3, 45.0, 44.9, 43.0, 43.0, 33.3, 33.3, 31.0 (2C), 30.8, 30.7, 27.6, 23.9, 14.6; HRMS (EI): calcd. for $C_{57}H_{106}O_{24}Na^+$ $[M+Na]^+$ 1197.6972, found 1197.6968.

References

1. Schneider, C. A.; Rasband, W. S.; Eliceiri, K. W. NIH Image to Image J. *Nat. Methods* **2012**, *9*, 671–675.
2. Deckert, G.; Warren, P. V.; Gaasterland, T.; Young, W. G.; Lenox, A. L.; Graham, D. E.; Overbeek, R.; Snead, M. A.; Keller, M.; Aujay, M.; Huber, R.; Feldman, R. A.; Short, J. M.; Olsen G. J.; Swanson, R. V. The complete genome of the hyperthermophilic bacterium Aquifex aeolicus. *Nature* **1998**, *392*, 353–358.
3. Chae, P. S.; Rasmussen, S. G. F.; Rana, R. R.; Gotfryd, K.; Chandra, R.; Goren, M. A.; Kruse, A. C.; Nurva, S.; Loland, C. J.; Pierre, Y.; Drew, D.; Popot, J.-L.; Picot, D.; Fox, B. G.; Guan, L.; Gether, U.; Byrne, B.; Kobilka, B.; Gellman, S. H. Maltose–neopentyl glycol (MNG) amphiphiles for solubilization, stabilization and crystallization of membrane proteins. *Nat. Methods* **2010**, *7*, 1003–1008.
4. Ethayathulla, A. S.; Yousef, M. S.; Amin, A.; Leblanc, G.; Kaback, H. R.; Guan, L. Structure-based mechanism for Na+/melibiose symport by MelB. *Nat. Commun.* **2014**, *5*, 3009.
5. Kaback, H. R. Bacterial Membranes. *Methods Enzymol.* **1971**, *22*, 99-120.
6. Short, S. A.; Kaback, H. R.; Kohn, L. D. D-lactate dehydrogenase binding in Escherichia coli dld-membrane vesicles reconstituted for active transport. *Proc. Natl. Acad. Sci. U. S. A.* **1974**, *71*, 1461-1465.
7. Guan, L.; Nurva, S.; Ankeshwarapu, S. P. Mechanism of melibiose/cation symport of the melibiose permease of Salmonella typhimurium. *J. Biol. Chem.* **2011**, *286*, 6367-6374.
8. Rosenbaum, D. M.; Cherezov, V.; Hanson, M. A.; Rasmussen, S. G.; Thian, F. S.; Kobilka, T. S.; Choi, H. J.; Yao, X. J.; Weis, W. I.; Stevens, R. C.; Bobilka, B. K. High-resolution crystal structure of an engineered human β2-adrenergic G protein–coupled receptor. *Science* **2007**, *318*, 1266–1273.
9. Swaminath, G. Steenhuis, J. Kobilka, B. Lee, T. W. Allosteric modulation of β2-adrenergic receptor by Zn^{2+}. *Mol. Pharmacol.* **2002**, *61*, 65-72.
10. Koehl, A., Hu, H., Maeda, S., Zhang, Y., Qu, Q., Paggi, J. M., Latorraca, N. R., Hilger, D., Dawson, R., Matile, H., Schertler, G. F. X., Granier, S., Weis, W. I., Dror, R. O., Manglik, A., Skiniotis, G., & Kobilka, B. K. Structure of the μ-opioid receptor-Gi protein complex. *Nature*, **2018**, *558*, 547–552.
11. Ruta, V., Jiang, Y., Lee, A., Chen, J. and MacKinnon, R. Functional analysis of an archaebacterial voltage-dependent K^+ channel. *Nature* **2003**, *422*, 180–185.
12. Ashton, P. R.; Boyd, S. E.; Brown, C. L.; Jayaraman, N.; Nepogodiev, S. A.; Stoddart, J. F. A convergent synthesis of carbohydrate-containing dendrimers. *Chem.-Eur. J.* **1996**, *2*, 1115-1128.

3.3. Synopsis (Manuscript 3)

In *Manuscript 3* the synthesis of three polymerizable, detergent-like amphiphiles, so-called surfmers is described and they were characterized in terms of their micellization, micellar size, and detergency.

Overall, the structure of these novel surfmers resembles the structure of the detergent gold standard DDM onto which either a methacrylamide (LC048 and LC049) or an acrylamide (LC058) moiety was grafted. In future studies, these **moieties are expected to enable polymerization** of the surfmers. Additionally, a CH_2 group in the hydrophobic chain of LC049 was substituted by one oxygen atom.

Micellization was explored by surface tensiometry (ST) and ITC. It turned out that the addition of different amide bonds lowered the hydrophobicity of the surfmers compared with DDM. This was reflected in higher CMC values as well as in lower entropic contributions ($T\Delta S^{o}_{mic}$) to the change in Gibbs free enthalpy (ΔG^{o}_{mic}) as determined for LC049 and LC058. This is readily explained by the polarity of amide bonds, which increases the hydrophilic interactions of the amphiphile with water. Comparison between LC048 and LC058 reveals that the effect of acrylamide addition was slightly stronger than that of methacrylamide. Comparison of LC048 and LC049 shows that the oxygen substitution remarkably lowers the hydrophobicity.

Contrary to micellization, only a minor influence of the amide bond was found regarding micelle sizes. This was revealed by DLS experiments which gave similar hydrodynamic diameters (d_H) for DDM micelles and all surfmer micelles.

To assess detergency of the surfmers, kinetic solubilization experiments for artificial POPC vesicles and shotgun MP extraction on *E. coli* membranes were performed. Because of its low water solubility, LC048 was omitted from these experiments. Instead, the monomeric unit of NAPol, LC027, was included for comparison.

The new surfmers readily solubilized POPC vesicles and **exhibited rather fast solubilization kinetics**: While LC027 took about 5 h to completely solubilize the POPC vesicles, the new surfmers took less than 1 h. However, LC049 either formed large mixed micelles with POPC or only partly solubilized the vesicles as the scattering intensity was considerably higher than for the other surfmers.

All new surfmers were shown to **extract MPs of various sizes from biological membranes**, as shown by SDS-PAGE. This indicates a wide potential application possibility in MP research. Quantification gave overall moderate extraction efficiencies for the three surfmers in comparison to DDM. For concentrations of 1 mM or 2 mM above the CMC, the surfmers outperformed DDM. However, at 10 mM above the CMC, they only yielded 30–50% of the MP extraction. Furthermore, the surfmers were applied to extract recombinantly produced MPs, namely human wild-type GPCR adenosine receptor ($A_{2A}R$) and the bacterial transporter AcrB. For $A_{2A}R$, the surfmers alone were similarly efficient as a reference detergent mixture. When used as additives to the reference mixture, the extraction yields even increased. In the case of AcrB, the surfmers performed rather poorly, reaching less than 50% of the extraction yield of DDM. However, no negative effects were observed when the new monomers were used as additives to DDM.

Taken together, these findings show that **chemical additions and substitutions can have variably strong effects** on different properties of small-molecule glyco-amphiphiles.

3.4. Manuscript 3

Detergent-Like Polymerizable Monomers: Synthesis, Physicochemical, and Biochemical Characterization

Christophe Bonnet, Pierre Guillet, Florian Mahler, Sébastien Igonet, Sandro Keller, Anass Jawhari, and Grégory Durand

European Journal of Organic Chemistry, **2020**, 33, 5340–5349

Contribution

For this work, I designed and performed experiments for CMC determination via ITC (Fig. 2A), determination of d_H via DLS (Fig. 2C), and assessment of detergency via artificial vesicle solubilization (Fig. 3) and native *E. coli* MP extraction (Fig. 4). I also analyzed and interpreted the corresponding data.

EurJOC
European Journal of Organic Chemistry

Full Paper
doi.org/10.1002/ejoc.202000540

Check for updates
Chemistry Europe
European Chemical Societies Publishing

Protein Extraction

Detergent-Like Polymerizable Monomers: Synthesis, Physicochemical, and Biochemical Characterization

Christophe Bonnet,[a,b] Pierre Guillet,[a,b] Florian Mahler,[c] Sébastien Igonet,[b,d] Sandro Keller,[c] Anass Jawhari,[b,d] and Grégory Durand*[a,b]

Abstract: Three monomers with a maltose polar head, an alkyl hydrogenated chain, and an acrylamide-based polymerizable moiety were synthesized. The self-assembly properties in aqueous solutions of these monomers were studied by means of isothermal titration calorimetry (ITC), surface tension (SFT) measurements, and dynamic light scattering (DLS), which indicated the formation of small micellar aggregates of about 6 nm diameter. The critical micellar concentration (CMC) was found to depend on the length of the alkyl chain and on the nature of the polymerizable moiety, ranging from 0.35 mM to ca. 10 mM. The monomers were found to solubilize phospholipid vesicles and to extract a broad range of proteins from *Escherichia coli* membranes. Finally, the extraction of two membrane proteins, namely, the full-length, wild-type human G-protein-coupled receptor (GPCR) adenosine A2A receptor ($A_{2A}R$) and the bacterial transporter AcrB was demonstrated.

Introduction

Membrane proteins (MPs) perform a wide range of essential cellular functions and are involved in a large number of pathologies, which makes them priority drug targets representing nearly 70 % of therapeutic targets.[1] Because MPs exhibit high insolubility in water and poor stability outside their native membrane environment, their extraction from the membrane is highly challenging and may result in denaturation and/or aggregation of the protein once removed from their native environment. The need of natively isolated, yet stable proteins has prompted the development of sophisticated chemically well-defined detergents over the recent years. Among these new, chemically homogeneous systems, one can cite neo-pentyl glycols derivatives,[2] derivatives with branched[3] or fluorinated chains,[4] as well as steroid-based and facial derivatives.[5]

Other approaches for handling and studying MPs relate to the use of heterogeneous systems such as protein-lipid nanodiscs,[6] A8–35 amphipol (APols),[7] and nanodiscs bounded by poly(styrene-*co*-maleic acid) (SMA)[8] and poly(diisobutylene-*alt*-maleic acid) (DIBMA)[9] copolymers. Amphipols adsorb onto the hydrophobic transmembrane surface of membrane proteins thanks to their alkyl chains and the complex thus formed remains water-soluble thanks to the hydrophilic groups. MP/amphipols complexes are indeed very stable even at high dilutions due to the slow dynamic of the polymer which remains tightly attached to the protein. Unlike the other heterogeneous systems, SMA and DIBMA can efficiently recruit MPs and associated lipids directly from natural or artificial membranes into nanoscale lipid-bilayer patches that closely mimic the lamellar organization of cellular membranes. However, one common limitation of A8–35, SMA, and DIBMA lies in the presence of carboxylic groups along the polymer chain that result in polymer aggregation at acidic pH or in the presence of multivalent cations.[10]

This limitation has prompted the development of several amphipol derivatives including zwitterionic,[11] sulfonated,[12] or phosphocholine-based amphipols[13] as well as non-ionic APols called NAPols.[14] A first series of glucose-based NAPols was obtained either from co-telomerization of hydrophilic and hydrophobic monomers[14b] or by homo-telomerization of hydrophilic monomers, followed by hydrophobization of the polymer.[15] These glycosylated NAPols showed good potency at keeping various MPs soluble in their native state in the absence of detergent.[14b,15] We further designed homopolymeric NAPols (Figure 1) consisting of an amphiphilic repeating unit[16] (called **LC027** in the current study).[14a] This more convenient synthetic route offers the advantage of resorting to only one amphiphilic monomer and to allow better batch-to-batch reproducibility and higher yields. **LC027** due to its amphiphilic

[a] C. Bonnet, Dr. P. Guillet, Dr. G. Durand
Institut des Biomolécules Max Mousseron (UMR 5247 UM-CNRS-ENSCM) & Avignon University,
Chimie Bioorganique et Systèmes amphiphiles
301 rue Baruch de Spinoza – 84916 AVIGNON cedex 9, France
E-mail: gregory.durand@univ-avignon.fr
http://www.chem2stab.org/
[b] C. Bonnet, Dr. P. Guillet, Dr. S. Igonet, Dr. A. Jawhari, Dr. G. Durand
CHEM2STAB,
301 rue Baruch de Spinoza – 84916 AVIGNON cedex 9, France
[c] F. Mahler, Prof. Dr. S. Keller
Molecular Biophysics, Technische Universität Kaiserslautern (TUK),
Erwin-Schrödinger-Str. 13, 67663 Kaiserslautern, Germany
[d] Dr. S. Igonet, Dr. A. Jawhari
CALIXAR
60A Avenue Rockefeller – 69008 Lyon, France
Supporting information and ORCID(s) from the author(s) for this article are available on the WWW under https://doi.org/10.1002/ejoc.202000540.

EurJOC
European Journal of Organic Chemistry

Full Paper
doi.org/10.1002/ejoc.202000540

Chemistry Europe
European Chemical Societies Publishing

chemical structure and its surface activity belongs to the family of surfmers.[17] Surfmers combine the functionalities of surface-active agents with the reactivity of monomers. The polymerization of surfmers has been successfully employed for several applications such as emulsion stabilization, nanomaterials synthesis, drug-delivery systems, and hydrogels.

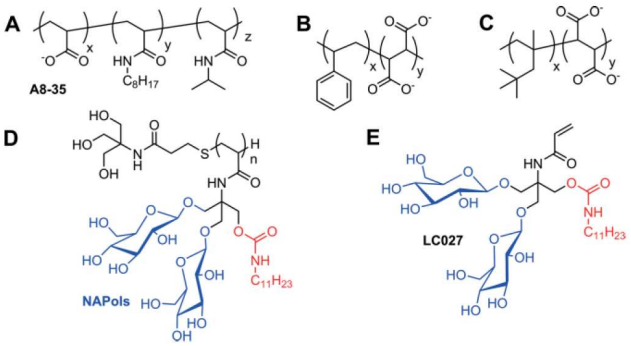

Figure 1. Structure of (**A**) A8–35 amphipol, (**B**) poly(styrene-*co*-maleic acid) (SMA) copolymer, (**C**) poly(diisobutylene-*alt*-maleic acid) (DIBMA) copolymer, (**D**) non-ionic amphipol (NAPol), and (**E**) its constituting detergent-like monomer (**LC027**).

The promising results obtained with this most advanced series of NAPols further confirmed their advantages over the classical A8–35 for specific applications such as cell-free synthesis, nuclear magnetic resonance (NMR) spectroscopy, and mass spectrometry (MS), to name but a few.[18] More recently, the first cryo-EM structure of the translocase of the outer membrane (TOM) core complex in NAPol has been reported.[19] However, like other amphipols, NAPols are unable to solubilize membrane proteins. It is therefore necessary to proceed in two distinct steps by doing first the extraction of the protein with a detergent and then performing the exchange with the polymer. As part of our long-term project, the work presented herein deals with the evaluation of the solubilizing properties of detergent-like monomers that could be further used in the synthesis of new NAPols. We expected that, while polymeric NAPols are very efficient stabilizing agents, the constituting monomers could exhibit solubilizing properties.

We report the synthesis of three detergent-like monomers refer to as surfmers and called **LC048**, **LC049**, and **LC058** that present chemical similarity with conventional *n*-dodecyl-β-D-maltopyranoside (DDM), which so far is considered as the gold standard for membrane-protein extraction. These new compounds are characterized by the presence of a maltose polar head, a hydrogenated alkyl chain, and an acrylamide or methacrylamide moiety that enables polymerization for further work. We chose to use acrylamide group instead of acryl ester due to higher stability of the amide bond compared to the ester one. For the sake of comparison, **LC027** was also included in the study. The colloidal properties of the four surfmers were evaluated by means of isothermal titration calorimetry (ITC), surface tension (SFT) measurements, as well as dynamic light scattering (DLS). Their potency to act as solubilizing agents was further evaluated with model membranes as well as with different membrane proteins from two cell membranes.

Results and Discussion

Synthesis. The synthesis followed a convergent synthetic pathway, based on three key steps: (i) synthesis of the hydrophobic parts; (ii) synthesis of the maltose polar head; (iii) coupling of the hydrophobic and hydrophilic parts (Scheme 1).

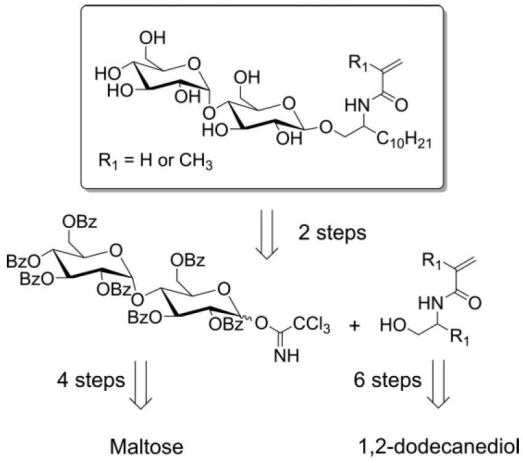

Scheme 1. Retrosynthetic pathway for compounds **LC048** and **LC058**.

Compounds **8a–b** were synthesized following an eight-step synthetic route starting from 1,2-dodecanediol (Scheme 2). Selective protection of the primary alcohol group was achieved using Et_3N and 1.2 equivalent of trityl chloride as previously reported.[20] Mesylation of the secondary alcohol group followed by nucleophilic substitution in the presence of NaN_3 afforded compound **3** in good yield (65 % in three steps). The azide group was next reduced under hydrogen atmosphere at room temperature, using catalytic amounts of Pd-C to lead to compound **4** in high yield. The insertion of the polymerizable moiety on the amine group was realized using either acryloyl chloride or methacryloyl chloride at room temperature in the presence of trimethylamine (TEA). Deprotection of **5a–b** in acidic condition led to compounds **6a–b**. In our hands, only moderate yields of deprotection were observed, that is, 55 and 63 %, respectively.

In order to obtain high-yield and stereoselective *O*-glycosylation leading to the β-anomer, activation of the anomeric position and protection of the other free hydroxy groups seemed preferable. We therefore activated maltose into its trichloroacetimidate form and used benzyl esters protecting groups.[21] Hepta-O-benzoyl-maltose-1-O-trichloroacetimidate was readily prepared from commercially available maltose following a four-step synthetic route[22] and was next condensed onto the hydrophobic parts **6a** and **6b** at room temperature following a Schmidt glycosylation[23] to give compounds **7a–b** in very good yields. Hydrolysis of benzoyl groups using catalytic amount of sodium methoxide in MeOH afforded compounds **8a–b** in good yields also called **LC048** and **LC058**, respectively. Analysis of the proton NMR spectra showed the formation β anomer witnessed by a doublet between 4.0 and 4.5 ppm with a coupling constant of ca. 8 Hz (J_{trans}) corresponding to the anomeric proton. The second anomeric proton between the two glucose

EurJOC
European Journal of Organic Chemistry

Full Paper
doi.org/10.1002/ejoc.202000540

Chemistry Europe
European Chemical Societies Publishing

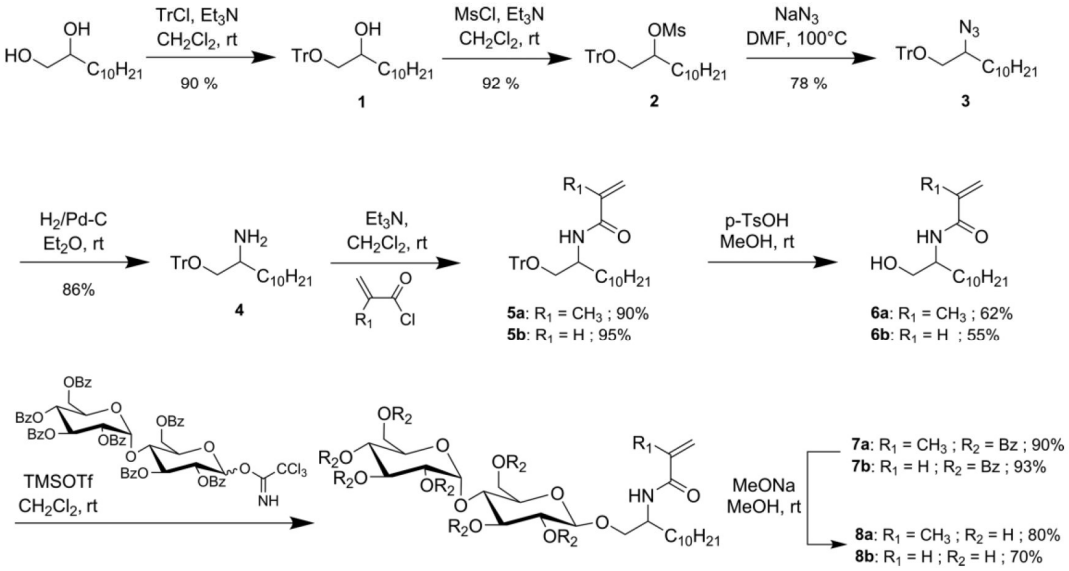

Scheme 2. Synthesis of **LC048 (8a)** and **LC058 (8b)**.

units appeared at 5.2 ppm with a coupling constant of ca. 4 Hz (J_{cis}).

LC049 was synthesized following an eleven-step synthetic route starting from glycerol (Scheme 3). The two hydroxyl groups were protected by reaction using 2,2-dimethoxypropane and catalytic amount of *p*TsOH in CH_3CN to afford compound **9** also called solketal.[24] The addition of the hydrogenated chain was achieved by an S_N2 reaction in the presence of sodium hydride (NaH) and 1.2 equivalent of octyl bromide to give compound **10** in 74 % yield. Then, hydrolysis in acidic conditions gave compound **11** in good yield, which was next put in reaction with Et_3N and 1.2 equivalent of trityl chloride to yield compound **12**. Mesylation of the secondary alcohol group followed by nucleophilic substitution in the presence of NaN_3, afforded compound **14** in good yield. The azide group was reduced at room temperature using a catalytic amount of Pd-C under hydrogen pressure to afford compound **15** in 64 % yield in three steps. Next, the insertion of the methacrylamide moiety on the amino group was achieved using triethylamine and methacryloyl chloride, followed by a deprotection in acidic conditions to lead to compound **17.** Hepta-O-benzoyl-maltose-1-O-trichloroacetimidate was condensed onto **17** at room temperature following a Schmidt glycosylation[23] to give compounds **18** in 80 % yield. Finally, hydrolysis of benzoyl groups using catalytic amount of sodium methoxide (MeONa) in MeOH afforded compound **19**, also called **LC049**. The overall yield for the synthesis of **19** is ca. 18 % while that of **8a** and **8b** is respectively, 22 and 19 %. Since we started from racemic starting ma-

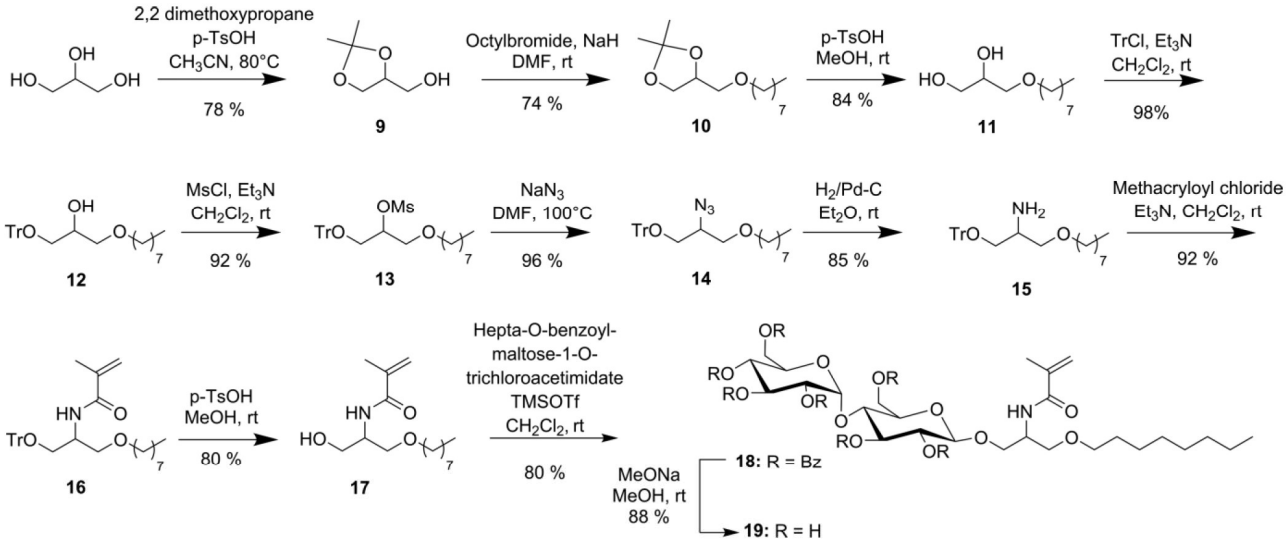

Scheme 3. Synthesis of **LC049 (19)**.

EurJOC
European Journal of Organic Chemistry

Full Paper
doi.org/10.1002/ejoc.202000540

Chemistry Europe
European Chemical Societies Publishing

Table 1. Self-aggregation properties of DDM, **LC027**, **LC048**, **LC058**, and **LC049**.

	Monomers	**DDM**[25]	**LC027**	**LC048**	**LC058**	**LC049**
	Molar mass (g/mol)	510.6	696.8	593.7	595.7	579.7
ITC[a]	CMC [mM]	0.147	0.55 ± 0.02	nd	0.70 ± 0.04	10.6 ± 0.04
	$-T\Delta S°$mic (kJ/mol)[b]	−35.1	−28.3 ± 0.10	nd	−29.0 ± 0.2	−25.3 ± 0.1
	$\Delta H°$mic (kJ/mol)[c]	3.8	−0.22 ± 0.01	nd	0.97 ± 0.1	4.02 ± 0.03
	$\Delta G°$mic (kJ/mol)[d]	−31.30	−28.6 ± 0.1	nd	−28.0 ± 0.1	−21.2 ± 0.02
	Δc [mM][e]		0.05 ± 0.02	nd	0.12 ± 0.03	0.86 ± 0.04
SFT[a]	CMC [mM]	0.17	0.51 ± 0.07	0.35 ± 0.02	0.64 ± 0.10	10.28[f]
	γ_{CMC} (mN/m)[g]	34.7	35.1 ± 2.8	34.4 ± 0.2	35.7 ± 2.2	32.9[f]
	$\Delta G°_{mic}$ (kJ/mol)[d]	−30.7	−28.8 ± 0.3	−29.7 ± 0.2	−28.8 ± 1.0	−21.1[f]
DLS	D_H [nm][h]	7.2	5.9	6.0	5.9	5.7

[a] Data are averages of three experiments. ± indicates 95 % confidence interval boundaries from a nonlinear least-squares fit for ITC. ± indicates standard errors from the three experiments for SFT. [b] Entropic contribution to micelle formation. [c] Enthalpic contribution to micelle formation. [d] Gibbs free energy of micellization. [e] Micellization concentration range. [f] Only one experiment. [g] Surface tension attained at the CMC. [h] Hydrodynamic diameter at 2 × (CMC + 5 mM) in buffer (50 mM Tris, 200 mM NaCl, pH 7.4).

terials, we expected the formation of mixture of diastereomers although neither NMR nor HPLC analysis allowed us to distinguish the presence of such diastereomers. Therefore, the investigated properties reported below are considered as the result of a mixture of diastereomers.

Micellization. The micellization processes of the monomers were characterized by means of high-sensitivity ITC and surface tension such as exemplified in Figure 2. CMC values derived from these two techniques (Table 1) were found to be in very good agreement between each other. **LC027**, **LC049**, and **LC058** were well soluble in aqueous solution; once the compounds were solubilized, the solutions remained transparent. By contrast, **LC048** tended to precipitate after solubilization. Several attempts at heating and using sonication failed to keep it soluble for long periods of time.

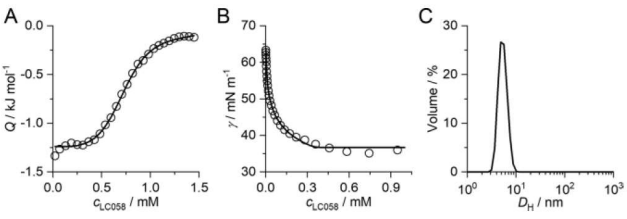

Figure 2. (A) ITC data for **LC058**. Shown are an experimental isotherm (open symbols) and a fit based on a generic sigmoidal function (solid line). (B) Surface tension vs. **LC058** concentration. The solid line represents the nonlinear fit of the experimental points. (C) Normalized volume-weighted particle size distributions for **LC058**.

The surface activity of surfactants in solution at the air–water interface was determined by the Wilhelmy plate technique for the four monomers. The two derivatives **LC048** and **LC058** exhibited CMC values of 0.35 and 0.64 mM, respectively. Compared with that of DDM (0.17 mM, see Table 1), these values indicate a strong influence of the polymerizable moiety. Indeed, introducing the acrylamide group contributes to shortening the alkyl chain from C12 to C10. This effect is likely due to the polarity of the amide bond directly attached to alkyl chain that can favor hydration. The CMC of **LC048** and **LC058** lie in between that of DDM and of the undecyl derivative UDM (0.65 mM). This indicates that the double bond of the acrylamide group brings also hydrophobicity to the molecule, the contribution of the methacrylamide being obviously more pronounced than that of the acrylamide. **LC049** has a CMC close to 10 mM, which is ca. 25 times higher than that of **LC048**, indicating that the position of the oxygen atom within the chain contributes to shortening it to a C8 alkyl chain. The CMC of **LC049** lies in between that of the *n*-nonylmaltoside (6 mM) and that of the octyl derivative (19.5 mM) in agreement with the slight hydrophobic contribution of the double bond of the acrylamide group. Since ITC requires good solubility of the tested compounds for preparation of stock solution at ca. 10 times the CMC, only **LC049**, **LC058**, and **LC027** were tested, as the rather limited water solubility of **LC048** made the preparation of such stock solutions impossible.

The changes in Gibbs free energy $\Delta G_{mic}^{m/aq,\circ}$, enthalpy $\Delta H_{mic}^{m/aq,\circ}$, and entropy $-T\Delta S_{mic}^{m/aq,\circ}$ accompanying the transfer of monomers from the aqueous solution into micelles are summarized in Table 1 and show that micellization was almost exclusively driven by entropy, with enthalpy making only a minor contribution that decreased and changed sign with increasing chain length. The contribution of the oxygen atom to micellization accounted for about ca. 8.0 kJ/mol, as deduced by a comparison between **LC049** and **LC048**, which is in rather good agreement with a reduction of the chain length of two CH_2 (typically −3.0 kJ/mol par CH_2 unit).

We next conducted DLS experiments in Tris buffer to determine the hydrodynamic diameters of the aggregates formed. Whatever monomer tested, volume size distribution indicated the presence of one population of aggregates of about 6 nm in diameter as exemplified in Figure 2C. This is similar to what is observed for DDM (6.6 nm), indicating that the additional polymerizable moiety did not substantially affect the morphology of the aggregates.

Complementary experiments were done in pure water and led to similar observation with only one population of aggregates of about 5 nm in diameter (Figure S40). Number size distribution also showed unimodal distribution with aggregates of about 4 nm in diameter while intensity distribution showed a bimodal distribution with main aggregates of about 5 to 6 nm and a second minor population of bigger aggregates (Figure S40).

EurJOC
European Journal of Organic Chemistry

Full Paper
doi.org/10.1002/ejoc.202000540

Chemistry Europe
European Chemical Societies Publishing

Detergency. Because of the rather limited water solubility of **LC048**, this compound was not further studied in the following biochemical validation. To investigate detergency, that is, the ability both to solubilize artificial lipid bilayers and to extract membrane proteins, we first investigated the solubilization of large unilamellar vesicles (LUVs) composed of monounsaturated zwitterionic phospholipid 1-plamitoyl-2-oleyl-*sn*-glycero-3-phosphocholine (POPC) into mixed micelles with the aid of light scattering measurements.[4a] The solubilization of 0.3 mM POPC in the form of LUVs was complete within a few hours for **LC027**, **LC049**, and **LC058** (Figure 3). While **LC058** enabled complete solubilization in less than an hour, **LC027** also allowed complete but slower solubilization over a time period of ca. 5 h. Finally, **LC049** achieved fast but only partial solubilization or formed larger mixed micelles than these obtained from **LC027** or **LC058**. POPC was chosen because – under the premise that a complex cellular membrane can be mimicked by one single phospholipid species – it is generally considered the most "typical" eukaryotic lipid.

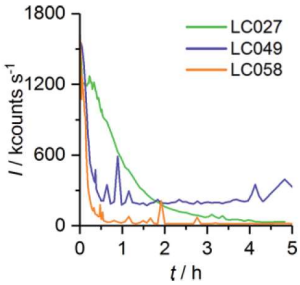

Figure 3. Vesicle solubilization by 5.55 mM **LC027**, 15.56 mM **LC049**, or 5.70 mM **LC058** (i.e., 5 mM above the respective CMC determined by ITC) at 25 °C as monitored in terms of the light scattering intensity recorded at an angle of 90°. Initially, each sample contained 0.3 mM POPC present in the form of LUVs.

Next, we investigated the extraction of integral membrane proteins from *E. coli* membranes in terms of sodium dodecyl sulfate polyacrylamide gel electrophoresis (SDS-PAGE) band patterns and overall amounts of extracted proteins. We compared the protein-extraction yields thus obtained with those afforded by DDM. As can be seen in Figure 4A, the three derivatives were able to extract MPs spanning a broad range of molar masses. Figure 4B shows the overall protein-extraction yields relative to the value obtained using 10 mM micellar DDM in dependence on the concentration of micellar detergent (i.e., total detergent concentration minus CMC). As expected, all protein-extraction yields were concentration-dependent, but this dependence varied clearly among the derivatives tested. At a concentration of 1 and 2 mM above the respective CMC, the three surfmers performed better than DDM, with **LC027** and **LC049** being the most efficient protein solubilizers. Increasing the concentration further to 5 and 10 mM above the CMC did not enhance the yields for **LC027** and **LC058** and slightly reduced that of **LC049**, whereas the protein-extraction yield of DDM continued to increase steeply as previously observed.[26] However, it needs to be pointed out that the superior performance of DDM at high concentrations was largely due to its unusually efficient extraction of a single abundant membrane protein, namely, outer membrane protein A (OmpA, ca. 35 kDa), as previously observed in other cases.[27]

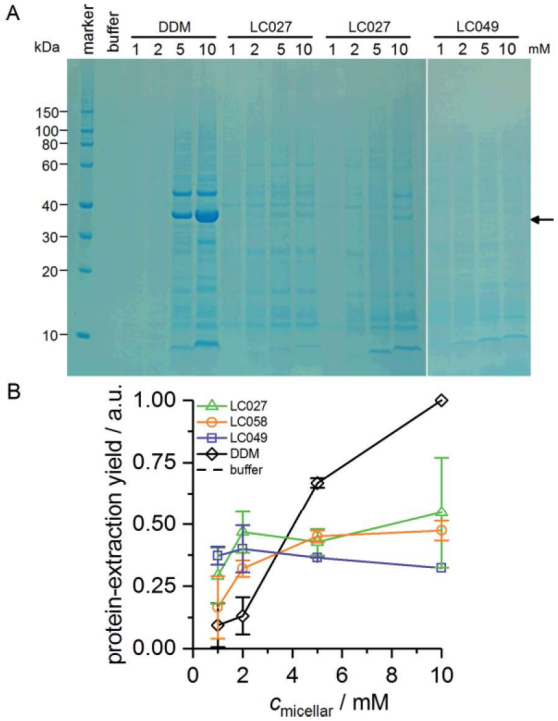

Figure 4. (A) SDS-PAGE of *E. coli* extracts upon exposure to different monomers at increasing micellar concentration (i.e., total detergent concentration minus CMC). The arrow indicates the position of the abundant outer-membrane porin OmpA, which was extracted extraordinarily well by DDM. (B) Relative protein-extraction yields as functions of the micellar concentration of **LC027**, **LC058**, **LC049**, or DDM. Extraction yields are reported relative to the yield obtained when DDM was used at 10 mM. Error bars indicate standard deviations of 2 experiments except for 10 mM micellar **LC049**.

In order to evaluate if the solubilizing properties of these surfmers can be extended to other membranes and other membrane proteins, we applied them to membrane proteins recombinantly produced in *E. coli* and insect cells (*Sf*9), namely, the bacterial transporter AcrB and the adenosine receptor $A_{2A}R$. These targets represent two important but distinct classes of membrane proteins, that is, transporters and G-protein-coupled receptors (GPCRs), respectively. Solubilization efficiency was assessed using stain-free SDS-PAGE and Western blots for total and target proteins, respectively, for both pure surfmers at 10 times the CMC and for DDM/monomer mixtures at a molar ratio of [10:1]. As previously reported, for solubilizing $A_{2A}R$, a DDM/cholesterol hemi-succinate [DDM:CHS] mixture was used as a reference condition, while we used DDM as reference for solubilizing AcrB. Solubilization of $A_{2A}R$ showed that **LC058** exhibited rather good extraction yields (≈79 %), while that of **LC049** remained moderate (≈49 %). When used as solubilization additives, both [DDM:**LC049**] and [DDM:**LC058**] mixtures outperformed the reference conditions, with extraction yields of ≈73 % and ≈90 %, respectively, indicating additive effects (Figure 5A). For the sake of comparison, **LC027** was also tested and showed good solubilizing properties (ca. 70 %) similar to the reference. Solubilization of AcrB led to lower extraction yields

EurJOC
European Journal of Organic Chemistry

Full Paper
doi.org/10.1002/ejoc.202000540

Chemistry Europe
European Chemical Societies Publishing

for both **LC049** and **LC058** monomers than for the reference. However, when [DDM:**LC049**] and [DDM:**LC058**] mixtures were used, extraction yields were as high as that of the reference (Figure 5B), indicating that, even if the new compounds failed to extract significant amounts of AcrB on their own, they did not preclude extraction by the reference detergent DDM. As has been observed numerous times before, there appears to be no obvious correlation between membrane composition, protein structure, and detergent chemistry on the one hand and their potency of protein extraction on the other.

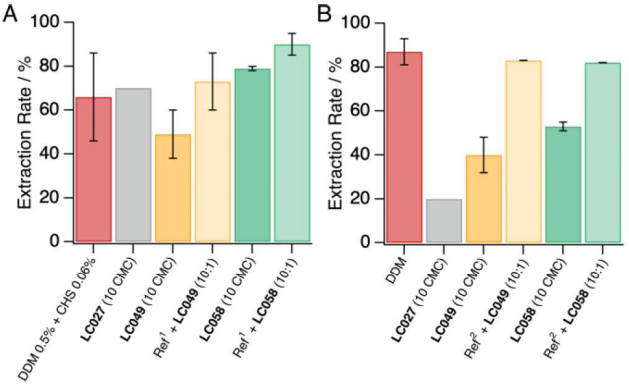

Figure 5. (A) Solubilization of $A_{2A}R$ (Ref^1 = DDM 0.5 % + CHS 0.06 %). (B) Solubilization of AcrB (Ref^2 = DDM 0.5 %).

Conclusion

We have synthesized a series of three amphiphilic monomers that are chemically similar to the conventional detergent DDM. **LC048** and **LC058** can be viewed as DDM molecules onto which were grafted, respectively, a methacrylamide and an acrylamide unit, while **LC049** differs from **LC048** by substitution of one oxygen atom for a CH_2 in the chain. The effect of attaching an amide bond within the chain contributes to shortening the length of the alkyl chain to 10 carbon atoms for **LC048** and **LC058**, and to 8 carbon atoms for **LC049**. All three monomers formed micellar aggregates of similar size (ca. 6 nm in diameter), indicating that the attached polymerizable moiety did not significantly affect the self-association properties. However, we noticed that the nature of the polymerizable moiety had a much stronger effect on the water solubility, the methacrylamide derivative **LC048** being poorly soluble above its CMC, which precluded its use in biochemical evaluation. **LC049**, **LC058**, and **LC027** a previously designed monomer that is used for the synthesis of non-ionic amphipols (NAPols) showed potency in solubilizing a model membrane system which is POPC preformed liposomes, and in extracting integral membrane proteins from *E. coli* membranes. Further, the potency of these surfmers to extract the full-length, wild-type human GPCR adenosine receptor ($A_{2A}R$) was demonstrated, while lower solubilization yields were observed for the bacterial transporter AcrB. Taken together, these findings demonstrate that the new amphiphilic monomers behave similarly to classical detergents. This warrants further development of poly-detergent based polymers that could be used for handling membrane proteins.

Experimental Section

Materials & Methods: All starting materials were commercially available and were used without further purification. Racemic 1,2-dodecanediol and racemic glycerol acetonide were used as starting materials. All solvents were of reagent grade and used as received unless otherwise indicated. MeOH was dried with Na under argon atmosphere. The progress of the reactions was monitored by thin layer chromatography. The compounds were detected either by exposure to ultraviolet light (254 nm) or by spraying with sulfuric acid (5 % ethanol) and/or ninhydrin (5 % ethanol), followed by heating at ca. 150 °C. ^1H and ^{13}C NMR analysis were performed at 400 and 100 MHz, respectively. Chemical shifts are given in ppm relative to the solvent residual peak as a heteronuclear reference for ^1H and ^{13}C. Abbreviations used for signal patterns are: s, singlet; d, doublet; t, triplet; q, quartet; m, multiplet; dd, doublet of doublet; dt, doublet of triplet. High-resolution mass spectra were determined on a Synapt G2-S (Waters) mass spectrometer with a TOF mass analyzer in a positive ionization mode. Milli-Q water (resistivity of 18.2 MΩ cm, surface tension of 71.45 mN/m at 25 °C) was employed for all physicochemical experiments.

(((2-Azidododecyl)oxy)methanetriyl)tribenzene (3): To a solution of **1** (24 g, 54.0 mmol, 1 equiv.) in anhydrous CH_2Cl_2, was added Et_3N (15.1 mL, 108.0 mmol, 2 equiv.). The solution was stirred for 20 minutes then methanesulfonyl chloride (5.0 mL, 64.8 mmol, 1.2 equiv.) was added dropwise. The reaction mixture was stirred for 16 h and the solution was filtered and concentrated in vacuo. The crude compound was purified by flash chromatography (cyclohexane/AcOEt, 95:5 v/v) to yield compound **2** as a white solid (26.0 g, 92 %) which was directly used in the next step. To a solution of **2** (22 g, 42.1 mmol, 1 equiv.) in anhydrous DMF was added NaN_3 (6.8 g, 84.2 mmol, 2 equiv.). The reaction mixture was stirred for 16 h at 100 °C. Then, the solution was diluted with water and extracted twice with AcOEt. The organic layer was dried with anhydrous Na_2SO_4, filtered and concentrated in vacuo. The crude compound was purified by flash chromatography (cyclohexane/AcOEt, 100:0 to 95:5 v/v) to yield compound **3** as a colorless oil (15.2 g, 78 %). R_f = 0.7 (cyclohexane/AcOEt, 95:5 v/v). ^1H NMR ($CDCl_3$, 400 MHz): δ = 7.48–7.24 (15H, m); 3.38 (1H, m); 3.29 (1H, dd, J = 4 Hz, J = 10 Hz); 3.16 (1H, dd, J = 8 Hz, J = 10 Hz); 1.40 (2H, m); 1.23 (16H, bs); 0.88 (3H, t, J = 8 Hz). $^{13}C^{[12]}$ NMR ($CDCl_3$, 100 MHz): δ = 143.7; 128.6–127.0; 87.0; 66.3; 62.6; 31.8; 30.8; 29.6; 29.5; 29.4; 29.3; 29.2; 25.9; 22.6; 14.1. HRMS (ESI-TOF) m/z: $[M + Na]^+$ Calcd for $C_{31}H_{39}N_3ONa$ 492.2991, found 492.2989.

1-(Trityloxy)dodecan-2-amine (4): To a solution of **3** (6 g, 12.8 mmol, 1 equiv.) in Et_2O was added to a suspension of Pd-C (640 mg) in Et_2O. The reaction mixture was stirred overnight under a pressure of H_2. Then, the solution was filtered through a pad of Celite and concentrated in vacuo. The crude compound was purified by flash chromatography (cyclohexane/AcOEt, 40:60 v/v) to yield compound **4** as a colorless oil (4.9 g, 86 %). R_f = 0.38 (cyclohexane/AcOEt, 40:60 v/v). ^1H NMR ($CDCl_3$, 400 MHz): δ = 7.50–7.21 (15H, m); 3.11 (1H, dd, J = 4 Hz, J = 8 Hz); 2.98 (1H, m); 2.90 (1H, m); 1.55 (2H, bs); 1.24 (18H, bs); 0.89 (3H, t, J = 8 Hz). ^{13}C {^1H} NMR ($CDCl_3$, 100 MHz): δ = 144.1; 128.7–126.9; 86.3; 68.6; 51.5; 34.2; 31.8; 29.7; 29.6; 29.5; 29.3; 26.0; 22.6; 14.0. HRMS (ESI-TOF) m/z: $[M + Na]^+$ Calcd for $C_{31}H_{41}NONa$ 466.3086, found 466.3088.

N-(1-(Trityloxy)dodecan-2-yl)methacrylamide (5a): To a solution of **4** (4.0 g, 9.0 mmol, 1 equiv.) in anhydrous CH_2Cl_2 was added Et_3N (2.5 mL, 18.0 mmol, 2 equiv.). The solution was stirred for 20 minutes then methacryloyl chloride (1.0 mL, 10.8 mmol, 1.2 equiv.) was added dropwise. The reaction mixture was stirred for 2 h and the solution was filtered and concentrated in vacuo. The crude com-

EurJOC
European Journal of Organic Chemistry

Full Paper
doi.org/10.1002/ejoc.202000540

Chemistry Europe
European Chemical Societies Publishing

pound was purified by flash chromatography (cyclohexane/AcOEt, 95:5 v/v) to yield compound **5a** as a colorless oil (4.1 g, 90 %). R_f = 0.40 (cyclohexane/AcOEt, 90:10 v/v). ^{1}H NMR ($CDCl_3$, 400 MHz): δ = 7.45–7.20 (15H, m); 5.99 (1H, d, J = 8 Hz); 5.64 (1H, s); 5.30 (1H, s); 4.10 (1H, m); 3.18 (2H, m); 1.95 (3H, s); 1.65 (2H, m); 1.24 (16H, bs); 0.88 (3H, t, J = 8 Hz). ^{13}C {^{1}H} NMR ($CDCl_3$, 100 MHz): δ = 167.7; 143.8; 140.4; 128.6–127.1; 118.9; 86.31; 64.4; 49.4; 32.2; 31.9; 29.6; 29.5; 29.3; 26.0; 22.7; 18.7; 14.1. HRMS (ESI+) m/z: [M + Na]$^+$ Calcd for $C_{35}H_{45}NO_2Na$ 534.3348, found 534.3353.

N-(1-(Trityloxy)dodecan-2-yl)acrylamide (5b): To a solution of **4** (4.1 g, 9.2 mmol, 1 equiv.) in anhydrous CH_2Cl_2 was added Et_3N (2.6 mL, 18.5 mmol, 2 equiv.). The solution was stirred for 20 minutes then acryloyl chloride (0.9 mL, 11.1 mmol, 1.2 equiv.) was added dropwise. The reaction mixture was stirred for 2 h and the solution was filtered and concentrated in vacuo. The crude compound was purified by flash chromatography (cyclohexane/AcOEt, 90:10 v/v) to yield compound **5b** as a colorless oil (4.3 g, 95 %). R_f = 0.40 (cyclohexane/AcOEt, 80:20 v/v). ^{1}H NMR ($CDCl_3$, 400 MHz): δ = 7.41–7.20 (15H, m); 6.22 (1H, d); 6.02 (1H, dd); 5.60 (1H, dd); 4.11 (1H, m); 3.18 (2H, m); 1.60 (2H, m); 1.24 (16H, bs); 0.86 (3H, t, J = 8 Hz). ^{13}C {^{1}H} NMR ($CDCl_3$, 100 MHz): δ = 164.9; 143.8; 131.2; 128.6–126.1; 86.4, 64.5; 49.4; 32.2; 31.9; 29.6; 29.5; 29.4; 29.3; 26.0; 22.7; 14.1. HRMS (ESI+) m/z: [M + Na]$^+$ Calcd for $C_{34}H_{43}NO_2Na$ 520.3186, found 520.3193.

N-(1-Hydroxydodecan-2-yl)methacrylamide (6a): To a solution of **5a** (3.6 g, 7.0 mmol, 1 equiv.) in MeOH was added *p*TsOH (121 mg, 0.7 mmol, 0.1 equiv.) and the reaction mixture was stirred for 6 h. Then the solution was neutralized by addition of Et_3N and concentrated in vacuo. The crude compound was purified by flash chromatography (cyclohexane/AcOEt, 60:40 v/v) to yield compound **6a** as a colorless oil (1.17 g, 62 %). R_f = 0.17 (cyclohexane/AcOEt, 60:40 v/v). ^{1}H NMR ($CDCl_3$, 400 MHz): δ = 6.15 (1H, d, J = 8 Hz); 5.68 (1H, s); 5.30 (1H, s); 3.95 (1H, m); 3.66 (1H, dd, J = 4 Hz, J = 12 Hz, CH_2O); 3.56 (1H, dd, J = 8 Hz, J = 12 Hz, CH_2O); 1.93 (3H, s, CH_3); 1.55 (1H, m, CH_2); 1.45 (1H, m, CH_2); 1.22 (16H, bs, CH_2); 0.85 (3H, t, J = 8 Hz, CH_3). ^{13}C {^{1}H} NMR ($CDCl_3$, 100 MHz): δ = 169.1; 139.8; 119.7; 65.2; 51.8; 31.8; 31.2; 29.5; 29.4; 29.2; 26.1; 22.6; 18.6; 14.0. HRMS (ESI-TOF) m/z: [M + H]$^+$ Calcd for $C_{16}H_{32}NO_2$ 270.2433, found 270.2438.

N-(1-Hydroxydodecan-2-yl)acrylamide (6b): To a solution of **5b** (3.0 g, 6.0 mmol, 1 equiv.) in MeOH was added *p*TsOH (0.1 g, 0.6 mmol, 0.1 equiv.) and the reaction mixture was stirred for 6 h. The solution was neutralized by addition of Et_3N and the solution was concentrated in vacuo. The crude compound was purified by flash chromatography (cyclohexane/AcOEt, 40:60 v/v) to yield compound **6b** as a white solid (0.8 g, 55 %). R_f = 0.2 (cyclohexane/AcOEt, 40:60 v/v). ^{1}H NMR ($CDCl_3$, 400 MHz): δ = 6.27 (1H, d, J = 16 Hz); 6.15 (1H, dd, J = 10 Hz, J = 16Hz); 5.63 (1H, d, J = 12 Hz); 3.98 (1H, m); 3.68 (1H, dd, J = 4H z, J = 12 Hz); 3.57 (1H, dd, J = 8 Hz, J = 12 Hz) 3.30 (1H, bs); 1.51 (2H, m); 1.24 (16H, bs); 0.86 (3H, t, J = 8 Hz). ^{13}C {^{1}H} NMR ($CDCl_3$, 100 MHz): δ = 166.3; 130.8; 126.7; 65.33; 52.0; 31.9; 31.2; 29.6; 29.5; 29.3; 26.1; 22.7; 14.0. HRMS (ESI-TOF) m/z: [M + H]$^+$ Calcd for $C_{15}H_{30}NO_2$ 256.2277, found 256.2282.

(2R,3R,4S,5R,6R)-2-((Benzoyloxy)methyl)-6-(((2R,3R,4S,5R,6R)-4,5-bis(benzoyloxy)-2-((benzoyloxy)methyl)-6-((2-methacrylamidododecyl)oxy)tetrahydro-2H-pyran-3-yl)oxy)tetrahydro-2H-pyran-3,4,5-triyl Tribenzoate (7a): To a solution of 6a (0.8 g, 3.0 mmol, 1 equiv.) and hepta-O-benzoyl-maltose-1-O-trichloroacetimidate[22] (3.6 g, 3.0 mmol, 1 equiv.) in anhydrous CH_2Cl_2 was added dropwise TMSOTf (0.54 mL, 3.0 mmol, 1 equiv.). The reaction mixture was stirred for 24 h. Then the solution was neutralized by addition of Et_3N and concentrated in vacuo. The crude compound was purified by flash chromatography (cyclohexane/AcOEt, 80:20 v/v) to yield compound 7a as a white solid (3.6 g, 90 %). R_f = 0.54 (cyclohexane/AcOEt, 60:40 v/v). ^{1}H NMR ($CDCl_3$, 400 MHz): δ = 8.07–7.24 (35H, m); 6.18 (1H, t, J = 10 Hz); 5.92 (1H, m); 5.73 (1H, t, J = 10 Hz); 5.61 (1H, s); 5.41 (1H, dd, J = 4 Hz, J = 10 Hz); 5.35 (1H, s); 4.95 (1H, t, J = 10 Hz); 4.85 (1H, m); 4.65–4.40 (5H, m); 4.10–3.80 (5H, m); 3.50 (1H, m); 1.87 (3H, s); 1.40 (2H, m); 1.25 (16H, bs); 0.90 (3H, t, J = 8 Hz). ^{13}C {^{1}H} NMR ($CDCl_3$, 100 MHz): δ = 167.9–165.1; 140.1; 133.5–128.3; 119.1; 100.2; 97.0; 78.5; 78.2; 75.4; 75.3; 74.7; 72.6; 71.5; 71.4; 70.5; 69.9; 68.9; 63.4; 62.7; 48.7; 31.9. 31.5; 31.3; 29.5; 29.3; 26.0; 22.6; 18.5; 14.0. HRMS (ESI-TOF) m/z: [M + H]$^+$ Calcd for $C_{77}H_{80}NO_{19}$ 1322.5319, found 1322.5350.

(2R,3R,4S,5R,6R)-2-(((2R,3R,4S,5R,6R)-6-((2-Acrylamidododecyl)oxy)-4,5-bis(benzoyloxy)-2-((benzoyloxy)methyl)tetrahydro-2H-pyran-3-yl)oxy)-6-((benzoyloxy)methyl)tetrahydro-2H-pyran-3,4,5-triyl Tribenzoate (7b): To a solution of 6b (0.75 g, 2.94 mmol, 1 equiv.) and hepta-O-benzoyl-maltose-1-O-trichloroacetimidate[22] (3.57 g, 2.94 mmol, 1 equiv.) in anhydrous CH_2Cl_2 was added dropwise TMSOTf (0.54 mL, 2.97 mmol, 1 equiv.). The reaction mixture was stirred for 24 h. Then the solution was neutralized by addition of Et_3N and concentrated in vacuo. The crude compound was purified by flash chromatography (cyclohexane/AcOEt, 80:20 v/v) to yield compound 7b as a white solid (3.57 g, 93 %). R_f = 0.7 (cyclohexane/AcOEt, 60:40 v/v). ^{1}H NMR ($CDCl_3$, 400 MHz): δ = 8.16–7.19 (35H, m); 6.08 (2H, m, CH); 5.78 (2H, m); 5.69 (1H, t, J = 10 Hz); 5.55 (1H, m); 5.32 (3H, m); 4.97 (1H, m); 4.75 (2H, m, CH); 4.86 (3H, m); 4.31 (1H, m); 4.10 (2H, m); 3.92 (1H, m); 3.62 (1H, m); 1.25 (18H, bs); 0.89 (3H, t, J = 8 Hz). ^{13}C {^{1}H} NMR ($CDCl_3$, 100 MHz): δ = 169.7–164.9; 133.6–126.0; 101.4; 96.5; 74.5; 73.4; 73.0; 72.7; 72.4; 71.9; 70.9; 69.9; 63.4; 62.5; 48.9; 31.9; 31.6; 31.2; 29.4; 26.9; 26.0; 22.7; 14.1. HRMS (ESI-TOF) m/z: [M + H]$^+$ Calcd for $C_{76}H_{78}NO_{19}$ 1308.5181, found 1308.5189.

N-(1-(((2R,3R,4R,5S,6R)-3,4-Dihydroxy-6-(hydroxymethyl)-5-(((2R,3R,4S,5S,6R)-3,4,5-trihydroxy-6-(hydroxymethyl)tetrahydro-2H-pyran-2-yl)oxy)tetrahydro-2H-pyran-2-yl)oxy)dodecan-2-yl)methacrylamide (8a): To a solution of 7a (3.6 g, 2.72 mmol, 1 equiv.) in MeOH was added catalytic amount of MeONa (58 mg, 1.1 mmol, 0.4 equiv.) and the reaction mixture was stirred for 16 h. Then IRC-50 was added, and the solution was filtered and concentrated in vacuo. The crude compound was purified by flash chromatography ($CHCl_3$/MeOH, 80:20 v/v) to yield compound 8a as a white solid (1.3 g, 80 %). R_f = 0.71 ($CHCl_3$/MeOH, 70:30 v/v). ^{1}H NMR (CD_3OD, 400 MHz): δ = 5.67 (1H, d, J = 4 Hz); 5.36 (1H, d, J = 4 Hz); 5.16 (1H, d, J = 4 Hz); 4.28 (1H, d, J = 8 Hz); 4.12 (1H, m); 3.95–3.20 (14H, m); 1.92 (3H, s); 1.60 (2H, m); 1.29 (16H, bs); 0.90 (3H, t, J = 8 Hz). ^{13}C {^{1}H} NMR (CD_3OD, 100 MHz): δ = 169.5; 139.6; 119.1; 103.1; 101.2; 79.7; 75.7; 74.7; 73.2; 72.7; 72.6; 72.1; 71.7; 71.3; 69.7; 61.2; 60.4; 49.4; 49.1; 31.3; 30.7; 29.0; 28.9; 28.8; 25.6; 25.5; 22.1; 17.8; 13.3. HRMS (ESI-TOF) m/z: [M + H]$^+$ Calcd for $C_{28}H_{52}NO_{12}$ 594.3490, found 594.3493.

N-(1-(((2R,3R,4R,5S,6R)-3,4-Dihydroxy-6-(hydroxymethyl)-5-(((2R,3R,4S,5S,6R)-3,4,5-trihydroxy-6-(hydroxymethyl)tetrahydro-2H-pyran-2-yl)oxy)tetrahydro-2H-pyran-2-yl)oxy)dodecan-2-yl)acrylamide (8b): To a solution of 7b (3 g, 2.29 mmol, 1 equiv.) in MeOH was added catalytic amount of MeONa (49 mg, 0.92 mmol, 0.4 equiv.) and the reaction mixture was stirred for 16 h. Then IRC-50 was added, and the solution was filtered and concentrated in vacuo. The crude compound was purified by flash chromatography ($CHCl_3$/MeOH, 80:20 v/v) to yield compound 8b as a white solid (0.93 g, 70 %). R_f = 0.55 ($CHCl_3$/MeOH, 70:30 v/v). ^{1}H NMR (CD_3OD, 400 MHz): δ = 6.22 (2H, m); 5.62 (1H); 5.13 (1H, dd); 4.25 (1H, d, J = 8 Hz); 4.07 (1H, m); 3.90–3.20 (14H, m); 1.55 (2H, m); 1.25 (16H, bs);

EurJOC
European Journal of Organic Chemistry

Full Paper
doi.org/10.1002/ejoc.202000540

Chemistry Europe
European Chemical Societies Publishing

0.86 (3H, t, J = 8 Hz). ^{13}C {^{1}H} NMR (CD_3OD, 100 MHz): δ = 167.9; 132.2; 126.7; 104.8; 102.8; 81.2; 77.6; 76.6; 74.9; 74.7; 74.6; 74.5; 74.0; 72.9; 71.5; 62.7; 62.1; 50.9; 50.6; 32.9; 32.3; 30.6; 30.5; 30.4; 27.0; 23.7. HRMS (ESI-TOF) m/z: [M + Na]$^+$ Calcd for $C_{27}H_{49}NO_{12}Na$ 602.3152, found 602.3153.

2,2-Dimethyl-4-((octyloxy)methyl)-1,3-dioxolane (10): To a suspension of NaH (3.0 g, 127.2 mol, 2.4 equiv.) in anhydrous DMF, was added a solution of **9**[24] (7 g, 53.0 mmol, 1 equiv.) in anhydrous DMF. The solution was stirred for 20 minutes and 1-bromooctane (11 mL, 63.6 mmol, 1.2 equiv.) was added dropwise. The reaction mixture was stirred for 24 h. Then water is added and the solution was extracted twice with AcOEt. The organic layer was dried with anhydrous Na_2SO_4, filtered and concentrated in vacuo. The crude compound was purified by flash chromatography (cyclohexane/AcOEt, 95:5 v/v) to yield compound **10** as a colorless oil (9.5 g, 74 %). R_f = 0.6 (cyclohexane/AcOEt, 90:10 v/v). **^{1}H NMR** ($CDCl_3$, 400 MHz): δ = 4.24 (1H, qt, J = 8 Hz); 4.03 (1H, dd, J = 6 Hz, J = 8 Hz); 3.71 (1H, dd, J = 6 Hz, J = 8 Hz); 3.45 (4H, m); 1.55 (2H, m); 1.40 (3H, s); 1.34 (3H, s); 1.25 (10H, bs); 0.86 (3H, t, J = 8 Hz). **^{13}C {^{1}H} NMR** ($CDCl_3$, 100 MHz): δ = 109.3; 74.8; 71.9; 71.8; 66.9; 31.8; 29.5; 29.4; 29.2; 26.7; 26.0; 25.4; 22.6; 14.0. **HRMS** (ESI-TOF) m/z: [M + H]$^+$ Calcd for $C_{14}H_{20}O_3$ 245.2112, found 245.2118.

3-(Octyloxy)propane-1,2-diol (11): To a solution of **10** (9.3 g, 38.0 mmol, 1 equiv.) in MeOH was added pTsOH (0.65 g, 3.8 mmol, 0.1 equiv.), and the reaction mixture was stirred for 6 h at 80 °C. Then the solution was neutralized by addition of Et_3N and concentrated in vacuo. The crude compound was purified by flash chromatography (cyclohexane/AcOEt, 60:40 v/v) to yield compound **11** as a colorless oil (6.5 g, 84 %). R_f = 0.35 (cyclohexane/AcOEt, 40:60 v/v). ^{1}H NMR ($CDCl_3$, 400 MHz): δ = 3.88 (1H, m); 3.71 (1H, dd, J = 4 Hz, J = 12 Hz); 3.64 (1H, dd, J = 8 Hz, J = 12 Hz); 3.55–3.45 (4H, m); 2.50 (2H, bs); 1.56 (2H, qt, J = 8 Hz); 1.26 (10H, bs); 0.87 (3H, t, J = 8 Hz). ^{13}C {^{1}H} NMR ($CDCl_3$, 400 MHz): δ = 72.4; 71.8; 70.5; 64.2; 31.8; 29.5; 29.4; 29.2; 26.0; 22.6; 14.0. HRMS (ESI-TOF) m/z: [M + H]$^+$ Calcd for $C_{11}H_{25}O_3$ 205.1804, found 205.1804.

1-(Octyloxy)-3-(trityloxy)propan-2-ol (12): To a solution of **11** (5.2 g, 21.3 mmol, 1 equiv.) in anhydrous CH_2Cl_2, was added Et_3N (6.0 mL, 42.6 mmol, 2 equiv.). The solution was stirred at r.t. for 20 min, and trityl chloride (7.2 g, 25.6 mmol, 1.2 equiv.) was added portion-wise. The reaction mixture was stirred for 24 h and the solution was filtered and concentrated in vacuo. The crude compound was purified by flash chromatography (cyclohexane/AcOEt, 90:10 v/v) to yield compound **12** as a colorless oil (9.3 g, 98 %). R_f = 0.32 (cyclohexane/AcOEt, 90:10 v/v). **^{1}H NMR** ($CDCl_3$, 400 MHz): δ = 7.47–7.20 (15H, m); 3.96 (1H, m); 3.54 (1H, dd, J = 4 Hz, J = 12 Hz); 3.48 (1H, dd, J = 8 Hz, J = 12 Hz); 3.44 (2H, m); 3.20 (2H, m); 2.45 (1H, m); 1.55 (2H, m); 1.28 (10H, bs); 0.89 (3H, t, J = 8 Hz). **^{13}C {^{1}H} NMR** ($CDCl_3$, 100 MHz): δ = 143.8; 128.6–127.0; 86.6; 72.0; 71.6; 69.8; 64.6; 31.8; 29.6; 29.4; 29.2; 26.0; 22.6; 14.0. **HRMS** (ESI-TOF) m/z: [M + H]$^+$ Calcd for $C_{30}H_{38}O_3Na$ 469.2713, found 469.2709.

((2-Azido-3-(octyloxy)propoxy)methanetriyl)tribenzene (14): To a solution of **12** (9.3 g, 20.8 mmol, 1 equiv.) in anhydrous CH_2Cl_2, was added Et_3N (5.8 mL, 41.6 mmol, 2 equiv.). The solution stirred for 20 minutes then methanesulfonyl chloride (1.9 mL, 25.0 mmol, 1.2 equiv.) was added dropwise. The reaction mixture was stirred for 16 h and the solution was filtered and concentrated in vacuo. The crude compound was purified by flash chromatography (cyclohexane/AcOEt, 95:5 v/v) to yield compound **13** as a colorless oil (10.0 g, 92 %) which was directly used without further characterization. To a solution of **13** (10.0 g, 19.0 mmol, 1 equiv.) in anhydrous DMF was added portion wise NaN_3 (2.47 g, 38.0 mmol, 2 equiv.). The reaction mixture was stirred for 16 h at 80 °C. Then the solution was diluted with water and extracted twice with AcOEt. The organic layer was dried with anhydrous Na_2SO_4, filtered and concentrated in vacuo. The crude compound was purified by flash chromatography (cyclohexane/AcOEt, 100:0 to 95:5 v/v) to yield compound **14** as a colorless oil (8.3 g, 96 %). R_f = 0.7 (cyclohexane/AcOEt, 95:5 v/v). ^{1}H NMR ($CDCl_3$, 400 MHz): δ = 7.46–7.24 (15H, m); 3.65 (1H, m); 3.55 (2H, m); 3.41 (2H, m); 3.26 (1H, dd, J = 4 Hz, J = 12 Hz); 3.21 (1H, dd, J = 8 Hz, J = 12 Hz); 1.55 (2H, m); 1.27 (10H, bs); 0.89 (3H, t, J = 8 Hz). ^{13}C {^{1}H} NMR ($CDCl_3$, 100 MHz): δ = 143.6; 128.6–127.1; 87.0; 71.6; 70.4; 63.3; 61.2; 31.8; 29.6; 29.4; 29.2; 25.9; 22.6; 14.1. HRMS (ESI-TOF) m/z: [M + H]$^+$ Calcd for $C_{30}H_{38}N_3O_2$ 472.2959, found 472.2957.

1-(Octyloxy)-3-(trityloxy)propan-2-amine (15): To a solution of **14** (8.3 g, 18.2 mmol, 1 equiv.) in Et_2O was added Pd-C (910 mg). The reaction mixture was stirred overnight under a pressure of H_2. Then the solution was filtered through a pad of Celite and concentrated in vacuo. The crude compound was purified by flash chromatography (cyclohexane/AcOEt, 40:60 v/v) to yield compound **15** as a colorless oil (6.9 g, 85 %). R_f = 0.51 (cyclohexane/AcOEt 40: 60 v/v). ^{1}H NMR ($CDCl_3$, 400 MHz): δ = 7.47–7.20 (15H, m); 3.49 (1H, dd, J = 4 Hz, J = 12 Hz); 3.44–3.31 (3H, m); 3.15 (2H, m); 3.05 (1H, m); 1.50 (4H, m); 1.28 (10H, bs); 0.89 (3H, t, J = 8 Hz). ^{13}C {^{1}H} NMR ($CDCl_3$, 100 MHz): δ = 144.1; 128.7–126.9; 86.5; 73.3; 71.5; 65.7; 51.4; 31.8; 29.7; 29.4; 26.9; 26.2; 22.6; 14.1. HRMS (ESI-TOF) m/z: [M + Na]$^+$ Calcd for $C_{30}H_{39}NO_2Na$ 468.2878, found 468.2869.

N-(1-(Octyloxy)-3-(trityloxy)propan-2-yl)methacrylamide (16): To a solution of **15** (6.9 g, 15.5 mmol, 1 equiv.) in anhydrous CH_2Cl_2 was added Et_3N (4.3 mL, 31.0 mmol, 2.0 equiv.). The solution was stirred for 20 minutes then methacryloyl chloride (1.8 mL, 18.6 mmol, 1.2 equiv.) was added dropwise. The reaction mixture was stirred for 2 h and the solution was filtered and concentrated in vacuo. The crude compound was purified by flash chromatography (cyclohexane/AcOEt, 90:10 v/v) to yield compound **16** as a yellow oil (7.32 g, 92 %). R_f = 0.51 (cyclohexane/AcOEt, 80:20 v/v). ^{1}H NMR ($CDCl_3$, 400 MHz): δ = 7.50–7.20 (15H, m); 6.15 (1H, d, J = 8 Hz); 5.65 (1H, s); 5.30 (1H, s); 4.30 (1H, m); 3.71 (1H, dd, J = 4 Hz, J = 8 Hz); 3.58 (1H, dd, J = 6 Hz, J = 10 Hz); 3.42 (2H, t, J = 8 Hz); 3.39 (1H, dd, J = 4 Hz, J = 12 Hz); 3.14 (1H, dd, J = 8 Hz, J = 12 Hz); 1.93 (3H, s); 1.55 (2H, m); 1.27 (10H, bs); 0.89 (3H, t, J = 8 Hz). ^{13}C {^{1}H} NMR ($CDCl_3$, 100 MHz): δ = 167.7; 143.9; 140.0; 128.6–127.0; 119.5; 86.5; 71.3; 69.1; 61.8; 60.3; 48.8; 31.8; 29.7; 29.4; 29.2; 26.1; 22.6; 18.6; 14.1. HRMS (ESI-TOF) m/z: [M + Na]$^+$ Calcd for $C_{34}H_{43}NO_3Na$ 536.3141, found 536.3136.

N-(1-Hydroxy-3-(octyloxy)propan-2-yl)methacrylamide (17): To a solution of **16** (0.92 g, 1.8 mmol, 1 equiv.) in MeOH was added pTsOH (0.03 g, 0.18 mmol, 0.1 equiv.) and the reaction mixture was stirred for 2 h. Then the solution was neutralized by addition of Et_3N and concentrated in vacuo. The crude compound was purified by flash chromatography (cyclohexane/AcOEt, 50:50 v/v) to yield compound **17** as a colorless oil (0.35 g, 80 %). R_f = 0.24 (cyclohexane/AcOEt, 50:50 v/v). ^{1}H NMR ($CDCl_3$, 400 MHz): δ = 6.54 (1H, d, J = 8 Hz); 5.71 (1H, s); 5.32 (1H, s); 4.08 (1H, m); 3.80–3.50 (5H, m); 3.41 (2H, m); 1.94 (3H, s); 1.52 (2H, m); 1.23 (8H, bs); 0.84 (3H, t, J = 8 Hz). ^{13}C {^{1}H} NMR ($CDCl_3$, 100 MHz): δ = 168.5; 139.6; 120.0; 71.6; 70.7; 64.0; 50.7; 31.7; 29.4; 29.3; 29.1; 26.0; 22.5; 18.5; 14.0. HRMS (ESI-TOF) m/z: [M + H]$^+$ Calcd for $C_{15}H_{30}NO_3$ 272.2226, found 272.2234.

(2R,3R,4S,5R,6R)-2-((Benzoyloxy)methyl)-6-(((2R,3R,4S,5R,6R)-4,5-bis(benzoyloxy)-2-((benzoyloxy)methyl)-6-(2-methacrylamido-3-(octyloxy)propoxy)tetrahydro-2H-pyran-3-yl)oxy)-tetrahydro-2H-pyran-3,4,5-triyl Tribenzoate (18): To a solution of 17 (0.35 g, 1.29 mmol, 1 equiv.) and hepta-O-benzoyl-maltose-1-O-

EurJOC
European Journal of Organic Chemistry

Full Paper
doi.org/10.1002/ejoc.202000540

Chemistry Europe
European Chemical Societies Publishing

trichloroacetimidate[22] (1.57 g, 1.29 mmol, 1 equiv.) in anhydrous CH_2Cl_2 was added dropwise TMSOTf (0.23 mL, 1.29 mmol, 1 equiv.). The reaction mixture was stirred for 24 h. Then the solution was neutralized by addition of Et_3N and concentrated in vacuo. The crude compound was purified by flash chromatography (cyclohexane/AcOEt, 80:20 v/v) to yield compound 18 as a white solid (1.37 g, 80 %). R_f = 0.49 (cyclohexane/AcOEt, 60:40 v/v). ^{1}H NMR ($CDCl_3$, 400 MHz): δ = 8.10–7.20 (35H, m); 6.20 (1H, t, J = 10 Hz); 5.95 (1H, m); 5.75 (1H, t, J = 10 Hz); 5.50 (1H, s); 5.44 (1H, dd, J = 4 Hz, J = 12 Hz); 5.13 (1H, s); 4.95 (1H, t, J = 10 Hz); 4.86 (1H, d, J = 12 Hz); 4.70–4.40 (5H, m); 4.25 (1H, m); 4.10–3.90 (4H, m); 3.65 (1H, dd, J = 6 Hz, J = 10 Hz); 3.45 (1H, dd, J = 4 Hz, J = 10 Hz); 3.35–3.20 (3H, m); 2.90 (1H, d, J = 4 Hz); 1.88 (3H, s); 1.46 (2H, m); 1.25 (10H, bs); 0.90 (3H, t, J = 8 Hz). ^{13}C {^{1}H} NMR ($CDCl_3$, 100 MHz): δ = 167.8–165.1; 139.6; 133.4–128.2; 119.5; 100.6; 96.9; 78.2; 75.4; 74.7; 72.6; 71.4; 71.2; 69.9; 69.1; 68.9; 68.4; 68.1; 67.7; 63.4; 62.7; 48.2; 31.7; 29.4; 29.3; 29.2; 25.9; 22.6; 18.3; 18.4; 14.0. HRMS (ESI-TOF) m/z: $[M + H]^+$ Calcd for $C_{76}H_{78}NO_{20}$ 1324.5117, found 1324.5132.

N-(1-(((2R,3R,4R,5S,6R)-3,4-Dihydroxy-6-(hydroxymethyl)-5-(((2R,3R,4S,5S,6R)-3,4,5-trihydroxy-6-(hydroxymethyl)tetrahydro-2H-pyran-2-yl)oxy)tetrahydro-2H-pyran-2-yl)oxy)-3-(octyloxy)propan-2-yl)methacrylamide (19): To a solution of 18 (1.3 g, 0.98 mmol, 1 equiv.) in MeOH was added catalytic amount of MeONa (21 mg, 0.39 mmol, 0.4 equiv.) and the reaction mixture was stirred for 16 h. Then IRC-50 was added, and the solution was filtered and concentrated in vacuo. The crude compound was purified by flash chromatography ($CHCl_3$/MeOH, 80:20 v/v) to yield compound 19 as a white solid (0.51 g, 88 %). R_f = 0.28 ($CHCl_3$/MeOH, 80:20 v/v). ^{1}H NMR (CD_3OD, 400 MHz): δ = 5.70 (1H, d, J = 4 Hz); 5.37 (1H, d, J = 4 Hz); 5.15 (1H, d, J = 4 Hz); 4.28 (2H, m); 4.10–3.20 (18H, m); 1.94 (3H, s, CH_3); 1.54 (2H, qt, J = 8 Hz); 1.28 (10H, bs); 0.89 (3H, t, J = 8 Hz). ^{13}C {^{1}H} NMR (CD_3OD, 100 MHz): δ = 171.3; 141.4; 120.5; 104.7; 102.9; 81.2; 77.7; 76.7; 75.0; 74.7; 74.6; 74.1; 72.3; 71.5; 70.4; 70.2; 69.8; 62.7; 62.2; 50.8; 33.0; 30.7; 30.5; 27.3; 23.7; 18.8; 14.4. HRMS (ESI-TOF) m/z: $[M + H]^+$ Calcd for $C_{27}H_{50}NO_{13}$ 596.3282, found 596.3283.

Isothermal Titration Calorimetry: High-sensitivity microcalorimetry was performed at 25 °C on a VP-ITC (Malvern Instruments, Malvern, UK) for **LC027** and on an iTC200 (Malvern Instruments) for **LC049** and **LC058**. All solutions were prepared in phosphate buffer (10 mM NaH_2PO_4/Na_2HPO_4 and 150 mM NaCl at pH 7.4). For demicellization experiments 10-µL aliquots of 7 mM **LC027** and 1.5-µL aliquots 8 mM **LC058** were titrated into buffer, whereas 1-µL aliquots of 70 mM **LC049** were titrated into a cell preloaded with 3 mM monomer. Time spacings between consecutive injections were chosen long enough to allow for complete re-equilibration. Baseline subtraction and peak integration were performed using NITPIC.[28] All reactions heats were normalized with respect to the molar amount of detergent. Non-linear least-squares fitting was performed using D/STAIN.[29]

Surface Tension Measurements: The surface activity of detergents in solution at the air/water interface was determined using a K100 tensiometer (Kruss, Hamburg, Germany). Surface tensions were determined by dilution of stock solutions (ca. 5 × CMC) using the Wilhelmy plate technique. In a typical experiment, 20–30 concentration steps were used with ca. 5–10 min between each concentration step. All measurements were performed at (25.0 ± 0.5) °C.

Dynamic Light Scattering: Hydrodynamic particle size distributions were determined on a Nano Zetasizer ZS90 (Malvern Instruments, UK) equipped with a He–Ne laser (λ = 633 nm). Except for **LC048** all measurements were performed at (25 ± 0.5) °C. Measurements for **LC048** were performed at 35 °C to keep the compound in solution. The concentration for each measurement was 2 × (CMC + 5 mM) in buffer (50 mM Tris, 200 mM NaCl, pH 7.4). The time dependent correlation function of the scattered light intensity was measured at an angle of 90°. The hydrodynamic diameter (D_H) of the particles was estimated from their diffusion coefficient (D) using the Stokes–Einstein equation, $D = k_BT/3\pi\eta D_H$, where k_B is Boltzmann's constant, T absolute temperature, and η the viscosity of the solvent.

Vesicle Solubilization: POPC in powder form was suspended in phosphate buffer (10 mM NaH_2PO_4/Na_2HPO_4 and 150 mM NaCl at pH 7.4). To obtain large unilamellar vesicles (LUVs), the suspension was extruded 35 times through two stacked polycarbonate membranes with a nominal pore diameter of 100 nm using a LiposoFast extruder (Avestin, Ottawa, Canada). Unimodal size distribution was confirmed by DLS. A 0.6 mM stock solution of POPC LUVs and detergent were mixed in a 3 mm × 3 mm quartz glass cuvette (Hellma, Müllheim, Germany) before the light scattering intensity was monitored at 25 °C using a Nano Zetasizer ZS90 (Malvern) equipped with a 633-nm He–Ne laser and a detection angle of 90°. To ensure quantitative comparability of scattering intensities, the attenuator was fixed to the maximum open position.

Extraction of MPs from *E. coli* Membranes: *E. coli* BL21(DE3) cells were transformed with an empty pET-24 vector and thus selected by kanamycin resistance. After incubation in lysogeny broth overnight at 37 °C under permanent agitation, cells were harvested by centrifugation and washed twice with saline (154 mM NaCl). Cell pellets were resuspended in ice-cold buffer (100 mM Na_2CO_3, pH 11.5) to a concentration below ca. 0.1 g mL^{-1} and ultrasonicated twice for 10 min in an S-250A sonifier (Branson Ultrasonics, Danbury, USA). To remove cell debris, the lysate was centrifuged at 4 °C for 30 min at 1000 *g*. The supernatant was centrifuged at 4 °C for 1 h at 100,000 *g* to separate membrane fragments from soluble and peripheral proteins. Membrane fragments were resuspended in buffer (50 mM Tris, 200 mM NaCl, pH 7.4) to a final concentration of 100 mg wet-weight pellet per 1 mL of buffer and mixed in a 1:1 volume ratio with stock solutions of DDM or monomers in buffer. Surfactant concentrations were chosen based on the CMC values determined in this study to ensure comparable extraction conditions. All samples were incubated for 16 h at 20 °C under gentle agitation. After ultracentrifugation at 4 °C for 1 h at 100,000 *g*, the supernatant containing micelles was analyzed using SDS-PAGE. Extraction yields were then determined densitometrically using ImageJ gel analysis.[30]

Solubilization of A_{2A}R and AcrB: Adenosine receptor (A_{2A}R) was expressed in insect cells as described.[31] AcrB was expressed in *E.coli* as previously reported.[32] Membrane fractions were incubated for 2 h at 4 °C at a final concentration of 5mg/mL in 50 mM Hepes buffer pH 7.4, 200 mM NaCl, 1X protease inhibitor cocktail, and with 10-fold the CMC of DDM in combination with CHS or LC compounds. After solubilization samples were centrifuged at 100000 g for 45 min at 4 °C and an aliquot of the total extract, the pellet and the supernatant from each solubilization condition was analyzed by SDS-PAGE and western-blot using an antibody A_{2A}R (7F6-G5-A2) and against the his-tag for AcrB, respectively. Solubilization efficiency was evaluated by comparing the band intensity (in western blot) of the Soluble (S) to the insoluble (P for Pellet) fractions.

Supporting Information (see footnote on the first page of this article): ^{1}H and ^{13}C NMR spectra of compounds; HPLC chromatograms of **LC027**, **LC048**, **LC049**, and **LC058**. Contin distribution plots in pure water for **LC027**, **LC048**, and **LC058**.

EurJOC
European Journal of Organic Chemistry

Full Paper
doi.org/10.1002/ejoc.202000540

Chemistry Europe
European Chemical Societies Publishing

Acknowledgments

This work was supported by the Agence Nationale de la Recherche (ANR) through grants no. ANR-14-LAB7-0002 and by the Deutsche Forschungsgemeinschaft (DFG) through grant no. KE 1478/7-1. Christophe Bonnet was the recipient of a PhD fellowship from "Région Provence Alpes Côte d'Azur".

Keywords: Detergents · Monomers · Surfmers · Extraction · Membrane proteins

[1] M. E. Bunnage, *Nat. Chem. Biol.* **2011**, *7*, 335–339.
[2] a) P. S. Chae, R. R. Rana, K. Gotfryd, S. G. F. Rasmussen, A. C. Kruse, K. H. Cho, S. Capaldi, E. Carlsson, B. Kobilka, C. J. Loland, U. Gether, S. Banerjee, B. Byrne, J. K. Lee, S. H. Gellman, *Chem. Commun.* **2013**, *49*, 2287–2289; b) P. S. Chae, S. G. F. Rasmussen, R. R. Rana, K. Gotfryd, R. Chandra, M. A. Goren, A. C. Kruse, S. Nurva, C. J. Loland, Y. Pierre, D. Drew, J.-L. Popot, D. Picot, B. G. Fox, L. Guan, U. Gether, B. Byrne, B. Kobilka, S. H. Gellman, *Nat. Methods* **2010**, *7*, 1003–1008.
[3] W.-X. Hong, K. A. Baker, X. Ma, R. C. Stevens, M. Yeager, Q. Zhang, *Langmuir* **2010**, *26*, 8690–8696.
[4] a) E. Frotscher, B. Danielczak, C. Vargas, A. Meister, G. Durand, S. Keller, *Angew. Chem. Int. Ed.* **2015**, *54*, 5069–5073; *Angew. Chem.* **2015**, *127*, 5158; b) C. Breyton, F. Gabel, M. Abla, Y. Pierre, F. Lebaupain, G. Durand, J.-L. Popot, C. Ebel, B. Pucci, *Biophys. J.* **2009**, *97*, 1–10.
[5] a) Q. Zhang, X. Ma, A. Ward, W.-X. Hong, V.-P. Jaakola, R. C. Stevens, M. G. Finn, G. Chang, *Angew. Chem. Int. Ed.* **2007**, *46*, 7023–7025; *Angew. Chem.* **2007**, *119*, 7153; b) S. C. Howell, R. Mittal, L. Huang, B. Travis, R. M. Breyer, C. R. Sanders, *Biochemistry* **2010**, *49*, 9572–9583; c) P. S. Chae, K. Gotfryd, J. Pacyna, L. J. W. Miercke, S. G. F. Rasmussen, R. A. Robbins, R. R. Rana, C. J. Loland, B. Kobilka, R. Stroud, B. Byrne, U. Gether, S. H. Gellman, *J. Am. Chem. Soc.* **2010**, *132*, 16750–16752.
[6] a) T. H. Bayburt, Y. V. Grinkova, S. G. Sligar, *Nano Lett.* **2002**, *2*, 853–856; b) I. G. Denisov, Y. V. Grinkova, A. A. Lazarides, S. G. Sligar, *J. Am. Chem. Soc.* **2004**, *126*, 3477–3487.
[7] J.-L. Popot, T. Althoff, D. Bagnard, J.-L. Banères, P. Bazzacco, E. Billon-Denis, L. J. Catoire, P. Champeil, D. Charvolin, M. J. Cocco, G. Crémel, T. Dahmane, L. M. de la Maza, C. Ebel, F. Gabel, F. Giusti, Y. Gohon, E. Goormaghtigh, E. Guittet, J. H. Kleinschmidt, W. Kühlbrandt, C. Le Bon, K. L. Martinez, M. Picard, B. Pucci, J. N. Sachs, C. Tribet, C. van Heijenoort, F. Wien, F. Zito, M. Zoonens, *Annual Rev. Biophys.* **2011**, *40*, 379–408.
[8] a) J. M. Dörr, M. C. Koorengevel, M. Schäfer, A. V. Prokofyev, S. Scheidelaar, E. A. W. van der Cruijsen, T. R. Dafforn, M. Baldus, J. A. Killian, *Proc. Natl. Acad. Sci. USA* **2014**, *111*, 18607–18612; b) T. J. Knowles, R. Finka, C. Smith, Y.-P. Lin, T. Dafforn, M. Overduin, *J. Am. Chem. Soc.* **2009**, *131*, 7484–7485.
[9] A. O. Oluwole, B. Danielczak, A. Meister, J. O. Babalola, C. Vargas, S. Keller, *Angew. Chem. Int. Ed.* **2017**, *56*, 1919–1924; *Angew. Chem.* **2017**, *129*, 1946.
[10] M. Picard, T. Dahmane, M. Garrigos, C. Gauron, F. Giusti, M. le Maire, J.-L. Popot, P. Champeil, *Biochemistry* **2006**, *45*, 1861–1869.
[11] J. K. Nagy, A. Kuhn Hoffmann, M. H. Keyes, D. N. Gray, K. Oxenoid, C. R. Sanders, *FEBS Lett.* **2001**, *501*, 115–120.
[12] T. Dahmane, F. Giusti, L. J. Catoire, J.-L. Popot, *Biopolymers* **2011**, *95*, 811–823.
[13] C. Diab, C. Tribet, Y. Gohon, J.-L. Popot, F. M. Winnik, *Biochim. Biophys. Acta* **2007**, *1768*, 2737–2747.
[14] a) K. S. Sharma, G. Durand, F. Gabel, P. Bazzacco, C. Le Bon, E. Billon-Denis, L. J. Catoire, J.-L. Popot, C. Ebel, B. Pucci, *Langmuir* **2012**, *28*, 4625–4639; b) K. S. Sharma, G. Durand, F. Giusti, B. Olivier, A.-S. Fabiano, P. Bazzacco, T. Dahmane, C. Ebel, J.-L. Popot, B. Pucci, *Langmuir* **2008**, *24*, 13581–13590.
[15] P. Bazzacco, K. S. Sharma, G. Durand, F. Giusti, C. Ebel, J.-L. Popot, B. Pucci, *Biomacromolecules* **2009**, *10*, 3317–3326.
[16] S. K. Sharma, G. Durand, B. Pucci, *Des. Monomers Polym.* **2011**, *14*, 499–513.
[17] a) P. Anton, P. Köberle, A. Laschewsky, *Makromol. Chem.* **1993**, *194*, 1–27; b) A. Guyot, *Curr. Opin. Colloid Interface Sci.* **1996**, *1*, 580–586; c) K. Nagai, H.-G. Elias, *Makromol. Chem.* **1987**, *188*, 1095–1127.
[18] a) P. Bazzacco, E. Billon-Denis, K. S. Sharma, L. J. Catoire, S. Mary, C. Le Bon, E. Point, J.-L. Baneres, G. Durand, F. Zito, B. Pucci, J.-L. Popot, *Biochemistry* **2012**, *51*, 1416–1430; b) C. Bechara, G. Bolbach, P. Bazzaco, K. S. Sharma, G. Durand, J.-L. Popot, F. Zito, S. Sagan, *Anal. Chem.* **2012**, *84*, 6128–6135.
[19] T. Bausewein, D. J. Mills, J. D. Langer, B. Nitschke, S. Nussberger, W. Kühlbrandt, *Cell* **2017**, *170*, 693–700e697.
[20] C. Bonnet, P. Guillet, S. Igonet, A. Meister, A. Marconnet, S. Keller, A. Jawhari, G. Durand, *J. Org. Chem.* **2019**, *84*, 10606–10614.
[21] K. J. Jensen, *J. Chem. Soc. Perkin Trans. 1* **2002**, 2219–2233.
[22] Á. G. Barrientos, J. M. de la Fuente, T. C. Rojas, A. Fernández, S. Penadés, *Chem. Eur. J.* **2003**, *9*, 1909–1921.
[23] H. Minamikawa, T. Murakami, M. Hato, *Chem. Phys. Lipids* **1994**, *67–74*, 111–118.
[24] M. Sutter, E. D. Silva, N. Duguet, Y. Raoul, E. Métay, M. Lemaire, *Chem. Rev.* **2015**, *115*, 8609–8651.
[25] a) A. Polidori, S. Raynal, L.-A. Barret, M. Dahani, C. Barrot-Ivolot, C. Jungas, E. Frotscher, S. Keller, C. Ebel, C. Breyton, F. Bonnete, *New J. Chem.* **2016**, *40*, 5364–5378; b) S.-C. Tso, F. Mahler, J. Höring, S. Keller, C. A. Brautigam, *Anal. Chem.* **2020**, *92*, 1154–1161.
[26] P. Guillet, F. Mahler, K. Garnier, G. Nyame Mendendy Boussambe, S. Igonet, C. Vargas, C. Ebel, M. Soulié, S. Keller, A. Jawhari, G. Durand, *Langmuir* **2019**, *35*, 4287.
[27] B. T. Arachea, Z. Sun, N. Potente, R. Malik, D. Isailovic, R. E. Viola, *Protein Expression Purif.* **2012**, *86*, 12–20.
[28] S. Keller, C. Vargas, H. Zhao, G. Piszczek, C. A. Brautigam, P. Schuck, *Anal. Chem.* **2012**, *84*, 5066–5073.
[29] a) M. Textor, S. Keller, *Anal. Biochem.* **2015**, *485*, 119–121;b) S.C. Tso, F. Mahler, J. Höring, S. Keller, C.A. Brautigam, *Anal. Chem.* **2020**, *92*, 1154–1161.
[30] C. A. Schneider, W. S. Rasband, K. W. Eliceiri, *Nat. Methods* **2012**, *9*, 671–675.
[31] S. Igonet, C. Raingeval, E. Cecon, M. Pučić-Baković, G. Lauc, O. Cala, M. Baranowski, J. Perez, R. Jockers, I. Krimm, A. Jawhari, *Sci. Rep.* **2018**, *8*, 8142.
[32] K. M. Pos, K. Diederichs, *Acta Crystallogr., Sect. D* **2002**, *58*, 1865–1867.

Received: April 20, 2020

Supporting Information

Detergent-Like Polymerizable Monomers: Synthesis, Physicochemical, and Biochemical Characterization

Christophe Bonnet, Pierre Guillet, Florian Mahler, Sébastien Igonet, Sandro Keller, Anass Jawhari, Grégory Durand*

Table of contents **Pages**

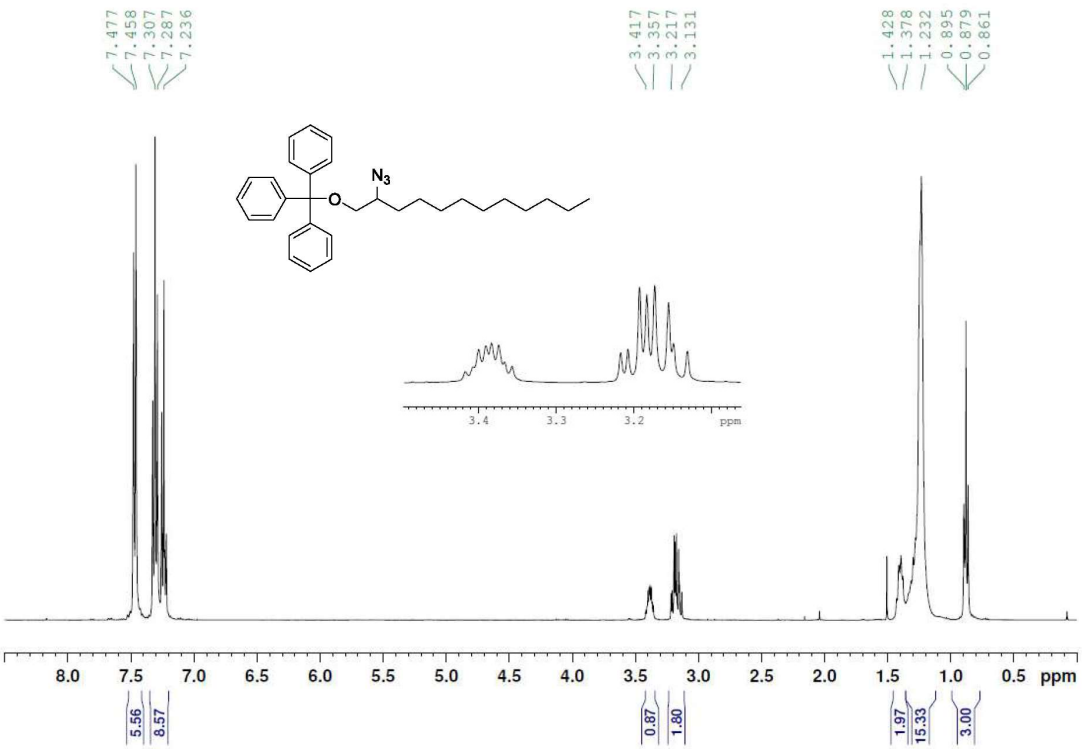

Figure S1. ^{1}H NMR spectrum of **3** in $CDCl_3$.

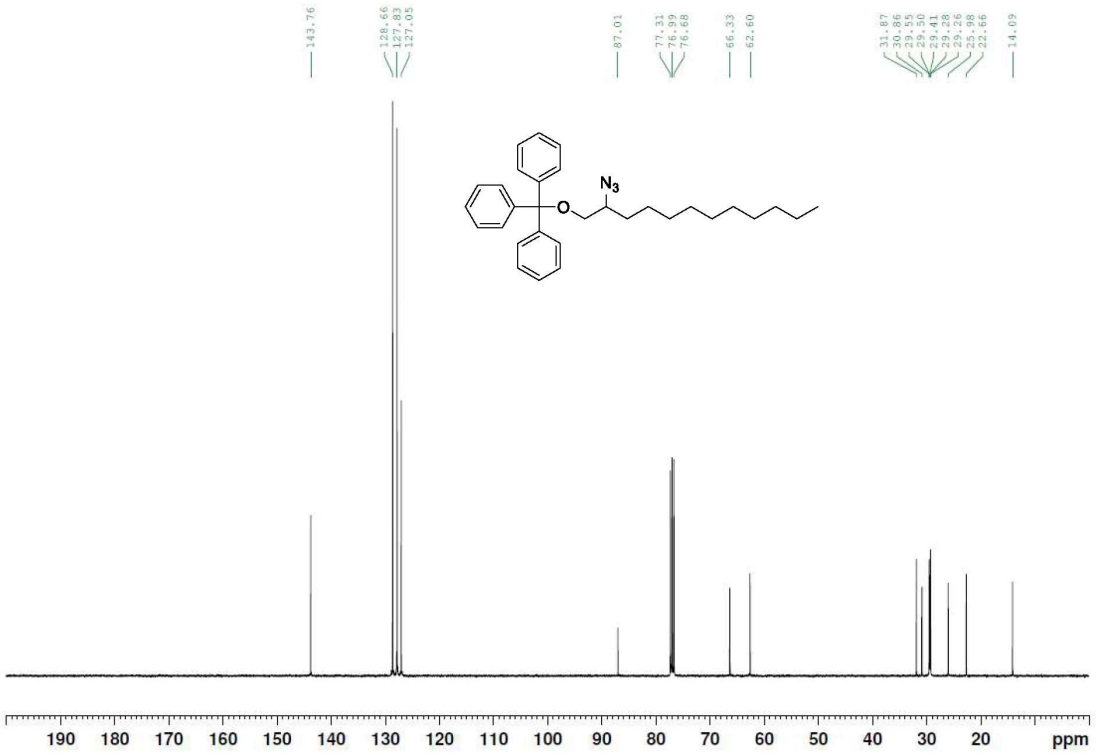

Figure S2. ^{13}C NMR spectrum spectrum of **3** in $CDCl_3$.

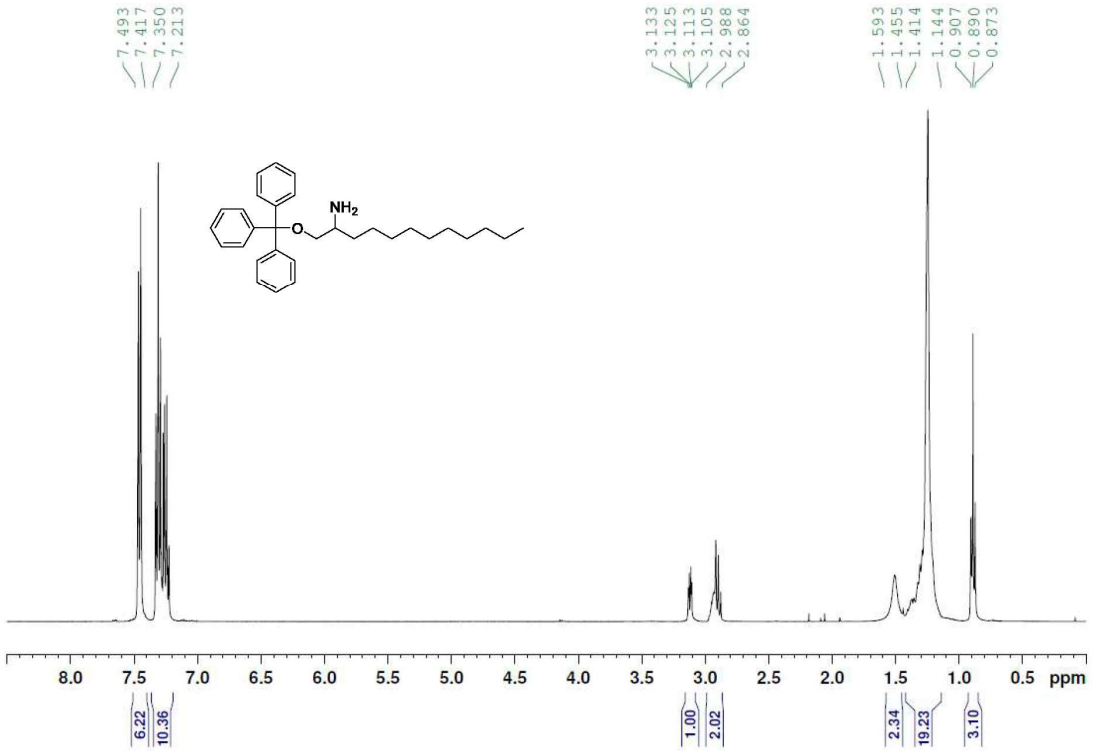

Figure S3. ^{1}H NMR spectrum of **4** in $CDCl_3$.

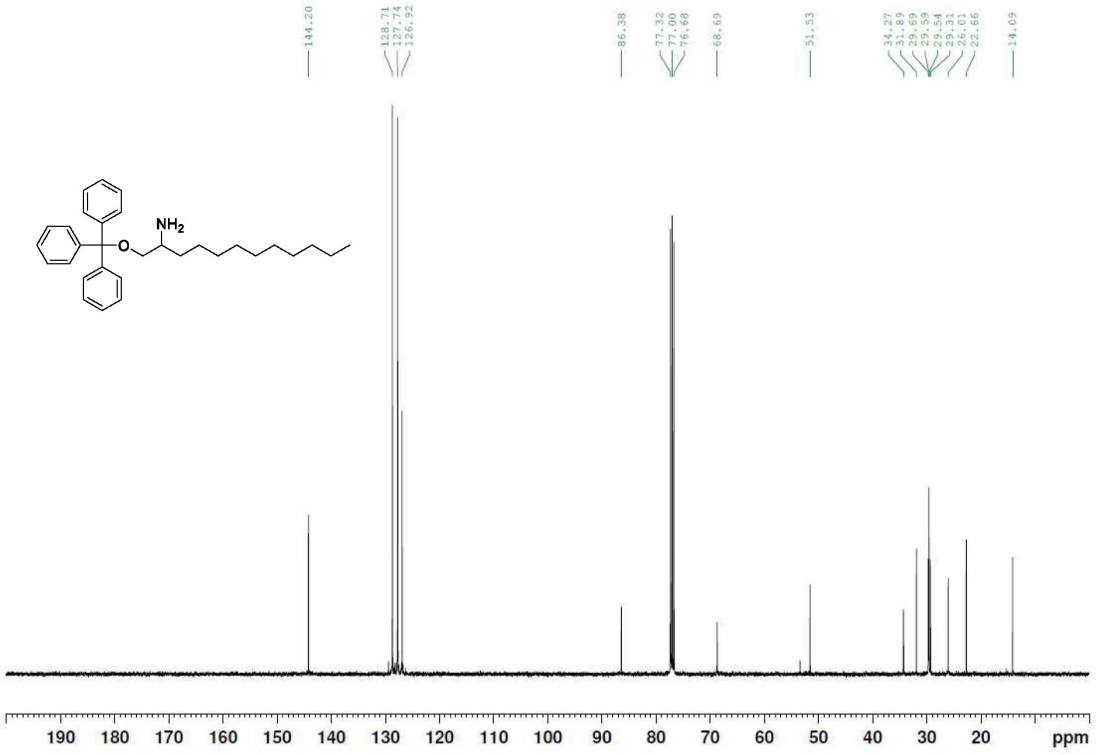

Figure S4. ^{13}C NMR spectrum spectrum of **4** in $CDCl_3$.

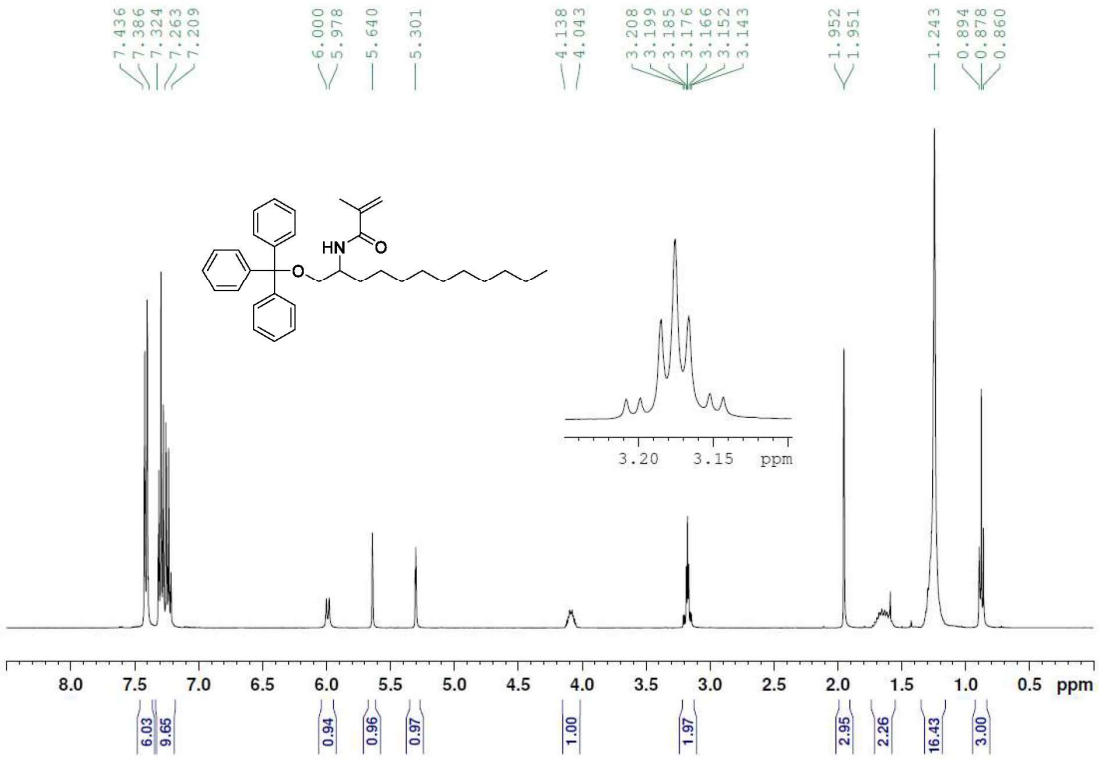

Figure S5. ^{1}H NMR spectrum of **5a** in $CDCl_3$.

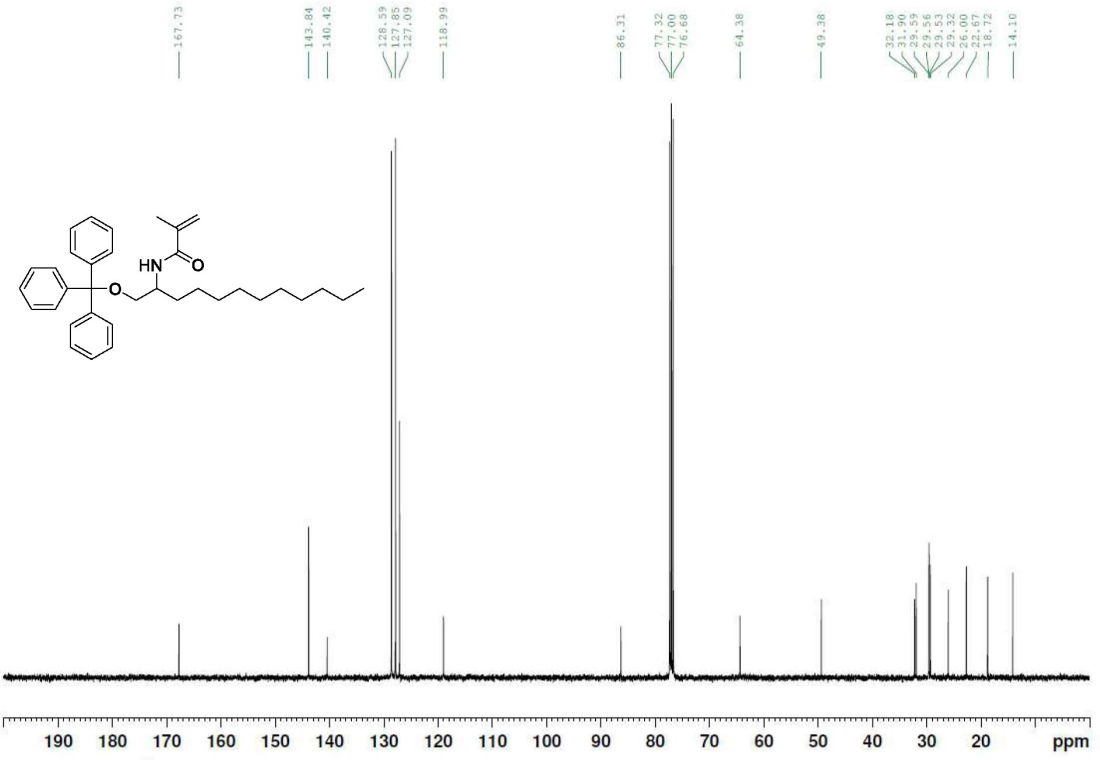

Figure S6. ^{13}C NMR spectrum spectrum of **5a** in $CDCl_3$.

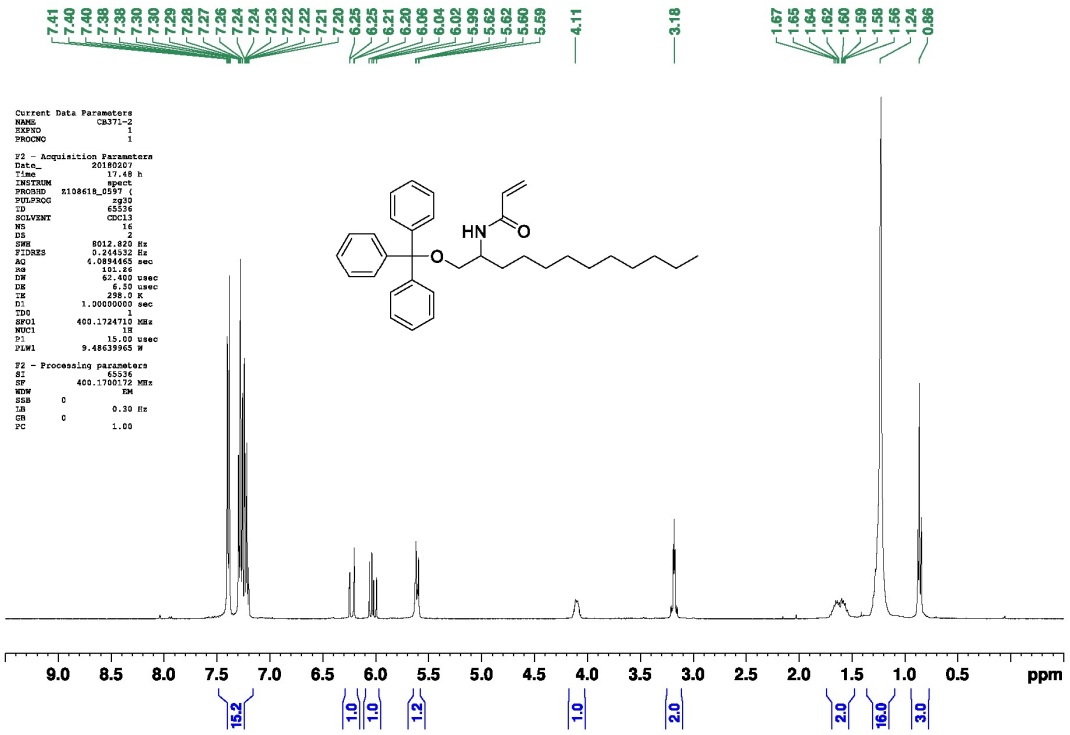

Figure S7. ^{1}H NMR spectrum of **5b** in $CDCl_3$.

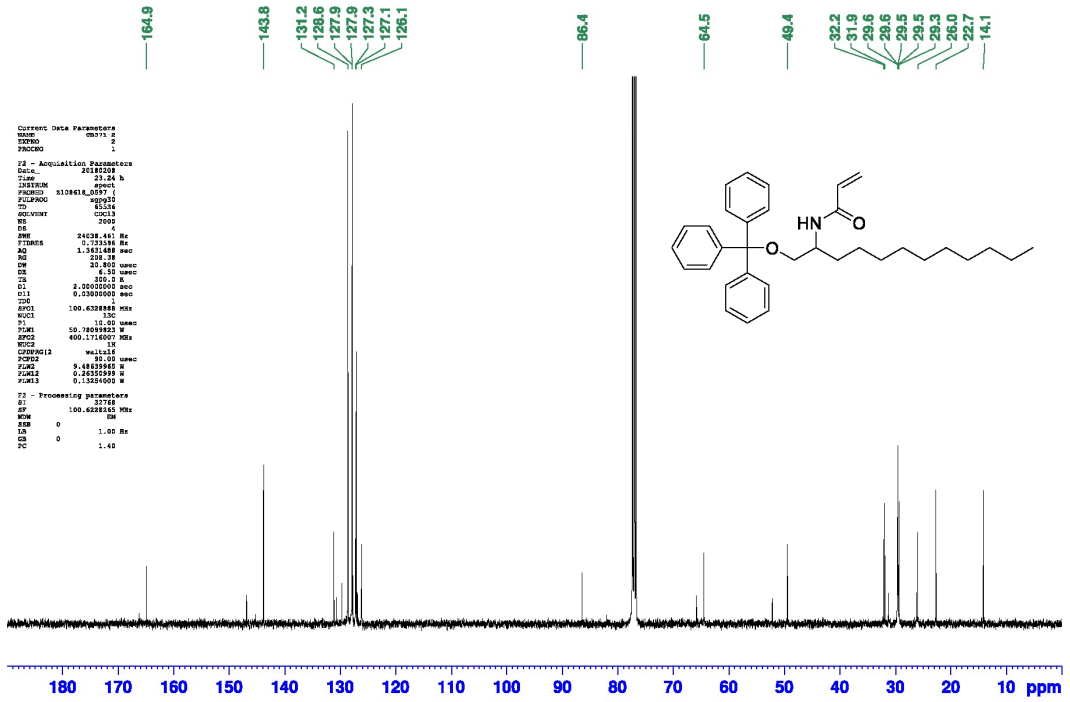

Figure S8. ^{13}C NMR spectrum spectrum of **5b** in $CDCl_3$.

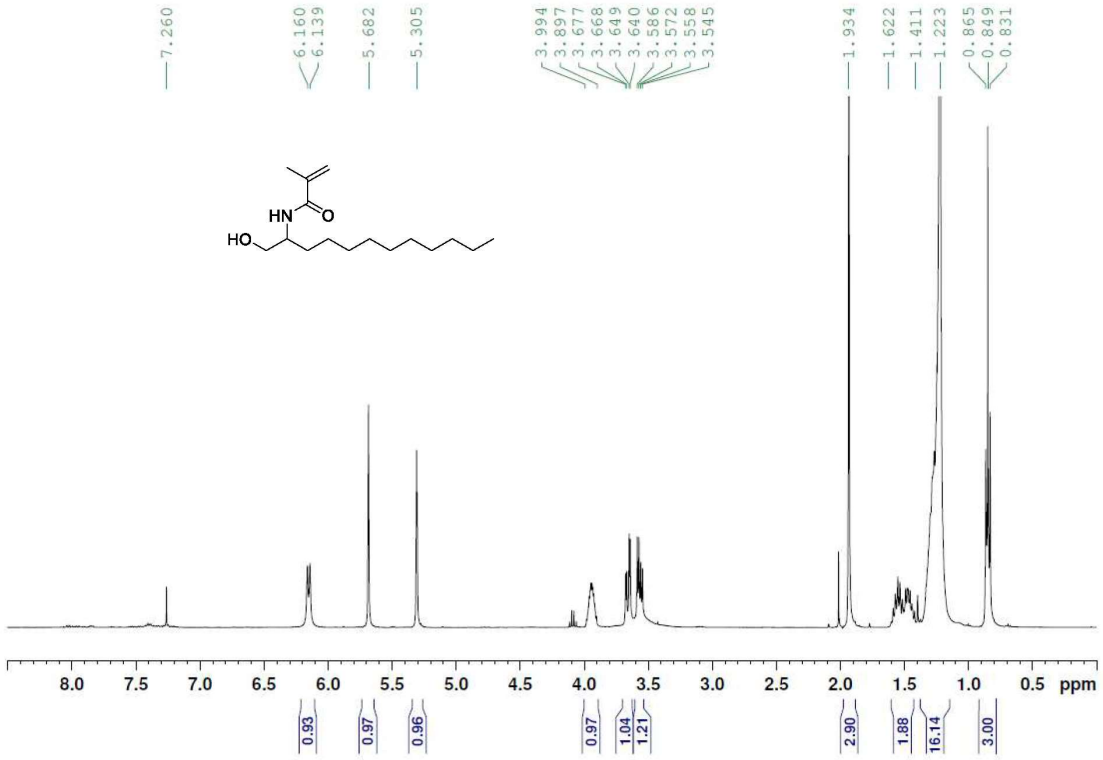

Figure S9. ^{1}H NMR spectrum of **6a** in $CDCl_3$.

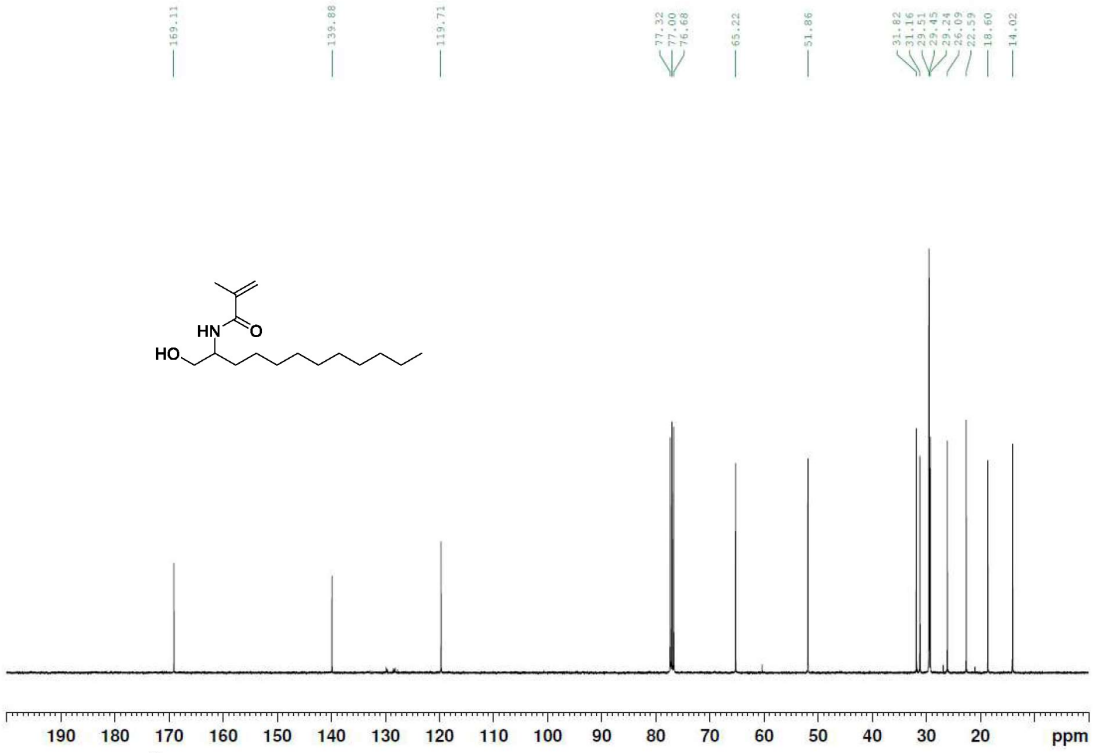

Figure S10. ^{13}C NMR spectrum spectrum of **6a** in $CDCl_3$.

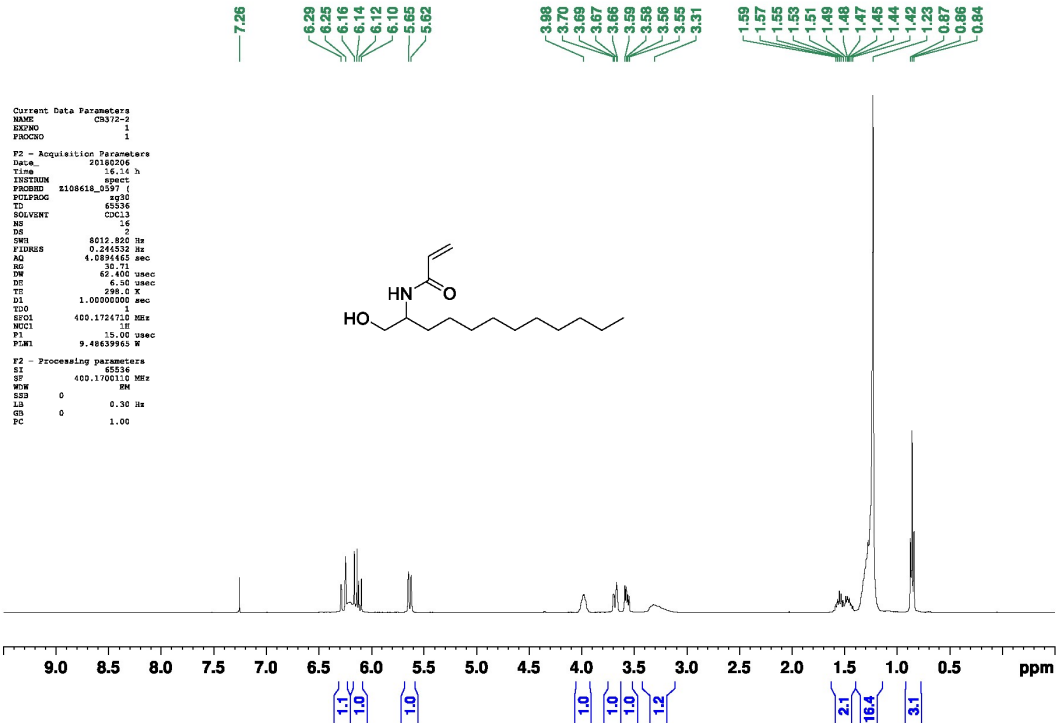

Figure S11. ^{1}H NMR spectrum of **6b** in $CDCl_3$.

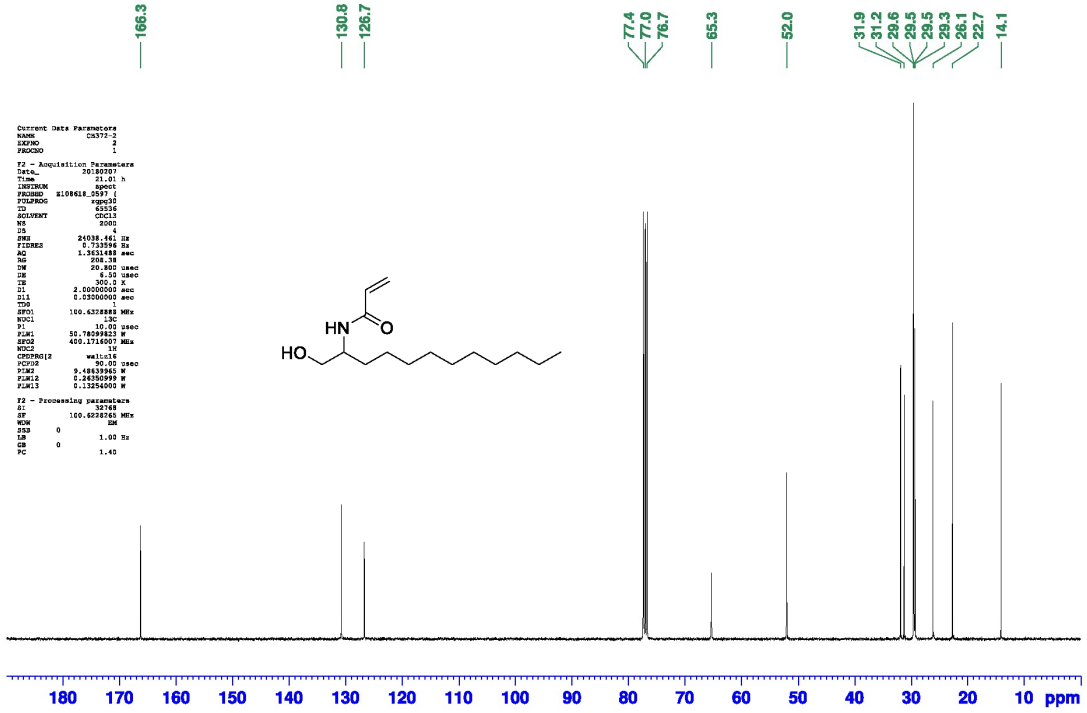

Figure S12. ^{13}C NMR spectrum spectrum of **6b** in $CDCl_3$.

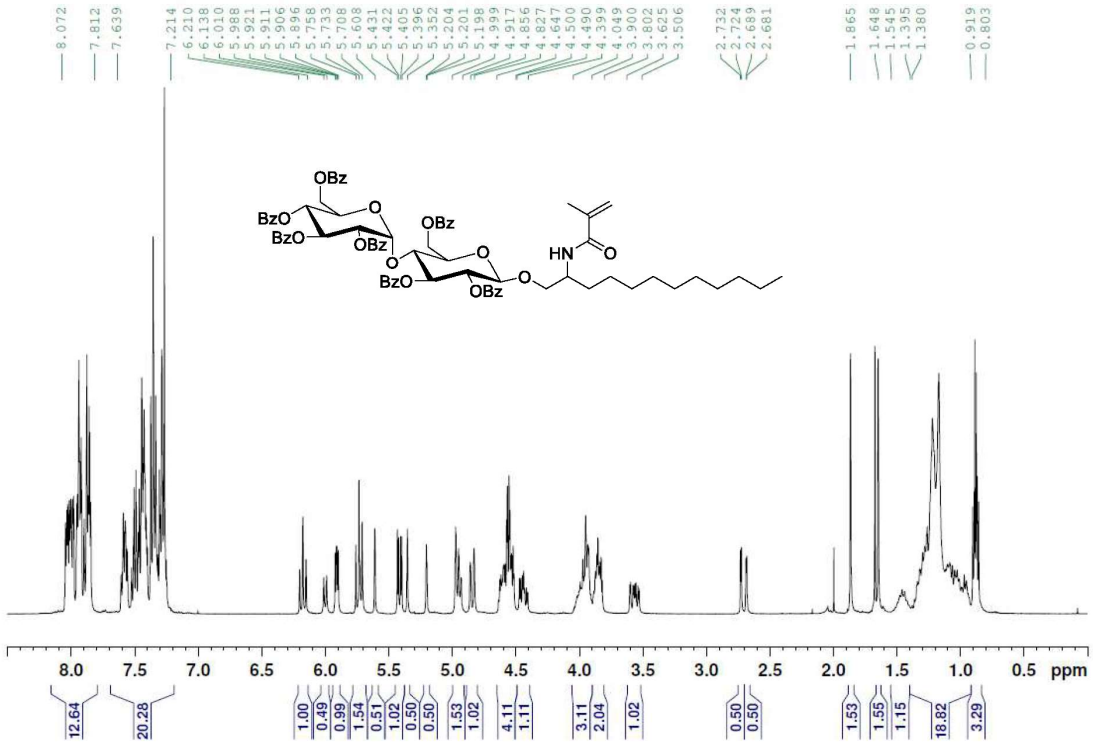

Figure S13. ^{1}H NMR spectrum of **7a** in $CDCl_3$.

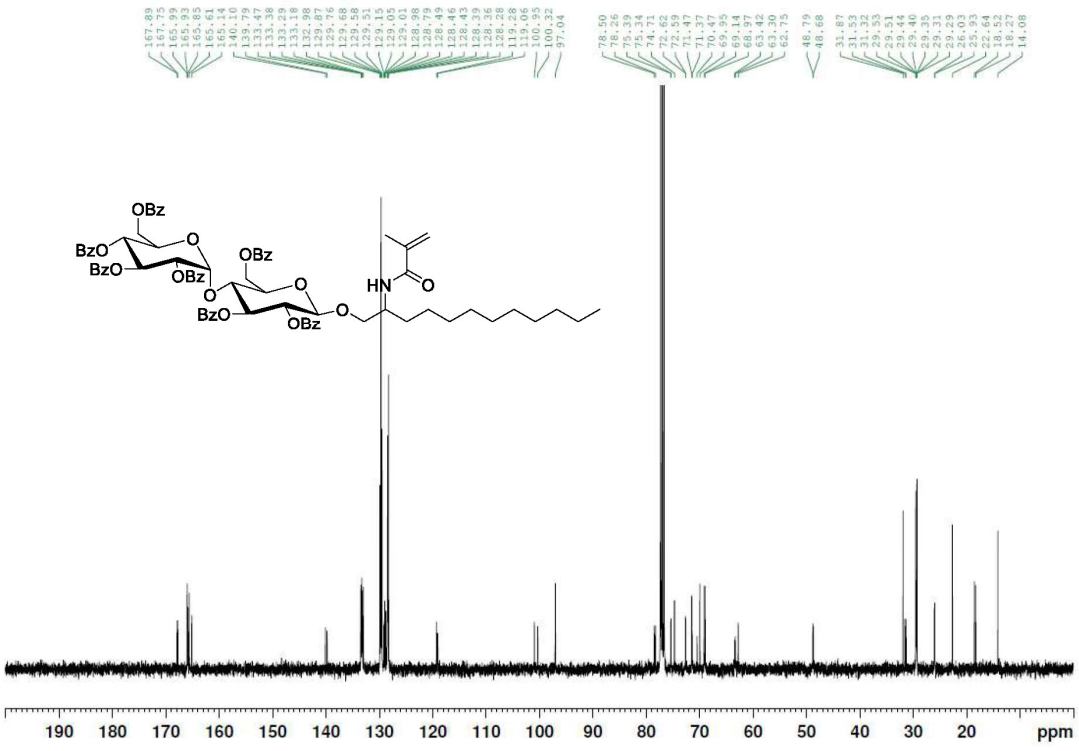

Figure S14. ^{13}C NMR spectrum spectrum of **7a** in $CDCl_3$.

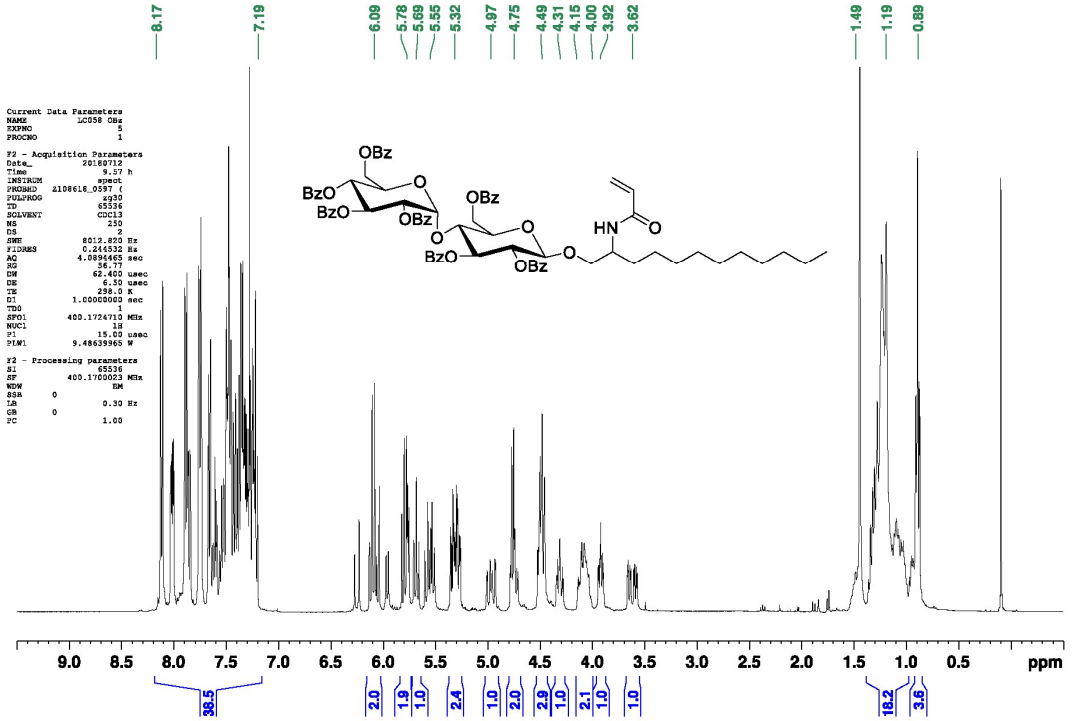

Figure S15. ^{1}H NMR spectrum of **7b** in $CDCl_3$.

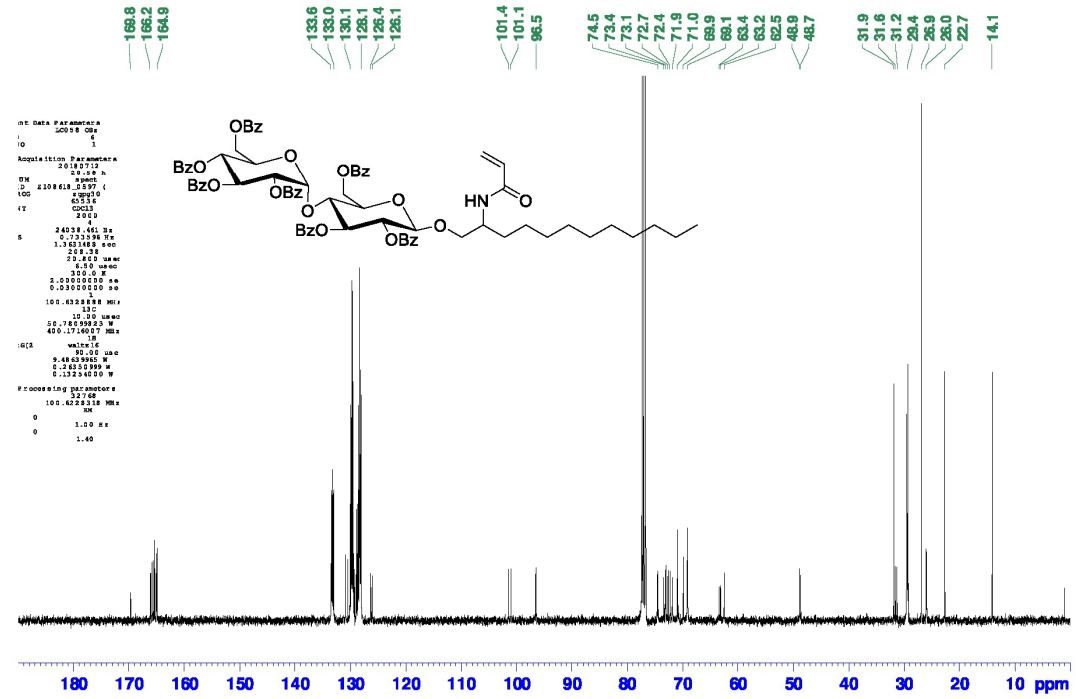

Figure S16. ^{13}C NMR spectrum spectrum of **7b** in $CDCl_3$.

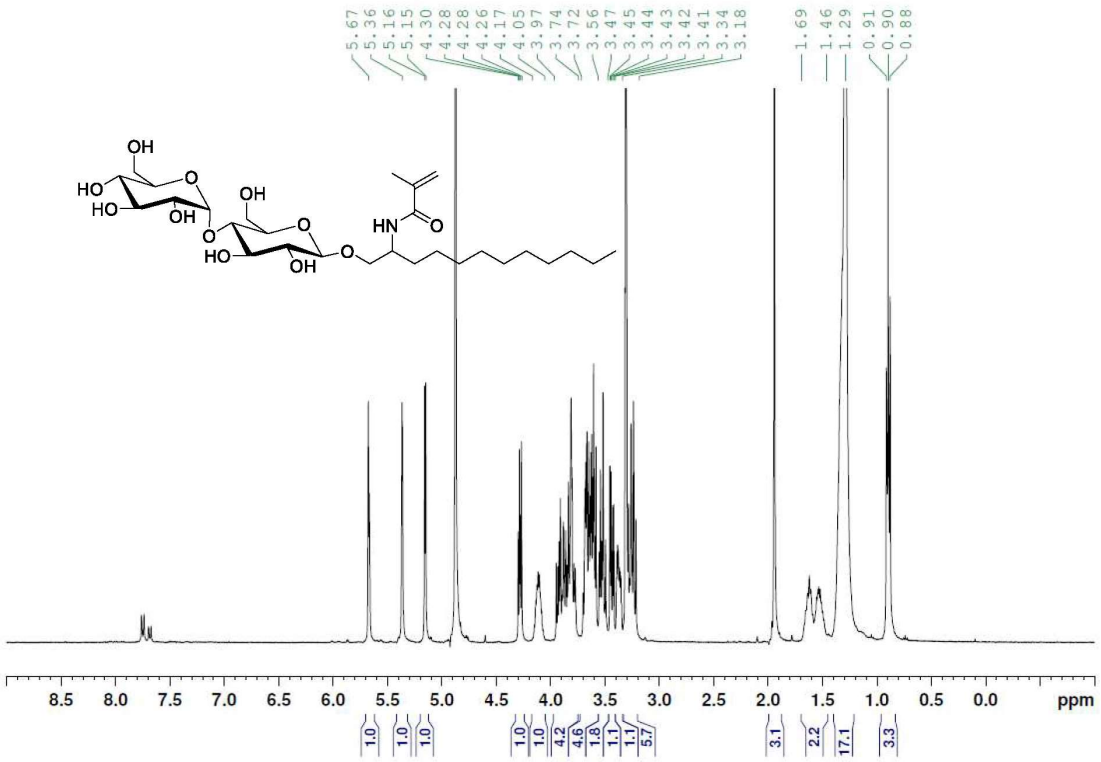

Figure S17. ^{1}H NMR spectrum of **8a** in CD_3OD.

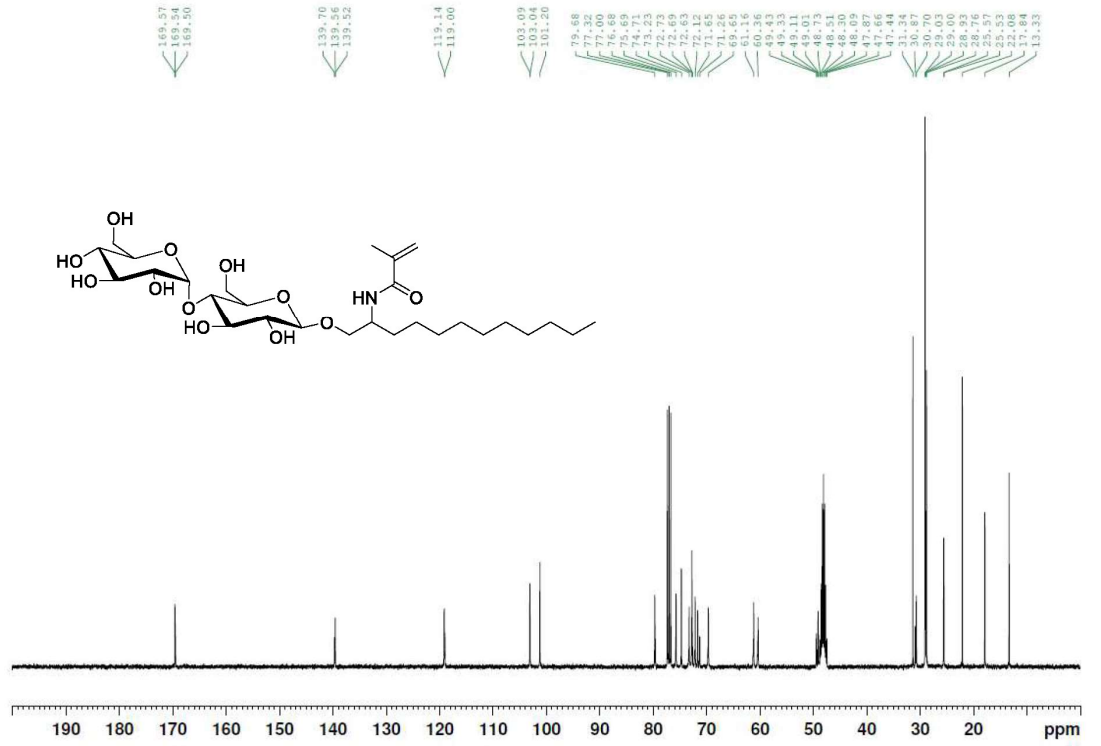

Figure S18. ^{13}C NMR spectrum spectrum of **8a** in CD_3OD.

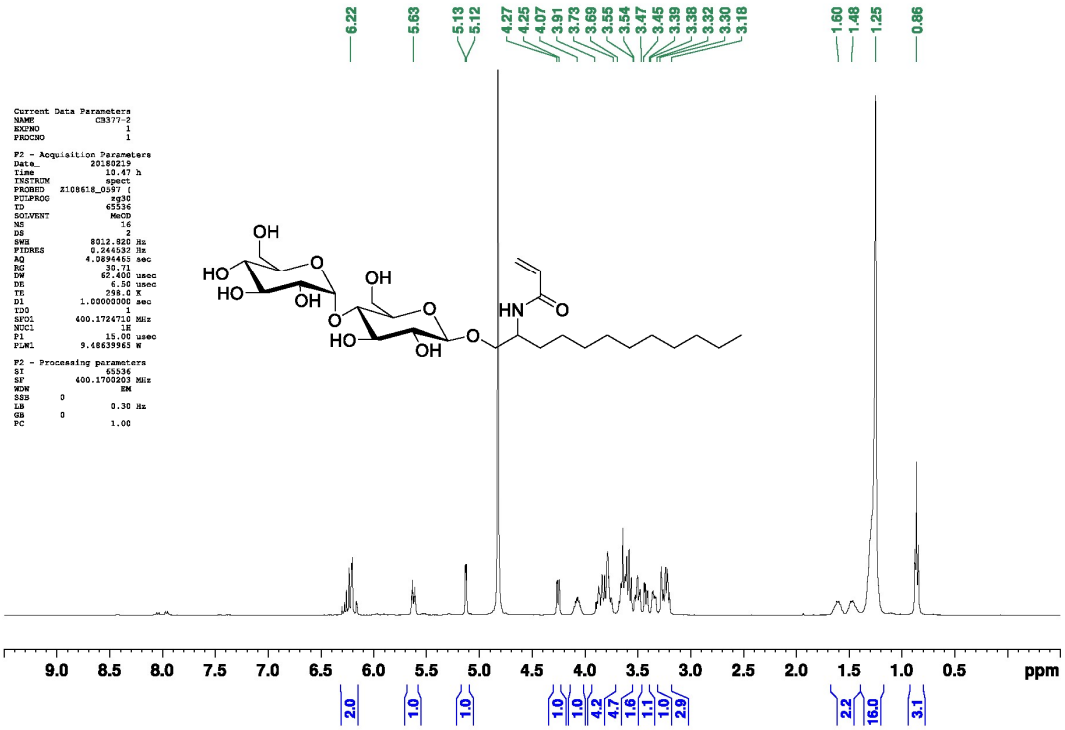

Figure S19. ^{1}H NMR spectrum of **8b** in CD_3OD.

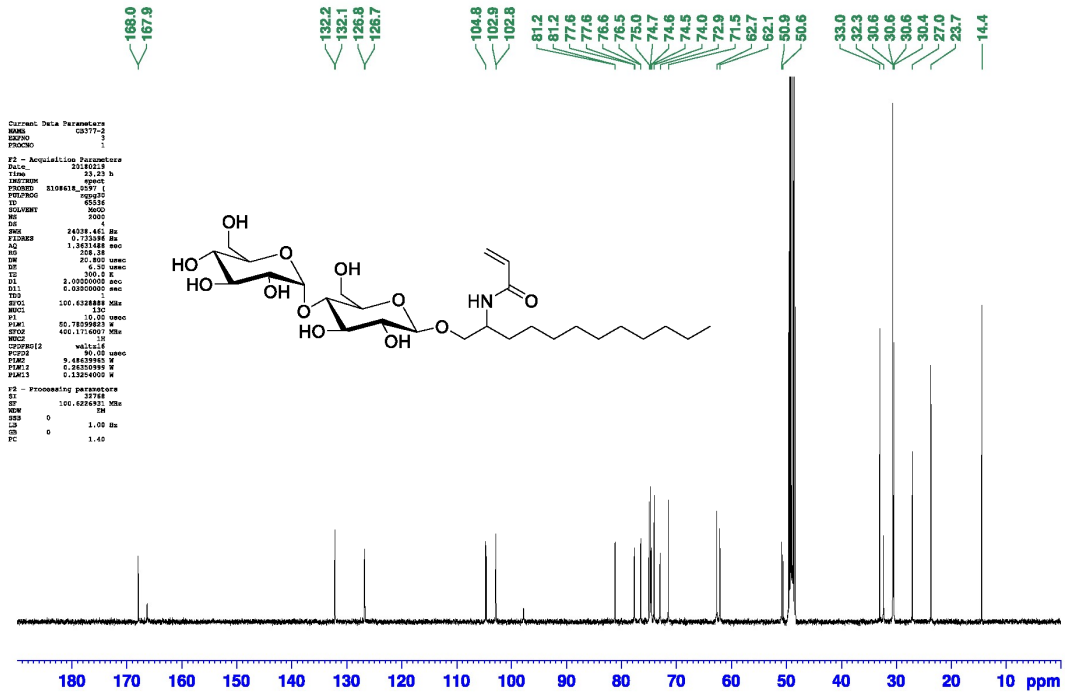

Figure S20. ^{13}C NMR spectrum spectrum of **8b** in CD_3OD.

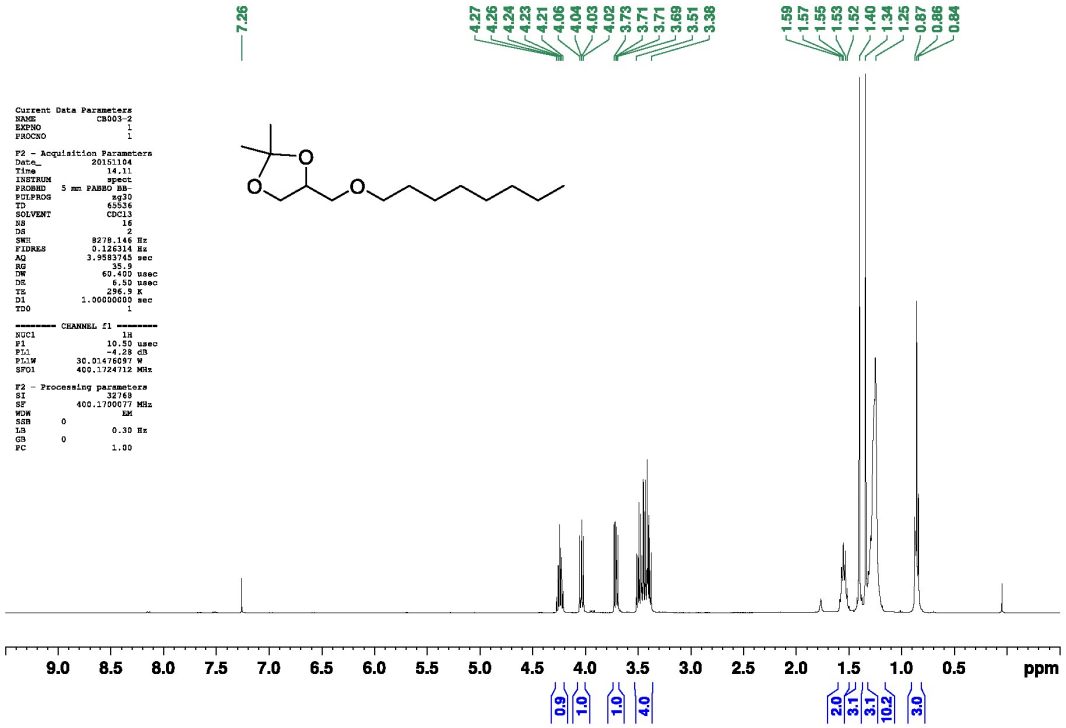

Figure S21. ^{1}H NMR spectrum of **10** in $CDCl_3$.

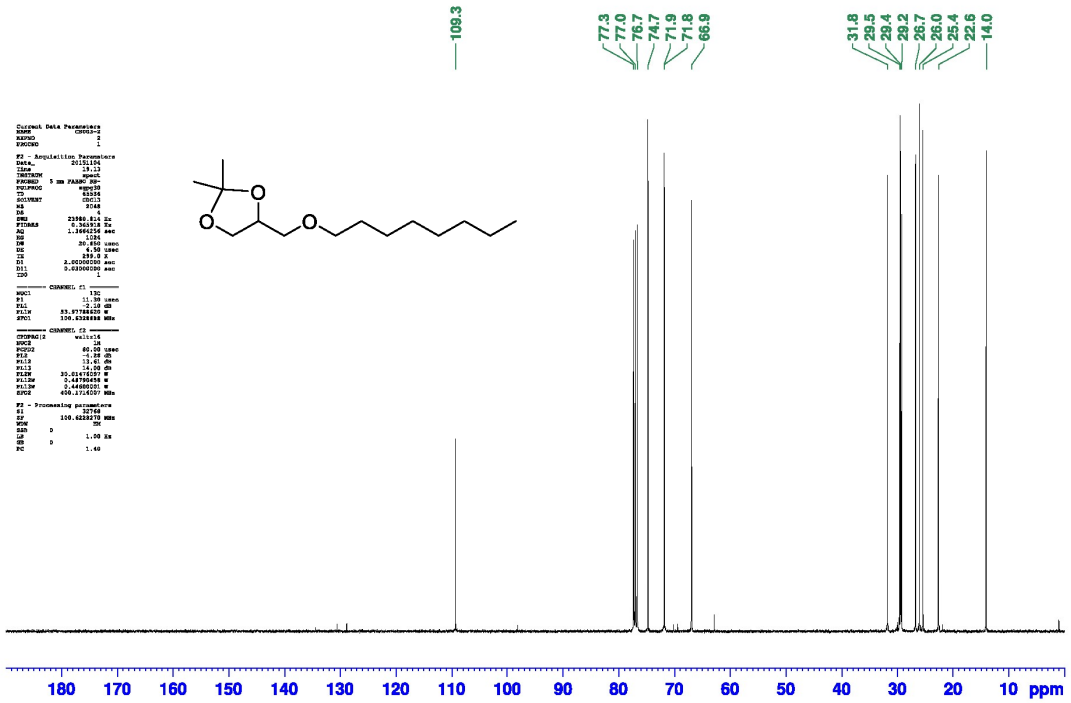

Figure S22. ^{13}C NMR spectrum spectrum of **10** in $CDCl_3$.

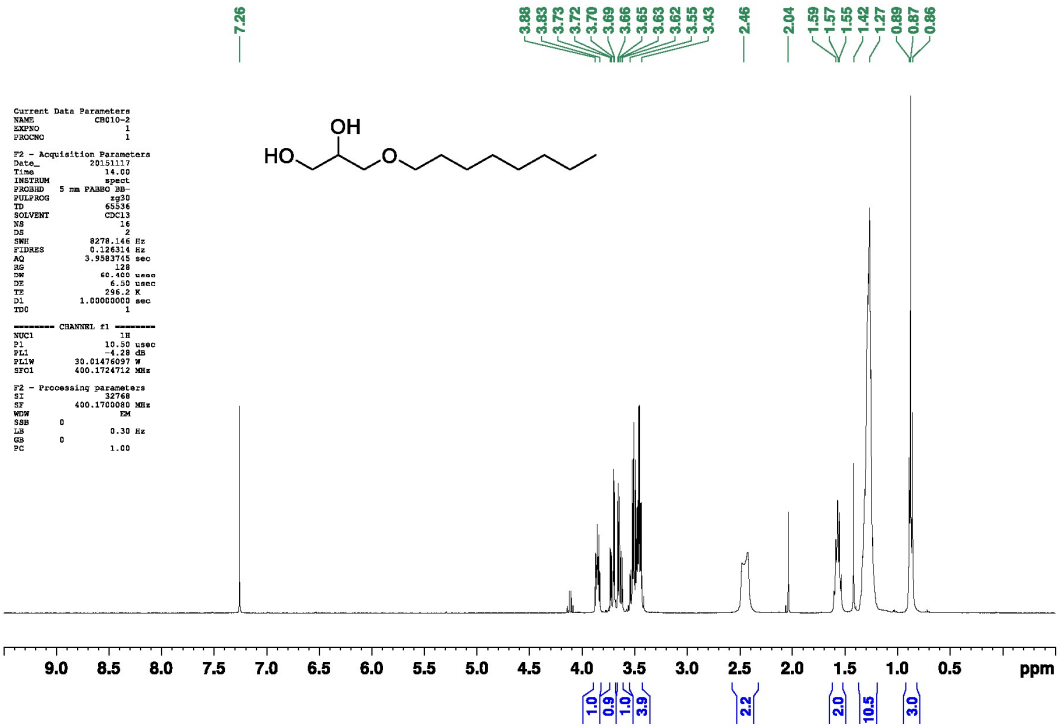

Figure S23. ^{1}H NMR spectrum of **11** in $CDCl_3$.

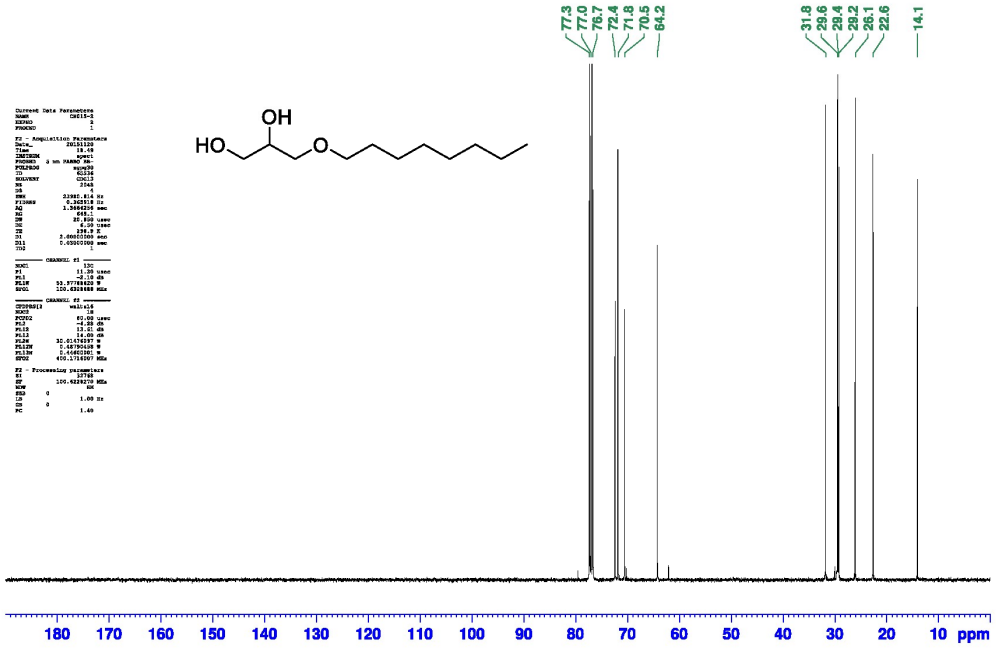

Figure S24. ^{13}C NMR spectrum spectrum of **11** in $CDCl_3$.

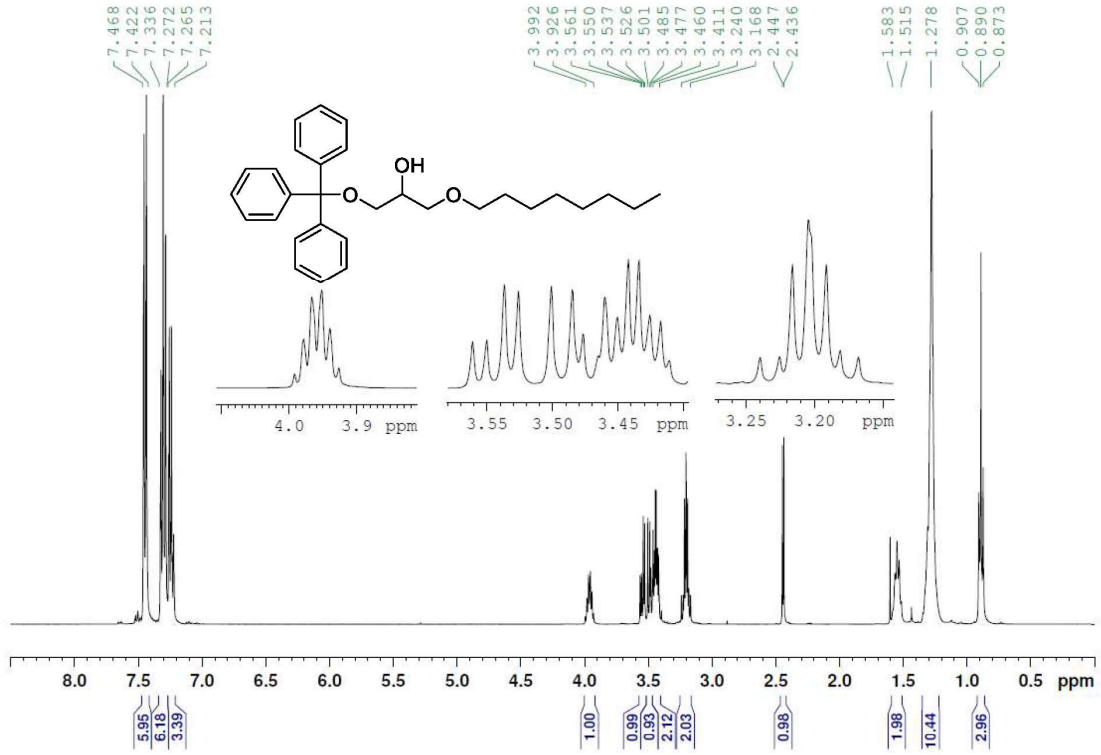

Figure S25. ^{1}H NMR spectrum of **12** in $CDCl_3$.

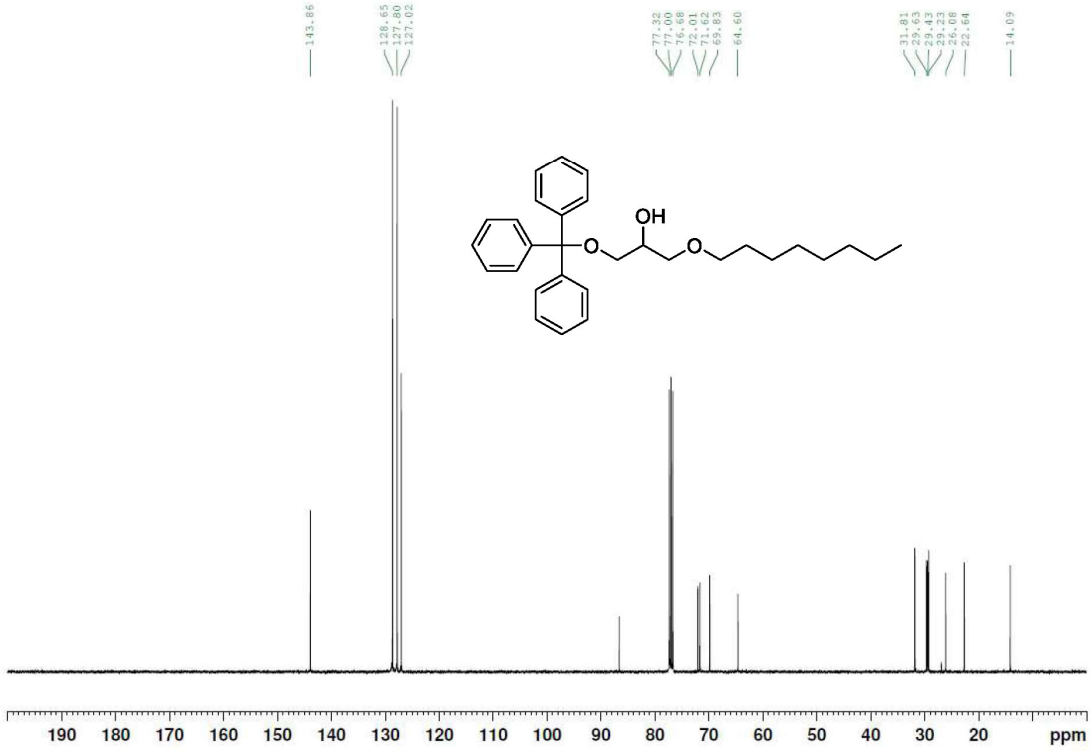

Figure S26. ^{13}C NMR spectrum spectrum of **12** in $CDCl_3$.

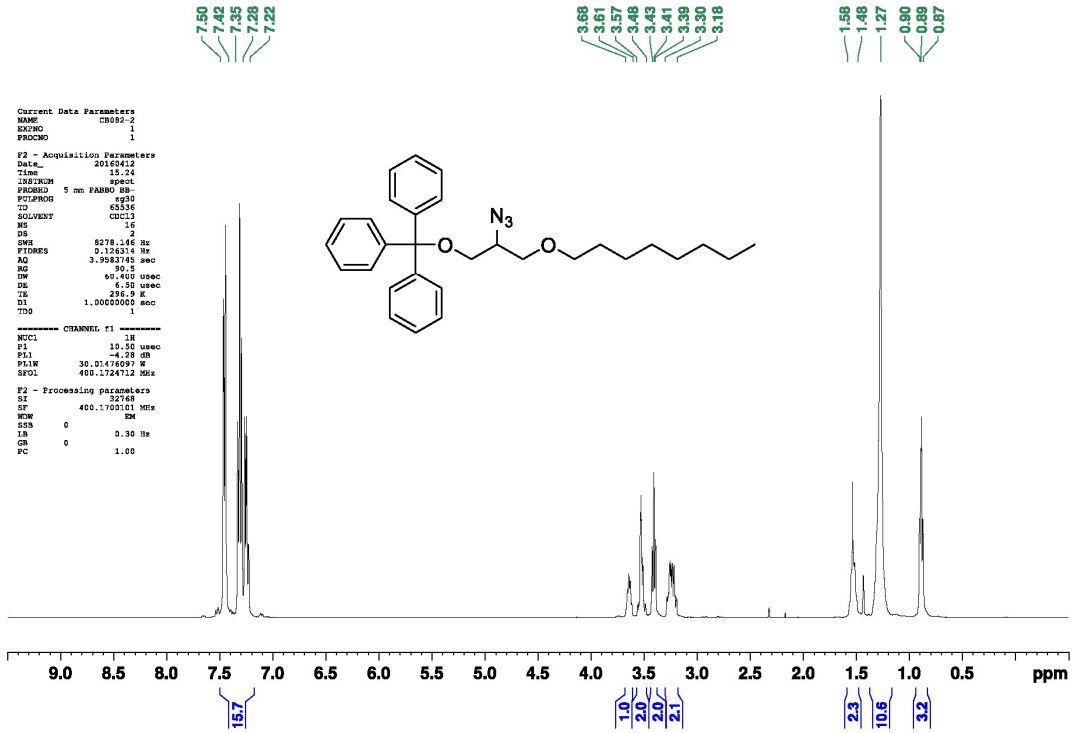

Figure S27. ^{1}H NMR spectrum of **14** in $CDCl_3$.

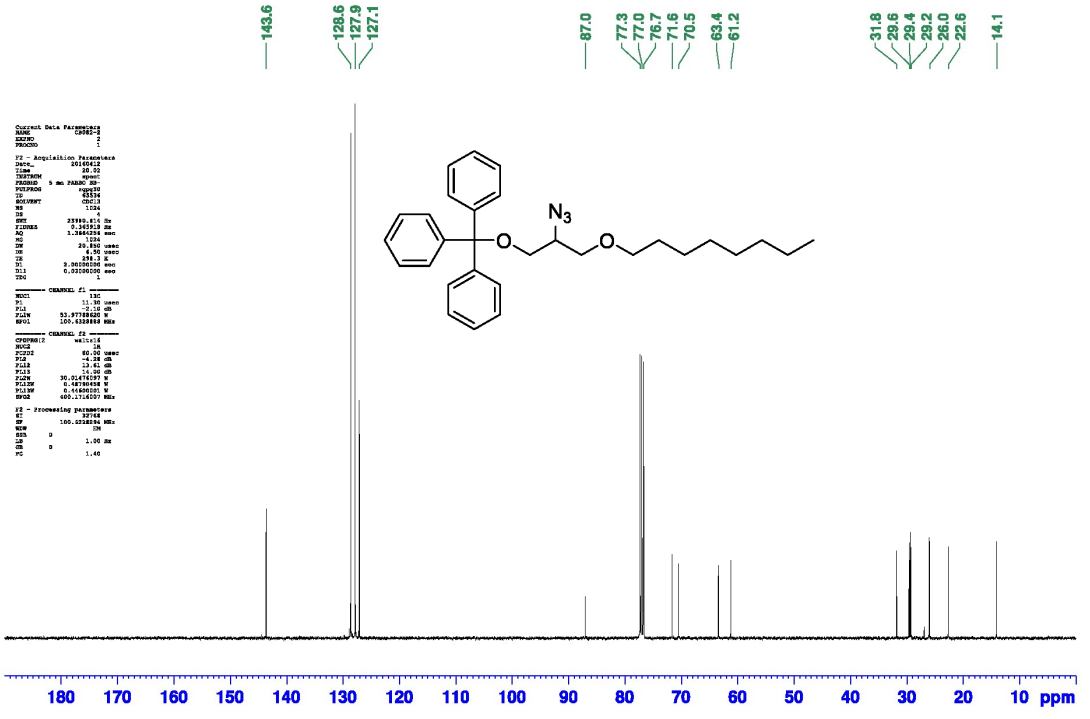

Figure S28. ^{13}C NMR spectrum spectrum of **14** in $CDCl_3$.

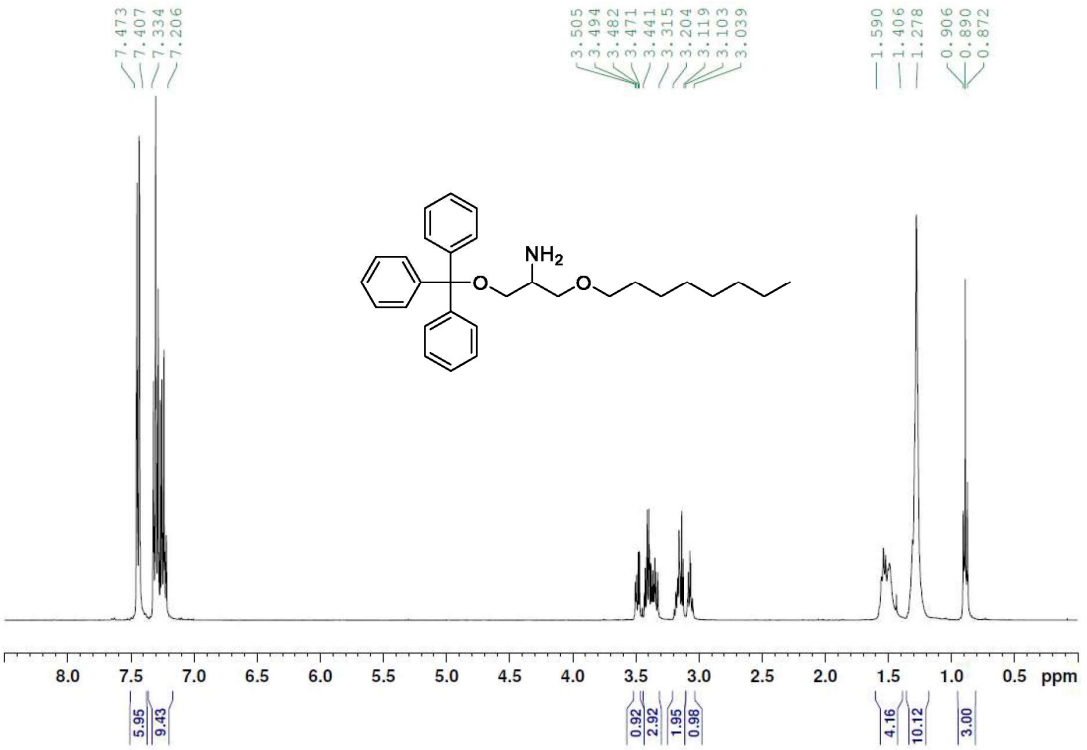

Figure S29. ^{1}H NMR spectrum of **15** in $CDCl_3$.

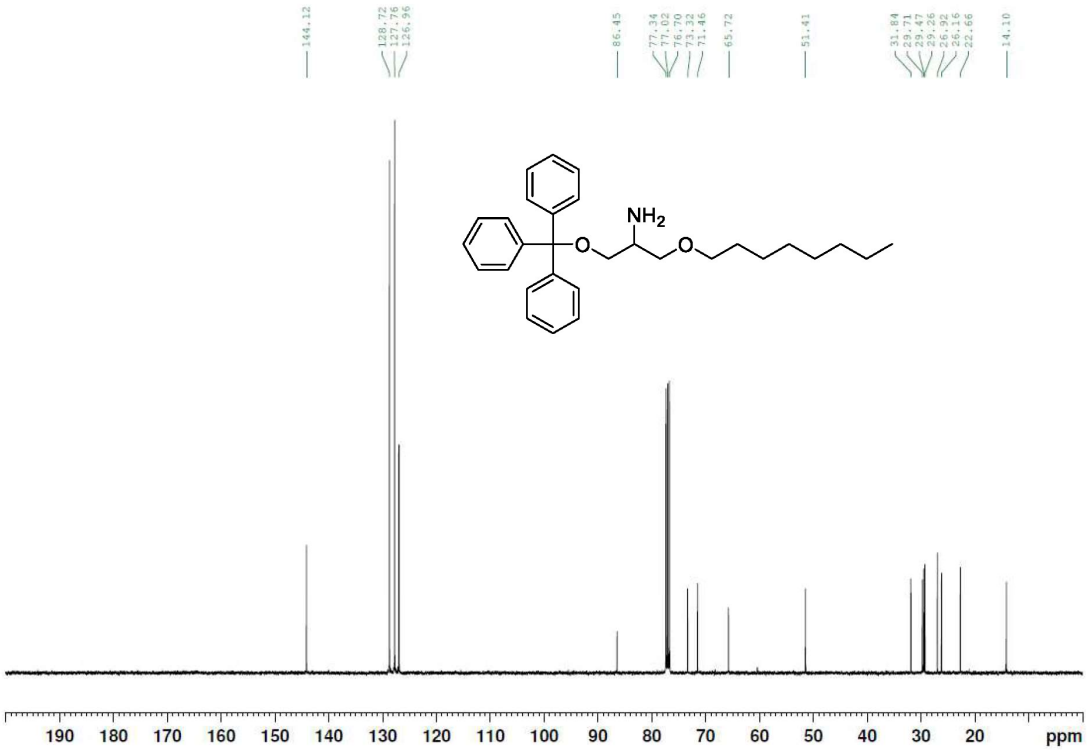

Figure S30. ^{13}C NMR spectrum spectrum of **15** in $CDCl_3$.

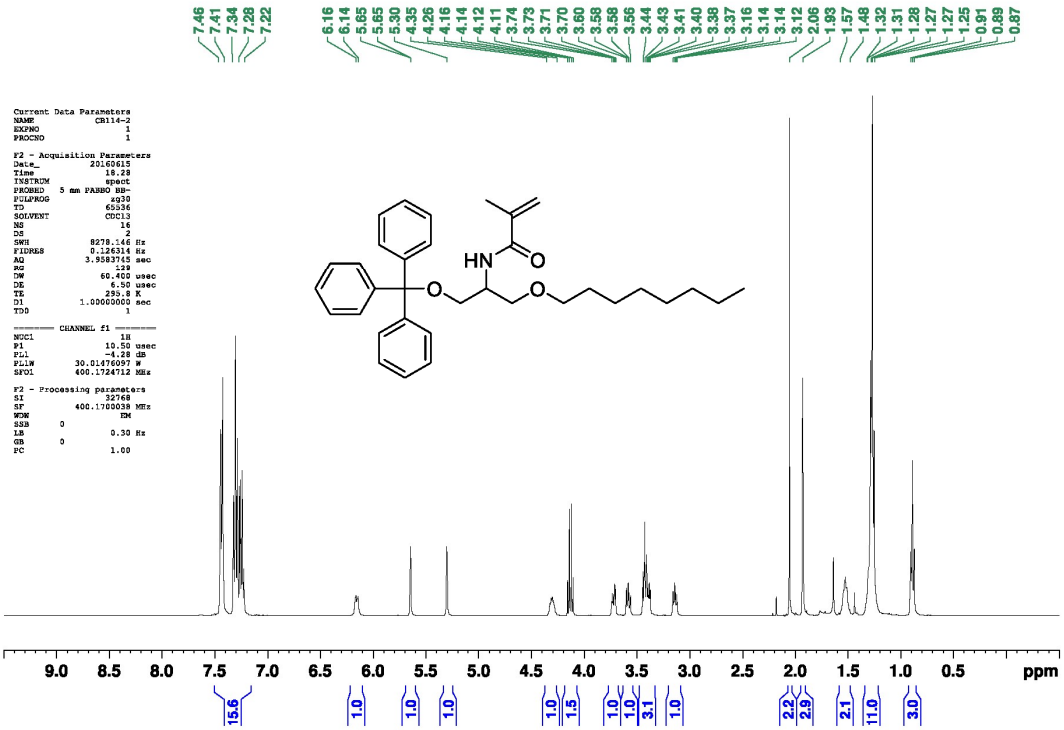

Figure S31. ^{1}H NMR spectrum of **16** in $CDCl_3$.

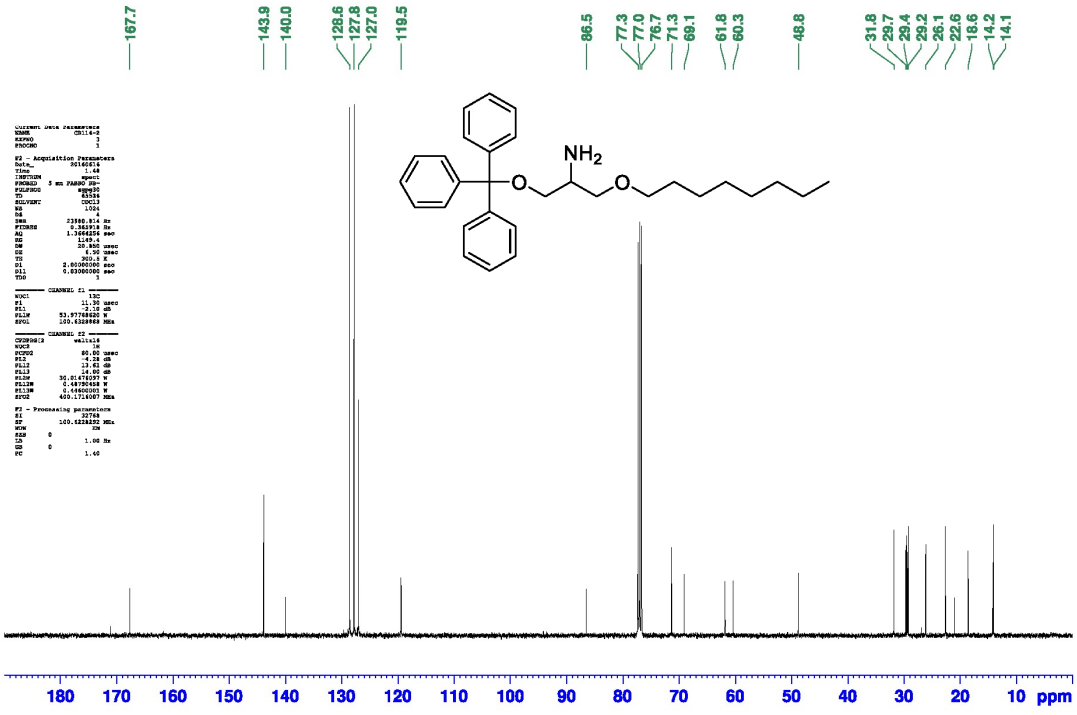

Figure S32. ^{13}C NMR spectrum spectrum of **16** in $CDCl_3$.

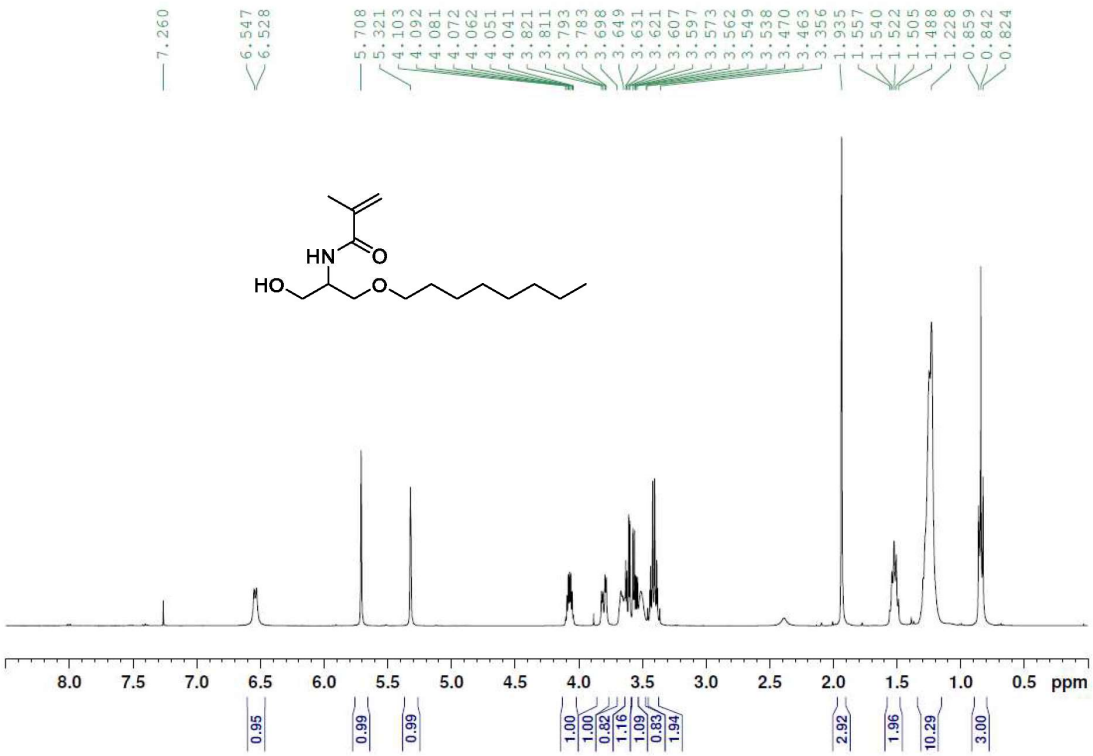

Figure S33. ^{1}H NMR spectrum of **17** in $CDCl_3$.

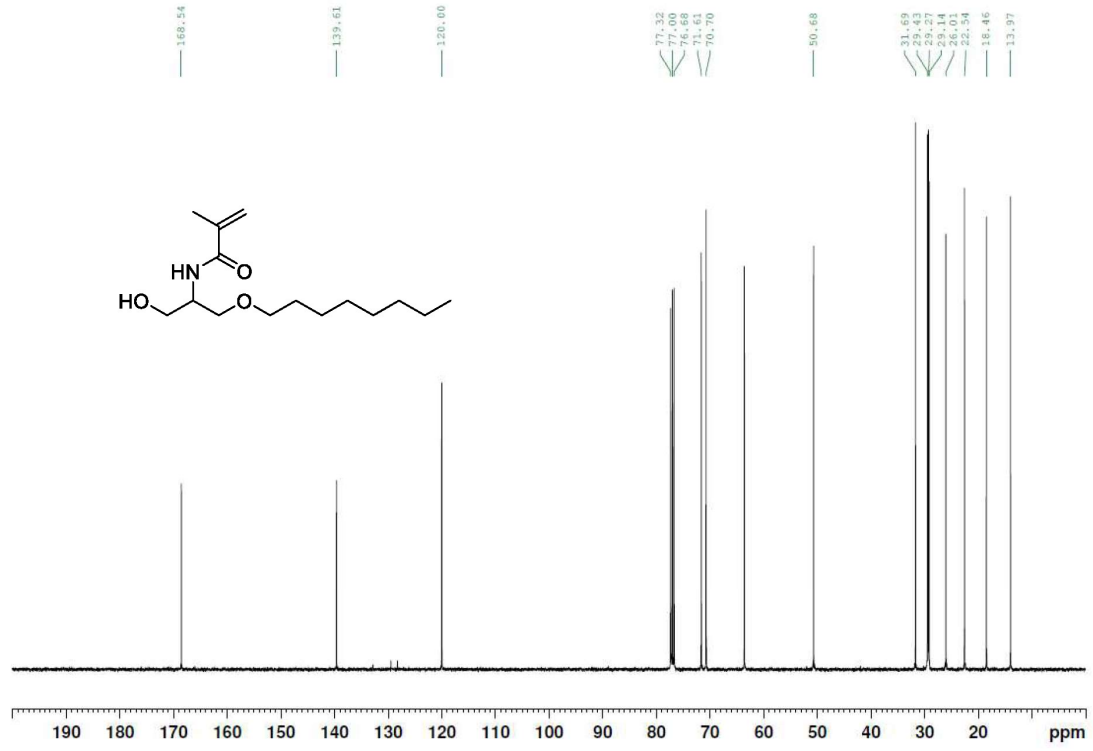

Figure S34. ^{13}C NMR spectrum spectrum of **17** in $CDCl_3$.

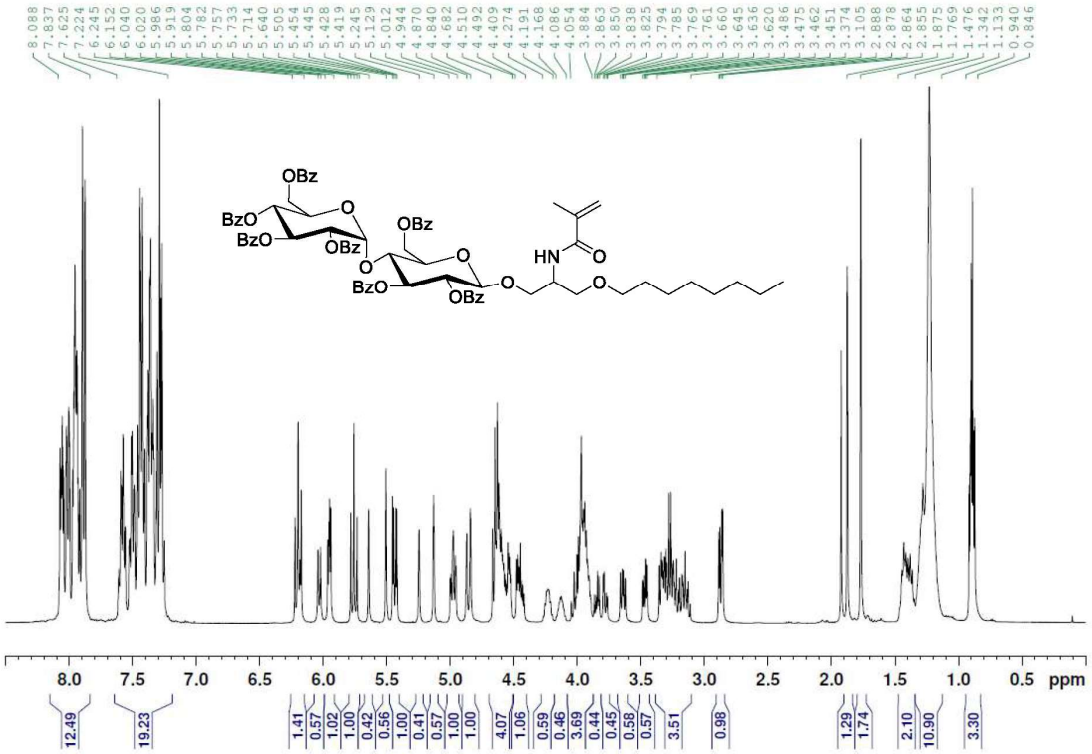

Figure S35. ^{1}H NMR spectrum of **18** in $CDCl_3$.

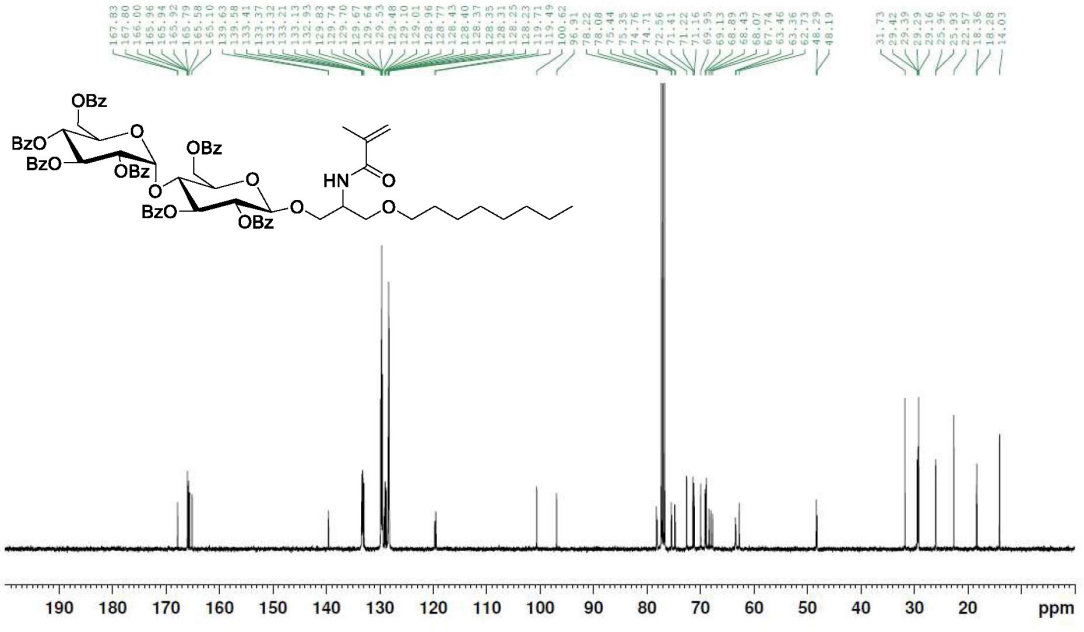

Figure S36. ^{13}C NMR spectrum spectrum of **18** in $CDCl_3$.

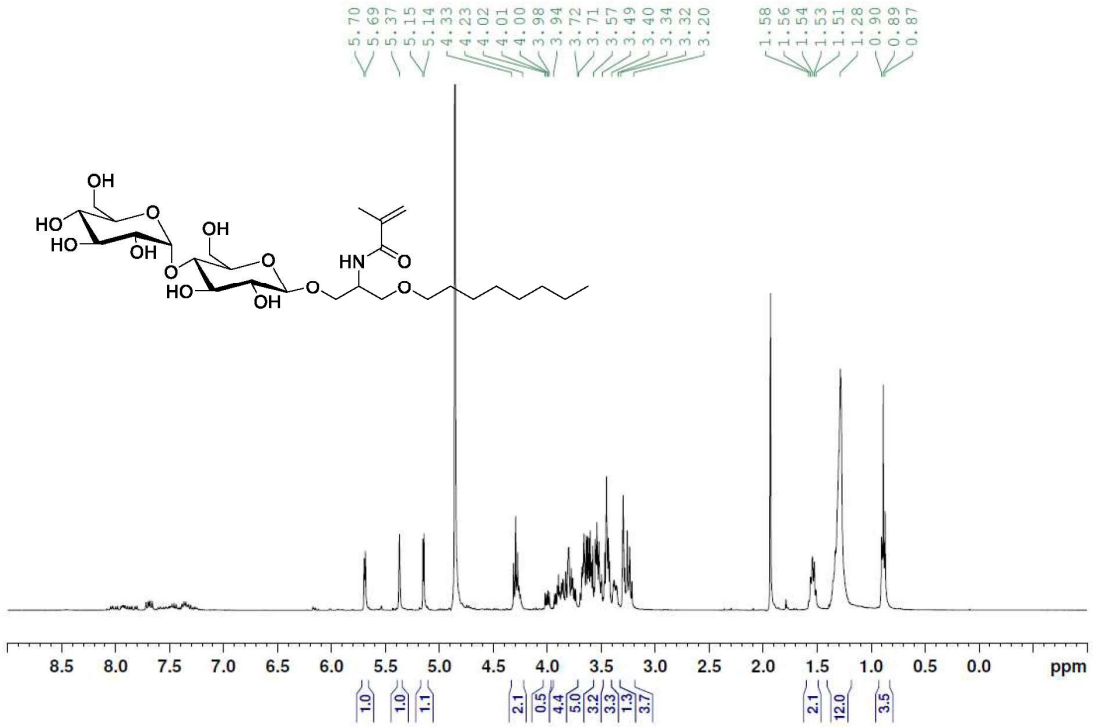

Figure S37. ^{1}H NMR spectrum of **19** in CD_3OD.

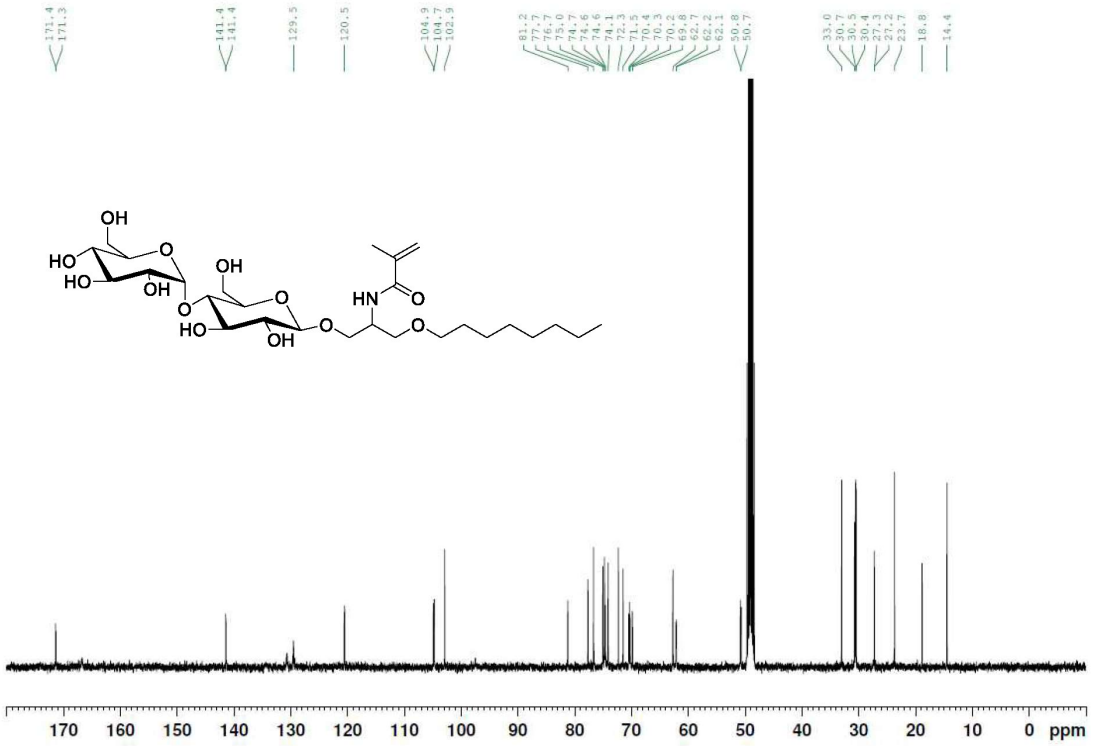

Figure S38. ^{13}C NMR spectrum spectrum of **19** in CD_3OD.

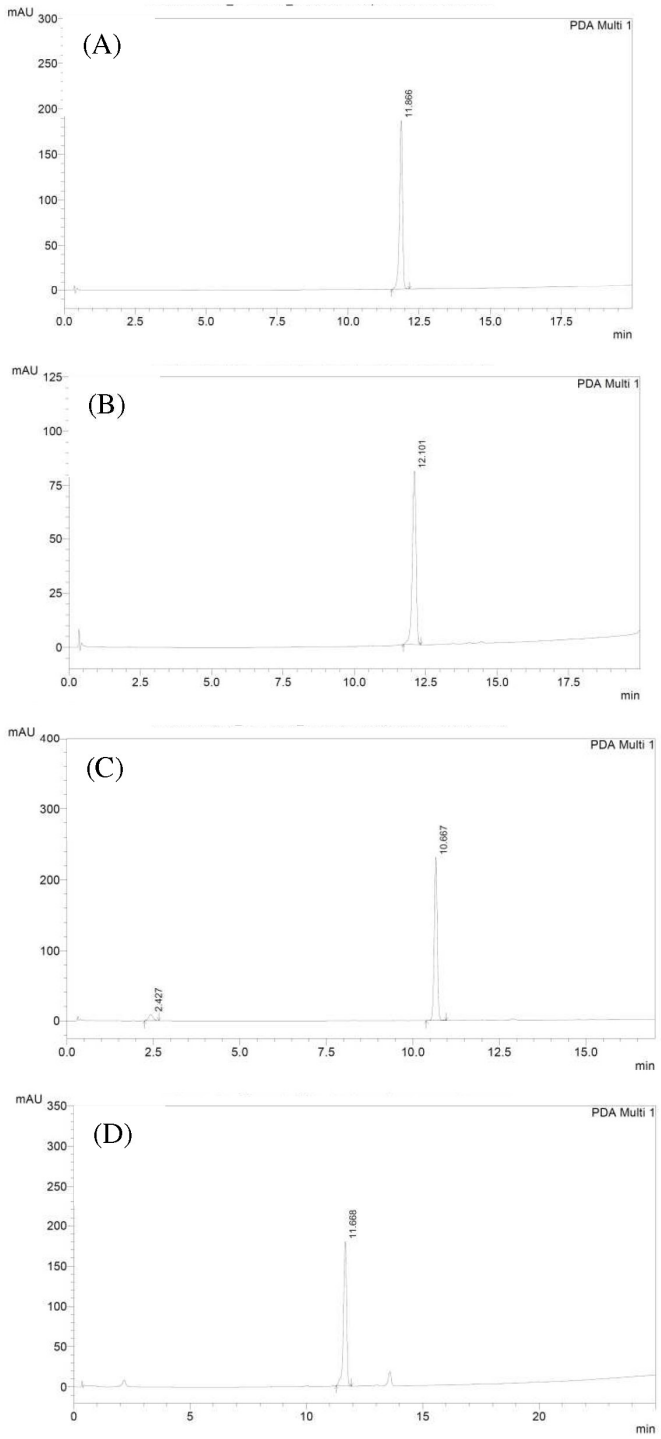

Figure S39. HPLC chromatogram of (A) **LC027**; (B) **LC048**; (C) **LC049**; (D) **LC058** at 254 nm. From 0 to 2 min.: isocratic 1:9 v/v (MeCN with 0.1% TFA)/(Water with 0.1% TFA); from 2 to 22 min.: gradient from 1:9 v/v (MeCN with 0.1% TFA)/(Water with 0.1% TFA) to 9.5:0.5 v/v (MeCN with 0.1% TFA)/(Water with 0.1% TFA); from 22 to 26 min.: isocratic 9.5:0.5 v/v (MeCN with 0.1% TFA)/(Water with 0.1% TFA). Column XTerra RP18, 5 µm, 2.1 x 100 mm, flow rate 1 mL/min.

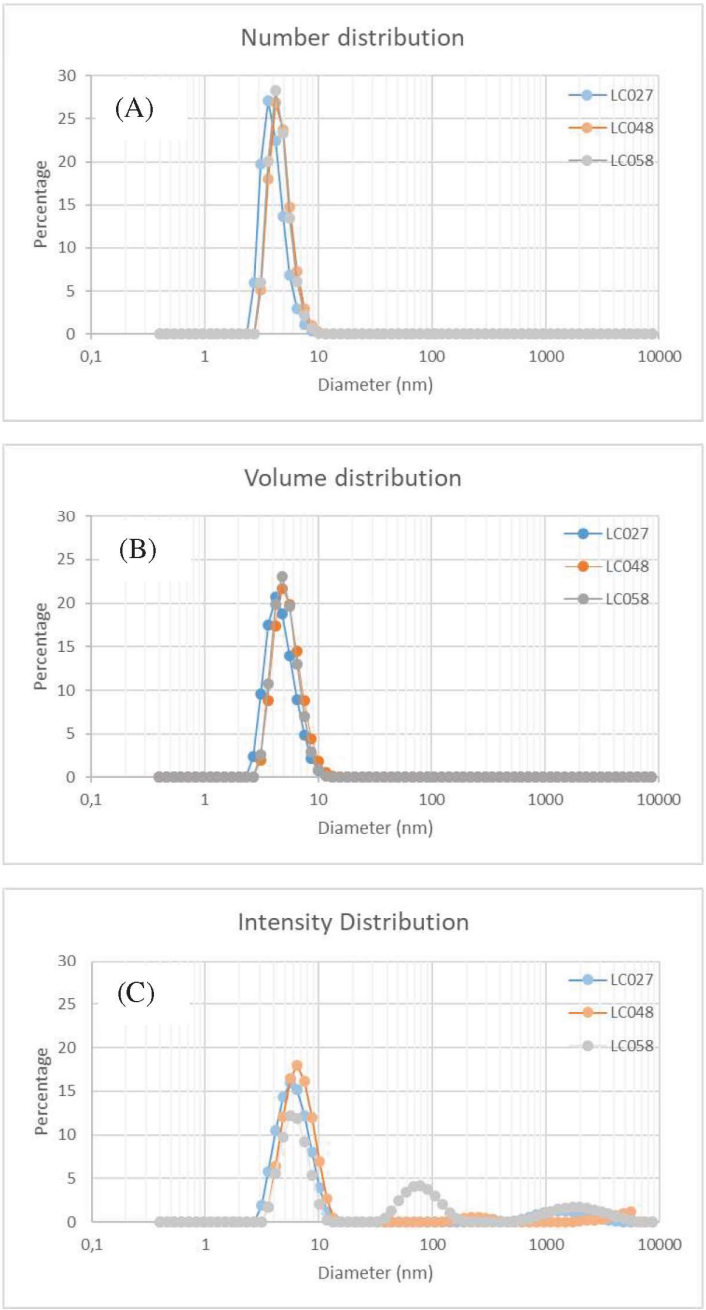

Figure S40. Contin distribution plots for **LC027**, **LC048** and **LC058.** Solution were prepared in pure MilliQ water mixtures at 5.64 mg/mL for **LC027**, 6.25 mg/mL for **LC048**, and 5.49 mg/mL for **LC058**. Solution were centrifuged 60 min at 15.200 rpm (25.830 g) before being analyzed. (**A**) Number distribution, (**B**) Volume distribution, and (**C**) Intensity distribution.

3.5. Synopsis (Manuscript 4)

In *Manuscript 4*, the self-assembly and the properties of native nanodiscs formed by either a hydrocarbon (DDDG) or a fluorocarbon (F_6ODG) diglucoside amphiphile and lipids were investigated. Both diglucoside amphiphiles contain the same headgroup consisting of mainly two branched glucose moieties, a linker group, and one hydrophobic chain. The latter consists of either a conventional C12 hydrocarbon chain in the case of DDDG or a polyfluorinated C8 fluorocarbon chain in the case of F_6ODG. The fluorination of the last 6 carbons renders F_6ODG not only hydrophobic but also lipophobic, which, in turn, conveys peculiar properties to the amphiphile and, subsequently, to the nanodiscs.

The diglucoside amphiphiles are able to directly extract lipids and proteins from artificial and biological membranes of different complexity and **form native nanodiscs with a lipid bilayer core**. These membranes include chemically defined, artificial vesicles with a model MP and, more importantly, highly heterogeneous, native *E. coli* membranes. The self-assembly of nanodiscs from 1,2-dimyristoyl-sn-glycero-3-phosphocholine (DMPC) and F_6ODG was investigated herein in great detail. With the combination of ^{19}F and ^{31}P NMR, DLS, and fluorescence spectroscopy, a sequential model for the self-assembly process was proposed. This model includes (i) the perforation of the DMPC bilayer at sub-solubilizing concentrations of the diglucoside amphiphile, (ii) the saturation of the DMPC bilayer and subsequent onset of nanodisc formation, and, (iii) the completion of nanodisc formation with all DMPC molecules present in nanodiscs and, thus, the completion of the solubilization process. Moreover, with the aid of ITC, the DMPC solubilization by DDDG and F_6ODG was tracked at varying lipid concentrations yielding pseudophase diagrams for mixtures with each diglucoside amphiphile.

The architecture of the nanodiscs containing various lipid species and MPs was determined by transmission electron microscopy (TEM) and DLS. Discoidal nanostructures with a thickness of about 5 nm and diameters between 10 nm and 40 nm were observed. Moreover, the integrity of the lipid bilayer core of DMPC nanodiscs was monitored by the solvent-sensitive fluorescence probe laurdan, differential scanning calorimetry (DSC), and time-resolved Förster resonance energy transfer (FRET). Laurdan fluorescence as well as DSC measurements revealed a thermotropic phase transition temperature (T_m) close to 24°C. This suggests a **low impact of the diglucoside amphiphiles on the harbored**

DMPC lipid bilayer core, because the physicochemical properties were only slightly affected. Comparing both diglucoside amphiphiles, it turned out that F_6ODG is the gentlest amphiphile to the membrane core, as reflected by small changes of T_m. Moreover, for F_6ODG, FRET experiments revealed a lower lipid exchange by lipid monomer diffusion and nanodisc collisions compared with DDDG. While the first emphasizes the high bilayer integrity, the latter shows that the lipophobicity of F_6ODG enhances the separation of the individual bilayer cores. The mild character of fluorocarbon nanodiscs was further emphasized by applying F_6ODG nanodiscs to the enzyme outer membrane phospholipase A1 (OmpLA). In fact, no difference in enzymatic activity could be observed for OmpLA present in vesicles and in fluorocarbon nanodiscs, whereas its activity in hydrocarbon nanodiscs was slightly decreased.

In summary, the findings presented in *Manuscript 4* are twofold. First, it shows that the **structure and molecular shape of amphiphiles are important** properties for the resulting aggregate formation with lipids. Second, the substitution of hydrocarbon by fluorocarbon is not only beneficial for MP/fluorinated amphiphile interactions. In this particular case, the interactions between MP-surrounding lipids and the **fluorinated amphiphile render a preferable environment** for MPs.

3.6. Manuscript 4

Self-Assembly of Protein-Containing Lipid-Bilayer Nanodisc from Small-Molecule Amphiphiles

Florian Mahler, Annette Meister, Carolyn Vargas, Grégory Durand, and Sandro Keller

Small, **2021**, 2103603

Contribution

For this work, I designed and performed all experiments except TEM imaging. For TEM, I prepared samples and grids containing POPC and DDDG (Fig. 2C), samples containing OmpLA (Fig. 8A), and samples containing native *E. coli* membranes (Fig. 8B). This manuscript contains minor contributions from my diploma thesis, namely, data for OmpLA solubilization and related activity measurements (Fig. 8D–E).

RESEARCH ARTICLE

NANO · MICRO small
www.small-journal.com

Self-Assembly of Protein-Containing Lipid-Bilayer Nanodiscs from Small-Molecule Amphiphiles

Florian Mahler, Annette Meister, Carolyn Vargas, Grégory Durand, and Sandro Keller**

When membrane proteins are removed from their natural environment, the quality of the membrane-solubilizing agent used is critical for preserving their native structures and functions. Nanodiscs that retain a lipid-bilayer core around membrane proteins have attracted great attention because they offer a much more native-like environment than detergent micelles. Here, two small-molecule amphiphiles with diglucose headgroups and either a hydrocarbon or a fluorocarbon hydrophobic chain are shown to directly assemble lipids and membrane proteins to form native nanodiscs rather than mixed micelles. Self-assembly of nanodiscs of increasing complexity from both defined, artificial vesicles as well as complex, cellular membranes is demonstrated. A detailed investigation of bilayer integrity and membrane-protein activity in these nanodiscs reveals gentle effects on the encapsulated bilayer core. The fluorinated amphiphile appears particularly promising because its lipophobicity results in gentle, non-perturbing interactions with the nanoscale lipid bilayer. A sequential model of nanodisc self-assembly is proposed that proceeds through perforation of the original membrane followed by saturation and complete solubilization of the bilayer. On this basis, pseudophase diagrams are established for mixtures of lipids and nanodisc-forming diglucoside amphiphiles, and the latter are used for the extraction of a broad range of membrane proteins from cellular membranes.

1. Introduction

Integral membrane proteins are delicate targets for in vitro studies because they usually need to be extracted from their native environment while hydrophobic surfaces need to be shielded from the aqueous solution by a membrane mimic. Traditionally, detergents have been applied to extract and purify membrane proteins, although they mimic the native environment only poorly and often lead to denaturation and loss of function.[1] Lipid-bilayer nanodiscs are excellent tools for studying membrane proteins under native-like yet well-controlled in vitro conditions. Such nanodiscs encapsulate membrane proteins in a nanosized membrane patch that, in spite of its small size, provides a native-like lipid environment.[2,3] All nanodiscs have in common that their lipid-bilayer core is surrounded by a belt composed of amphiphilic molecules that serve to shield the lipid acyl chains at the rim of the patch from contact with water. Yet, different types of nanodiscs drastically differ from one another in terms of their ability to self-assemble and their dynamics once formed. On the one hand, nanodiscs encapsulated by membrane scaffold proteins (MSPs) are kinetically trapped, static structures that require solubilization by conventional detergents before the latter are removed to drive nanodisc assembly.[4] On the other hand, both bicelles ("bilayered micelles") made from certain lipid mixtures[5] as well

F. Mahler, C. Vargas, S. Keller
Molecular Biophysics
Technische Universität Kaiserslautern (TUK)
67663 Kaiserslautern, Germany

A. Meister
HALOmem and Institute of Biochemistry
Martin-Luther-Universität Halle–Wittenberg
06108 Halle (Saale), Germany

C. Vargas, S. Keller
Biophysics, Institute of Molecular Biosciences (IMB)
NAWI Graz
University of Graz
Graz 8010, Austria
E-mail: sandro.keller@uni-graz.at

The ORCID identification number(s) for the author(s) of this article can be found under https://doi.org/10.1002/smll.202103603.

DOI: 10.1002/smll.202103603

C. Vargas, S. Keller
Field of Excellence BioHealth
University of Graz
Graz, Austria

C. Vargas, S. Keller
BioTechMed-Graz
Graz, Austria

G. Durand
Equipe Chimie Bioorganique et Systèmes Amphiphiles
Institut des Biomolécules Max Mousseron
Avignon University
Avignon 84916, France
E-mail: gregory.durand@univ-avignon.fr

G. Durand
CHEM2STAB
Avignon 84916, France

ADVANCED SCIENCE NEWS
www.advancedsciencenews.com

NANO · MICRO small
www.small-journal.com

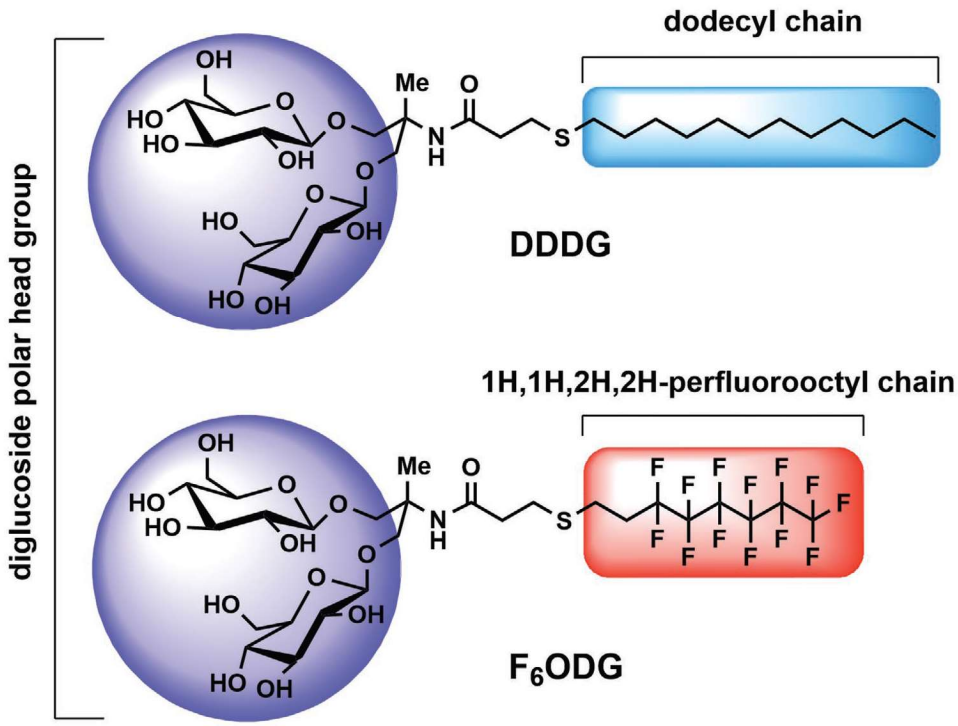

Figure 1. Chemical structures and names of nanodisc-forming diglucoside (DG) amphiphiles.

as polymer-encapsulated native nanodiscs[6] are capable of self-assembly in the absence of conventional detergents and, once formed, continue to exhibit fast dynamics of content exchange.

Here, we show that small-molecule diglucoside (DG) amphiphiles are able to recruit lipids and proteins directly into discoidal nanoparticles that retain the native-like bilayer organization of the parent membrane. Both amphiphiles possess a strongly hydrated diglucose headgroup and a hydrophobic chain and, thus, structurally resemble conventional head-and-tail detergents (**Figure 1**). While one of these amphiphiles contains a C12-hydrocarbon chain (hence, DDDG) as its hydrophobic moiety, the other carries a C8-fluorocarbon chain (hence, F_6ODG), which is expected to confer not only hydrophobicity but also lipophobicity. We have recently reported the basic physicochemical properties of two series of such detergent-like amphiphiles and their application to extract and stabilize membrane proteins in an aqueous solution.[7,8] On the one hand, a series of hydrogenated DG amphiphiles have proven superior to an established, commonly used detergent system in stabilizing essential but sensitive integral membrane proteins such as G-protein-coupled receptors (GPCRs).[8] On the other hand, a series of fluorinated DG amphiphiles have been shown to be the first fluorinated surfactants able to extract membrane proteins in amounts similar to those obtained with the aid of conventional detergents.[7]

Here, we report the unexpected finding that the solubilization of both artificial lipid vesicles and native cellular membranes by these new DG amphiphiles results in the formation of lipid-bilayer nanodiscs rather than mixed micelles. Both DG amphiphiles retain a lipid-bilayer architecture and preserve the thermotropic phase transition of saturated phospholipids yet allow rapid collisional exchange of their lipid contents. Hence, the DG amphiphiles combine the desirable features of bilayer-preserving membrane mimics with the fast dynamics typical of micelle-forming detergents. Furthermore, we demonstrate that DDDG and F_6ODG can recruit both reconstituted membrane proteins from chemically defined proteoliposomes as well as a broad range of membrane proteins directly from native cellular membranes into lipid-bilayer nanodiscs.

2. Results & Discussion

2.1. Morphology of Nanodiscs Made from Artificial Lipid Vesicles

Negative-stain transmission electron microscopy (TEM) revealed that both DG amphiphiles spontaneously formed nanodiscs when added to unilamellar lipid vesicles made from the saturated phospholipid 1,2-dimyristoyl-*sn*-glycero-3-phosphocholine (DMPC; **Figure 2**A,B). Moreover, the hydrogenated, more lipophilic DG amphiphile DDDG was also effective in accommodating the singly unsaturated phospholipid 1-palmitoyl-2-oleoyl-*sn*-glycero-3-phosphocholine (POPC) in nanodiscs (Figure 2C). Under negative-stain conditions, nanodiscs tend to form stacks—sometimes referred to as rouleaux—that are not observed in suspension. Although these stacks are staining artifacts, they allow for a straightforward analysis of some important geometrical properties of nanodiscs. Specifically, we estimated the average thickness of a nanodisc by measuring the height of a stack of nanodiscs and dividing it by the number of nanodiscs in the stack (Figure 2D). For DMPC encapsulated by F_6ODG or DDDG, we thus determined thicknesses of, respectively, (6.1 ± 0.6) nm and (5.9 ± 0.6) nm, which are typical of hydrated lipid bilayers.[9,10] For POPC encapsulated by DDDG,

ADVANCED SCIENCE NEWS
www.advancedsciencenews.com

NANO · MICRO small
www.small-journal.com

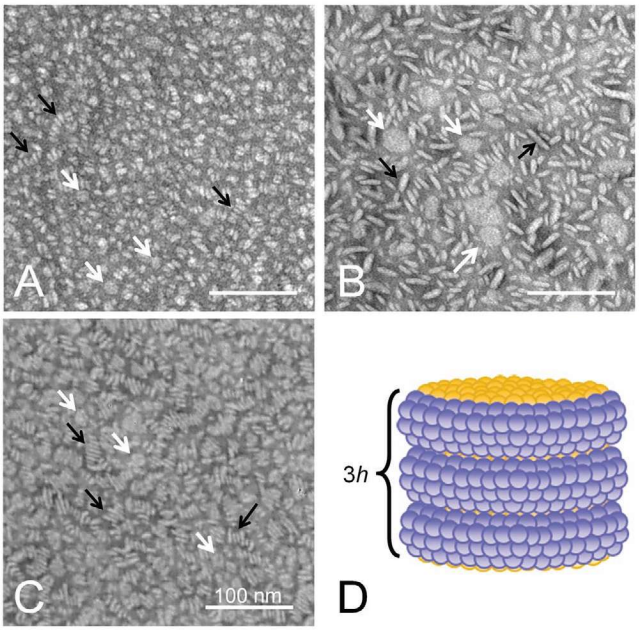

Figure 2. Formation of lipid-bilayer nanodiscs. TEM images of DG nanodiscs made from A) 0.3 mM DMPC and 1.0 mM DDDG at 30 °C, B) 0.3 mM DMPC and 0.6 mM F_6ODG at 30 °C, and C) 0.3 mM POPC and 1.0 mM DDDG at room temperature. Black arrows exemplarily indicate edge-on views of nanodiscs or nanodisc rouleaux, and white arrows point to face-on views of nanodiscs. D) Schematic measurement of bilayer thickness exploiting rouleaux formation.

we determined a thickness of (4.9 ± 0.5) nm, which is in good agreement with literature values.[9] These observations indicate that the thickness of DG nanodiscs is largely determined by the encapsulated lipids rather than the amphiphile surrounding them, which may be important for accommodating structurally and functionally diverse membrane proteins within a near-native lipid environment.

2.2. Preservation of Lipid Bilayers in Nanodiscs

2.2.1. Thermotropic Lipid Phase Transitions in Nanodiscs

Membrane proteins are embedded in a lipid bilayer; therefore, the structure and dynamics of the lipid molecules in the bilayer have a direct influence on the membrane protein. Thus, an essential criterion for gauging the usefulness of any nanodisc system is the extent to which it affects the structure and dynamics of the lipid molecules it harbors. To address this point, we exploited the main gel-to-fluid phase transition of the fully saturated phospholipid DMPC. At atmospheric pressure, this transition takes place around T_m = 24 °C and, therefore, is readily monitored by various kinds of spectroscopy and calorimetry. Here, we exploited the fluorescence properties of the membrane probe 6-dodecanoyl-2-dimethylaminonaphthalene (Laurdan), which sensitively reports on the temperature-dependent hydration state of the lipid headgroups. In particular, the influence of temperature on the hydration state of the bilayer and, consequently, the thermotropic phase transition of the membrane can be tracked by monitoring the

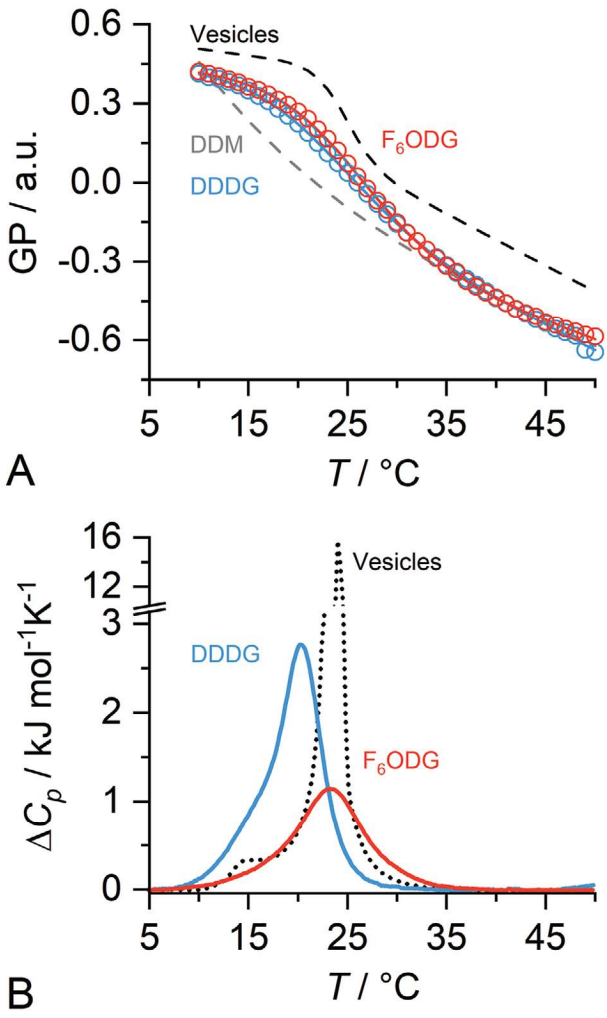

Figure 3. Gel-to-fluid phase transition of DMPC in DG nanodiscs by Laurdan fluorescence and DSC. A) Laurdan generalized polarization (GP) for hydrocarbon and fluorocarbon nanodiscs, DDM/DMPC mixed micelles, and unilamellar DMPC vesicles. DMPC (2 mM) in the form of unilamellar vesicles containing 0.5 mol% Laurdan was solubilized by addition of 5 mM DDM, 3 mM DDDG, or 3 mM F_6ODG. B) Differential isobaric heat capacity, ΔC_p, derived from DSC upscans for vesicles, hydrocarbon nanodiscs, and fluorocarbon nanodiscs. For nanodiscs, 4 mM DMPC in the form of vesicles was solubilized with 4 mM DDDG or F_6ODG.

so-called generalized polarization (GP, Equation 1, Supporting Information).[11,12] We determined T_m by fitting Equation 2 to the calculated GP values.

We thus made two major observations: First, we found only moderate changes in the inflection points of GP temperature scans, indicating minor effects of the DG amphiphiles on T_m (**Figure 3**A). In detail, T_m decreased from 24.6 °C for vesicles to 21.7 °C for DDDG and even slightly increased to 25.3 °C for F_6ODG nanodiscs. Second, the width of the transition from high GP values reflecting lower hydration in the gel phase to low GP values reflecting stronger hydration was reduced in nanodiscs as compared with vesicles, indicating a reduction in the size of the cooperative unit in the former as compared with the latter. In other words, the number of lipid molecules that undergo

ADVANCED SCIENCE NEWS
www.advancedsciencenews.com

NANO · MICRO small
www.small-journal.com

the thermotropic phase transition in a cooperative manner was found to be considerably smaller in nanodiscs than in unilamellar vesicles, which is readily explained by a simple calculation: Our nanoscale lipid bilayers contain fewer than 800 lipid molecules, whereas more than 100 000 lipid molecules would be contained in a 100 nm vesicle. Further to DMPC vesicles, we used the nonionic detergent *n*-dodecyl-*β*-D-maltoside (DDM) as an additional reference that allowed us to compare DG nanodiscs with conventional detergent/lipid mixed micelles. At low temperatures, the values for both DG nanodiscs lie between those of lipid-only vesicles and mixed micelles. Above ≈30 °C, however, the hydration state of DG nanodiscs as captured by GP was found to be similar to the one of DDM/DMPC mixed micelles (Figure 3A).

We turned to differential scanning calorimetry (DSC) to study the gel-to-fluid phase transition of nanoscale phospholipid patches encapsulated by DG amphiphiles in more detail. DSC measures the difference in the isobaric heat capacity ΔC_p between the sample and a buffer reference, which results in a pronounced peak when the former undergoes a thermotropic phase transition. The dependences of T_m and the size of the cooparative unit on the DG/DMPC ratio agree well with the results from fluorescence measurements: Nanodisc formation affected T_m by only a few degrees Celsius, as reflected in a slight temperature shift of the maximum in ΔC_p (Figure 3B). Specifically, T_m decreased from 24.0 °C for vesicles to 23.4 °C and 20.2 °C for fluorocarbon and hydrocarbon nanodiscs, respectively. Again, we observed the expected decrease in the size of the cooperative unit for nanodiscs compared with vesicles, as reflected in the broadening of the transition peaks (Figure 3B). In addition, we ensured that DG nanodiscs are present below T_m, that is, when vesicular DMPC bilayers are in the gel phase. TEM of samples prepared at 10 °C (Figure S1, Supporting Information) confirmed that DG nanodiscs self-assemble at such low temperatures.

In conclusion, fluorescence and DSC experiments demonstrated that DMPC molecules in DG nanodiscs retain their characteristic main phase transition, experience rather low perturbation in their acyl chain region, and have well-hydrated headgroups above T_m. Comparing DDDG and F_6ODG, the latter turns out to be the gentler amphiphile, as one might expect from the general properties of fluorinated surfactants.[7,13] T_m is even better preserved than is the case for DMPC nanodiscs encapsulated by the amphiphilic styrene maleic acid copolymer SMA(2:1), addition of which leads to a decrease in T_m well below 20 °C.[3] Overall, these are promising properties for a nanodisc system, as membrane proteins are likely to benefit from such a near-native lipid-bilayer environment.

2.2.2. Kinetics and Mechanisms of Lipid Exchange

The kinetics and the mechanisms of lipid exchange belong to the key distinguishing properties of membrane–mimetic systems. While MSP nanodiscs exchange lipids with one another only slowly by diffusional transfer of individual lipid monomers,[14] polymer-encapsulated nanodiscs exchange lipids with each other as well as with other membrane systems much faster by collisional transfer.[15–18] Quantifying the kinetics of lipid exchange is important because it determines whether a lipid-bilayer nanoparticle represents an equilibrium or rather a kinetically trapped structure. This, in turn, has far-reaching implications for the interpretation of experiments aiming at extracting membrane proteins and lipids.

In order to monitor lipid exchange, we used two fluorescently labeled lipids, namely, *N*-(7-nitrobenz-2-oxa-1,3-diazol-4-yl)-1,2-dihexadecanoyl-*sn*-glycero-3-phosphoethanolamine (NBD-DHPE) and rhodamine B 1,2-dihexadecanoyl-*sn*-glycero-3-phosphoethanolamine (Rh-DHPE). When these lipids are colocalized within the same nanodisc, they give rise to efficient Förster resonance energy transfer (FRET). This is, the excited NBD label transfers its energy without radiation to the Rh label, which, in turn, emits light at its own characteristic emission wavelength. Using a stopped-flow device, we mixed a population of unlabeled nanodiscs containing DMPC only with a population of doubly labeled nanodiscs containing NBD-DHPE and Rh-DHPE, each at 1 mol%, and monitored time-resolved FRET (**Figure 4**A).[17] We thus found that the kinetics of donor dequenching steeply depended on the concentration of unlabeled lipid, suggesting a dominant role of collisional over diffusional lipid exchange.

Correspondingly, a global fit (Equation 3) across all lipid concentrations yielded quantitative information on the contributions of diffusional and collisional lipid exchange. In the case of diffusional lipid exchange, the lipid is transferred from one nanodisc to another by diffusion of monomers through the aqueous phase. The kinetics of this type of exchange is given by the exchange rate k_{dif}, whose value is determined by the integrity of the lipid bilayer. We found $k_{dif} = (5.35 \pm 0.02)10^{-4}$ s^{-1} for fluorocarbon nanodiscs and $k_{dif} = (93.5 \pm 0.4)10^{-4}$ s^{-1} for hydrocarbon nanodiscs. These values indicate a higher bilayer integrity in fluorocarbon nanodiscs than in hydrocarbon nanodiscs, as reflected in our observation that lipids can dissociate from the membrane more easily in the latter case. This finding fits well with the above results from fluorescence and DSC measurements that fluorocarbon nanodiscs are the milder alternative.

In addition to the exchange of individual lipid monomers, direct nanodisc/nanodisc collisions may allow for mass transfer of lipids. Here, the corresponding rate constant k_{col} reflects both the likelihood that a collisional encounter of two nanodiscs is "productive" in the sense that it allows lipid exchange and the efficiency of this kind of exchange. For fluorocarbon nanodiscs, this lipid exchange was found to be characterized by $k_{col} = (0.301 \pm 0.001)$ s^{-1} M^{-1} and for hydrocarbon nanodiscs by $k_{col} = (3.65 \pm 0.02)$ s^{-1} M^{-1}. This considerably slower collisional lipid exchange between fluorocarbon nanodiscs indicates a much stronger separation of individual bilayer patches compared with hydrocarbon nanodiscs. In the case of DMPC vesicles, this type of lipid exchange was not observed at all.

Through a comparison with other membrane mimics, it is seen that nanodiscs formed by the hydrocarbon DG amphiphile exhibited exchange rates similar to those previously observed for lipid-bilayer nanodiscs encapsulated by SMA(2:1) (Figure 4B). By contrast, fluorocarbon nanodiscs exhibited considerably slower exchange, which, however, was still more than one or two orders of magnitude faster than for MSP nanodiscs and unilamellar vesicles, respectively. The slower lipid exchange

ADVANCED SCIENCE NEWS
www.advancedsciencenews.com

NANO · MICRO small
www.small-journal.com

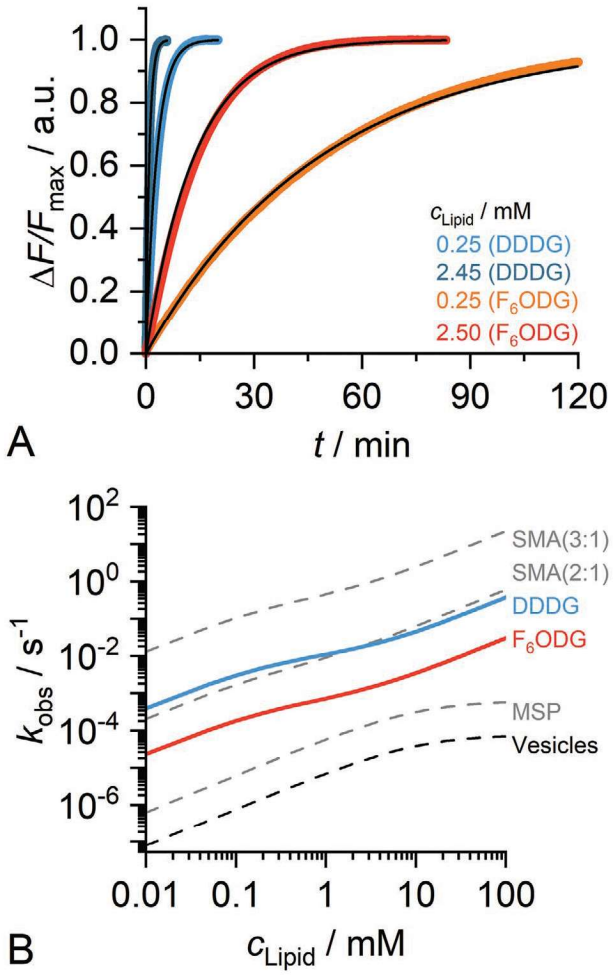

Figure 4. Investigation and comparison of lipid exchange kinetics at 35 °C. A) DMPC vesicles with and without NBD- and Rh-labeled lipids were solubilized into 25 nm-sized nanodiscs by DDDG and F_6ODG. Shown are four examples of normalized fluorescence dequenching curves. B) Resulting exchange rates of various membrane mimics across a broad range of lipid concentrations. Values for DDDG and F_6ODG were derived from the results shown in panel A. Values for SMA(3:1),[15] SMA(2:1),[18] MSP,[19] and vesicles[14] were obtained from the literature.

among MSP nanodiscs is due to the fact that they exchange lipids almost exclusively by diffusion, with negligible contributions coming from collisional exchange. The similar k_{dif} values found here for fluorocarbon nanodiscs (5.35×10^{-4} s^{-1}) and previously[19] for MSP nanodiscs (6.3×10^{-4} s^{-1}) hint at a similar degree of bilayer integrity in both nanoscale membranes. Together with their fast collisional exchange of lipid molecules, this renders fluorocarbon nanodiscs a highly promising membrane mimic that combines a near-native lipid-bilayer patch with a flexible, dynamic amphiphile belt into an equilibrium nanoparticle.

2.2.3. Mild Effects of Fluorocarbon Chains on DG Nanodiscs

Taken together, it is obvious that the fluorocarbon chains in fluorocarbon nanodiscs have a gentler effect on the bilayer properties of the core compared with the hydrocarbon chains in hydrocarbon nanodiscs. We reason that the higher T_m values (Figure 3) as compared with hydrocarbon nanodiscs are caused by (i) lower perturbation of the bilayer patch owing to a lower number of defects in lipid-bilayer packing and (ii) dehydration of the phospholipid headgroups due to slightly increased lateral pressure caused by the F_6ODG belt. Both points can be explained by a high degree of segregation between hydrocarbon lipids and fluorocarbon amphiphiles. Because lipids and lipophobic fluorocarbon compounds mix rather poorly, F_6ODG molecules are excluded from the bilayer patch and are largely restricted to the belt surrounding the nanodisc. First, this is expected to reduce the number of defects in lipid packing that otherwise would be introduced by conventional detergents. Second, this leads to a higher lateral pressure because unfavorable lipid/fluorocarbon interactions are minimized at the core/belt interface. Similar effects could also be observed by reconstitution of membrane proteins into fluorocarbon lipid bilayers, leading to higher stability of oligomers.[20,21] Furthermore, segregation explains the slower collisional lipid transfer found for fluorocarbon nanodiscs as compared with hydrocarbon nanodiscs, as the lipids have to cross the fluorocarbon belt and, thereby, would give rise to unfavorable hydrocarbon/fluorocarbon interactions. These unfavorable interactions render nanodisc/nanodisc collisions less efficient for fluorocarbon nanodiscs compared with hydrocarbon nanodiscs.

2.3. Detailed Investigation of The Solubilization Process

2.3.1. Nanodisc Self-Assembly

In order to gain a deeper understanding of the self-assembly process, we combined dynamic light scattering (DLS), NMR spectroscopy, fluorescence spectroscopy, and calorimetry to dissect the different stages leading to the formation of nanodiscs from fluid-phase DMPC at 35 °C. Considering a transition from large particles (vesicles) to small ones (nanodiscs), two straightforward parameters that can be extracted from DLS experiments are the size distribution and the average hydrodynamic diameter d_H. For vesicles in the absence of F_6ODG, we found a unimodal distribution peaking at about 100 nm as expected (**Figure 5**A). While the particle size distribution remained unimodal for all F_6ODG concentrations, we observed drastic changes in d_H. An initial increase in d_H from 100 nm to ≈2500 nm indicated vesicle aggregation upon incorporation of DG amphiphiles into the vesicular bilayer. This was followed by a drastic drop to ≈40 nm, which marked the onset of vesicle solubilization and, concomitantly, of nanodisc formation. Finally, a smooth decrease in d_H to 16 nm reflected the completion of the solubilization process (Figure 5B). Such a dependence of particle size on amphiphile concentration is well known for vesicle solubilization[22] and allows one to determine two threshold concentrations: At the saturating concentration, lipid vesicles start to disintegrate into nanodiscs because the stress induced by DG amphiphiles can no longer be accommodated in the vesicular lipid bilayer. At the solubilizing concentration, solubilization is completed, and all lipid molecules are present in the form of nanodiscs. In between these concentrations, DG

ADVANCED SCIENCE NEWS
www.advancedsciencenews.com

NANO · MICRO small
www.small-journal.com

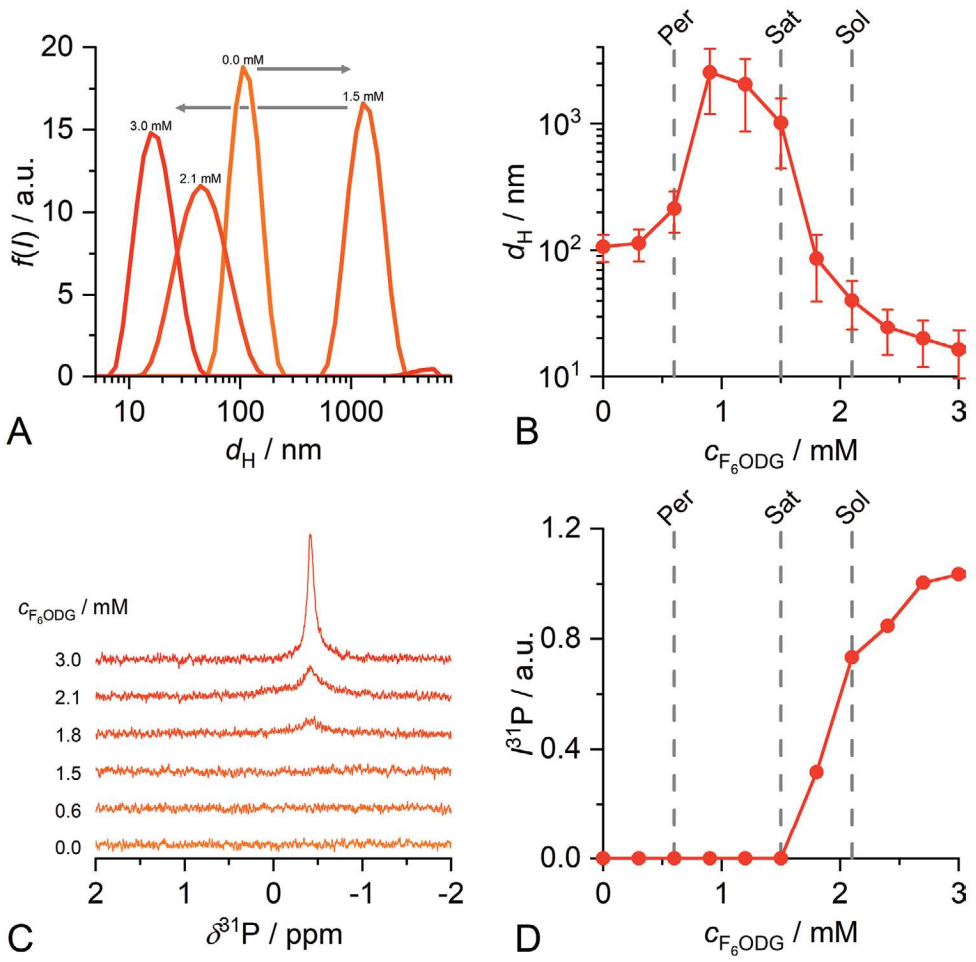

Figure 5. Solubilization of 2.8 mM DMPC vesicles with increasing F_6ODG concentrations at 35 °C. A) Intensity-weighted size distributions determined by DLS. B) Hydrodynamic diameters, d_H, derived from DLS size distributions. "Error bars" are derived from the polydispersity index. C) ^{31}P-NMR spectra of the same samples as in panel A. D) Peak intensities of ^{31}P-NMR spectra. Dashed lines indicate threshold concentrations for bilayer perforation (Per), saturation (Sat), and complete solubilization (Sol).

amphiphile-saturated vesicles and large nanodiscs coexist. In the case at hand, we thus found a saturating concentration of 1.5 mM and a solubilizing concentration of 2.1 mM F_6ODG for 2.8 mM DMPC at 35 °C.

To corroborate these values, we exploited ^{31}P-NMR, another technique that is highly sensitive to changes in the size of lipid aggregates. Lipid molecules within vesicles yield an NMR signal that is broadened beyond detection because of the slow rotational diffusion of such large structures.[23] By contrast, nanodiscs tumble much faster and, thus, give rise to a sharp ^{31}P-NMR signal. Accordingly, no peak could be detected for F_6ODG concentrations up to 1.5 mM (Figure 5C). Above this concentration, further addition of F_6ODG gave rise to an isotropic peak with increasing intensity. The break points of the resulting concentration/intensity plot agreed well with the saturation and solubilization concentrations obtained by DLS (Figure 5D). The moderate increase in the ^{31}P-NMR signal observed even beyond the solubilization was most likely due to the fact that, although solubilization was complete at this point of the titration, the nanodiscs were still relatively large (about 40 nm) and further decreased in size as more F_6ODG was added.

2.3.2. F_6ODG-Induced Lipid Vesicle Perforation

^{19}F-NMR has been applied to fluorinated surfactants in order to monitor micellization[13,7] or mixing with conventional hydrocarbon surfactants[24–26] and lipids.[13] Similarly, we used ^{19}F-NMR to monitor the change in the environment of the terminal CF_3 group of F_6ODG throughout the solubilization process. We observed a continuous change in the chemical shift to lower values with increasing F_6ODG concentrations (**Figure 6**A). The change in the chemical shift was more pronounced between 0.6 mM and 1.2 mM OF F_6ODG (Figure 6B). This shift reflected a change in the group's environment from polar to nonpolar, that is, from monomers in the aqueous solution to the bilayer-bound state. Interestingly, this pronounced change did not coincide with the saturation concentration (Figure 6B). Rather, it hints at a significant change going on in the lipid bilayer even before the latter becomes saturated with F_6ODG. This process must enable fast tumbling or flip-flopping of the incorporated F_6ODG molecules because, as mentioned above, solution NMR is insensitive to slow-tumbling nuclei. The most obvious

ADVANCED SCIENCE NEWS
www.advancedsciencenews.com

NANO · MICRO small
www.small-journal.com

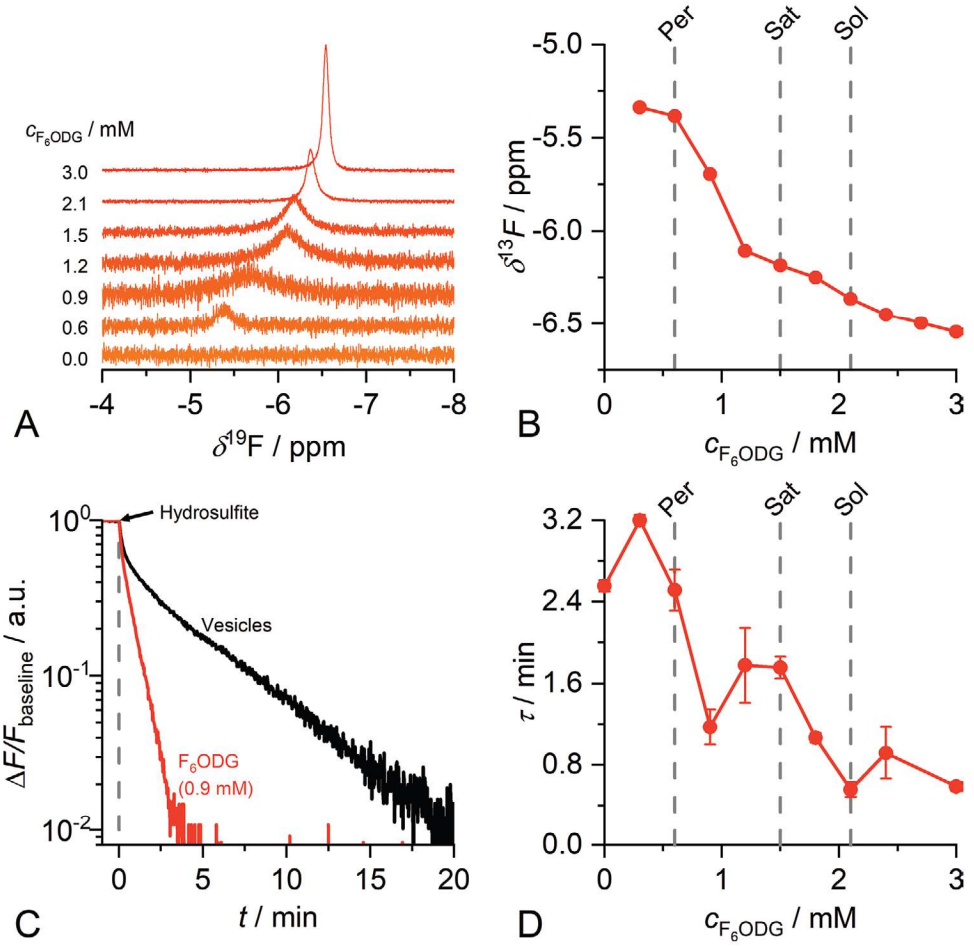

Figure 6. Detailed investigation of the solubilization process. Solubilization of 2.8 mM DMPC vesicles by increasing F_6ODG concentrations at 35 °C. A) ^{19}F-NMR spectra focusing on the peak corresponding to the CF_3 group of F_6ODG. Vertical scaling is not uniform to emphasize the shift of the maximum of the peak. B) ^{19}F-NMR chemical shifts, $\delta^{19}F$, of the CF_3 group in dependence on the F_6ODG concentration. C) Normalized NBD fluorescence as a function of the time after the addition of the bleaching agent hydrosulfite. NBD-labeled DMPC vesicles and nanodiscs were treated with hydrosulfite at timepoint zero (arrow). D) Characteristic NBD bleaching times, τ, in dependence on the F_6ODG concentration as derived from the area under the $\Delta F/F_{bl}$ curve such as those shown in panel C. Error bars are standard errors derived from replicates. Dashed lines indicate threshold concentrations for bilayer perforation (Per), saturation (Sat), and complete solubilization (Sol).

explanation for this observation would be the formation of transmembrane pores by F_6ODG. It seems particularly likely that pores may form at the interface between the bulk of the vesicular bilayer consisting of DMPC and domains rich in F_6ODG.

To test this hypothesis, we quantified the permeability of vesicular lipid bilayers to a small solute. To this end, we incubated NBD-labeled DMPC vesicles with F_6ODG and treated the samples with hydrosulfite anions to monitor the time-dependent bleaching of the NBD labels (Figure 6C). Immediately after the addition of hydrosulfite, we observed a drop in the fluorescence intensity within the first few minutes. This initial bleaching is attributed to the NBD labels on the outside of the DMPC vesicles, which are immediately accessible to hydrosulfite. Subsequently, the fluorescence intensity continued to decrease exponentially at a much slower rate. This second bleaching phase was caused by the slow diffusion of hydrosulfite through the DMPC bilayer. The time dependence of this process was captured by the characteristic bleaching time, τ. With increasing F_6ODG concentration τ decreased, indicating increasing accessibility of the interior NBD labels (Figure 6D). Closer inspection shows that the most pronounced change in τ occurred at 0.6 mM F_6ODG, where τ dropped from 2.4 min to 1.2 min. This is also the F_6ODG concentration at which ^{19}F-NMR spectroscopy revealed the most pronounced change, strongly suggesting that both methods follow the perforation of vesicular DMPC membranes upon incorporation of F_6ODG. We henceforth refer to this concentration as the perforating (Per) concentration.

2.3.3. Pseudophase Diagrams of DG Amphiphile/DMPC Mixtures

For certain applications, it is of particular importance to control the amphiphile/lipid ratio necessary to reach a desired colloidal state. On the one hand, the most common requirement in membrane-protein research might be complete solubilization. On the other hand, the perforation stage might be

ADVANCED SCIENCE NEWS
www.advancedsciencenews.com

NANO · MICRO small
www.small-journal.com

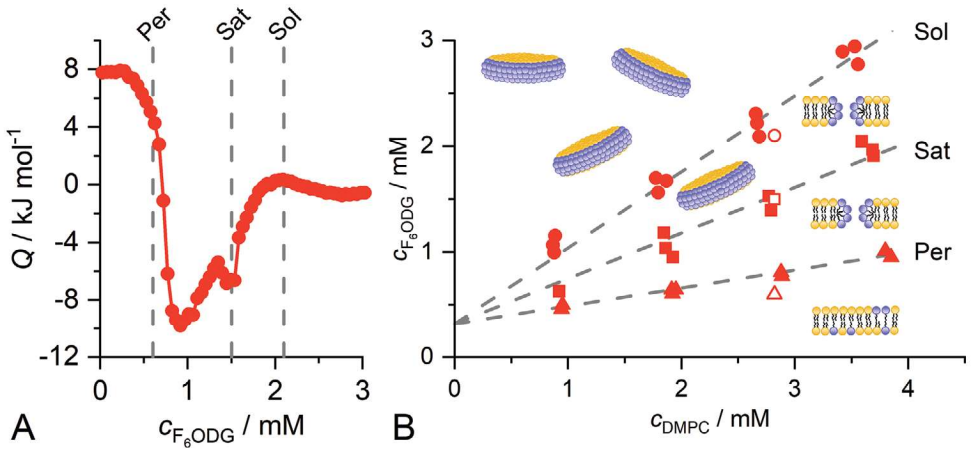

Figure 7. Pseudophase diagram of F_6ODG and DMPC. A) ITC isotherm of the solubilization of initially 3 mM DMPC by F_6ODG. Threshold concentrations obtained from other methods (i.e., DLS, NMR, and NBD bleaching) are indicated by dashed lines. B) Pseudophase diagram constructed from ITC measurements such as in panel A (solid symbols). Global fitting was performed to yield phase boundaries (dashed lines). Threshold concentrations from other methods are shown for comparison (open symbols).

interesting for other applications such as drug release. Therefore, we monitored the solubilization process for various DMPC concentrations using isothermal titration calorimetry (ITC). We titrated a concentrated DG amphiphile solution into a suspension of DMPC vesicles and measured the heat Q released upon each injection (**Figure 7**A). For all titrations, the initial injections gave rise to endothermic reactions, as often observed for membrane-partitioning processes involving nonionic small-molecule amphiphiles.[27] After a drastic drop in Q, the sign turned negative reflecting an exothermic reaction. Within this exothermic part of the self-assembly process, the thermogram followed a W shape, with the first minimum being lower than the second one. This W shape was more pronounced at higher lipid concentrations. Finally, for higher F_6ODG concentrations, a flat maximum was observed before Q declined to zero. Such complex isotherms can be explained neither in terms of a simple three-stage model nor by so-called "breaking-in"[28,29] or "staying-out"[30] mechanisms. Notwithstanding, the characteristic points observed above by DLS and ^{31}P NMR (Figure 5) as well as by ^{19}F NMR and NBD bleaching experiments (Figure 6) can be matched with the initial drop in Q (perforation), the second minimum in Q (saturation), and the flat positive maximum (solubilization). Hence, we were able to use ITC to monitor the concentration dependence of those characteristic points by performing titrations at various DMPC concentrations (Figure 7).

A systematic evaluation of all isotherms obtained at various DMPC concentrations yielded the expected linear relationships between the F_6ODG concentration resulting in a particular feature in the isotherm and the corresponding DMPC concentration (Figure 7B).[31,32,22,33] These linear relationships are described by slopes for perforation, R_{Per}, saturation, R_{Sat}, and solubilization, R_{Sol}, together with one common y-axis intercept, c_{mon} (**Table 1**). These values determine the boundaries of a pseudophase diagram that separates concentration ranges in which different colloidal states are populated. The slopes of these boundaries reflect the extreme DG/DMPC molar ratios in the various colloidal assemblies, while the y-axis intercept gives the monomer concentration, c_{mon}, of the respective DG amphiphile. c_{mon} is utterly important, as this concentration of amphiphile is always present in the aqueous phase and, therefore, needs to be considered when diluting DG nanodiscs. Potentially, these amphiphile monomers in the aqueous phase could interact directly with water-exposed parts of nanodisc-embedded membrane proteins. It is noteworthy that the pseudophase boundaries derived from different methods agree very well with one another (Figure 7B). Comparing the pseudophase boundaries obtained here (Table 1) with those previously found for SMA(2:1)/DMPC mixtures under similar conditions,[3] one can see that SMA(2:1) is the more potent solubilizing agent on a molar scale. However, comparisons of small-molecule with polymeric amphiphiles on a molar basis have to be taken with caution because of the large difference in molar mass. Comparison of the pseudophase boundaries on a mass scale (Table S1, Supporting Information) reveals that the slopes of the pseudophase boundaries are similar for the two systems, with those of the DG amphiphiles being less than twice as steep as those of SMA(2:1).

Overall, isotherms obtained by titrating DDDG into DMPC vesicles look similar (Figure S2A, Supporting Information), suggesting a similar sequence of events during the self-assembly process. In this case, however, we observed signs of large aggregates between the second minimum in Q and the flat maximum for all DMPC concentrations tested. This included reproducible shifts in the baseline heating power as well as increased noise in the raw thermogram. Thus, we were able to establish a pseudophase diagram for DDDG as well (Figure S2B, Supporting Information) by determining the same

Table 1. Parameters derived from pseudophase diagrams of DG/DMPC mixtures at 35 °C.

	F_6ODG	DDDG
R_{Per}	0.17 ± 0.06	0.11 ± 0.08
R_{Sat}	0.43 ± 0.06	0.45 ± 0.09
R_{Sol}	0.72 ± 0.06	0.82 ± 0.09
c_{mon} / mM	0.32 ± 0.14	0.12 (0.00 – 0.34)

ADVANCED SCIENCE NEWS
www.advancedsciencenews.com

NANO · MICRO small
www.small-journal.com

set of parameter values detailed above. Comparison of the pseudophase boundaries (Table 1) shows that, despite its lipophobic nature, F_6ODG solubilized fluid-phase DMPC with similar efficiency as DDDG. Hence, F_6ODG not only provides a native-like lipid-bilayer environment but also turns out to be highly efficient in directly fragmenting vesicular membranes to form nanodiscs.

2.4. Model of Nanodisc Self-Assembly

On the basis of the above solubilization experiments, we propose the following sequential model of nanodisc self-assembly mediated by DG amphiphiles (Figure 7B):

In the first stage, only vesicles having an intact lipid bilayer are present. Although an increasing amount of DG amphiphile is incorporated into the bilayer upon titration with the latter, the overall structure and integrity of the lipid-bilayer membrane are not compromised. In the second stage at higher DG contents in the vesicles, the bilayer becomes perforated, that is, it loses its barrier function to polar compounds. This perforation is connected to the appearance of fast flip-flopping DG amphiphiles in the lipid bilayer (Figure 6) and is explained by the formation of transmembrane pores in or at the edge of domains rich in DG. In the third stage, the DMPC bilayers can no longer take up more DG amphiphiles, which causes solubilization and, thus, the coexistence of DG amphiphile-saturated vesicles with lipid-saturated nanodiscs (Figure 5). Finally, in the fourth stage, all DMPC is present exclusively in nanodiscs. Further addition of DG amphiphile leads to the formation of smaller nanodiscs (Figure 5B) and, ultimately, to the appearance of mixed micelles as lipids are further diluted within the colloidal assemblies.

Of course, the reason for the peculiar ability to form nanodiscs ultimately lies in the molecular structure of the DG amphiphiles. The branched arrangement of the glucose moieties leads to a large and bulky headgroup, as reflected in a high surface area per molecule observed by surface tensiometry.[34] Previous work[35] has revealed that similar amphiphiles bearing a single glucose moiety form rod-shaped micelles, whereas the DG amphiphiles studied here as well as homologous ones carrying three glucose moieties give rise to small, well-defined globular micelles in the absence of lipid. In addition, the sulfide group in the linker region of the DG amphiphiles induces a kink in the hydrophobic chain, as the C–S–C angle is known to be smaller than 100°.[36] We speculate that the decisive molecular properties that confer upon F_6ODG and DDDG the ability to form nanodiscs when combined with lipid bilayers are as follows: (i) a bulky, branched, and strongly hydrated polar headgroup, which confers high curvature, (ii) a kinked overall structure, which is expected to be poorly compatible with the relatively pronounced order within a phospholipid bilayer, and (iii) long chains that are not only hydrophobic but, in the case of F_6ODG, also lipophobic, which further enhances segregation.

2.5. Solubilization of Membrane Proteins into Nanodiscs

To explore the usefulness of hydrocarbon and fluorocarbon nanodiscs for membrane-protein research, we turned our attention to the extraction of membrane proteins from both chemically well-defined, vesicular lipid bilayers and complex, native cellular membranes. To address the first aspect, we reconstituted the bacterial membrane protein outer-membrane phospholipase A (OmpLA) into POPC vesicles and solubilized these proteoliposomes with the aid of DDDG. This treatment resulted in the formation of hydrocarbon nanodiscs having a diameter of around 25 nm, as borne out by negative-stain EM (**Figure 8**A). Moreover, we have previously found that both DG amphiphiles are able to extract membrane proteins from *Escherichia coli* membranes.[7,8] Thus, we extended our investigation of DG nanodiscs to these highly heterogeneous, native membranes. TEM images showed that F_6ODG formed native nanodiscs with a diameter of around 20 nm (Figure 8B). Moreover, it is notable that stacking, which was observed for nanodiscs formed from protein-free artificial vesicles (Figure 2), was completely suppressed by the presence of OmpLA or native *E. coli* proteins. We reason that this is chiefly due to the protrusion of soluble parts or even domains of embedded membrane proteins, which could prevent face-to-face interactions between nanodiscs encircled by DG amphiphiles (Figure 8C).

The ability to form *native nanodiscs*—that is, to recruit proteins and lipids directly from cellular membranes without abolishing the bilayer architecture of the latter—sets DG amphiphiles clearly apart from bicelle-forming amphiphiles such as DHPC or CHAPS. For this reason, we here use operational definitions of, on the one hand, *bicelles* as self-assemblies formed by small-molecule amphiphiles that are unable to extract membrane proteins directly and, on the other hand, *native nanodiscs* as self-assembled structures that do possess this highly desirable property. This is especially remarkable for F_6ODG, as fluorinated amphiphiles have long been thought to be unable to solubilize membranes. We consider the formation of bilayered nanodisc structures as opposed to mixed micelles as a possible reason for the relatively good extraction efficiency of F_6ODG as compared with other fluorinated amphiphiles, which tend to form mixed micelles.[13] Intriguingly, DDDG is even similarly efficient in extracting integral membrane proteins as the "benchmark" solubilizing agents DDM[7] and SMA(2:1)[3] (Figure S3, Supporting Information).

Further to the extraction properties, an essential aspect of using DG amphiphiles in membrane-protein research is their ability to preserve the native structures and functions of solubilized proteins once embedded into nanodiscs. We thus checked the integrity of solubilized OmpLA by SDS-PAGE and enzymatic activity measurements. Both types of DG nanodiscs were able to keep OmpLA in a folded state upon incorporation into nanodiscs, as determined by the differential migration behavior of boiled and unboiled samples in SDS-PAGE (Figure 8D). OmpLA is a phospholipase, whose enzymatic activity can be induced by the addition of divalent cations such as Ca^{2+}. The addition of $CaCl_2$ to nanodisc-embedded OmpLA resulted in an initially linear increase in absorbance reflecting a steady increase in the concentration of product (Figure 8E). While the enzymatic activity was virtually the same for OmpLA in lipid-only vesicles and fluorocarbon nanodiscs, it was slightly reduced in hydrocarbon nanodiscs. The gentler nature of F_6ODG correlates with the lower bilayer perturbation caused by its fluorocarbon chains (Figure 3 and k_{dif} values) and renders

ADVANCED SCIENCE NEWS
www.advancedsciencenews.com

NANO · MICRO small
www.small-journal.com

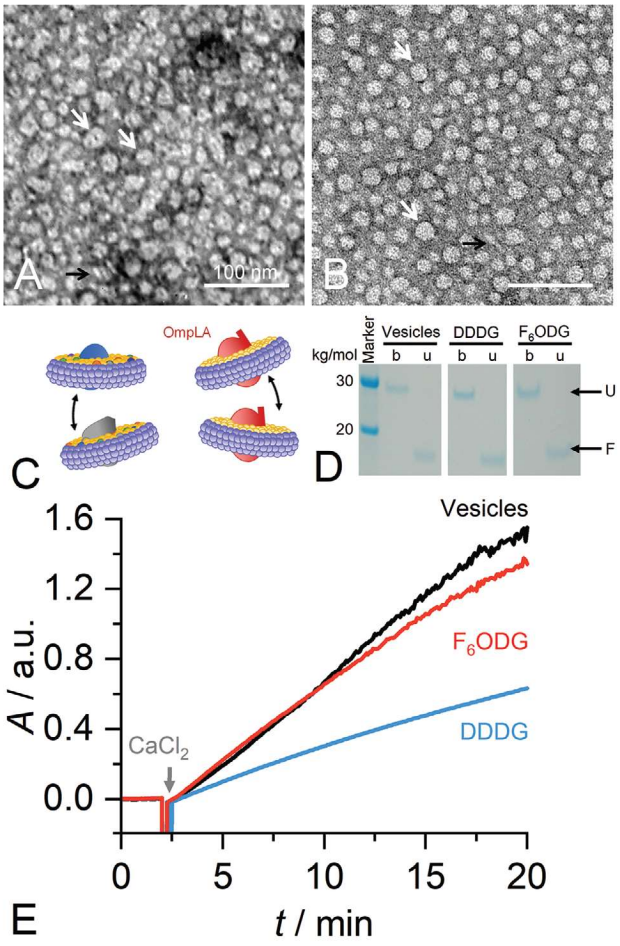

Figure 8. A,B) TEM images of DG nanodiscs made from A) 0.3 mM POPC, 1 µM OmpLA, and 1.0 mM DDDG or B) 0.25 mg ml^{-1} *E. coli* membrane and 0.2 mM F_6ODG. White arrows exemplarily indicate face-on views of nanodiscs, and black arrows indicate edge-on views of nanodiscs. C) Schematic depiction of DG nanodiscs containing the membrane protein OmpLA or complex protein/lipid mixtures. D) SDS-PAGE of OmpLA-containing samples. Boiled (b) and unboiled (u) samples were loaded to assess the folding state of OmpLA in terms of folded (F) and unfolded (U) protein. E) Ca^{2+}-induced enzyme activity measurements of OmpLA-containing vesicles, hydrocarbon nanodiscs, and fluorocarbon nanodiscs.

this compound a particularly interesting candidate for representing a new class of nanodisc-forming amphiphiles for membrane-protein research.

3. Conclusions

We have demonstrated that the diglucoside amphiphiles F_6ODG and DDDG solubilize lipids as well as protein-containing membranes to form lipid-bilayer nanodiscs rather than mixed micelles. We propose a sequential model of nanodisc self-assembly including (i) the perforation of lipid bilayers at sub-solubilizing concentrations of DG amphiphiles in the membrane, (ii) the saturation of the membrane and the onset of nanodisc formation, and (iii) the completion of the solubilization process once all lipid molecules have been transferred to nanodiscs. Contrary to bicelle-forming amphiphiles, the novel nanodisc systems presented here are capable of extracting membrane proteins directly from chemically defined, artificial proteoliposomes and, more importantly, also from highly heterogeneous, native cellular membranes. The lipophobic nature of the F_6ODG fluorocarbon chain renders the nanodiscs formed by this amphiphile remarkably gentle, as reflected by the better preservation of the bilayer architecture compared with the popular nanodisc-forming agent SMA(2:1). In summary, F_6ODG combines the advantages of (i) efficient membrane-solubilizing and protein-extracting agents, (ii) mild fluorinated surfactants having both hydrophobic and lipophobic properties, and (iii) native-like lipid-bilayer nanodiscs to provide a valuable new tool for in vitro studies of membrane proteins embedded in a nanoscale lipid bilayer (Table 2).

4. Experimental Section

Materials: All chemicals were obtained in the highest available purity. POPC and DMPC were kindly gifted by Lipoid (Ludwigshafen, Germany). DDDG and F_6ODG were synthesized as described elsewhere.[7,8] Tris(hydroxylmethyl)aminomethane (TRIS) and ethylenediaminetetraacetic acid (EDTA) were purchased from Carl Roth (Karlsruhe, Germany). NaCl was from VWR (Darmstadt, Germany). NBD-PE and Rhodamine-PE were purchased from Biotium

Table 2. Properties of different native nanodiscs versus other membrane mimics.

	Discoidal morphology	Lipid-bilayer core	Fast content exchange	Direct lipid solubilization	Direct protein extraction
Native nanodiscs					
F_6ODG	+	+	+	+	+
DDDG	+	+	+	+	+
SMA(2:1)	+	+	+	+	+
DIBMA	+	+	+	+	+
Other membrane mimics					
Micelle-forming detergents (e.g., DDM)	–	–	+	+	+
Bicelles	+	+	+	+/–[a)]	–
MSP nanodiscs	+	+	–	–	–

[a)]Lipid solubilization for direct formation of bicelles is limited to a narrow range of lipid compositions and experimental conditions.

ADVANCED SCIENCE NEWS
www.advancedsciencenews.com

NANO · MICRO small
www.small-journal.com

(Fremont, USA). Laurdan, Na_5CO_3, H_3PO_4, $C_2F_3NaO_2$, hydrosulfite, D_2O, and 5,5'-dithiobis-(2-nitrobenzoic acid) (DTNB) were purchased from Sigma–Aldrich (Steinheim, Germany). 2-hexadecanoylthio-1-ethylphosphorylcholine (HEPC) was from Cayman Chemical (Ann Arbor, USA) and LDAO from Anatrace (Maumee, USA).

All experiments were performed in 50 mM Tris, 200 mM NaCl, and at pH 7.4, unless stated otherwise.

Vesicle Preparation: Unlabeled large unilamellar vesicles were prepared by dissolving lipid powders in buffer and shaking for several minutes. For DMPC, heating to 35 °C was required. POPC suspensions were extruded using a LiposoFast extruder (Avestin, Mannheim, Germany) at room temperature; DMPC suspensions were extruded using a Mini-Extruder (Avanti Polar Lipids, Alabaster, USA) at 35 °C. In all cases, extrusion was performed with at least 35 repeats through two stacked polycarbonate membranes with a pore diameter of 100 nm (Cytiva, Freiburg, Germany). Hydrodynamic vesicle diameters were confirmed by DLS. DMPC vesicles labeled with either 0.5 mol% Laurdan, 0.5 mol% NBD-PE, or 1 mol% NBD-PE and Rh-PE each, were prepared by dissolving the corresponding powders in chloroform, followed by mixing of DMPC and the respective dyes. Then, the chloroform was evaporated under a continuous stream of N_2 followed by drying in a vacuum desiccator overnight. Dried lipid films were resuspended in buffer and subjected to five freeze-thaw cycles with liquid N_2 to ensure homogeneous distribution. Finally, all suspensions were extruded as described above.

Transmission Electron Microscopy (TEM): Samples were prepared by mixing stock solutions to achieve the indicated concentrations and subsequent shaking overnight. Negative stained TEM samples were prepared by applying 5 µl of the sample solution to a Cu grid coated with formvar film (Plano, Wetzlar, Germany). After 1 min of incubation time, the excess sample was blotted off with filter paper. Five microliters of 1% (*w/v*) aqueous uranyl acetate solution was applied to the grid for 30 s and was blotted once more. Specimens were dried and examined on an EM 900 transmission electron microscope (Carl Zeiss Microscopy, Oberkochen, Germany), and micrographs were recorded with an SM-1k-120 slow-scan charge-coupled device (slow-scan CCD) camera (TRS, Moorenweis, Germany). The height of nanodisc stacks was measured using Fiji's (ImageJ) measure function.[37,38]

Laurdan Emission Spectroscopy: We used the fluorescence probe Laurdan in order to investigate the thermotropic phase transition of DMPC. To this end, we used a FluoTime300 spectrometer (PicoQuant, Berlin, Germany). 2 mM Laurdan-probed DMPC vesicles (cf. above) were incubated with either 3 mM DDDG, 3 mM F_6ODG, or 5 mM DDM at 35 °C overnight. All samples were excited using a 347 nm LED and perpendicular polarizer settings. Emission spectra were recorded from 380 nm to 600 nm with a detection bandwidth of 10 nm and an integration time of 1 s for temperatures of 10–50 °C with 2 min equilibration time in between. Spectra were decomposed by nonlinear least-squares fitting[39] of two Gaussian peaks corresponding to the two hydration states. Background fluorescence and scattering were negligible. Generalized polarization, GP,[11,12] was calculated as

$$\mathrm{GP} = \left(I_{440\,nm} - I_{490\,nm}\right) / \left(I_{440\,nm} + I_{490\,nm}\right) \quad (1)$$

where $I_{440\ nm}$ and $I_{490\ nm}$ are the emission intensities at 440 nm and 490 nm, respectively.

The resulting temperature dependence of GP values was then fitted by nonlinear least-square fitting according to

$$\mathrm{GP}(T) = \frac{m_1 T + b_1 - m_2 T - b_2}{1 + \exp\left(\frac{T - T_m}{\Delta T}\right)} + m_2 T + b_2 \quad (2)$$

where T denotes the experimental temperature, T_m is the phase-transition temperature, and ΔT is the width of the transition range, which was included as a fitting parameter. m_i and b_i are the slope and *y*-axis intercept of the pre- and post-transition baselines, respectively.

Differential Scanning Calorimetry: DSC was performed on a MicroCal VP-DSC (Malvern Instruments, Malvern, UK). DMPC (4 mM) was incubated with 4 mM DG amphiphile at 35 °C overnight. Reference and sample cells were filled with buffer and sample, respectively, before both cells were repeatedly heated and cooled. Samples containing nanodiscs were heated and cooled at a rate of 0.5 °C min^{-1}. Samples containing DMPC vesicles only were heated and cooled at a rate of 1.0 °C min^{-1}. Except for the first upscan, successive heating and cooling scans are overlaid very closely. Data were averaged, blank-subtracted, and normalized against the DMPC concentration using the MicroCal Origin 7.0 software (OriginLab, Northampton, USA). The melting temperature, T_m, was taken as the temperature at which the isobaric heat capacity difference, ΔC_p, reached its maximum.

Time-Resolved Förster Resonance Energy Transfer: Fluorescently labeled DG nanodiscs were produced by incubating 0.25 mM NBD- and rhodamine-labeled DMPC vesicles (cf. above) with DDDG and F_6ODG, respectively, in order to obtain nanodiscs with a diameter of (25 ± 5) nm, as verified by DLS (see below). Unlabeled DG nanodiscs of the same size were produced by incubating DMPC vesicles at various concentrations with corresponding DG amphiphile concentrations. Experiments were performed on an SF.3 stopped-flow apparatus (Applied Photophysics, Leatherhead, UK) equipped with a 470 nm LED and an OD 2 filter. Time-resolved donor dequenching was detected by a photomultiplier at a 90° angle at (528 ± 15) nm using an OD 6 band pass filter (Edmund Optics, Karlsruhe, Germany). Drive syringes, tubings, and the quartz glass cell were thermostatted at 35 °C. Samples were equilibrated for at least 10 min prior to measurements. Then, 75 µl of labeled and unlabeled DG nanodiscs were mixed rapidly. Each measurement was repeated five to seven times with 1000 or 10 000 data points per repeat. The resulting traces were averaged and fitted globally as described.[17] In brief, rate constants for lipid exchange by diffusion, k_{dif}, and by collision, k_{col}, can be extracted from the equation

$$\frac{\Delta F}{F_{max}} = 1 - \exp\left(\frac{k_{dif} c_L}{c_L^0 + c_L} + k_{col} c_L\right) \quad (3)$$

Here, $\Delta F/F_{max}$ is the normalized fluorescence intensity change. k_{dif} and k_{col} are treated as global fitting parameters, while c_L and c_L^0 are the lipid concentrations of unlabeled and labeled DG nanodiscs, respectively, specific to the particular experiment. Best-fit parameter values and corresponding to 95% confidence intervals were obtained by nonlinear least-square fitting using Excel (Microsoft, Redmond, USA) as described in detail elsewhere.[39]

Dynamic Light Scattering: Measurements were performed on a Nano Zetasizer ZS90 (Malvern Instruments, Malvern, UK) equipped with a He–Ne laser and a detection angle of 90° using a 45 µl quartz glass cuvette (Hellma, Müllheim, Germany). Measurements were performed at 25 °C for POPC and at 35 °C for DMPC after both the instrument and the cuvettes had equilibrated at the respective temperature.

NMR Spectroscopy: Experiments were performed on an Avance 600 spectrometer (Bruker BioSpin, Rheinstetten, Germany) operating at a ^{31}P resonance frequency of 242.9 MHz and a ^{19}F resonance of 564.6 MHz. For all measurements, 2.8 mM DMPC vesicles (cf. above) were incubated with 0–3 mM F_6ODG at 35 °C overnight before being transferred into NMR tubes. All samples contained 10% (v/v) D_2O as a lock signal. Samples were incubated at 35 °C for 20 min inside the spectrometer prior to measurements. ^{31}P spectra were acquired with 265 scans per sample. We applied a 5 mm broadband inverse probe, an inverse-gated gated ^1H decoupling pulse sequence with an acquisition time of 1.5 s, a sweep width of 7310 Hz, and a relaxation delay of 2 s. Data were multiplied by an exponential function with a line-broadening factor of 1.0 Hz before Fourier transformation. ^{19}F spectra were acquired with 128 scans per sample. We also applied a 5-mm broadband inverse probe, an inverse gated ^1H decoupling pulse sequence with an acquisition time of 2.2 s, a sweep width of 45 045 Hz, and a relaxation delay of 1 s. Data were multiplied by an exponential function with a line-broadening factor of 0.3 Hz before Fourier transformation. ^{31}P and ^{19}F chemical shifts were referenced to H_3PO_4 and $C_2F_3NaO_2$ in D_2O, respectively, as external standards at 0 ppm. Peak areas and chemical shifts were obtained by using the TopSpin 4.0.8 software (Bruker BioSpin).

ADVANCED SCIENCE NEWS
www.advancedsciencenews.com

NANO · MICRO small
www.small-journal.com

NBD Bleaching Assay: Experiments were performed on a FLUOstar Omega (BMG Labtech, Ortenberg, Germany) using its fluorescence intensity mode with λ_{ex} = 485 nm and λ_{em} = 520 nm. For all measurements, 2.8 mM NBD-labeled DMPC vesicles (cf. above) were incubated with 0–3 mM F_6ODG at 35 °C overnight. A total of 148.5 µl of each sample was transferred to a flat-bottomed 96-well microplate (Greiner Bio-One, Kremsmünster, Austria) and measured every 2 s. After 10 min, 1.5 µl of a 1 M hydrosulfite solution was added to each well, resulting in a final concentration of 10 mM hydrosulfite and ≈2.8 mM DMPC/NBD-PE, and the plate was shaken for 2 s. Measurements continued for about 20 min. Fluorescence intensity decays were normalized in order to eliminate concentration errors and scattering artifacts. To this end, the average values of the last 5 min of each measurement were subtracted and the result was divided by the average value of the initial 10 min baseline. Due to this normalization, the characteristic bleaching time τ could be directly obtained from numerical integration of the values from 10 to 30 min.

Isothermal Titration Calorimetry: All experiments were performed on an iTC200 (Malvern Instruments, Malvern, UK) in 50 mM Tris, 200 mM NaCl at pH 7.4 at 35 °C. The sample cell was loaded with 1–4 mM DMPC vesicles (cf. above) and the syringe with the respective DG amphiphile. For all experiments, a first injection of 0.4 µl was followed by 80 injections of 0.5 µl, and time spacings were chosen long enough to allow baseline re-equilibration before the next injection. Baseline subtraction and peak integration were performed using NITPIC.[40] The first injection was omitted from further analysis.

Preparation of OmpLA-Containing Vesicles: Vesicles containing outer membrane phospholipase A, OmpLA, were prepared by drop dilution of 3.22 mg ml^{-1} OmpLA in 12 mM LDAO into 1 mM POPC vesicles (cf. above) in 20 mM Tris and 2 mM EDTA at pH 8.3 to a final volume of 500 µl (20 times 0.78 µl) under permanent agitation (900 rpm) at 20 °C. After overnight incubation at 4 °C, OmpLA-containing vesicles were dialyzed for 24 h against a 500-fold excess volume of 50 mM Tris, 2 mM EDTA, and 200 mM NaCl at pH 7.4.

Escherichia coli Solubilization: *E. coli* BL21(DE3) cells were transformed with an empty pET-24 vector and selected by kanamycin resistance. After overnight incubation at 37 °C in LB medium under permanent agitation, cells were harvested and washed twice with saline by centrifugation. The resulting pellets were resuspended in ice-cold alkaline buffer (100 mM Na_5CO_3, pH 11.5) and sonicated two times for 10 min with an MS-73 SonoPlus tip sonicator (Bandelin, Berlin, Germany). Cell debris was removed by centrifugation for 30 min at 4 °C and 1000 × *g*. For separation of membrane fragments from soluble and peripheral proteins, the supernatant was ultracentrifuged for 1 h at 4 °C and 100 000 × *g*. The resulting pellets were resuspended in Tris buffer and ultracentrifuged again. Washed pellets were resuspended in Tris buffer containing complete protease inhibitor (Roche, Basel, Switzerland). Final membrane concentrations were 100 mg ml^{-1}. *E. coli* membrane suspensions were mixed with F_6ODG to final concentrations of 0.25 mg ml^{-1} membrane and 0.2 mM F_6ODG. The resulting samples were shaken at room temperature overnight.

OmpLA activity assay: The activity of OmpLA in vesicles and DG nanodiscs was monitored by a spectrophotometric assay. To this end, we solubilized OmpLA-containing vesicles with DG amphiphile stock solutions in a 1:5 ratio (proteoliposome/DG amphiphile) and incubated them for 24 h at 20 °C. In the case of F_6ODG, we heated the samples to 45 °C to ensure solubilization of the POPC vesicles. After equilibration at 20 °C for at least 1 h, samples were mixed with enzyme activity buffer containing 50 mM Tris, 150 mM NaCl, 1.3 mM HEPC, and 1.0 mM DTNB in a 3:7 ratio (buffer/sample). Samples were then incubated at 20 °C for another 2 h. Absorption measurements were performed on a Jasco V-630 UV-VIS spectrometer (Jasco Germany, Groß-Umstadt, Germany) at 412 nm using a 3 mM quartz glass cuvette (Hellma). Before inducing the color reaction via the addition of 20 mM Ca^{2+} each sample was measured for 2 min to determine the baseline absorption that was set to 0. After the addition of Ca^{2+} OmpLA could dimerize and hydrolyze HEPC, products of which, in turn, react with DTNB[41,42] and could be observed via spectroscopy.

Supporting Information

Supporting Information is available from the Wiley Online Library or from the author.

Acknowledgements

The authors are indebted to Dr. Harald Kelm and Prof. Dr. Michael Schroda (both TUK) for providing access to NMR spectroscopy and a plate reader, respectively. The authors thank Johannes Klingler (TUK) and Kevin Janson (Martin-Luther-Universität Halle–Wittenberg) for helpful comments and discussions on solubilization experiments and NBD fluorescence experiments, respectively. This work was partly funded by the Agence Nationale de la Recherche (ANR) through LabCom Chem2staB (ANR14-LAB7-0002-01) as well as by the ANR and the Deutsche Forschungsgemeinschaft (DFG) through the French–German FLUOR initiative (GD: ANR-16-CE92-0001; AM: ME 4165/2-1; SK: KE 1478/7-1).

Conflict of Interest

The authors declare no conflict of interest.

Data Availability Statement

Research data are not shared.

Keywords

fluorinated surfactants, membrane proteins, protein solubilization, self-assembly, small-molecule amphiphiles

Received: June 20, 2021
Revised: August 24, 2021
Published online:

[1] R. M. Garavito, S. Ferguson-Miller, *J. Biol. Chem.* **2001**, *276*, 32403.
[2] T. H. Bayburt, Y. V. Grinkova, S. G. Sligar, *Nano Lett.* **2002**, *2*, 853.
[3] A. Grethen, A. O. Oluwole, B. Danielczak, C. Vargas, S. Keller, *Sci. Rep.* **2017**, *7*, 11517.
[4] F. Hagn, M. L. Nasr, G. Wagner, *Nat. Protoc.* **2018**, *13*, 79.
[5] A. A. de Angelis, S. J. Opella, *Nat. Protoc.* **2007**, *2*, 2332.
[6] S. Scheidelaar, M. C. Koorengevel, C. A. van Walree, J. J. Dominguez, J. M. Dörr, J. A. Killian, *Biophys. J.* **2016**, *111*, 1974.
[7] G. N. M. Boussambe, P. Guillet, F. Mahler, A. Marconnet, C. Vargas, D. Cornut, M. Soulié, C. Ebel, A. Le Roy, A. Jawhari, F. Bonneté, S. Keller, G. Durand, *Methods* **2018**, *147*, 84.
[8] P. Guillet, F. Mahler, K. Garnier, G. N. M. Boussambe, S. Igonet, C. Vargas, C. Ebel, M. Soulié, S. Keller, A. Jawhari, G. Durand, *Langmuir* **2019**, *35*, 4287.
[9] N. Kučerka, M.-P. Nieh, J. Katsaras, *Biochim. Biophys. Acta, Biomembr.* **2011**, *1808*, 2761.
[10] D. Marsh, *Handbook of Lipid Bilayers*, CRC Press, Boca Raton, FL **2013**.
[11] T. Parasassi, G. de Stasio, G. Ravagnan, R. M. Rusch, E. Gratton, *Biophys. J.* **1991**, *60*, 179.
[12] F. M. Harris, K. B. Best, J. D. Bell, *Biochim. Biophys. Acta, Biomembr.* **2002**, *1565*, 123.

ADVANCED SCIENCE NEWS
www.advancedsciencenews.com

NANO · MICRO small
www.small-journal.com

[13] E. Frotscher, B. Danielczak, C. Vargas, A. Meister, G. Durand, S. Keller, *Angew. Chem., Int. Ed. Engl.* **2015**, *54*, 5069.
[14] M. Nakano, M. Fukuda, T. Kudo, H. Endo, T. Handa, *Phys. Rev. Lett.* **2007**, *98*, 238101.
[15] R. Cuevas Arenas, B. Danielczak, A. Martel, L. Porcar, C. Breyton, C. Ebel, S. Keller, *Sci. Rep.* **2017**, *7*, 45875.
[16] B. Danielczak, S. Keller, *Eur. Polym. J.* **2018**, *109*, 206.
[17] B. Danielczak, S. Keller, *Methods* **2020**, *180*, 27.
[18] A. Grethen, D. Glueck, S. Keller, *J. Membr. Biol.* **2018**, *251*, 443.
[19] M. Nakano, M. Fukuda, T. Kudo, M. Miyazaki, Y. Wada, N. Matsuzaki, H. Endo, T. Handa, *J. Am. Chem. Soc.* **2009**, *131*, 8308.
[20] H. Takahashi, M. Yoshino, K. Morita, T. Takagi, Y. Yokoyama, T. Kikukawa, H. Amii, T. Kanamori, M. Sonoyama, *Biochim. Biophys. Acta, Biomembr.* **2019**, *1861*, 631.
[21] M. Yoshino, T. Kikukawa, H. Takahashi, T. Takagi, Y. Yokoyama, H. Amii, T. Baba, T. Kanamori, M. Sonoyama, *J. Phys. Chem. B* **2013**, *117*, 5422.
[22] D. Lichtenberg, E. Opatowski, M. M. Kozlov, *Biochim. Biophys. Acta, Biomembr.* **2000**, *1508*, 1.
[23] M. Roux, P. Champeil, *FEBS Lett.* **1984**, *171*, 169.
[24] P. Barthélémy, V. Tomao, J. Selb, Y. Chaudier, B. Pucci, *Langmuir* **2002**, *18*, 2557.
[25] E. Frotscher, J. Höring, G. Durand, C. Vargas, S. Keller, *Anal. Chem.* **2017**, *89*, 3245.
[26] L. Nordstierna, I. Furó, P. Stilbs, *J. Am. Chem. Soc.* **2006**, *128*, 6704.
[27] H. Heerklotz, J. Seelig, *Biophys. J.* **2000**, *78*, 2435.
[28] A. Hildebrand, R. Neubert, P. Garidel, A. Blume, *Langmuir* **2002**, *18*, 2836.
[29] H. Heerklotz, *Biophys. J.* **2001**, *81*, 184.
[30] H. Y. Fan, D. Das, H. Heerklotz, *Langmuir* **2016**, *32*, 11655.
[31] D. Lichtenberg, H. Ahyayauch, A. Alonso, F. M. Goñi, *Trends Biochem. Sci.* **2013**, *38*, 85.
[32] D. Lichtenberg, H. Ahyayauch, F. M. Goñi, *Biophys. J.* **2013**, *105*, 289.
[33] H. Heerklotz, *Q. Rev. Biophys.* **2008**, *41*, 205.
[34] M. Abla, G. Durand, B. Pucci, *J. Org. Chem.* **2008**, *73*, 8142.
[35] C. Breyton, F. Gabel, M. Abla, Y. Pierre, F. Lebaupain, G. Durand, J.-L. Popot, C. Ebel, B. Pucci, *Biophys. J.* **2009**, *97*, 1077.
[36] T. Iijima, S. Tsuchiya, M. Kimura, *Bull. Chem. Soc. Jpn.* **1977**, *50*, 2564.
[37] J. Schindelin, I. Arganda-Carreras, E. Frise, V. Kaynig, M. Longair, T. Pietzsch, S. Preibisch, C. Rueden, S. Saalfeld, B. Schmid, J.-Y. Tinevez, D. J. White, V. Hartenstein, K. Eliceiri, P. Tomancak, A. Cardona, *Nat. Methods* **2012**, *9*, 676.
[38] C. A. Schneider, W. S. Rasband, K. W. Eliceiri, *Nat. Methods* **2012**, *9*, 671.
[39] G. Kemmer, S. Keller, *Nat. Protoc.* **2010**, *5*, 267.
[40] S. Keller, C. Vargas, H. Zhao, G. Piszczek, C. A. Brautigam, P. Schuck, *Anal. Chem.* **2012**, *84*, 5066.
[41] N. Dekker, K. Merck, J. Tommassen, H. M. Verheij, *Eur. J. Biochem.* **1995**, *232*, 214.
[42] G. L. Ellman, *Arch. Biochem. Biophys.* **1959**, *82*, 70.

NANO MICRO small

Supporting Information

for *Small,* DOI: 10.1002/smll.202103603

Self-Assembly of Protein-Containing Lipid-Bilayer Nanodiscs from Small-Molecule Amphiphiles

Florian Mahler, Annette Meister, Carolyn Vargas, Grégory Durand, and Sandro Keller**

WILEY-VCH

Supporting Information

Self-Assembly of Protein-Containing Lipid-Bilayer Nanodiscs from Small-Molecule Amphiphiles

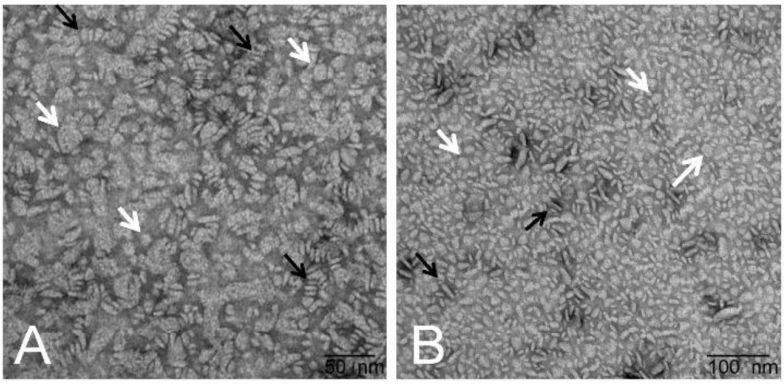

Florian Mahler, Annette Meister, Carolyn Vargas, Grégory Durand, and Sandro Keller**

Figure S1. Formation of lipid-bilayer nanodiscs at 10°C. TEM images of DG nanodiscs made from (A) 0.3 mM DMPC and 0.4 mM DDDG or (B) 0.3 mM DMPC and 0.6 mM F_6ODG. Black arrows exemplarily indicate edge-on views of nanodiscs or nanodisc rouleaux, and white arrows point to face-on views of nanodiscs.

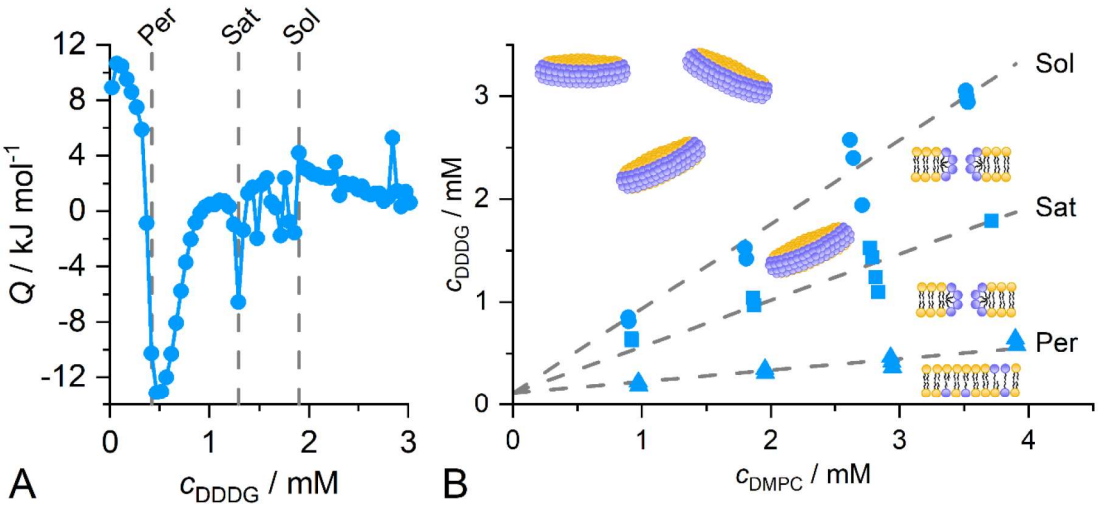

Figure S2. Pseudophase diagram of DDDG and DMPC (A) ITC isotherm of the solubilization of initially 3 mM DMPC by DDDG. Threshold concentrations (*dashed lines*) are estimated by similar features as found for F_6ODG. (B) Pseudophase diagram constructed from ITC measurements such as in panel A (*symbols*). Global fitting was performed to yield phase boundaries (*dashed lines*).

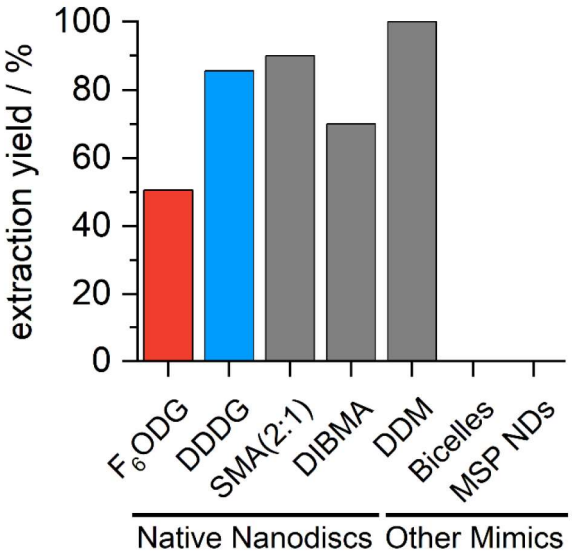

Figure S3. Direct membrane-protein extraction yield from *E. coli* membranes, normalized to the extraction yield afforded by 10 mM DDM. Molar concentrations were 10.4 mM F_6ODG,[7] 10.1 mM DDDG,[8] 9.3 mM SMA(2:1),[3] and 3.0 mM DIBMA.[43] For bicelles and MSP nanodiscs (NDs), no direct extraction of membrane proteins has been reported.[44]

Table S1: Parameters derived from pseudophase diagrams converted to mass scale.

	F_6ODG	DDDG	SMA(2:1)[a)]
R_{Per}	0.22 ± 0.08	0.11 ± 0.08	-
R_{Sat}	0.55 ± 0.08	0.45 ± 0.09	0.35
R_{Sol}	0.92 ± 0.08	0.82 ± 0.009	0.52
c_{mon} / g L^{-1}	0.28 ± 0.12	0.08 (0.00 – 0.23)	0.0

[a)] 30°C, taken from the literature.[3]

References

[1] G. N. M. Boussambe, P. Guillet, F. Mahler, A. Marconnet, C. Vargas, D. Cornut, M. Soulié, C. Ebel, A. Le Roy, A. Jawhari, F. Bonneté, S. Keller, G. Durand, *Methods* **2018**, 147, 84.
[2] P. Guillet, F. Mahler, K. Garnier, G. Nyame Mendendy Boussambe, S. Igonet, C. Vargas, C. Ebel, M. Soulié, S. Keller, A. Jawhari, G. Durand, *Langmuir* **2019**, 35, 4287.
[3] A. Grethen, A. O. Oluwole, B. Danielczak, C. Vargas, S. Keller, *Sci. Rep.* **2017**, 7, 11517.
[4] A. O. Oluwole, B. Danielczak, A. Meister, J. O. Babalola, C. Vargas, S. Keller, *Angew. Chem. Int. Ed.* **2017**, 56, 1919.
[5] J.-L. Popot, *Membrane Proteins in Aqueous Solutions,* Springer, **2018**.

3.7. Associated Results (Manuscript 4)

In *Manuscript 4*, it was shown that DDDG and F_6ODG self-assemble into native nanodiscs upon addition to lipid bilayers of different composition. Moreover, the fluorocarbon chain of F_6ODG conveys peculiar properties onto the nanodiscs. In this section, the results of the corresponding experiments that were performed using decyl diglucoside (DDG) are presented. These experiments **elucidate the impact of the hydrophobic chain length** of the amphiphiles on the nanodisc architecture, integrity, and self-assembly. Moreover, F_6ODG and DDG were designed to have similar hydrophobicities, that is, similar CMC values.

3.7.1. Experimental and Theoretical Section

Experimental Procedure

All experiments were performed as described in *Manuscript 4*. Concentration differences are indicated in the respective figure captions.

Theoretical Background

Free energies for the transfer of lipid (L) or surfactant (S, i.e., amphiphile) from a vesicular bilayer (v) to a nano-sized micelle (m) or nanodisc (d) can be calculated with the information obtained by a pseudophase diagram (e.g., Fig. 3.5B) for lipid/amphiphile mixtures. In detail, the slopes of the pseudophase boundaries for saturation of the vesicular bilayer (R_{Sat}) and the completion of solubilization (R_{Sol}) can be used to calculate the critical mole fractions of the surfactant in the vesicular and the nanodisc/micelle phase, $X_S^{v,Sat}$ and $X_S^{d,Sol}$, respectively:

$$X_S^{v,Sat} = \frac{R_{Sat}}{1+R_{Sat}} \quad (1)$$

$$X_S^{d,Sol} = \frac{R_{Sol}}{1+R_{Sol}} \quad (2)$$

Furthermore, the partition coefficients characterizing the transfer of lipids and surfactant from the vesicular phase to the nanodisc/micelle phase are given by the ratios of the critical mole fractions:

$$K_L^{v\rightarrow d} = \frac{X_L^{d,Sol}}{X_L^{v,Sat}} = \frac{1-X_S^{d,Sol}}{1-X_S^{v,Sat}} = \frac{1+R_{Sat}}{1+R_{Sol}} \quad (3)$$

$$K_S^{v\rightarrow d} = \frac{X_S^{d,Sol}}{X_S^{v,Sat}} = \frac{R_{Sol}(1+R_{Sat})}{R_{Sat}(1+R_{Sol})} = \frac{R_{Sol}}{R_{Sat}} K_L^{v\rightarrow d} \quad (4)$$

Finally, these partition coefficients can be used to calculate the corresponding change in standard molar Gibbs free energies of transfer from the vesicular phase into the nanodisc/micelle phase:

$$\Delta G_L^{v\rightarrow d,o} = -RT\ln(K_L^{v\rightarrow d}) \quad (5)$$

$$\Delta G_S^{v\rightarrow d,o} = -RT\ln(K_S^{v\rightarrow d}) \quad (6)$$

3.7.2. Results

Bilayer Architecture and Integrity

Upon addition of DDG to lipid bilayers of different composition, the mixture spontaneously reorganized into discoidal structures. This was observed for pure artificial vesicles formed by either DMPC or POPC (Fig. 3.1A–B), as well as for artificial POPC vesicles containing the model MP OmpLA (Fig. 3.1C). For the mentioned samples, discoidal structures with a diameter of roughly 20 nm were visible in TEM images, similar to those shown in *Manuscript 4*. This suggests that **DDG also induces nanodisc self-assembly**. Unfortunately, no clear disc formation could be observed for DDG/*E. coli* membrane mixtures with TEM.

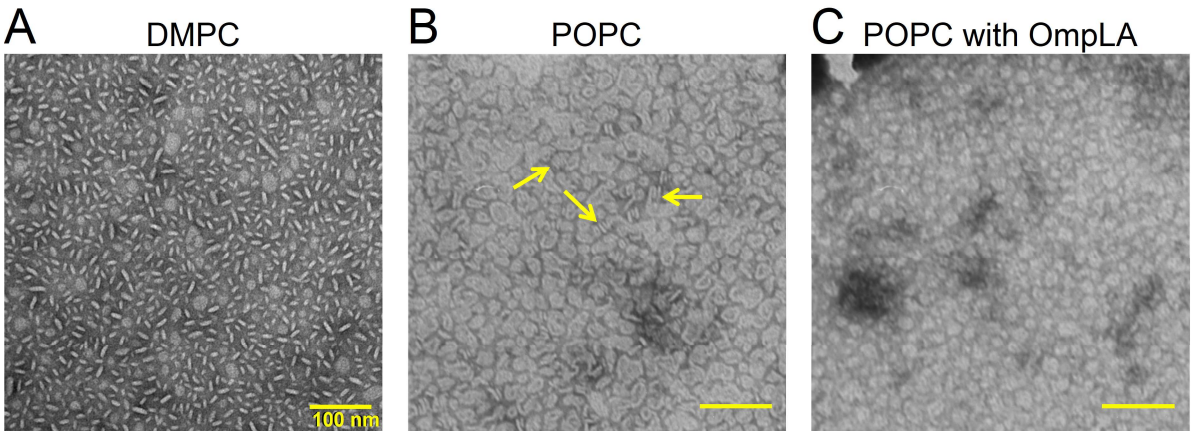

Figure 3.1. Formation of lipid-bilayer nanodiscs. TEM images of diglucoside nanodiscs made from (A) 0.3 mM DMPC solubilized by 0.8 mM DDG at 30°C, (B) 0.3 mM POPC solubilized by 3.2 mM DDG at room temperature, and (C) 0.3 mM POPC with 1 µM OmpLA solubilized by 3.2 mM DDG at room temperature. Scale bars for all micrographs are 100 nm, as indicated in micrograph A. Arrows indicate edge-on views of nanodisc rouleaux.

To investigate the integrity of the bilayer core of DDG nanodiscs in terms of gel-to-fluid phase transition, laurdan fluorescence and DSC experiments were performed. Similarly to DDDG and F_6ODG, the generalized polarization (GP) values over the measured temperature range were between those measured for DMPC vesicles and DDM/DMPC mixed micelles (Fig. 3.2A). However, the sigmoidal shape was only weakly pronounced, which suggests a small cooperative unit of lipids for the phase transition in DDG nanodiscs. Therefore, the generic, model-free fit as described in *Manuscript 4* failed to yield a reasonable value for T_m. Instead, the numerical derivative of the fit was calculated to determine the inflection point (i.e.,

the minimum of the derivative), which yielded T_m = 23.0°C. Moreover, DSC upscans gave similar results: The peak in the change of differential isobaric heat capacity (ΔC_p) of DDG nanodiscs was poorly defined and its maximum yielded T_m = 21.7°C.

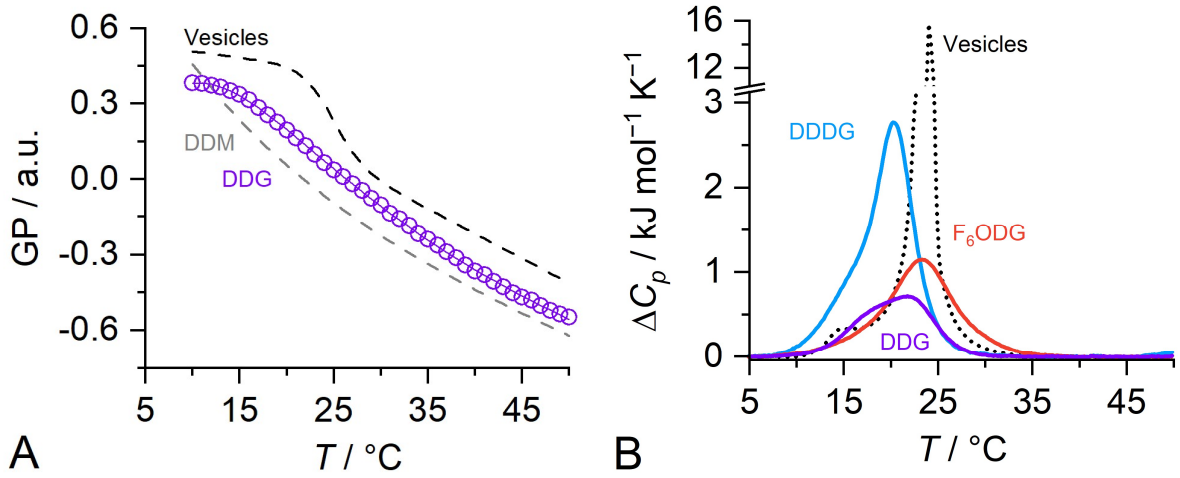

Figure 3.2. Gel-to-fluid phase transition of DMPC in diglucoside nanodiscs by laurdan fluorescence and DSC. (A) Laurdan generalized polarization (GP) for DDG nanodiscs, DDM/DMPC mixed micelles, and unilamellar DMPC vesicles. 2 mM DMPC in the form of unilamellar vesicles containing 0.5 mol% laurdan was solubilized by addition of 5 mM DDM or 3.5 mM DDG. (B) Change in differential isobaric heat capacity (ΔC_p) derived from DSC upscans for vesicles, hydrocarbon nanodiscs, and fluorocarbon nanodiscs. For nanodiscs, 4 mM DMPC in the form of vesicles was solubilized with 4 mM DDDG, DDG, or F_6ODG. This graph is an extended version of the one shown in *Manuscript 4*.

Furthermore, the kinetics of lipid exchange among DDG nanodiscs were investigated with the aid of nanodiscs containing two fluorescently labeled lipids that act as a FRET pair: *N*-(7-nitrobenz-2-oxa-1,3-diazol-4-yl)-1,2-dihexadecanoyl-*sn*-glycero-3-phosphoethanolamine (NBD-DHPE) and rhodamine B 1,2-dihexadecanoyl-*sn*-glycero-3-phosphoethanolamine (Rh-DHPE). Figure 3.3A shows that with increasing concentrations of unlabeled nanodiscs, the donor fluorescence reaches equilibrium faster. Global fitting allowed for dissection into contributions from diffusional lipid transfer (k_{dif}) and collisional transfer (k_{col}; cf., Equation 3 in *Manuscript 4*). The comparison to other membrane mimics revealed that the **exchange kinetics were similar to that of DDDG** and SMA(2:1) nanodiscs (Fig. 3.3B). In more detail, k_{dif} was less than $1 \cdot 10^{-3}$ s^{-1} smaller for DDG compared with DDDG nanodiscs and k_{col} was about 2 times higher for DDG. This reflects a similar bilayer integrity for both hydrogenated diglucoside amphiphiles but a considerably faster lipid exchange by collisions for DDG nanodiscs. For comparison, detailed numeric values are summarized in Table 1.

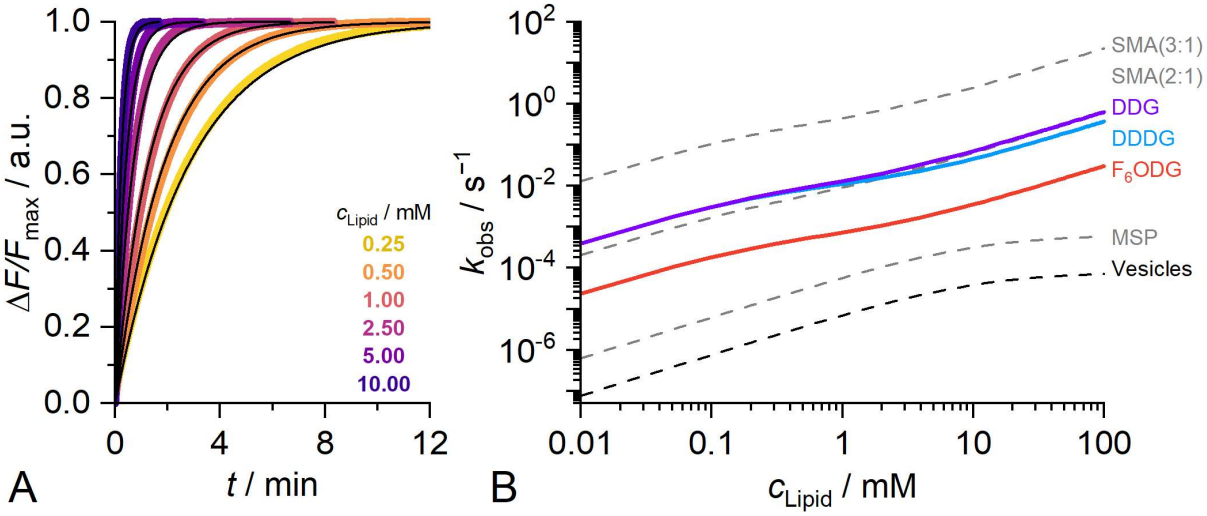

Figure 3.3. Lipid exchange among fluorescently labeled and unlabeled nanodiscs formed by diglucoside amphiphiles at 35°C. (A) DMPC vesicles with and without NBD- and Rh-labeled lipids were solubilized into 25 nm-sized nanodiscs by DDG. Shown are normalized fluorescence dequenching curves (*colored*) and corresponding global best-fits (*black*). (B) Observed lipid-exchange rate constants (k_{obs}) of various membrane mimics across a broad range of lipid concentrations. Values for DDG were derived from the results shown in panel A. Values for SMA(3:1),[72] SMA(2:1),[73] MSP,[74] and vesicles[75] were obtained from the literature. Values for DDDG and F_6ODG are from *Manuscript 4*.

Table 1: Transfer rates determined by global fitting of time-resolved FRET data for diffusional lipid exchange (k_{dif}) and collisional lipid exchange (k_{col}). Given are best-fit values and 95% confidence intervals.

Amphiphile	k_{dif} / 10^{-3} s^{-1}	k_{col} / s^{-1} M^{-1}	Chain length
F_6ODG	0.535 ± 0.002	0.301 ± 0.001	C8
DDG	8.56 ± 0.02	6.29 ± 0.01	C10
DDDG	9.35 ± 0.04	3.65 ± 0.02	C12

Bilayer Perforation and Self-Assembly Process of Hydrogenated Diglucoside Amphiphiles

To monitor the perforation process of DDDG- and DDG-mediated vesicle solubilization, NBD bleaching kinetics were evaluated for labeled DMPC vesicles treated with increasing DDDG and DDG concentrations. The determined characteristic NBD bleaching times (τ) decreased already at low concentrations of diglucoside amphiphile (Fig. 3.4). Contrary to the results for F_6ODG, τ values between the starting value and the values for medium concentrations were observed, most likely indicating different degrees of perforation. However, it

cannot be distinguished whether only a small number of vesicles became permeable, or all vesicles became partially permeable. For medium concentrations, the NBD bleaching for DDG-treated vesicles was **considerably faster than for vesicles treated with DDDG or F_6ODG**.

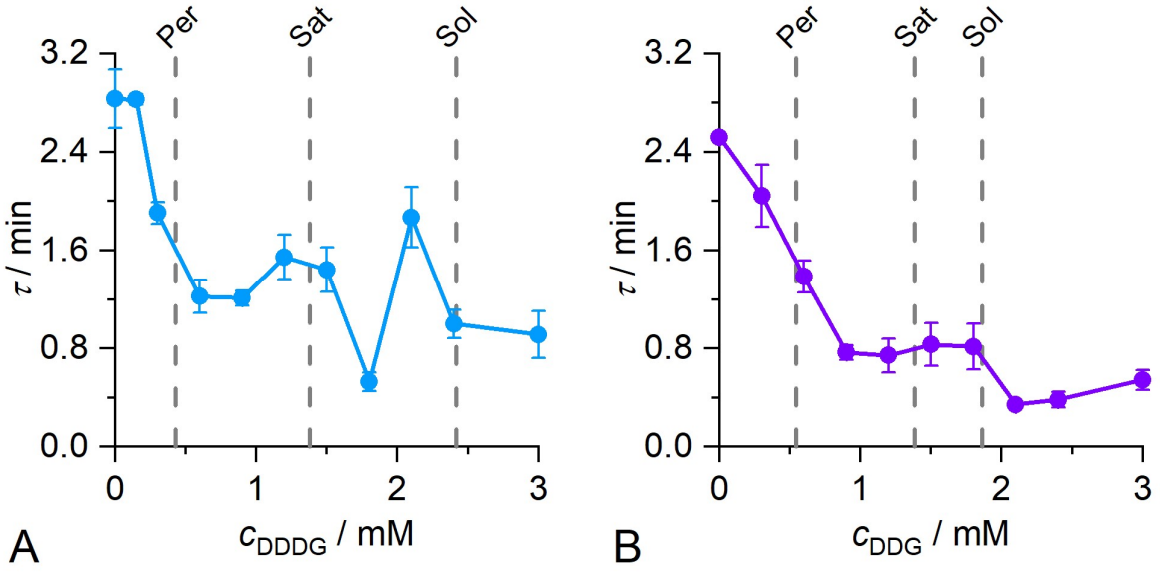

Figure 3.4. Characteristic NBD bleaching times, τ, in dependence of (A) the DDDG concentration and (B) the DDG concentration. τ values were derived from the area under the $\Delta F/F_{bl}$ curves. Error bars are standard errors derived from replicates. Dashed lines indicate threshold concentrations for bilayer perforation (Per), saturation (Sat), and complete solubilization (Sol).

Similarly to F_6ODG and DDDG, as outlined in *Manuscript 4*, the self-assembly process of DDG was monitored by ITC solubilization experiments (Fig. 3.5). The isotherm showed a short plateau of endothermic reaction heats before the signal inverted around the perforation concentration to largely exothermic heats for increasing DDG concentrations. For further increasing DDG concentrations, the heats raised again close to zero before noise signal dominated. This noise is indicative for the formation of large aggregates and was used to estimate the onset (i.e., saturation) and completion of solubilization (cf., DDDG in *Manuscript 4*). Finally, a broad endothermic peak was observed for high concentrations, which decreased to zero with further titrations (Fig. 3.5A).

Performing ITC solubilization experiments at different DMPC concentrations enabled the **establishment of a pseudophase diagram for DDG/DMPC mixtures** at 35°C (Fig. 3.5B). To this end, the DDG and DMPC concentrations of the inflection point of the first, large inversion of heats representing the perforation concentration, the beginning of the noise-dominated concentration range

indicating the saturation concentration, and the end of this range indicating the complete solubilization concentration, were plotted. Furthermore, the pseudophase boundaries were determined by global fitting of individual slopes for each boundary and one common *y*-axis intercept (c_{mon}) indicating the DDG-monomer concentration present in the aqueous phase (Table 2).

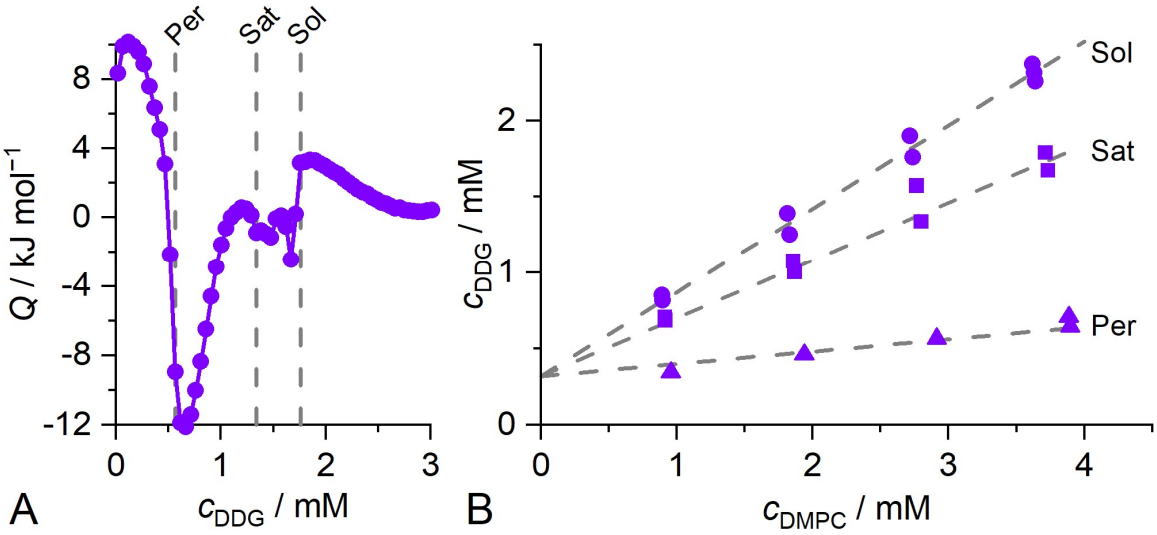

Figure 3.5. DDG/DMPC pseudophase diagram. (A) ITC isotherm of the solubilization of initially 3 mM DMPC by DDDG. Threshold concentrations (*dashed lines*) were estimated by similar features as found for DDDG. (B) Pseudophase diagram established from ITC measurements such as in panel A (*symbols*). Global fitting was performed to yield phase boundaries (*dashed lines*).

Table 2: Parameters of the diglucoside/DMPC pseudophase diagrams at 35°C and derived transfer free energies for lipids (L) and diglucosides (S). Given are the best-fit values and 95% confidence intervals.

Amphiphile	F_6ODG	DDDG	DDG
c_{mon} / mM	0.32 ± 0.14	0.12 (0.00–0.34)	0.32 ± 0.15
R_{Per}	0.17 ± 0.06	0.11 ± 0.08	0.08 ± 0.05
R_{Sat}	0.43 ± 0.06	0.45 ± 0.09	0.38 ± 0.05
R_{Sol}	0.72 ± 0.06	0.82 ± 0.09	0.55 ± 0.05
$\Delta G_L^{v\rightarrow d,o}$ / kJ mol^{-1}	0.47	0.58	0.30
$\Delta G_S^{v\rightarrow d,o}$ / kJ mol^{-1}	−0.85	−0.96	−0.65

Moreover, from the diglucoside amphiphile/DMPC ratios R_{Sat} and R_{Sol} the transfer free energies from vesicles (v) to discs (d) for lipid molecules, $\Delta G_L^{v\rightarrow d,o}$, and surfactants (i.e., amphiphiles), $\Delta G_S^{v\rightarrow d,o}$, could be calculated according to Equations 1–6 (Table 2). The ratio of these transfer energies can be used to

estimate the solubilization power of different solubilizing agents.[76] To this end, the values for diglucoside amphiphiles were plotted with those of comparable solubilizing agents, which are nanodisc-forming polymers and a fluorinated surfactant (Fig. 3.6). From this plot it becomes apparent that membrane solubilization by amphiphilic copolymers is characterized by low lipid transfer free energies, whereas for the fluorinated F_6OM this value is about 10-fold higher. Except for DIBMA, all amphiphiles plotted exhibited similar amphiphile/surfactant standard molar transfer free energies slightly below −1 kJ mol^{-1}. The values for the three diglucoside amphiphiles lie close together just below the empirical boundary $\Delta G_L^{v\rightarrow d,o} = -0.65\ \Delta G_S^{v\rightarrow d,o}$, separating weak and strong solubilizers.[76]

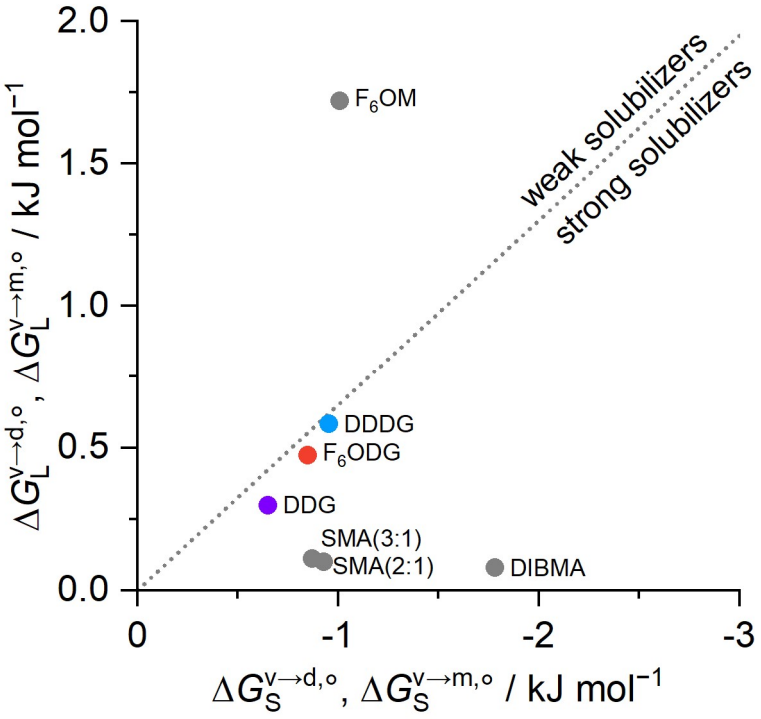

Figure 3.6. Thermodynamic classification of membrane-solubilizing amphiphiles. Free energies of vesicle-to-micelle (F_6OM) or vesicle-to-nanodisc (rest) transfer for lipid (L) and surfactant (S), $\Delta G_L^{v\rightarrow d,o}$ and $\Delta G_S^{v\rightarrow d,o}$, respectively. Data for the diglucoside amphiphiles can be found in Table 2. Data for F_6OM,[77] SMA(2:1),[78] SMA(3:1),[76] and DIBMA[51] are from the literature. The dotted line, separating weak and strong solubilizers is an empirically determined threshold defined by $\Delta G_L^{v\rightarrow d,o} = -0.65\ \Delta G_S^{v\rightarrow d,o}$.[76]

Chapter 4: Discussion

4.1. Novel Small-Molecule Glyco-Amphiphiles for Membrane-Protein Research

This work focused on the biophysical characterization of novel small-molecule glyco-amphiphiles, which make use of **different design principles to render them milder** compared with conventional detergents. To this end, the self-assembly as well as solubilization properties towards artificial membranes and natural membranes containing MPs were investigated. Moreover, extraction and stabilization of different model MPs were evaluated for selected novel amphiphiles.

The obtained results provide valuable information on the advantages and disadvantages of each amphiphile. For example, these are solubilization properties towards artificial and natural membranes and, most important, stabilization properties, which were probed for different model MPs.

4.2. Characterization of Micelle Self-Assembly

4.2.1. CMC values

Precise knowledge of the CMC under distinct experimental conditions is pivotal for selection and application of small-molecule amphiphiles in MP research. The QPSA presented in *Manuscript 1* proved to yield robust thermodynamic parameters and CMC values from demicellization isotherms in this manuscript, in *Manuscript 3*, and another recently published study.[79] Additionally, demicellization isotherms of several hitherto unpublished fluorinated amphiphiles were successfully analyzed. Moreover, the distribution as a stand-alone software with several practical and comfort features allows easy, automated, and reliable characterization of the mentioned parameters for scientists of different expertise levels. This is an improvement over earlier approaches as they needed to be set up in a spreadsheet software and, thus, required basic programming knowledge or the spreadsheet needed to be requested from the authors.[80,81]

As mentioned above, with the aid of the QPSA, *Manuscript 3* revealed that addition of polymerizable (meth)acrylamide groups decreases the hydrophobicity of the surfmers compared with the similar DDM. This was reflected by the increased CMCs of LC048 and LC058 and lower gains in free enthalpy upon micellization. However, for LC049, the additional substitution of the fourth carbon of the hydrophobic chain by an oxygen atom led to a much more pronounced decrease of hydrophobicity

and thus an about 30 times higher CMC and even lower gains in free enthalpy. Similar observations were made for classical maltosides and maltosides with either an additional oxygen atom or an amide bond in the alkyl chain.[33] Comparison of n-tridecyl-β-D-maltopyranoside (TDM) and a derivative with an oxygen atom substituting a CH_2 group revealed that the CMC of this derivate was 33 times higher than that of TDM, which is very close to the factor determined for LC048 and LC049. This leads to the conclusion that the chemical **nature of a modification can be much more important than its size**.

The investigation of branched amphiphiles in *Manuscript 2* revealed two distinct features influencing their CMC. First, the influence of different stereo confirmations was investigated and second, the influence of alkyl chain lengths could be investigated. The effect of the latter is well known for conventional head-and-tail amphiphiles. However, the decrease in CMC in dependence on hydrophobic chain length for detergents with two hydrophobic chains deviates from Traube's law as no common factor was found for different amphiphile series.[82–87] In fact, the group from which the CPMs were derived did not even show a constant factor within the homologous series.[84] For the presented CPMs, an additional CH_2 group in each alkyl chain decreased the CMCs by a factor of ~0.75, regardless of the *cis* and *trans* confirmation. This falls into the range of the factors observed for NBMs.

When comparing NBMs and CPMs, they exhibit the same trend of *trans* isomers having slightly lower CMC values than their *cis* isomers. Comparing the parent NBMs to the analog CPMs shows a difference between the two stereo isomers. When changing from the norbornane core to the cyclopentane core, by removing one restrictive C–C bond, almost no change of the CMC could be observed for CPM-*C*11. On the other hand, the CMC of CPM-*T*11 was lowered by factor of 0.8 compared with *X*-NBM-C11. Although the change in CMC is rather minor, it is surprising to find a difference between the *trans* isomers because density-functional theory calculations revealed very similar energy-optimized conformations for NBMs and CPMs in *trans* configuration. However, this shows that **stereochemistry influences self-aggregation** properties of branched amphiphiles just as it does for head-and-tail amphiphiles.[66,68,69] Moreover, it shows that the amphiphile stereochemistry can be tuned by relatively small changes like removal of a single C–C bond.

Fluorocarbon amphiphiles such as presented in *Manuscript 4* are well-known for their low perturbation towards MPs but also for their high hydrophobicity.[88,89]

Because of the low polarizability of fluorine in fluorocarbon compounds, they are **more hydrophobic than analog hydrocarbon compounds**. In particular, for highly fluorinated carbon chains, the contribution of one CF_2 group can be estimated to the contribution of 1.5 CH_2 groups.[90,91] This could be verified with several other fluorocarbon surfactants,[92] as well as with a series of diglucoside surfactants[93,94] which the fluorinated compound from *Manuscript 4* belongs to. Therefore, the CMC values of F_6ODG (C8) and DDG (C10) are similar despite their different chain lengths.

4.2.2. Micelle Architecture

Among all amphiphiles investigated, the biggest impact on micellar shape was found for CPM-*T*11. In detail, when the C–C bond of *X*-NBM-C11, which restricts the flexibility of the two maltose moieties, was removed in order to derive CPM-*T*11, d_H of the micelles decreased from 34.6 nm to 7.6 nm. This is readily explained by an altered molecular geometry. While *X*-NBM-C11 with its particularly restricted maltose moieties and two long alkyl chains possesses a cylindrical shape and most likely assembles into rod-like micelles,[84,95] CPM-*T*11 has more flexible maltose moieties, which led to a conical shape and subsequent to self-assembly into spherical micelles. A similar difference was observed for shorter chain *X*-NBM variants. Owed to the shorter alkyl chains, the molecular geometry was more conical; therefore, shorter NBM variants assembled into small, spherical micelles.[84] Similarly, the popular LMNG was also found to form large, rod-like micelles[96] whereas shorter chain analogs formed small, spherical micelles.[83]

On the contrary, removing the C–C bond of *D*-NBM-C11 in order to derive CPM-*C*11, showed almost no difference in micellar size. Considering the drastically different conformations revealed by density-function theory calculations, this was rather surprising. The *trans* isomers with their envelope conformation are similar to the conformation of NBM whereas the *cis* isomers adapted a half-chair conformation, which led to a twisted arrangement of its functional groups. However, this finding shows that drastic conformational changes not necessarily convey drastic changes to micellar aggregation but even **small modifications of amphiphile structure can lead to drastic changes** in their self-assembly.

Comparing the CPMs among each other, one can see that the CPM-*C*s form slightly smaller micelles than the CPM-*T*s with the same alkyl chain length. This trend is similar to what has been observed for the parental NBM series.[84] Finally, when

the alkyl chain length was increased from C11 to C12, the micellar diameter hardly changed compared with that of conventional detergents.[97]

The additions of methacrylamide and acrylamide to DDM that yielded the monomers LC048 and LC058 from *Manuscript 3*, led to a slight decrease in micellar diameter from 7.2 nm for DDM to ~6 nm for the monomers. This minor decrease in micelle diameter can be explained by a slightly more conical shape, which is caused by the presence of the rather hydrophilic (meth)acrylamide (cf., 4.2.1. CMC values). Since these groups were attached at the second carbon atom of the alkyl chain, these **additional hydrophilic groups can likely interact with water** molecules at the interface and consequently increase the required space for the headgroup. Contrarily, an increase in micellar size could be observed when short, hydrophobic hydrocarbon[98] or fluorocarbon[99] chains were added at similar positions of the alkyl chain.

It is of note that, although the substitution by an oxygen atom in the structure of LC049 had a major impact on the CMC, it had almost no influence on d_H of the micelle. Compared with LC048, the diameter decreased by 0.3 nm. Hence, it can be concluded that for additional groups located near the headgroup, the hydrophobicity plays a major role in how the micellar size is affected, this is, if it is decreased or increased. Moreover, the size of the group also determines how strong this influence is.

The micellar properties of the diglucoside amphiphiles presented in *Manuscript 4* were described in earlier publications, separately.[93,94,100] Note that F_6ODG was named F_6H_2-DigluM in the respective study. By combining the results for the hydrogenated and the fluorinated series, it becomes obvious that **fluorination of the hydrophobic chains leads to an increase in micellar d_H**. This observation is readily explained by the stiffer and bulkier nature of fluorocarbon chains compared with hydrocarbon chains, leading to a rather extended chain conformation.[31] This is a direct result of the peculiar properties that are conveyed by the fluorocarbon chain.

4.3. Investigation of Detergency

4.3.1. Solubilization of Artificial Membranes

Artificial lipid vesicles consisting of only one or a few lipid species represent a simple and easy-to-handle model system, not just for MP research but also for initial amphiphile characterization. To this end, the solubilization efficiency of

newly developed amphiphiles are often tested on artificial vesicles in order to extrapolate those results to MP extraction. However, this type of experiments relies on the assumption that—in the case of *Manuscripts 2–4*—one single lipid species, namely POPC, can mimic the most essential properties of a complex and heterogenous natural bilayer membrane. Thus, solubilization properties towards artificial membranes do not necessarily translate into similar properties towards natural bilayers and vice versa.

Most tested amphiphiles were shown to solubilize POPC vesicles at 25°C in a reasonable time (i.e., within 24 h). The most potent solubilizers were the monomers LC049 and LC058 from *Manuscript 3*. They required less than 30 min to completely solubilize the POPC vesicles. In contrast, the monomeric unit of NAPol, LC027, took ~4 h to achieve complete solubilization under the same conditions. The major differences between the structures of LC027 and the new monomers are, on the one hand, the branched arrangement of the two glucose moieties in the headgroup and, on the other hand, the length of the hydrophobic chain. The latter is owed to an additional linker group between the headgroup and the alkyl chain because of different synthetic routes. Thus, the molecular geometry between the maltose monomers and LC027 is different, which was shown to be a determining factor for the solubilization kinetics and mechanism.[101,102] An particularly crucial factor is **how fast amphiphiles can translocate** from the accessible outer leaflet of a vesicle into the inner leaflet of a vesicle.[103–105] This flipping is largely determined by the charge/polarity and size of the hydrophilic headgroup.[104,105] Hence, the slower solubilization of LC027 can be explained by the bulkier diglucose headgroup[106] compared with the maltose groups of LC049 and LC058. Moreover, considering the hydrogenated diglucoside amphiphiles related with *Manuscript 4*, the headgroup dependence is further emphasized. The two longer chained diglucosides both required 1.5 h for complete solubilization, while the shortest variant, octyl diglucoside (ODG), even required ~6 h.[94] The slow solubilization by ODG can possibly be explained by a low partitioning into the lipid bilayer related to its low hydrophobicity (cf., its CMC[94]).

The only studied amphiphiles that required heating to solubilize the POPC vesicles, are the fluorinated diglucoside amphiphiles related to *Manuscript 4*.[93] The necessity of heating to solubilize vesicles indicates insufficient translocation across the membrane at ambient temperatures.[107] This is related to (i) the relatively high lipophobicity of the fluorocarbon chains and (ii), again, to the bulky diglucose

headgroup. In contrast, fluorinated, maltose-bearing amphiphiles exhibited vesicle solubilization already at 25°C.[77,92] This also indicates, that a **branched diglucose headgroup conveys worse solubilization properties** towards POPC vesicles compared with a linear maltose headgroup. Within the fluorinated diglucoside series, POPC solubilization kinetics at 50°C were determined by the length of the fluorocarbon chain, resulting in slower solubilization for the longer and thus more lipophobic amphiphiles.[93] Overall, this demonstrates how crucial it is for fluorinated amphiphiles to find a balance between fluorination—rendering the amphiphile mild—and solubilization power.

Unfortunately, only selected branched amphiphiles were tested in certain experiments in *Manuscript 2*. Hence, solubilization properties of the commercially available *X*-NBM-C11 and the most promising CPM-*C*12 were tested, although they are not directly related. It was found that the straight and restricted *X*-NBM-C11 required 15–20 h for complete solubilization. On the contrary, the kinked and more flexible CPM-*C*12 completely solubilized the POPC vesicles within ~2 h, which is similar to the hydrogenated head-and-tail amphiphiles. This finding is particularly interesting as the headgroups of these branched amphiphiles is much larger compared with the tested head-and-tail amphiphiles. Overall, the large difference in solubilization kinetics between CPM-*C*12 and *X*-NBM-C11 emphasizes the **importance of seemingly minor changes**, such as stereochemistry and single restrictive bonds in the amphiphile structure.

4.3.2. Solubilization of Natural Membranes

When assessing the MP extraction efficiency of newly developed amphiphiles, there are basically two approaches. One is to study the extraction efficiency of one or more model MPs. The obtained results on the extraction of the individual model MPs can be extrapolated to MPs of interest, provided they have a similar structure. However, since this information is rather sparse on MPs in general, one should at least choose models from the same class of MPs. The other approach is to simply solubilize natural membranes and monitor the total MP extraction in a "shotgun" extraction experiment. Provided that the amphiphile is non-selective towards a wide range of MPs, the potential overall extraction can be estimated by such shotgun extractions. Such experiments were performed in *Manuscript 2* and *3*, as well as in the previous publications about the diglucoside amphiphiles.[93,94] However, it is of note that DDM exhibits a particularly high specificity for the outer membrane protein A (OmpA), which can be seen as a particularly strong band

around 35 kDa in SDS-PAGE. Moreover, one must keep in mind that extraction experiments are affected by two factors: (i) the initial extraction efficiency and (ii) the stabilizing ability of an amphiphile keeping the MPs soluble.

All tested amphiphiles showed distinct band patterns on the SDS-PAGE indicating the **extraction of different subsets of the *E. coli* membrane proteome**. Moreover, for some amphiphiles the concentration dependent total extraction showed individual differences as well. However, as expected, most amphiphiles revealed an increase in total extraction with increasing concentration. Together, this already emphasizes the importance of both MP-specific requirements and amphiphile-specific extraction properties. Interestingly, except for two fluorinated diglucoside amphiphiles, all novel amphiphiles outperformed the gold standard DDM at concentrations just 1 and 2 mM above the CMC. Such high extraction efficiencies at low amphiphile concentrations are particularly interesting for techniques such as electron microscopy because large amounts of, for example, empty micelles lower the quality of electron micrographs.[108,109]

To make the shotgun MP extraction results easier to compare to each other, the total extraction yield was calculated by summing up the extraction yields for all four tested concentrations and dividing it by the total extraction yield of DDM. These normalized total MP extractions are summarized in Table 3. For CPM-*C*12, this revealed a normalized total extraction yield of 1.77 relative to DDM. Surprisingly, its stereoisomer CPM-*T*12 performed substantially worse, extracting only half as much as CPM-*C*12. Considering the total extraction yield of *X*-NBM-C11, which was roughly the same as for DDM, the importance of stereo conformation becomes apparent again. The half-chair conformation of CPM-*C*12 leads most likely to superior MP extraction properties. The reasons for the superior extraction properties of the half-chair conformation are twofold. First, the alkyl chains are not arranged in parallel. The twisting of the cyclopentane ring places one chain in an axial position and the other in an equatorial position. This **asymmetric conformation results in greater packing defects** when the amphiphiles are incorporated in the membrane. Moreover, different effective hydrophobic lengths of these chains are adapted, which is beneficial for favorable interactions with MPs. Similar observations were made for asymmetric MNGs, for which certain MPs were substantially better stabilized by specific, asymmetric alkyl chain combinations.[110] Second, the twisting of the cyclopentane ring leads to a greater spatial separation of the two maltose moieties and thus to an effectively

larger headgroup. The latter, in turn, leads to a more conical shape and thus to better solubilization and extraction because a **greater membrane curvature stress is induced** when incorporating into the membrane.[111]

However, large differences in amphiphile molecular weights should be taken into account when comparing solubilization and extraction efficiencies on a molar concentration scale (e.g., comparison of pseudophase boundaries of diglucoside amphiphiles and SMA(2:1) in *Manuscript 4*). As the tested branched amphiphiles resemble the structure of two linked DDM molecules, the molecular weight is about twice that of DDM. Hence, the mass concentrations of the CPMs and *X*-NBM-C11 are ~2-fold higher than that of DDM. This means that, on a mass scale, CPM-*C*12 performs similarly to DDM.

Among the head-and-tail amphiphiles, DDG and DDDG slightly outperformed DDM in terms of total MP extraction. Again, this improved extraction can be explained by the **larger diglucose headgroup, leading to a more conical shape**. Considering the shorter ODG,[94] a more complex dependence becomes apparent. Overall, the total MP extraction of hydrocarbon diglucoside amphiphiles can be ranked DDG > DDDG > ODG. This suggests that DDG has the optimal hydrophobic chain length among these three amphiphiles. However, headgroups of different sizes can result in largely different optimal chain lengths for small-molecule glyco-amphiphiles.[112] Together, this suggests that there might be an optimal molecular geometry suitable for broad-range extraction of MPs from native membranes.

As expected, when substituting the hydrocarbon chain of diglucoside amphiphiles for fluorocarbon chains, the total MP extraction was substantially lower, owed to their peculiar lipophobicity.[22,31] However, the fluorinated diglucoside amphiphiles were among the first fluorinated amphiphiles that could extract MPs in reasonable amounts.[93] The role of the fluorocarbon chain is further emphasized as shorter fluorocarbon chains gave a better total extraction, which could be also observed for fluorinated maltosides.[92] Interestingly, the nanodisc formation described in *Manuscript 4* does not only render diglucoside amphiphiles particularly interesting membrane mimics for sensitive MPs, but also poses a potential reason for the good extraction properties of F_6ODG. This is discussed in detail below. However, particularly in the design of fluorinated amphiphiles, a **balance between extraction power and mildness must be found**.

Comparing the surfmer monomers from *Manuscript 3*, the novel monomers bearing maltose headgroups extract MPs in the same order of magnitude as DDM.

In particular, the normalized total MP extraction yields of LC049 and LC058 were about 75% of DDM. However, the good performance at MP extraction of DDM is by a large part a result of the extraordinarily efficient extraction of the very abundant OmpA. Interestingly, the addition of the polymerizable moieties led to a complete loss of this specificity although the headgroups and chain lengths were the same as for DDM. This suggests that the high specificity of DDM towards OmpA is based on interactions in the headgroup region of the amphiphile. Thus, this is a good example of the individual requirements for interactions between certain MPs and amphiphiles. Omitting these very prominent SDS-PAGE bands, the impact of the polymerizable moieties is less drastic. Compared to the novel surfmers, the LC027 showed similar concentration dependencies of the protein extraction. However, judging by the total MP extraction, LC027 was almost as efficient as DDM and thus, slightly outperformed the novel monomers. Although there is a slight difference in architecture regarding the linker group, the better performance of LC027 emphasizes the **positive effect of the large diglucose headgroup towards MP extraction**, which contrasts with its poor solubilization power.

In addition to the MP shotgun extraction experiments, the extraction power of the novel amphiphiles from *Manuscripts 2* and *3* was tested on either one or two challenging model MPs. In particular, the CPMs and their parental NBM molecules were applied to extract recombinantly produced and overexpressed $MelB_{St}$ from *E. coli* membranes. $MelB_{St}$ is an α-helical transporter for disaccharides.[113] Compared to DDM, most amphiphiles showed an extraction yield around 100%. However, *X*-NBM-C11 and CPM-*T*12 performed considerably worse and reached only a yield of ~50% and ~37%, respectively. While these results compare relatively well with the results for the respective amphiphiles in the shotgun extraction experiment, the good performance of CPM-*T*11 is surprising because of the poor performance of CPM-*T*12. A possible explanation is that CPM-*T*12 micelles are about 1 nm bigger in diameter compared with the other CPMs. Hence, the hydrophobic core of the CPM-*T*12 micelles might be unsuitable for the hydrophobic surface of the MP, therefore leading to a hydrophobic mismatch. Similarly, negative correlations between hydrophobic chain lengths and extraction were found for different head-and-tail amphiphiles.[112,114] Indirectly, this hints to the **favorable conformation of its counterpart CPM-*C*12**. Despite having the same nominal chain lengths, the half-chair conformation of the cyclopentane core leads to a shorter effective hydrophobic length. Paired with the thus effectively

asymmetric alkyl chains, this can provide easier adaption to the hydrophobic surface of different proteins.[110]

The surfmer monomers from *Manuscript 3* were tested on two MPs with α-helical transmembrane domains from two different classes, namely, the multidrug efflux transporter, AcrB,[115] and the GPCR adenosine A_{2A} receptor, A_{2A}R.[116] AcrB and A_{2A}R were recombinantly expressed in *E. coli* and insect cells (*Sf*9), respectively. In the case of AcrB extraction, LC049 and LC058 performed substantially worse than DDM extracting only ~40% of the available AcrB. Hence, similarly to OmpA in the shotgun extraction experiments, particular interactions might be diminished by the addition of the polymerizable moiety. Moreover, LC027, with its branched diglucose headgroup, performed even worse extracting only ~20% of the target protein. Considering the results from the *E. coli* extraction for LC027, it is likely that its poor extraction of AcrB was caused by missing MP/amphiphile interactions. Interestingly, in the case of A_{2A}R extraction from insect cells, all monomers performed similarly to a mixture of DDM and cholesteryl hemisuccinate (CHS), which has gained immense popularity in recent years.[64] Therefore, these amphiphiles and, later, their polymerized form, might be interesting candidates for GPCR research.

A_{2A}R recombinantly expressed in *Sf*9 cells was previously used to determine the extraction properties of hydrogenated diglucoside amphiphiles.[94] While ODG performed as good as DDM in the extraction, DDG and DDDG extracted more A_{2A}R therefore being potential valuable tools for GPCR research (cf., 4.4. Stabilization of Model Membrane Proteins). Although the origin of the membranes was different and only a single model MP was monitored, the dependence on the hydrophobic chain was the same as observed in shotgun extraction experiments: DDG extracted the largest amount of A_{2A}R, indicating an optimum in hydrophobic chain length. In addition, the extraction properties of the hydrogenated diglucoside amphiphiles were further tested with the bacterial ATP-binding cassette transporter, BmrA, recombinantly expressed in *E. coli*. In this case, the hydrogenated diglucoside amphiphiles performed overall similarly to DDM and showed the same hydrophobic chain length dependence as mentioned before.

Table 3: Summarized ranking for POPC vesicle solubilization kinetics and total *E. coli* membrane-protein extraction relative to DDM for novel small-molecule glyco-amphiphiles.

Amphiphile	Estimated solubilization time for POPC vesicles (h)	normalized total MP extraction
CPM-*C*12	2.2	1.77
CPM-*T*12	not tested	0.86
X-NBM-C11	17.0	1.07
F_6ODG	16.0*	0.76
DDG	2.0	1.25
DDDG	2.0	1.14
LC049	0.6	0.77
LC058	0.6	0.74
LC027	4.0	0.92

* measurement at 50°C

4.4. Stabilization of Model Membrane Proteins

After successfully extracting MPs from their biological environment, one key issue is the stability of the MP in the chosen amphiphile. To this extent, different approaches can be done. On the one hand, assessing the (thermal) stability of extracted MPs is broadly applicable to many proteins. It can be assessed, for example, by different spectroscopic techniques or altered migration behavior in SDS-PAGE or chromatographic methods. On the other hand, monitoring enzymatic activity or ligand binding are more protein specific. If the MP has enzymatic activity or binds a ligand, activity or binding measurements can be done to investigate whether the MP is disturbed in its function.

The stabilizing properties of the branched amphiphiles in *Manuscript 2* were tested with diverse model MPs. The stability of most of these MPs was assessed by ligand binding. This included the bacterial leucine transporter, LeuT, the disaccharide transporter $MelB_{St}$, and the human β_2 adrenergic receptor, β_2AR. In all cases, the novel branched amphiphiles showed similar preservation of the binding activity of the model MPs, which is indicative for structural preservation. The only exception was the poor stabilization of β_2AR by CPM-*T*12, which is coherent with its poor extraction power. In addition, the thermal stability of model MPs in CPMs were

tested for $MelB_{St}$ and for MOR, another GPCR. In the case of $MelB_{St}$, extraction at different temperatures suggested that, similarly to DDM and *X*-NBM-C11, CPM-*T*12 stabilized $MelB_{St}$ up to 45°C. On the contrary, the other three CPMs stabilized $MelB_{St}$ up to 55°C. Moreover, the stabilizing properties of these three CPMs were further tested with MOR and compared with DDM as well as LMNG, which is known for stabilizing GPCRs.[34] As expected, DDM was the worst amphiphile in stabilizing this delicate model MP. While CPM-*T*11 performed similarly to LMNG (less than 1°C difference in T_m), CPM-*C*11 and CPM-*C*12 increased the T_m of MOR by 2.6°C and 5.6°C compared with LMNG, respectively. In general, the **CPM amphiphiles are particularly good at stabilizing MPs**, like the prominent LMNG. Despite their structural difference, CPMs and LMNG can be viewed as a "dimer" of linked conventional head-and-tail detergents, similar to DDM. Recently, molecular dynamics simulations showed that single LMNG molecules exhibit much less motion in a micelle containing a MP, compared with DDM.[34] This is owed to the higher molecular mass of such a "dimer" but also to specific interactions between maltose moieties of different LMNG molecules leading to further restrictions in the individual molecular motion. The resulting **low mobility of the amphiphiles preserves native protein–protein and protein–lipid interactions**, thus explaining the superior stabilization properties of branched amphiphiles.

The stabilizing properties of nanodisc-forming diglucoside amphiphiles in *Manuscript 4* were assessed by enzymatic activity of OmpLA. Interestingly, the fluorocarbon nanodiscs preserved the activity of OmpLA dimers similar to what was observed in POPC vesicles, whereas the activity was lower in hydrocarbon nanodiscs. This suggests, that OmpLA was either affected in its integrity, in dimer formation, or that hydrogenated diglucoside monomers from the aqueous phase interact with the OmpLA dimer and inhibit its enzymatic activity. However, to unravel the reason for the lower activity, further experiments investigating the MP structure would be necessary. Together with the depression of the main gel-to-fluid phase transition in hydrocarbon nanodiscs containing DMPC, this emphasizes the **influence of the rim-forming agent on the integrity of the bilayer patch and harbored MPs**. Similar observations were made with another GPCR and different nanodisc-forming copolymers.[117] Here, certain types of polymer-bounded nanodiscs restricted the embedded GPCR in its conformational changes.

However, despite the rather poor stabilization of OmpLA by DDDG, it was shown that the shorter hydrocarbon diglucoside amphiphiles ODG and DDG were

promising candidates in stabilizing $A_{2A}R$.[94] Unfortunately, DDDG was excluded from this experiment because of experimental considerations. Hence, DDDG should not be considered a poor stabilizing agent, but the investigation of its applicability should be further extended.

4.5. Nanodisc-Forming Glyco-Amphiphiles

4.5.1. Hydrophobic Chain Length Influence on Nanodisc Architecture, Integrity, and Self-Assembly

From *Manuscript 4*, it can be concluded that the fluorinated F_6ODG is the milder nanodisc-forming diglucoside amphiphile compared with DDDG. However, in addition to the difference in chemical nature of the hydrophobic chains, the chain length differs by 4 carbon groups (C8 versus C12); therefore, it is unclear whether the **chemical modification or the different chain lengths are the main reason** for the preferable properties of F_6ODG. To clarify this question, experiments were repeated using the shorter C10 homolog from the hydrogenated diglucoside series, DDG[94] (3.7. Associated Results).

While DDG formed nanodiscs of similar architecture as DDDG when mixed with artificial vesicles (Fig. 3.1), the influence on the integrity of the DMPC bilayer core was slightly milder than for DDDG. In particular, laurdan fluorescence spectroscopy and DSC measurements revealed DMPC main gel-to-fluid phase transitions at slightly higher T_m values (Fig. 3.2), indicating a slightly higher integrity of the bilayer core. However, when comparing T_m for nanodiscs formed by DDG or DDDG, these values were similarly decreased compared with DMPC vesicles.

Moreover, lipid exchange, studied by time-resolved FRET, revealed observed lipid exchange rates (k_{obs}) for DDG similar to those of DDDG, thus suggesting a similar exchange behavior (Fig. 3.3B). In particular, when accounting for the contribution of diffusional exchange, the slightly lower value for DDG nanodiscs (Table 1) corroborates the slightly higher bilayer integrity as observed in terms of smaller changes in T_m. However, the value for F_6ODG nanodiscs was still about 1 order of magnitude smaller, confirming superior stabilization properties of the fluorocarbon chain. Furthermore, the shorter C10 hydrophobic chain of DDG led to an increase in collisional lipid exchange compared with DDDG and its C12 hydrophobic chain (Table 1). This faster exchange is caused by an **easier crossing of the nanodisc rim region** most likely owed to the shorter and thus, more flexible C10 hydrocarbon chain. This is contrary to the lower values observed for F_6ODG,

containing the shorter, polyfluorinated C8 chain. Therefore, it can be excluded that the preferable properties of F_6ODG nanodiscs come from the shorter hydrophobic chain but are **exclusively conveyed by the fluorocarbon chain**.

The self-assembly process of DDG nanodiscs was similar to that of the other diglucoside amphiphiles, as judged by ITC solubilization experiments. Titration with DDG gave the same overall shape of the isotherm with initially endothermic titration heats followed by a W-shaped exotherm titration range (Fig. 3.5A). This suggests that the sequential self-assembly model, established in *Manuscript 4*, also applies for DDG-mediated nanodisc formation. While the characteristic features were found for all three diglucoside amphiphiles, DDG showed signs of aggregation that were similar to what was observed for DDDG. This included shifts in the heating power baseline and signal noise for the resulting titration heats.

Another difference between the self-assembly of the hydrogenated nanodiscs and F_6ODG nanodiscs was seen for the bilayer perforation. Contrary to the well-defined perforation threshold concentration that was found for F_6ODG/DMPC mixtures, the perforation for hydrogenated diglucoside/DMPC mixtures turned out to be more gradual (Fig. 3.4). This was reflected in intermediate characteristic bleaching times that could be calculated. One possible explanation for this gradual behavior is a higher perturbation of the vesicular bilayer induced by the incorporation of hydrogenated diglucoside monomers prior pore formation. While the lipophobic F_6ODG monomers most likely form clusters within the bilayer in order to **minimize the fluorocarbon–hydrocarbon interfacial area**, the hydrogenated diglucoside monomers can readily disperse in the vesicular bilayer.[118] Hence, hydrogenated diglucosides potentially induce many small membrane defects before forming pores in the bilayer and consequently already facilitate the hydrosulfite permeation.

4.5.2. Thermodynamic Considerations for Nanodisc Formation

From the slopes of the determined pseudophase diagrams for diglucoside/DMPC mixtures at 35°C from *Manuscript 4* and the associated results (Fig. 3.5B), free energies for the transfer from the vesicle to the nanodisc for the diglucoside amphiphile $\Delta G_S^{v\rightarrow d,o}$ and for DMPC $\Delta G_L^{v\rightarrow d,o}$ were calculated (Eq. 1–6). These values offer an **estimate for the underlying thermodynamics**, although, strictly speaking, the formed nanodiscs are no pseudophases because of the segregation between lipid and diglucoside amphiphile.[76] An analysis of such transfer free energies for head-and-tail amphiphiles, bile salts, and novel amphiphiles led to the

empiric relationship of $\Delta G_L^{v\rightarrow d,o} < -0.65\ \Delta G_S^{v\rightarrow d,o}$ for strong solubilizing agents, which do not include any head-and-tail amphiphiles.[76] According to this definition, the diglucoside amphiphiles are classified as strong DMPC-solubilizing agents under the respective conditions, including the fluorinated diglucoside amphiphile. Considering its lipophobic character, the classification as strong solubilizing agent might seem surprising, but the segregation and resulting **bilayer-core formation thermodynamically facilitate the lipid transfer** from the vesicle to the nanodisc (i.e., solubilization). The presence of the bilayer core in the nanodisc provides a membrane-like environment, which leads to much lower endergonic $\Delta G_L^{v\rightarrow d,o}$ values compared with formation of mixed micelles with fluorinated amphiphiles such as F_6OM (Fig. 3.6). In short, this illustrates that the great solubilization power is due to the accommodation of diglucoside amphiphiles in the nanodisc rim and the accommodation of lipid in the bilayer core, which only slightly opposes the solubilization process.

4.6. Structure–Efficacy Relationships

As mentioned in the beginning, finding a relationship between the structure of small-molecule (glyco-)amphiphiles is desirable because their properties could thus be predicted. Although, some tendencies are known, such as the dependence of the CMC on the chain length within a homologous series,[24] a quantitative prediction of amphiphile properties remains highly challenging. For example, mathematical models relating different molecular descriptors with certain properties have been developed to predict the CMC[119,120] and other physicochemical properties.[121] Although these physicochemical properties, of course, dictate the interaction with lipid bilayers, the precise relation remains elusive. Therefore, simple guidelines or trends for structure–efficacy relationships for the properties discussed above are extracted.

4.6.1. Headgroup diameter

An increase of the headgroup diameter generally **hampered the lipid solubilization** kinetics as could be seen for diglucoside (*Manuscript 4*) and CPM (*Manuscript 2*) amphiphiles (cf., Table 3). The underlying mechanism is most likely the slow translocation between the outer and the inner leaflet of the lipid bilayer. However, this does not translate to MP extraction. Indeed, the **MP extraction efficiency was higher** compared with DDM as estimated by *E. coli* MP extraction for the hydrogenated diglucosides and CPMs (cf., Table 3). Similar observations

were made for other nonionic small-molecule amphiphiles.[122] Fluorinated diglucoside amphiphiles extracted MPs to a lower extent compared with DDM but compared with other fluorinated amphiphiles,[22,31] they exhibited a great extraction potential.

4.6.2. Branching and Fluorination—Increasing Rigidity

As mentioned before, branching (*Manuscript 2*) or fluorination (*Manuscript 4*) of the hydrophobic part of the amphiphile is already **considered to be beneficial for MP stability**.[34,96,123–125] This is generally attributed to the low mobility of these hydrophobic groups resulting in a **rather rigid hydrophobic environment** for the MP. In general, the use of branched amphiphiles might be more favorable over the use of fluorinated amphiphiles because their extraction yield is generally higher and the solubilization kinetics are less affected. Nonetheless, the nanodiscs that can be provided by the fluorinated F_6ODG present and interesting option for certain proteins and experiments.

4.6.3. Asymmetric Hydrophobic Chain Lengths

Regarding the branched CPMs, the results from *Manuscript 2* indicate that **asymmetric effective hydrophobic chain lengths** of certain stereo conformers are beneficial for the stabilization of MPs. This is most likely due to a **better adaption of the amphiphile** to the uneven hydrophobic surface of the MP. Similar observations were made for branched glyco-amphiphiles containing two hydrophobic chains with different nominal chain lengths.[110]

Chapter 5: Conclusions

5.1. Summary

Novel small-molecule glyco-amphiphiles designed on the basis different principles were investigated and characterized in terms of (i) their self-assembly into micelles as well as (ii) interactions with lipid bilayers and MPs. On the one hand, this led directly to the identification of new promising amphiphiles, which can be applied in MP research. On the other hand, important conclusions about structure–efficacy relationships could be drawn that will aid the design of next-generation amphiphiles.

Diastereomeric cyclopentane-based maltosides were investigated. They contain a CP core group onto which two maltose groups as hydrophilic moiety and two alkyl chains as hydrophobic moiety were grafted (*Manuscript 2*).

- The *cis* and *trans* stereoisomers exhibit different conformations of the CP core and thus have different arrangements of the two maltose groups as well as of the hydrophobic chains. This results in different physicochemical and biophysical properties between the stereoisomers.
- Overall, CPMs exhibit good stabilizing properties towards various model MPs. This is most likely rooted in the presence of two hydrocarbon chains as hydrophobic moiety, which form relatively rigid micelles around the MPs, comparable to other branched amphiphiles.[34] Additionally, the *cis* stereoisomers turned out to be more stabilizing, which can most likely be attributed to the half-chair conformation of the CP core. This conformation leads to uneven effective hydrophobic chain lengths that are beneficial for adapting the hydrophobic chains to the uneven hydrophobic surface of the MP, inside the amphiphile/MP complex.[110]
- CPM-*C*12 could be identified as a particularly interesting amphiphile for GPCR studies, as it exhibits superior stabilization properties towards this class of MPs. It increased the thermal stability of a GPCR by several degree Celsius compared with the prominent LMNG, DDM, and other CPMs.
- Moreover, CPM-*C*12 exhibits great extraction properties as it extracts large amounts of MPs from natural *E. coli* membranes. In doing so, it is more efficient than DDM, which is up to now still the gold standard in MP purification,[64] and the related *X*-NBM-C11. Hence, CPM-*C*12 can be used to

extract the target MP and to stabilize it during purification and subsequent analysis, avoiding a tedious exchange of amphiphiles.

- Among the tested novel amphiphiles in this thesis, CPM-*C*12 showed mediocre solubilization kinetics for artificial POPC vesicles. The slower solubilization, compared with novel amphiphiles containing only one hydrocarbon chain, can be attributed to the relatively large size of the branched amphiphile. However, even if this translates to MP extraction and prolongs the necessary incubation time for MP extraction, CPM-*C*12's stabilization properties outweigh the slightly longer incubation times.

Furthermore, detergent-like polymerizable amphiphiles that resemble the structure of DDM were investigated. To make these amphiphiles polymerizable, a reactive acrylamide or a methacrylamide group was added to enable polymerization (*Manuscript 3*).

- Minor chemical modifications have a low impact on the micellar diameter but, depending on the hydrophobicity, can greatly affect the CMC. While the micellar diameter was slightly reduced irrespective of the polymerizable group type, the CMCs clearly differed from each other depending on the attached polymerizable group. This points out, that the additional methyl group in methacrylamide has neglectable influence on the overall shape of the amphiphile, yet its contribution to hydrophobicity impacts the overall hydrophobicity and consequently the CMC of the amphiphile. Furthermore, similar behavior could be seen for the substitution of a CH_2 group by an oxygen atom. While this substitution did not alter the shape of the amphiphile and thus resulted in similar micellar diameters, the CMC was drastically increased due to the high hydrophilicity of such ether bonds.
- The tested two novel surfmers exhibited a rather quick solubilization of artificial POPC vesicles, compared with the other novel amphiphiles from this thesis. This can probably be attributed to the smaller headgroup diameter of the linear arrangement in the maltose headgroup, compared with the branched arrangements of the other novel amphiphiles.
- The extraction efficiency of the two novel surfmers was rather good in terms of total extraction of the membrane proteome from *E. coli* as well as in the extraction of two model MPs. It is noteworthy, that the additional polymerizable groups have considerable impact on extraction yields of

distinct MPs. For example, the high OmpA extraction specificity of DDM is completely abolished by the addition of these groups.

The self-assembly of diglucoside nanodiscs from both, artificial membranes and biological membranes was investigated (*Manuscript 4*). To this end, two hydrogenated diglucosides and one fluorinated diglucoside were used.

- All three tested diglucosides self-assemble into nanodiscs when mixed with lipid bilayers. F_6ODG readily forms nanodiscs with both artificial vesicles and natural cell membranes. However, DDG and DDDG could not be shown to form nanodiscs with natural membranes, but only with artificial vesicles.
- The impact of the diglucosides on physicochemical properties of the lipid core within formed nanodisc is low. F_6ODG turned out to be the gentlest diglucoside, which can be attributed to its fluorinated, lipophobic chain. This is beneficial for MPs that are located inside such a nanodisc, as for example, OmpLA. The enzymatic activity of OmpLA was unaffected by transfer from vesicles into fluorinated nanodiscs, whereas the transfer into hydrogenated nanodiscs lowered the activity.
- Diglucoside nanodiscs are dynamic nano assemblies that exchange lipids by monomer diffusion and nanodisc collisions. While the exchanges among DDG and DDDG nanodiscs are rather similar to each other, the lipid exchange among fluorinated nanodiscs is considerably slower. This can be explained by the lipophobicity of the fluorinated hydrophobic chains forming the nanodisc rim, which hampers the transfer of lipids across this part of the nanodisc.
- Based on pseudophase diagrams, a model for diglucoside nanodisc self-assembly was proposed in which the DMPC bilayer is perforated at sub-solubilizing concentrations. With increasing diglucoside concentrations the bilayer is then becoming saturated and starts to disintegrate into nanodiscs until complete solubilization is reached.
- From a thermodynamic viewpoint, the diglucosides can be classified as strong solubilizers towards DMPC bilayers, like other nanodisc-forming amphiphiles. The main reason for this is the low transfer free energy of lipids in this self-assembly process, probably owed to the presence of the bilayer core.

5.2. Future Directions

As the small-molecule glyco-amphiphiles covered in this thesis all follow different rationales and originated from collaborations with different partners, each one offers individual future directions.

Regarding the branched CPMs from *Manuscript 2*, the group of Prof. Dr. Pil Seok Chae already synthesized a set of amphiphiles similar to the CPMs but in which the connecting cyclopentane carbon is removed. Thus, the **maltose branches are even more flexible** allowing to further explore the effect of different degrees of restriction in headgroups for branched glyco-amphiphiles. Their properties in MP handling are currently under investigation. Certainly, the observations made for the beneficial asymmetric effective hydrophobic chain lengths should be further explored and considered when designing new branched amphiphiles.

As mentioned above, the new surfmers introduced in *Manuscript 3* are planned to be used in (i) their detergent-like monomeric form as solubilizing agent and (ii) in their polymerized form as stabilizing agent. Thus, **MP/monomer/polymer complexes should be formed**, from which the monomer can subsequently be depleted by dilution well below the CMC of the monomer, resulting in a stabilizing MP/polymer complex. Currently, the group of Prof. Dr. Grégory Durand is working on the best polymerization conditions. Once these conditions are found, biochemical investigations using MPs can be performed and, eventually, the design of the monomers can be further improved.

With the comprehensive characterization of the new diglucoside nanodiscs from *Manuscript 4* and their properties at hand, application towards different membrane compositions, additional model organisms, and individual MPs can be tackled. Currently, the group of Prof. Dr. Sandro Keller is investigating the solubilization properties of **diglucoside amphiphiles towards different negatively charged artificial membranes**. Solubilization of negatively charged membranes would set diglucoside amphiphiles apart from prominent negatively charged copolymers, such as SMA and DIBMA, as Coulombic repulsion is irrelevant to the non-ionic diglucoside amphiphiles.

Overall, small-molecule glyco-amphiphiles accomplished a great success, which is evident from their use in MP structure determination over the last decade.[64] In particular, branched glyco-amphiphiles, which combine good extraction efficiency and MP stabilization, are potentially becoming the new gold standard of MP research. However, **many more types of glyco-amphiphiles are designed** and

synthesized, which for example, bear even more than two hydrophobic chains[126,127] or have restricted, cyclic hydrophobic groups.[128–130] Moreover, an increasing number of amphiphiles is being synthesized combining several approaches in their structure.[131,132]

References

Note that this list does not include references that appear within the manuscripts.

[1] W. Mäntele, *Biophysik*, UTB GmbH, Stuttgart **2012**.

[2] C. Tanford, *Science* **1978**, Vol. 200, 1012–1018.

[3] G. Adam, P. Läuger, G. Stark, *Physikalische Chemie und Biophysik,* Springer Berlin Heidelberg, Berlin, Heidelberg **2009**.

[4] A. Shevchenko, K. Simons, *Nat. Rev. Mol. Cell Biol.* **2010**, Vol. 11, 593–598.

[5] H. Watson, *Essays Biochem.* **2015**, Vol. 59, 43–69.

[6] B. Alberts, *Molecular biology of the cell*, Garland Science, New York **2002**.

[7] R. Santos, O. Ursu, A. Gaulton, A. P. Bento, R. S. Donadi, C. G. Bologa, A. Karlsson, B. Al-Lazikani, A. Hersey, T. I. Oprea, J. P. Overington, *Nat. Rev. Drug Discov.* **2017**, Vol. 16, 19–34.

[8] M. Uhlén, L. Fagerberg, B. M. Hallström, C. Lindskog, P. Oksvold, A. Mardinoglu, Å. Sivertsson, C. Kampf, E. Sjöstedt, A. Asplund, I. Olsson, K. Edlund, E. Lundberg, S. Navani, C. A.-K. Szigyarto, J. Odeberg, D. Djureinovic, J. O. Takanen, S. Hober, T. Alm, P.-H. Edqvist, H. Berling, H. Tegel, J. Mulder, J. Rockberg, P. Nilsson, J. M. Schwenk, M. Hamsten, K. von Feilitzen, M. Forsberg, L. Persson, F. Johansson, M. Zwahlen, G. von Heijne, J. Nielsen, F. Pontén, *Science* **2015**, Vol. 347, 1260419.

[9] V. Pomerleau, E. Harvey-Girard, F. Boucher, *Biochim. Biophys. Acta Biomembr.* **1995**, Vol. 1234, 221–224.

[10] C. Hunte, S. Richers, *Curr. Opin. Struct. Biol.* **2008**, Vol. 18, 406–411.

[11] K. Renard, B. Byrne, *Int. J. Mol. Sci.* **2021**, Vol. 22.

[12] A. Arkhipov, Y. Shan, R. Das, N. F. Endres, M. P. Eastwood, D. E. Wemmer, J. Kuriyan, D. E. Shaw, *Cell* **2013**, Vol. 152, 557–569.

[13] K. Gupta, J. A. C. Donlan, J. T. S. Hopper, P. Uzdavinys, M. Landreh, W. B. Struwe, D. Drew, A. J. Baldwin, P. J. Stansfeld, C. V. Robinson, *Nature* **2017**, Vol. 541, 421–424.

[14] Y. Norimatsu, K. Hasegawa, N. Shimizu, C. Toyoshima, *Nature* **2017**, Vol. 545, 193–198.

[15] I. Liko, M. T. Degiacomi, S. Lee, T. D. Newport, J. Gault, E. Reading, J. T. S. Hopper, N. G. Housden, P. White, M. Colledge, A. Sula, B. A. Wallace, C. Kleanthous, P. J. Stansfeld, H. Bayley, J. L. P. Benesch, T. M. Allison, C. V. Robinson, *Proc. Natl. Acad. Sci. U.S.A.* **2018**, Vol. 115, 6691–6696.

[16] Y. Gohon, T. Dahmane, R. W. H. Ruigrok, P. Schuck, D. Charvolin, F. Rappaport, P. Timmins, D. M. Engelman, C. Tribet, J.-L. Popot, C. Ebel, *Biophys. J.* **2008**, Vol. 94, 3523–3537.

[17] M. Le Maire, P. Champeil, J. V. Møller, *Biochim. Biophys. Acta Biomembr.* **2000**, Vol. 1508, 86–111.

[18] T. Nakae, *Biochem. Biophys. Res. Commun.* **1976**, Vol. 71, 877–884.

[19] T. J. Knowles, R. Finka, C. Smith, Y.-P. Lin, T. Dafforn, M. Overduin, *J. Am. Chem. Soc.* **2009**, Vol. 131, 7484–7485.

[20] T. H. Bayburt, Y. V. Grinkova, S. G. Sligar, *Nano Lett.* **2002**, Vol. 2, 853–856.

[21] U. H. N. Dürr, M. Gildenberg, A. Ramamoorthy, *Chem. Rev.* **2012**, Vol. 112, 6054–6074.

[22] J.-L. Popot, *Membrane Proteins in Aqueous Solutions,* Springer International Publishing, Cham **2018**.

[23] D. Lichtenberg, H. Ahyayauch, A. Alonso, F. M. Goñi, *Trends Biochem. Sci.* **2013**, Vol. 38, 85–93.

[24] J. Traube, *Liebigs Ann.***1891**, Vol. 265, 27–55.

[25] D. P. Tieleman, D. van der Spoel, H. J. C. Berendsen, *J. Phys. Chem. B* **2000**, Vol. 104, 6380–6388.

[26] W. Al-Soufi, M. Novo, *Molecules* **2021**, Vol. 26.

[27] R. M. Garavito, S. Ferguson-Miller, *J. Biol. Chem.* **2001**, Vol. 276, 32403–32406.

[28] S. Bogusz, R. M. Venable, R. W. Pastor, *J. Phys. Chem. B* **2000**, Vol. 104, 5462–5470.

[29] J. Deisenhofer, H. Michel, *EMBO J.* **1989**, Vol. 8, 2149–2170.

[30] O. Vinogradova, F. Sönnichsen, C. R. Sanders, *J. Biomol. NMR* **1998**, Vol. 11, 381–386.

[31] G. Durand, M. Abla, C. Ebel, C. Breyton, “New Amphiphiles to Handle Membrane Proteins: “Ménage à Trois” Between Chemistry, Physical Chemistry, and Biochemistry”, in: Mus-Veteau, I., ed., *Membrane Proteins Production for Structural Analysis,* Springer, New York, NY, pp. 205–251 **2014**.

[32] J.-L. Popot, *Annu. Rev. Biochem.* **2010**, Vol. 79, 737–775.

[33] P. S. Chae, S. G. F. Rasmussen, R. R. Rana, K. Gotfryd, R. Chandra, M. A. Goren, A. C. Kruse, S. Nurva, C. J. Loland, Y. Pierre, D. Drew, J.-L. Popot, D. Picot, B. G. Fox, L. Guan, U. Gether, B. Byrne, B. Kobilka, S. H. Gellman, *Nat. Methods* **2010**, Vol. 7, 1003–1008.

[34] S. Lee, S. Ghosh, S. Jana, N. Robertson, C. G. Tate, N. Vaidehi, *Biochemistry* **2020**, Vol. 59, 2125–2134.

[35] T. Althoff, D. J. Mills, J.-L. Popot, W. Kühlbrandt, *EMBO J.* **2011**, Vol. 30, 4652–4664.

[36] C. Tribet, R. Audebert, J.-L. Popot, *Proc. Natl. Acad. Sci. U.S.A.* **1996**, Vol. 93, 15047–15050.

[37] K. S. Sharma, G. Durand, F. Gabel, P. Bazzacco, C. Le Bon, E. Billon-Denis, L. J. Catoire, J.-L. Popot, C. Ebel, B. Pucci, *Langmuir* **2012**, Vol. 28, 4625–4639.

[38] Y. Gohon, F. Giusti, C. Prata, D. Charvolin, P. Timmins, C. Ebel, C. Tribet, J.-L. Popot, *Langmuir* **2006**, Vol. 22, 1281–1290.

[39] M. Picard, T. Dahmane, M. Garrigos, C. Gauron, F. Giusti, M. Le Maire, J.-L. Popot, P. Champeil, *Biochemistry* **2006**, Vol. 45, 1861–1869.

[40] P. Champeil, T. Menguy, C. Tribet, J.-L. Popot, M. Le Maire, *J. Biol. Chem.* **2000**, Vol. 275, 18623–18637.

[41] M. Zoonens, F. Zito, K. L. Martinez, J.-L. Popot, "Amphipols: A General Introduction and Some Protocols", in: Mus-Veteau, I., ed., *Membrane Proteins Production for Structural Analysis,* Springer, New York, NY, pp. 173–203 **2014**.

[42] D. P. Tieleman, M. S. Sansom, H. J. Berendsen, *Biophys. J.* **1999**, Vol. 76, 40–49.

[43] C. Sohlenkamp, O. Geiger, *FEMS Microbiol. Rev.* **2016**, Vol. 40, 133–159.

[44] J. Klingler, C. Vargas, S. Fiedler, S. Keller, *Anal. Biochem.* **2015**, Vol. 477, 10–12.

[45] B. J. Frisken, C. Asman, P. J. Patty, *Langmuir* **2000**, Vol. 16, 928–933.

[46] D. J. Paterson, J. Reboud, R. Wilson, M. Tassieri, J. M. Cooper, *Lab Chip* **2014**, Vol. 14, 1806–1810.

[47] K. Karamdad, R. V. Law, J. M. Seddon, N. J. Brooks, O. Ces, *Lab Chip* **2015**, Vol. 15, 557–562.

[48] E. A. Morrison, K. A. Henzler-Wildman, *Biochim. Biophys. Acta* **2012**, Vol. 1818, 814–820.

[49] T. Raschle, S. Hiller, M. Etzkorn, G. Wagner, *Curr. Opin. Struct. Biol.* **2010**, Vol. 20, 471–479.

[50] F. Hagn, M. L. Nasr, G. Wagner, *Nat. Protoc.* **2018**, Vol. 13, 79–98.

[51] A. O. Oluwole, B. Danielczak, A. Meister, J. O. Babalola, C. Vargas, S. Keller, *Angew. Chem. Int. Ed.* **2017**, Vol. 56, 1919–1924.

[52] K. M. Burridge, B. D. Harding, I. D. Sahu, M. M. Kearns, R. B. Stowe, M. T. Dolan, R. E. Edelmann, C. Dabney-Smith, R. C. Page, D. Konkolewicz, G. A. Lorigan, *Biomacromolecules* **2020**, Vol. 21, 1274–1284.

[53] I. G. Denisov, Y. V. Grinkova, A. A. Lazarides, S. G. Sligar, *J. Am. Chem. Soc.* **2004**, Vol. 126, 3477–3487.

[54] G. G. Privé, *Methods* **2007**, Vol. 41, 388–397.

[55] A. J. Y. Jones, F. Gabriel, A. Tandale, D. Nietlispach, *Molecules* **2020**, Vol. 25.

[56] A. K. Bhuyan, *Biopolymers* **2010**, Vol. 93, 186–199.

[57] A. L. Shapiro, E. Viñuela, J. V. Maizel, *Biochem. Biophys. Res. Commun.* **1967**, Vol. 28, 815–820.

[58] J. Lauterwein, C. Bösch, L. R. Brown, K. Wüthrich, *Biochim. Biophys. Acta Biomembr.* **1979**, Vol. 556, 244–264.

[59] S. Scheidelaar, M. C. Koorengevel, C. A. van Walree, J. J. Dominguez, J. M. Dörr, J. A. Killian, *Biophys. J.* **2016**, Vol. 111, 1974–1986.

[60] A. Rahman, C. W. Brown, *J. Appl. Polym. Sci.* **1983**, Vol. 28, 1331–1334.

[61] M. L. Corrin, W. D. Harkins, *J. Am. Chem. Soc.* **1947**, Vol. 69, 683–688.

[62] B. Lukanov, A. Firoozabadi, *Langmuir* **2014**, Vol. 30, 6373–6383.

[63] A. H. Kopf, J. M. Dörr, M. C. Koorengevel, F. Antoniciello, H. Jahn, J. A. Killian, *Biochim. Biophys. Acta Biomembr.* **2020**, Vol. 1862, 183125.

[64] B. C. Choy, R. J. Cater, F. Mancia, E. E. Pryor, *Biochim. Biophys. Acta Biomembr.* **2021**, Vol. 1863, 183533.

[65] F. Lebaupain, A. G. Salvay, B. Olivier, G. Durand, A.-S. Fabiano, N. Michel, J.-L. Popot, C. Ebel, C. Breyton, B. Pucci, *Langmuir* **2006**, Vol. 22, 8881–8890.

[66] C. Pagliano, S. Barera, F. Chimirri, G. Saracco, J. Barber, *Biochim. Biophys. Acta* **2012**, Vol. 1817, 1506–1515.

[67] F. Caussanel, C. Andre-Barrès, S. Lesieur, I. Rico-Lattes, *Colloids Surf. B* **2001**, Vol. 22, 193–203.

[68] J. M. Hutchison, Z. Lu, G. C. Li, B. Travis, R. Mittal, C. L. Deatherage, C. R. Sanders, *Biochemistry* **2017**, Vol. 56, 5481–5484.

[69] S. Abel, F.-Y. Dupradeau, E. P. Raman, A. D. MacKerell, M. Marchi, *J. Phys. Chem. B* **2011**, Vol. 115, 487–499.

[70] T. Vanaken, S. Foxall-Vanaken, S. Castleman, S. Ferguson-Miller, “Alkyl glycoside detergents: Synthesis and applications to the study of membrane proteins”, in: *Biomembranes Part M,* Academic Press, Amsterdam, pp. 27–35 **1986**.

[71] S. Keller, C. Vargas, H. Zhao, G. Piszczek, C. A. Brautigam, P. Schuck, *Anal. Chem.* **2012**, Vol. 84, 5066–5073.

[72] R. Cuevas Arenas, B. Danielczak, A. Martel, L. Porcar, C. Breyton, C. Ebel, S. Keller, *Sci. Rep.* **2017**, Vol. 7, 45875.

[73] A. Grethen, D. Glueck, S. Keller, *J. Membr. Biol.* **2018**, Vol. 251, 443–451.

[74] M. Nakano, M. Fukuda, T. Kudo, M. Miyazaki, Y. Wada, N. Matsuzaki, H. Endo, T. Handa, *J. Am. Chem. Soc.* **2009**, Vol. 131, 8308–8312.

[75] M. Nakano, M. Fukuda, T. Kudo, H. Endo, T. Handa, *Phys. Rev. B* **2007**, Vol. 98, 238101.

[76] C. Vargas, R. C. Arenas, E. Frotscher, S. Keller, *Nanoscale* **2015**, Vol. 7, 20685–20696.

[77] E. Frotscher, B. Danielczak, C. Vargas, A. Meister, G. Durand, S. Keller, *Angew. Chem. Int. Ed.* **2015**, Vol. 54, 5069–5073.

[78] A. Grethen, A. O. Oluwole, B. Danielczak, C. Vargas, S. Keller, *Sci. Rep.* **2017**, Vol. 7, 11517.

[79] E. Grousson, F. Mahler, S. Keller, C. Contino-Pépin, G. Durand, *J. Org. Chem.* **2021**, Vol. 86, 14672–14683.

[80] J. Broecker, S. Keller, *Langmuir* **2013**, Vol. 29, 8502–8510.

[81] M. Textor, S. Keller, *Anal. Biochem.* **2015**, Vol. 485, 119–121.

[82] K. H. Cho, H. E. Bae, M. Das, S. H. Gellman, P. S. Chae, *Chem. Asian J.* **2014**, Vol. 9, 632–638.

[83] K. H. Cho, M. Husri, A. Amin, K. Gotfryd, H. J. Lee, J. Go, J. W. Kim, C. J. Loland, L. Guan, B. Byrne, P. S. Chae, *Analyst* **2015**, Vol. 140, 3157–3163.

[84] M. Das, Y. Du, O. Ribeiro, P. Hariharan, J. S. Mortensen, D. Patra, G. Skiniotis, C. J. Loland, L. Guan, B. K. Kobilka, B. Byrne, P. S. Chae, *J. Am. Chem. Soc.* **2017**, Vol. 139, 3072–3081.

[85] K. H. Cho, Y. Du, N. J. Scull, P. Hariharan, K. Gotfryd, C. J. Loland, L. Guan, B. Byrne, B. K. Kobilka, P. S. Chae, *Chem. Eur. J.* **2015**, Vol. 21, 10008–10013.

[86] M. Ehsan, H. Wang, C. Cecchetti, J. S. Mortensen, Y. Du, P. Hariharan, A. Nygaard, H. J. Lee, L. Ghani, L. Guan, C. J. Loland, B. Byrne, B. K. Kobilka, P. S. Chae, *ACS Chem. Biol.* **2021**, Vol. 16, 9, 1779–1790.

[87] M. Ehsan, Y. Du, N. J. Scull, E. Tikhonova, J. Tarrasch, J. S. Mortensen, C. J. Loland, G. Skiniotis, L. Guan, B. Byrne, B. K. Kobilka, P. S. Chae, *J. Am. Chem. Soc.* **2016**, Vol. 138, 3789–3796.

[88] M. Monduzzi, *Curr. Opin. Colloid Interface Sci.* **1998**, Vol. 3, 467–477.

[89] J. C. Ravey, M. J. Stébé, *Colloids Surf. A* **1994**, Vol. 84, 11–31.

[90] V. M. Sadtler, F. Giulieri, M. P. Krafft, J. G. Riess, *Chem. Eur. J.* **1998**, Vol. 4, 1952–1956.

[91] K. Shinoda, M. Hato, T. Hayashi, *J. Phys. Chem.* **1972**, Vol. 76, 909–914.

[92] M. Wehbie, K. K. Onyia, F. Mahler, A. Le Roy, A. Deletraz, I. Bouchemal, C. Vargas, J. O. Babalola, C. Breyton, C. Ebel, S. Keller, G. Durand, *Langmuir* **2021**, Vol. 37, 2111–2122.

[93] G. N. M. Boussambe, P. Guillet, F. Mahler, A. Marconnet, C. Vargas, D. Cornut, M. Soulié, C. Ebel, A. Le Roy, A. Jawhari, F. Bonneté, S. Keller, G. Durand, *Methods* **2018**, Vol. 147, 84–94.

[94] P. Guillet, F. Mahler, K. Garnier, G. Nyame Mendendy Boussambe, S. Igonet, C. Vargas, C. Ebel, M. Soulié, S. Keller, A. Jawhari, G. Durand, *Langmuir* **2019**, Vol. 35, 4287–4295.

[95] Jacob N. Israelachvili, *Intermolecular and Surface Forces,* Academic Press, Amsterdam **2011**.

[96] C. Breyton, W. Javed, A. Vermot, C.-A. Arnaud, C. Hajjar, J. Dupuy, I. Petit-Hartlein, A. Le Roy, A. Martel, M. Thépaut, C. Orelle, J.-M. Jault, F. Fieschi, L. Porcar, C. Ebel, *Biochim. Biophys. Acta Biomembr.* **2019**, Vol. 1861, 939–957.

[97] R. C. Oliver, J. Lipfert, D. A. Fox, R. H. Lo, S. Doniach, L. Columbus, *PlOS ONE* **2013**, Vol. 8, e62488.

[98] W.-X. Hong, K. A. Baker, X. Ma, R. C. Stevens, M. Yeager, Q. Zhang, *Langmuir* **2010**, Vol. 26, 8690–8696.

[99] C. Bonnet, P. Guillet, S. Igonet, A. Meister, A. Marconnet, S. Keller, A. Jawhari, G. Durand, *J. Org. Chem.* **2019**, Vol. 84, 10606–10614.

[100] M. Abla, G. Durand, C. Breyton, S. Raynal, C. Ebel, B. Pucci, *J Fluor. Chem.* **2012**, Vol. 134, 63–71.

[101] D. Lichtenberg, H. Ahyayauch, F. M. Goñi, *Biophys. J.* **2013**, Vol. 105, 289–299.

[102] M. C. A. Stuart, E. J. Boekema, *Biochim. Biophys. Acta* **2007**, Vol. 1768, 2681–2689.

[103] H. Heerklotz, *Biophys. J.* **2001**, Vol. 81, 184–195.

[104] M. G. Lete, B. G. Monasterio, M. I. Collado, M. Medina, J. Sot, A. Alonso, F. M. Goñi, *Colloids Surf. B.* **2019**, Vol. 183, 110430.

[105] H. Y. Fan, D. Das, H. Heerklotz, *Langmuir* **2016**, Vol. 32, 11655–11663.

[106] M. Abla, G. Durand, B. Pucci, *J. Org. Chem.* **2008**, Vol. 73, 8142–8153.

[107] S. Keller, H. Heerklotz, N. Jahnke, A. Blume, *Biophys. J.* **2006**, Vol. 90, 4509–4521.

[108] D. Kampjut, J. Steiner, L. A. Sazanov, *iScience* **2021**, Vol. 24, 102139.

[109] H. E. Autzen, D. Julius, Y. Cheng, *Curr. Opin. Struct. Biol.* **2019**, Vol. 58, 259–268.

[110] H. E. Bae, Y. Du, P. Hariharan, J. S. Mortensen, K. K. Kumar, B. Ha, M. Das, H. S. Lee, C. J. Loland, L. Guan, B. K. Kobilka, P. S. Chae, *Chem. Sci.* **2019**, Vol. 10, 1107–1116.

[111] H. Heerklotz, A. Blume, "5.5 Detergent Interactions with Lipid Bilayers and Membrane Proteins", in: *Comprehensive Biophysics,* Elsevier, Amsterdam, pp. 63–91 **2012**.

[112] B. W. Berger, R. Y. García, A. M. Lenhoff, E. W. Kaler, C. R. Robinson, *Biophys. J.* **2005**, Vol. 89, 452–464.

[113] A. S. Ethayathulla, M. S. Yousef, A. Amin, G. Leblanc, H. R. Kaback, L. Guan, *Nat. Commun.* **2014**, Vol. 5, 3009.

[114] R. K. Wong, C. P. Nichol, M. C. Sekar, B. D. Roufogalis, *Biochem. Cell Biol.* **1987**, Vol. 65, 8–18.

[115] S. Murakami, R. Nakashima, E. Yamashita, A. Yamaguchi, *Nature* **2002**, Vol. 419, 587–593.

[116] V.-P. Jaakola, M. T. Griffith, M. A. Hanson, V. Cherezov, E. Y. T. Chien, J. R. Lane, A. P. Ijzerman, R. C. Stevens, *Science* **2008**, Vol. 322, 1211–1217.

[117] R. L. Grime, R. T. Logan, S. A. Nestorow, P. Sridhar, P. C. Edwards, C. G. Tate, B. Klumperman, T. R. Dafforn, D. R. Poyner, P. J. Reeves, M. Wheatley, *Nanoscale* **2021**, Vol. 13, 13519–13528.

[118] M. Nazari, M. Kurdi, H. Heerklotz, *Biophys. J.* **2012**, Vol. 102, 498–506.

[119] T. Gaudin, P. Rotureau, I. Pezron, G. Fayet, *Ind. Eng. Chem. Res.* **2016**, Vol. 55, 11716–11726.

[120] M. Mattei, G. M. Kontogeorgis, R. Gani, *Ind. Eng. Chem. Res.* **2013**, Vol. 52, 12236–12246.

[121] T. Gaudin, H. Lu, G. Fayet, A. Berthauld-Drelich, P. Rotureau, G. Pourceau, A. Wadouachi, E. van Hecke, A. Nesterenko, I. Pezron, *Adv. Colloid Interface Sci.* **2019**, Vol. 270, 87–100.

[122] E. Chabaud, P. Barthélémy, N. Mora, J.-L. Popot, B. Pucci, *Biochimie* **1998**, Vol. 80, 515–530.

[123] C. Breyton, E. Chabaud, Y. Chaudier, B. Pucci, J.-L. Popot, *FEBS Lett.* **2004**, Vol. 564, 312–318.

[124] J.-C. Talbot, A. Dautant, A. Polidori, B. Pucci, T. Cohen-Bouhacina, A. Maali, B. Salin, D. Brèthes, J. Velours, M.-F. Giraud, *J. Bioenerg. Biomembr.* **2009**, Vol. 41, 349–360.

[125] T. S. Owen, D. Salom, W. Sun, K. Palczewski, *Biochemistry* **2018**, Vol. 57, 1022–1030.

[126] A. Sadaf, S. Kim, H. E. Bae, H. Wang, A. Nygaard, Y. Uegaki, Y. Du, C. F. Munk, S. Katsube, H. Sung Lee, J. Bae, C. W. Choi, H.-J. Choi, B. Byrne, S. H. Gellman, L. Guan, C. J. Loland, B. K. Kobilka, W. Im, P. S. Chae, *Acta Biomater.* **2021**, Vol. 128, 393–407.

[127] A. Sadaf, M. Ramos, J. S. Mortensen, Y. Du, H. E. Bae, C. F. Munk, P. Hariharan, B. Byrne, B. K. Kobilka, C. J. Loland, L. Guan, P. S. Chae, *ACS Chem. Biol.* **2019**, Vol. 14, 1717–1726.

[128] J. W. Missel, N. Salustros, E. R. Becares, J. H. Steffen, A. G. Laursen, A. S. Garcia, M. M. Garcia-Alai, Č. Kolar, P. Gourdon, K. Gotfryd, *Curr. Res. Struct. Biol.* **2021**, Vol. 3, 85–94.

[129] J. Hovers, M. Potschies, A. Polidori, B. Pucci, S. Raynal, F. Bonneté, M. J. Serrano-Vega, C. G. Tate, D. Picot, Y. Pierre, J.-L. Popot, R. Nehmé, M. Bidet, I. Mus-Veteau, H. Busskamp, K.-H. Jung, A. Marx, P. A. Timmins, W. Welte, *Mol. Membr. Biol.* **2011**, Vol. 28, 171–181.

[130] M. Ehsan, A. Kumar, J. S. Mortensen, Y. Du, P. Hariharan, K. K. Kumar, B. Ha, B. Byrne, L. Guan, B. K. Kobilka, C. J. Loland, P. S. Chae, *Chem. Asian J.* **2019**, Vol. 14, 1926–1931.

[131] M. Ehsan, Y. Du, J. S. Mortensen, P. Hariharan, Q. Qu, L. Ghani, M. Das, A. Grethen, B. Byrne, G. Skiniotis, S. Keller, C. J. Loland, L. Guan, B. K. Kobilka, P. S. Chae, *Chem. Eur. J.* **2019**, Vol. 25, 11545–11554.

[132] K. H. Cho, B. Byrne, P. S. Chae, *ChemBioChem* **2013**, Vol. 14, 452–455.

Abbreviations and Variables

amphipol	short amphiphilic polymer
APol	(ionic) amphiphilic polymers
bicelle	bilayered micelle
c	concentration
CMC	critical micellization concentration
col	collisional (subscript)
CP	cyclopentane
CPM	cyclopentane-based maltoside
CPM-*C*	CPM *cis* stereoisomer
CPM-*T*	CPM *trans* stereoisomer
d	nanodisc (superscript)
DDDG	dodecyl diglucoside
DDG	decyl diglucoside
DDM	n-dodecyl-β-D-maltopyranoside
d_H	hydrodynamic diameter
DHPC	1,2-dihexanoyl-*sn*-glycero-3-phosphocholine
DIBMA	di-isobutylene/maleic acid
dif	diffusional (subscript)
DLS	dynamic light scattering
DMPC	1,2-dimyristoyl-*sn*-glycero-3-phosphocholine
DSC	differential scanning calorimetry
F_6ODG	1H,1H,2H,2H-perfluorooctyl diglucoside
FDA	food and drug administration
FRET	Förster resonance energy transfer
GP	generalized polarization
GPCR	G protein-coupled receptors
ITC	isothermal titration calorimetry

K	partition coefficient
k	exchange rate
KvAP	voltage-dependent potassium ion channel
L	lipid (subscript)
LeuT	leucine transporter
LMNG	lauryl maltose neopentylglycol
m	micelle (superscript)
$MelB_{St}$	melibiose permease
mic	micelle; micellar; micellization (subscript)
mon	monomer (subscript)
MOR	*μ*-opioid receptor
MP/MPs	membrane protein/membrane proteins
MSP	membrane scaffold protein
NAPol	non-ionic Amphiphilic Polymer
NBD-DHPE	*N*-(7-nitrobenz-2-oxa-1,3-diazol-4-yl)-1,2-dihexadecanoyl-*sn*-glycero-3-phosphoethanolamine
NBM	norbonane-based maltosides
NMR	nuclear magnetic resonance
obs	observed (subscript)
ODG	octyl diglucoside
OG	n-octyl-β-D-glucopyranoside
OmpA	outer membrane protein A
OmpLA	outer membrane phospholipase A1
PAGE	polyacrylamide gel electrophoresis
Per	perforation
POPC	1-palmitoyl-2-oleoyl-*sn*-glycero-3-phosphocholine
QPSA	quasiphenomenological sigmoid algorithm
R	amphiphile/lipid ratio; gas constant

Rh-DHPE	rhodamine B 1,2-dihexadecanoyl-*sn*-glycero-3-phosphoethanolamine
S	surfactant (subscript)
Sat	saturation
SDS	sodium dodecyl sulfate
SMA	styrene/maleic acid
Sol	solubilization
ST	surface tensiometry
T	temperature
TDM	n-tridecyl-β-D-maltopyranoside
TEM	transmission electron microscopy
Tm	thermotropic phase transition temperature
v	vesicle (superscript)
X	critical mole fraction
β_2AR	β_2 adrenergic receptor
ΔC_p	change in isobaric heat capacity
$\Delta G°$	change in standard molar Gibbs free energy
$\Delta H°$	change in standard molar enthalpy
$\Delta S°$	change in standard molar entropy
τ	characteristic NBD bleaching time

Acknowledgements

With this, I want to thank all the people who were involved in realizing this work. In particular I want to thank:

- Prof. Dr. Sandro Keller (Universität Graz, Austria) for giving me the opportunity to work in his former laboratory at the Technische Universität Kaiserslautern on these interesting projects, as well for outstanding supervision and guidance in the past 5 years.
- Prof. Dr. Matthias Hahn (TUK) for agreeing on being my second advisor for this thesis.
- Prof. Dr. Stefan Kins (TUK) for agreeing to act as a chairman for the defense.
- Prof. Dr. Grégory Durand and his group (University of Avignon) for great collaboration and providing us with a manifold of compounds including the diglucoside amphiphiles and the surfmers presented in this work.
- Prof. Dr. Pil Seok Chae (Hanyang University, South Korea) and Dr. Manabendra Das (formerly Hanyang University and TUK) for good collaboration and providing us with the branched CPMs.
- PD Dr. Annette Meister (Martin-Luther-Universität, Halle-Wittenberg) and Dr. Harald Kelm (TUK) for their invaluable support with TEM and NMR spectroscopy, respectively.
- Our former collaboration partners from Quench Bio for funding.
- All other collaboration partners I worked with during my time as PhD student.
- All former members of the Molecular Biophysics group: Dr. Carolyn Vargas, Andreas Werle–Rutter, Simone Adkins, Dr. Eugenio Pérez Patallo, Dr. Manabendra Das, Jessica Klement, Dr. Abraham Olusegun Oluwole, Johannes Klingler, Dr. Erik Frotscher, Dr. Bartholomäus Danielczak, Dr. Anne Grethen, Kenechi Onyia, Patricia Ogochukwu Mmeka, Michael Tope Agbadaola, Jonas Höring, David Glück, Kevin Janson, Melike Aksu, Dr. Tim Diederichs, Moritz Häffner, Jan Schatteburg, Dirk Himbert, Felix Jung, Duc Nguyen, Dr. Johannes Schnur, Sophie Weyrauch, Julia Lenz, Kai Zwara, Ann-Cathrin Schlapp, and Lisa Hamsch for the great working environment and great times in and outside the lab.
- Dr. Eugenio Pérez Patallo, Dr. Anne Grethen, Johannes Klingler, David Glück, Kevin Janson, and Jonas Höring for their support throughout the years, scientific advice, excellent comments on the thesis, and great friendship.
- Jonas Höring for everything that was said, specifically not said, and written in highly official e-mails.
- Simone Adkins for her indispensable support with all organizational matters and her help with many administration issues.
- The TU-Nachwuchsring for funding attendance to the Okinawa Colloids 2019.
- My family and friends for their support and interest in this "soap stuff".
- Jennifer Kleinschmidt for her dear support in all the things we lived through.

Curriculum Vitae

Personal Data

Name	Florian Mahler
Place of Birth	Karlsruhe
Date of Birth	28. August 1992
Nationality	German

Employment

03/2018 – 08/2021 **Technische Universität Kaiserslautern, Germany**
Research associate in the group of *Molecular Biophysics* with Prof. Sandro Keller

Education

Since 03/2018 **Technische Universität Kaiserslautern, Germany**
PhD student in the group of *Molecular Biophysics* with Prof. Sandro Keller

10/2012 – 02/2018 **Technische Universität Kaiserslautern, Germany**
Studies in *Biophysics*

Diploma thesis about "Interactions of Fluorinated Surfactants with Model Lipid Bilayers" in the group of *Molecular Biophysics* with Prof. Sandro Keller

09/2009 – 06/2021 **Bertha-von-Suttner-Schule Ettlingen, Germany**

(Biotechnological Orientation)

Higher education entrance qualification/A-levels (Abitur)

09/2003 – 06/2009 **Realschule Rheinstetten, Germany**

Secondary school certificate/O-levels (Mittlere Reife)

Conferences

03/2020 DGfB - Membrane Biophysics Meeting Drübeck 2020, Drübeck, Germany

Poster presentation

11/2019	Okinawa Colloids 2019 An International Conference on Colloids & Surface Science, Okinawa, Japan *Oral presentation*
03/2018	665. WE-Heraeus-Seminar on ‚Physical Approaches to Membrane Asymmetry', Bad Honnef, Germany *Poster presentation*

List of Publications

Peer-reviewed

1. Glyco-DIBMA: A Glycosylated Diisobutylene/Maleic Acid Copolymer with Improved Nanodisc Properties.
   B. Danielczak, M. Rasche, E. Pérez Patallo, S. Weyrauch, **F. Mahler**, M. Tope Agbadaola, J. Lenz, A. Meister, J. Oyebamiji Babalola, C. Vargas, C. Kolar, and S. Keller *Nanoscale* (2021) *accepted*
2. Hybrid Fluorocarbon-Hydrocarbon Surfactants: Synthesis and colloidal characterization.
   E. Grousson, **F. Mahler**, S. Keller, C. Contino-Pépin, and G. Durand *J. Org. Chem.* (2021) 86, 21, 14672-14683
3. Self-Assembly of Protein-Containing Lipid-Bilayer Nanodiscs from Small-Molecule Amphiphiles.
   F. Mahler, A. Meister, C. Vargas, G. Durand, and S. Keller *Small* (2021) 2103603 *in print*
4. Maltose-Based Fluorinated Surfactants for Membrane-Protein Extraction and Stabilization.
   M. Wehbie, **F. Mahler**, K. Onyia, A. Le Roy, A. Deletraz, I. Bouchemal, C. Breyton, C. Ebel, S. Keller, and G. Durand *Langmuir* (2021) 37, 6, 2111-2122.
5. Diastereomeric Cyclopentane-Based Maltosides (CPMs) as Tools for Membrane Protein Study.
   M. Das, **F. Mahler**, P. Hariharan, H. Wang, Y. Du, J. S. Mortensen, E. Pérez Patallo, L. Ghani, D. Glück, H. J. Lee, B. Byrne, C. J. Loland, B. K. Kobilka, S. Keller, and P. Seok Chae *J. Am. Chem. Soc.* (2020) 142, 51, 21382-21392.
6. Detergent-Like Polymerizable Monomers: Synthesis, Physicochemical, and Biochemical Characterization.
   C. Bonnet, P. Guillet, **F. Mahler**, S. Igonet, S. Keller, A. Jawhari, and G. Durand *Eur. J. Org. Chem.* (2020) 5340-5349.
7. Fast and robust quantification of detergent micellization thermodynamics from isothermal titration calorimetry.
   S.-C. Tso, **F. Mahler**, J. Höring, S. Keller, and C. A. Brautigam *Anal. Chem.* (2019) 92, 1, 1154-1161.

8. Hydrogenated diglucose detergents for membrane-protein extraction and stabilization.
   P. Guillet, **F. Mahler**, K. Garnier, G. N. M. Boussambe, S. Igonet, C. Vargas, C. Ebel M. Soulié, S. Keller, A. Jawhari, and G. Durand *Langmuir* (2019) 35, 12, 4287-4295.
9. Fluorinated diglucose detergents for membrane-protein extraction.
   G. N. M. Boussambe, P. Guillet, **F. Mahler**, A. Marconnet, C. Vargas, D. Cornut, M. Soulié, C. Ebel, A. Le Roy, A. Jawhari, F. Bonneté, S. Keller, and G. Durand *Methods* (2018) 147, 84-94.

Preprints

10. The secreted hypersensitive response inducing protein 1 from *Botrytis cinerea* displays non-canonical PAMP-activity.
    T. Jeblick, T. Leisen, C. Steidele, J. Müller, **F. Mahler**, F. Sommer, S. Keller, R. Hückelhoven, M. Hahn, and D. Scheuring *bioRxiv* (2020).

Eidesstattliche Erklärung

Hiermit erkläre ich, dass mir die Promotionsordnung des Fachbereichs Biologie der Technischen Universität Kaiserslautern in der derzeit gültigen Fassung bekannt ist. Ich versichere, dass ich die vorliegende Arbeit selbstständig verfasst, keine anderen als die angegebenen Quellen und Hilfsmittel verwendet, sowie die Ergebnisse anderer Mitarbeiter beziehungsweise Autoren klar gekennzeichnet habe. Ich habe diese Arbeit oder Teile daraus keinem anderen Fachbereich der Technischen Universität Kaiserslautern vorgelegt und mich zu keinem früheren Zeitpunkt um den Doktorgrad beworben.

Florian Mahler

Kaiserslautern, November 2021